Identification and functional characterisation of synaptic AMPA receptor-interacting proteins

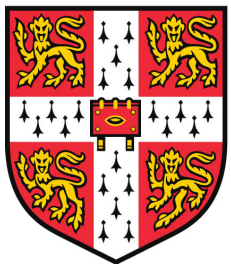

Peter Michael Matthews

Supervisor: Dr Ingo H. Greger

MRC Laboratory of Molecular Biology
University of Cambridge

This dissertation is submitted for the degree of
Doctor of Philosophy

Wolfson College

March 2021

A synaptic fishing trip

Preface

This thesis is the result of my own work and includes nothing which is the outcome of work done in collaboration except as declared below and specified in the text.

A subset of glutamate spillover experiments in Chapter 3 were conducted with the support of Dr Jake F Watson and Dr Alexandra Pinggera, who performed single-cell electroporation transfections of organotypic slice cultures and stereotactic injections of neonatal pups. Individual contributions are mentioned throughout the text. Investigations were conducted under the supervision of Dr Ingo Greger.

This thesis is not substantially the same as any work that I have submitted, or, is being concurrently submitted for a degree or diploma or other qualification at the University of Cambridge or any other University or similar institution. I further state that no substantial part of my thesis has already been submitted, or, is being concurrently submitted for any such degree, diploma or other qualification at the University of Cambridge or any other University or similar institution.

This thesis contains less than 60,000 words excluding the bibliography, appendix and figure legends.

Peter Michael Matthews
March 2021

Identification and functional characterisation of synaptic AMPA receptor-interacting proteins

Peter Michael Matthews

Abstract

Neuronal communication occurs at specialised sites, known as synapses. Presynaptic neurotransmitter release from one neuron acts on the postsynaptic receptors of another, facilitating transfer of electrical impulses between neurons. At glutamatergic synapses, ionotropic glutamate receptors (iGluRs) respond to presynaptically released L-glutamate, the predominant excitatory neurotransmitter. Excitatory synaptic transmission is mediated primarily by AMPA-type glutamate receptors (AMPARs), and is crucial for the transfer and storage of information in the brain. The AMPAR engages in numerous protein interactions, modulating receptor trafficking, channel gating, synaptic positioning, and ultimately synaptic strength.

iGluR family members bind synaptic proteins through their N-terminal domain (NTD), influencing synaptic and neuronal circuit function. The AMPAR NTD encompasses 50% of the receptor, extending midway into the synaptic cleft, exposing it to a protein-rich environment. The strength of synaptic transmission is dependent on the AMPAR NTD, likely by positioning receptors at the synapse. This mechanism is thought to be regulated through direct protein interactions with the NTD. The identity and functional importance of these protein interactions however, are unknown. Therefore, this study aims to identify and characterise the synaptic function of AMPAR NTD-interacting proteins.

Aided by the development of a novel proximity-labelling proteomics technique, synaptic proteins enriched for the AMPAR NTD were determined. This permitted identification of transient NTD interactors, previously unresolved using classical affinity-purifications. Furthermore, this technique provides a comprehensive list of diverse synaptic cleft proteins, which may influence AMPAR function through direct or indirect mechanisms. Candidate interactors were later screened for direct interactions with iGluR NTDs by establishing a cell-based binding assay. This confirmed known iGluR NTD interactors and uncovered neuronal pentraxin-1 (Nptx1) as an AMPAR NTD-interacting protein. Facilitated by structural biology, the Nptx1 binding site was deduced using AMPAR NTD mutants. The functional consequence of this interaction was then studied at synapses onto principle neurons of the hippocampus using different electrophysiological and imaging approaches, demonstrating Nptx1 as a subunit-specific regulator of AMPAR-mediated synaptic transmission. These findings have profound implications for understanding the role of AMPAR-interacting proteins in regulating the strength of synaptic connections.

A subset of figures and ideas presented in this document have been published in the following:

Matthews, P.M., Pinggera, A.*, Kampjut, D., Greger, I.H. 2021. Biology of AMPA receptor interacting proteins - From biogenesis to synaptic plasticity. Neuropharmacology, doi: https://doi.org/10.1016/j.neuropharm.2021.108709 (* authors contributed equally)*

Acknowledgments

Firstly, I would like to thank the Medical Research Council (MRC) for funding this study and the scientific facilities and support services of the MRC Laboratory of Molecular Biology for making this project possible. I would like to thank Dr Ingo Greger in particular, for his supervision, advice and enthusiastic discussion throughout this project. Furthermore, I would like to thank Prof. Ole Paulsen for his guidance and expertise with electrophysiological recordings, for which I am very grateful.

I have thoroughly enjoyed working with past and present members of the Greger lab and would like to thank them all for their insightful technical and theoretical ideas, which have inspired a number of experiments conducted in this study. More specifically, I would like to thank Dr Alexandra Pinggera for her technical expertise with fluorescence microscopy of neuronal cultures and for her intuitive discussion and critical reading of this work, which helped formulate a number of experimental ideas used in this study. I would also like to thank Dr Remigijus Lape and Dr Ondrej Cais for their expertise with performing fast-glutamate application experiments and Dr Remigijus Lape for critical reading of a subset of this work.

I am greatly indebted to Dr Sew-Yeu Peak-Chew for her proficiency and perseverance with performing extensive mass spectrometry experiments, which enabled the identification of candidate synaptic AMPAR-interacting proteins. I am extremely grateful for her hard-work and assistance over the duration of this project. I would also like to thank Dr Radu Aricescu and Dr Veronica Chang for providing X-ray crystal structures of neuronal pentraxin-1 in complex with the AMPAR NTD, as this information formed the basis of a significant part of this study. Additionally, I am grateful for Dr Kunimichi Suzuki's helpful discussion and guidance in establishing the cell-based binding assay and for providing specific antibodies against neuronal pentraxin-1.

Finally, I would like to thank Jade Shoulder for her encouragement and support throughout this project and last but not least my cat Milo, for his words of wisdom.

Table of contents

Abbreviations

ΔNptx1	- neuronal pentraxin-1 binding site mutant
ΔNTD	- N-terminal domain-deleted receptor
A/N	- AMPAR/NMDAR ratio
AAV	- adeno-associated virus
ACSF	- artificial cerebrospinal fluid
aEPSC	- asynchronous excitatory postsynaptic current
AF	- Alexa Fluor
ANOVA	- analysis of variance
AMPAR	- α-amino-3-hydroxy-5-methyl-4-isoxazolepropionic acid receptor
AP-MS	- affinity purification-mass spectrometry
APEX	- ascorbate peroxidase
ATP	- adenosine 5'-triphosphate
AZ	- active zone
BirA	- biotin ligase
BirA*	- promiscuous biotin ligase
BSA	- bovine serum albumin
C1q	- complement component 1q
CA1	- *cornu ammonis 1*
Ca^{2+}	- calcium ions
CA3	- *cornu ammonis 3*
CAM	- cell-adhesion molecule
CaMKII	- calcium/calmodulin-dependent protein kinase II
Cbln	- cerebellin
CMW	- cytomegalovirus

Abbreviations

CNIH - cornichon

CP-AMPAR - calcium-permeable AMPA receptor

CPT1c - carnitine O-palmitoyltransferase 1c

CPTX - cerebellar pentraxin

CTD - C-terminal domain

CUB - complement C1r/C1s, Uegf, Bmp1

CV - coefficient of variation

D-APV - D-(-)-2-Amino-5-phosphonopentanoic acid

DAPI - 4′,6-diamidino-2-phenylindole

DG - dentate gyrus

DIV - days *in vitro*

DL-TBOA - DL-threo-β-Benzyloxyaspartic acid

DMEM - Dulbecco′s Modified Eagle′s Medium

DNA - deoxyribonucleic acid

DPI - days post-infection

DPT - days post-transfection

DTT - dithiothreitol

EAAT - excitatory amino-acid transporter

ECS - extracellular solution

eEPSC - evoked excitatory postsynaptic current

EGFP - enhanced green fluorescent protein

EGTA - ethylene glycol-bis(β-aminoethyl ether)-N,N,N′,N′-tetraacetic acid

EPSC - excitatory postsynaptic current

ER - endoplasmic reticulum

FBS - fetal bovine serum

FRRS1l - ferric chelate reductase 1 like

GBSS - Gey's Balanced Salt Solution

GFP - green fluorescent protein

HEPES - 4-(2-hydroxyethyl)-1-piperazineethanesulfonic acid

HRP - horse radish peroxidase

ICS - intracellular solution

iGluR - ionotropic glutamate receptor

IRES - internal ribosome entry site

ISI - inter-stimulus interval

ITR - inverted terminal repeat

IV - current/voltage relationship

IVA - *In vivo* assembly

KAR - kainate receptor

LBD - ligand binding domain

LC-MS/MS - liquid chromatography with tandem mass spectrometry

Lrrtm - leucine-rich repeat transmembrane protein

LTD - long-term depression

LTP - long-term potentiation

MEM - Minimal Essential Medium

mEPSC - miniature excitatory postsynaptic current

Mg^{2+} - magnesium ions

mGluR - metabotropic glutamate receptor

MS - mass spectrometry

Na^{+} - sodium ions

NBQX - 2,3-Dioxo-6-nitro-1,2,3,4-tetrahydrobenzo[f]quinoxaline-7-sulfonamide disodium salt

Neto - neuropilin and tolloid like

NMDAR - N-methyl-D-aspartate receptor

Abbreviations

Nptx	- neuronal pentraxin (1/2/r - receptor)
NTD	- N-terminal domain (also known as amino-terminal domain)
OE	- overexpression
Olfm	- olfactomedin
P2A	- porcine teschovirus-1 2a
PBS	- phosphate buffered saline
PCR	- polymerase chain reaction
PFA	- paraformaldehyde
PL	- proximity-labelling
PL-MS	- proximity labelling-mass spectrometry
PMSF	- phenylmethylsulfonyl fluoride
PPF	- paired-pulse facilitation
PPR	- paired-pulse ratio
PSD	- postsynaptic density
PTX	- pentraxin
PV-IN	- parvalbumin-positive interneurons
RI	- rectification index
SCE	- single-cell electroporation
SDS-PAGE	- sodium dodecyl sulphate-polyacrylamide gel electrophoresis
SEM	- standard error of the mean
sEPSC	- spontaneous excitatory postsynaptic current
SPR	- surface plasmon resonance
SS	- signal sequence
STED	- stimulated emission depletion microscopy
STORM	- stochastic optical reconstruction microscopy
SynGO	- synaptic gene ontology

TARP	- transmembrane AMPA receptor regulatory protein
TFB-TBOA	- (3S)-3-[[3-[[4-(Trifluoromethyl)benzoyl]amino]phenyl]methoxy]-L-aspartic acid
TMD	- transmembrane domain
TTX	- tetrodotoxin
WB	- western blot

Chapter 1

Introduction

1.1 Glutamatergic synaptic transmission

Neuronal communication occurs at specialised connections called synapses. At these neuronal junctions, neurotransmitter is released from the presynaptic cell, activating receptors expressed on the postsynaptic cell (Figure 1.1; Lisman et al., 2007). At excitatory synapses, L-glutamate is principally released by exocytosis into the synaptic cleft where it binds to postsynaptic AMPA receptors (AMPARs) and other glutamate receptors (Collingridge and Lester, 1983). The strength of communication at these sites can be modified by changes in the presynaptic and/or postsynaptic machinery.

At presynaptic terminals, neurotransmitter-containing vesicles are fused with the plasma membrane upon activation of the SNARE complex. More specifically, action potential depolarisation, driven by sodium (Na^+) channel activation, depolarises voltage-gated calcium channels (VGCCs) at the presynaptic terminal leading to an influx of calcium (Ca^{2+}). VGCCs are positioned within close proximity to the presynaptic release machinery to ensure Ca^{2+}-dependent activation of the SNARE complex and subsequent vesicle fusion. Glutamate is then released through the fusion pore and into the synaptic cleft (Lisman et al., 2007). Synaptic glutamate concentrations are thought to be >1 mM for a duration of <10 ms, rapidly returning to concentrations of <20 nM, due to the uptake of glutamate into neighbouring astrocytes (Dzubay and Jahr, 1999). Postsynaptic ionotropic glutamate receptors (iGluRs) are subsequently activated by their ligand, glutamate. This then permits flux of Na^+, and in some cases Ca^{2+}, into the postsynaptic cell generating an excitatory postsynaptic current (EPSC) (Figure 1.1B).

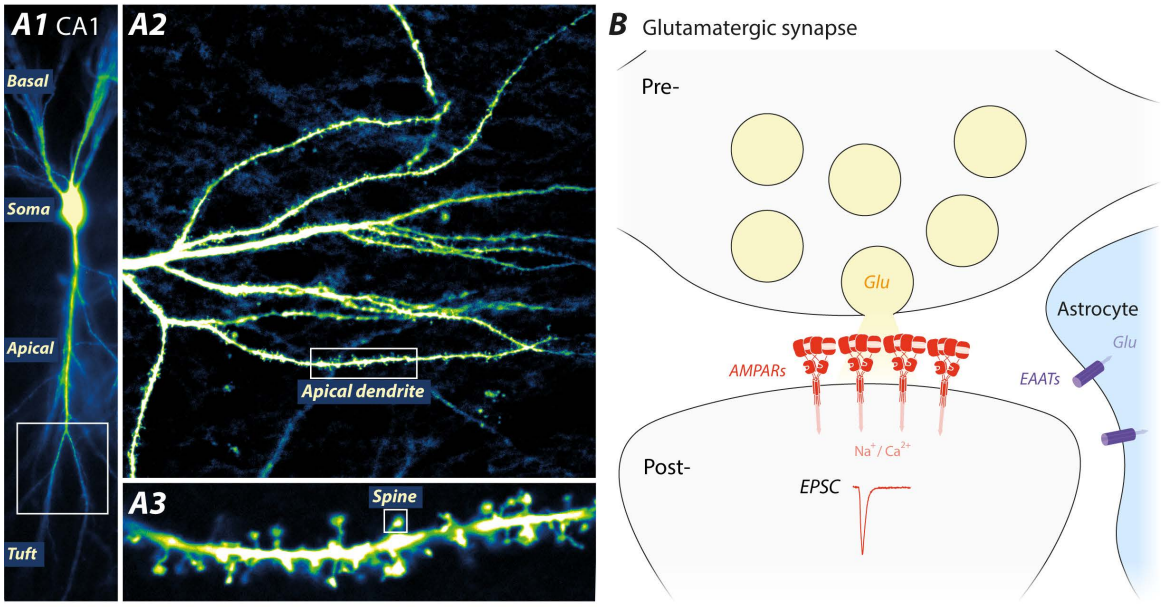

Figure 1.1 ***The glutamatergic synapse.*** *(**A1**) Hippocampal CA1 pyramidal neuron with apical and basal dendritic trees and a characteristic pyramidal soma. (**A2**) Apical dendritic tree, containing dendritic spines. (**A3**) Dendritic spines are protrusions on the dendrite where excitatory synapses are formed. (**B**) 'Tri-partite' excitatory synapse consisting of a presynaptic (Pre-) terminal where excitatory neurotransmitter glutamate (Glu; yellow) is released by exocytosis from vesicles, binding to postsynaptic (Post-) AMPA-type glutamate receptors (AMPARs; red), permitting Na^+, and in some cases, Ca^{2+} ion flow (arrows) and resultant depolarisation of the postsynaptic membrane. This results in the generation of an excitatory postsynaptic current (EPSC) detectable using electrophysiology (current trace). The concentration of glutamate in the synaptic cleft is tightly controlled by glutamate uptake into neighbouring astrocytes (blue) via excitatory amino acid transporters (EAATs) (purple).*

Excitatory pyramidal neurons are the major excitatory neurons in the hippocampus and cortex, characterised by their apical and basal dendritic spines and their pyramidal soma (Figure 1.1A1). Excitatory synapses are formed at membrane protrusions from the dendrite referred to as 'spines' (Figure 1.1A3; Spruston, 2008). 'Tri-partite' excitatory synapses are composed of pre- and post-synaptic terminals surrounded by astrocytic processes capable of clearing glutamate from the synaptic cleft through excitatory amino acid transporters (EAATs; Figure 1.1B). EAATs therefore, control the spatrio-temporal concentration of glutamate, influencing spillover onto extra-synaptic receptors and neighbouring synapses (Tzingounis and Wadiche, 2007).

Glutamate receptors can be broadly divided into ionotropic (iGluR; ligand-gated ion channels) and metabotropic (mGluR; G-protein coupled receptors) glutamate receptors. These receptors regulate fast and slow components of the EPSC respectively, and are essential for long-term changes in synaptic efficacy (synaptic plasticity), considered to be the cellular correlate of learning and memory. Our understanding of this family of receptors has been progressed significantly by specific pharmacology (Watkins and Evans, 1981) and molecular cloning (Hollmann and Heinemann, 1994). More recently, our appreciation of the cellular and molecular processes by which glutamate receptors modulate synaptic strength has improved significantly with the development of new molecular biology techniques. This study focuses on the molecular mechanisms of AMPARs in excitatory synaptic transmission and plasticity.

1.2 Ionotropic glutamate receptors

Ionotropic glutamate receptors (iGluR) comprise members of the AMPA (α -amino-3-hydroxy-5-methyl-4-isoxazolepropionic acid) receptor (AMPAR), NMDA (N-Methyl-D-aspartic acid) receptor (NMDAR), kainate receptor (KAR) and delta receptor subfamilies. These receptors are tetramers composed of 4 pore-forming subunits and have a similar amino acid sequence homology (50% sequence similarity; Traynelis et al., 2010) and overall structure (Figure 1.2A/C). iGluRs are composed of an N-terminal domain (NTD), ligand binding domain (LBD), transmembrane domain (TMD) and C-terminal domain (CTD). These channels are gated by the excitatory neurotransmitter, L-glutamate (with the exception of delta receptors), released from presynaptic terminals. Each subfamily and receptor subtype have distinct biophysical, pharmacological and signalling properties in the central nervous system (CNS).

1.2.1 AMPA receptors

AMPARs are tetrameric receptors composed of 4 pore-forming subunits GluA1-4, assembled into homo- and/or heteromeric complexes, with different subunit arrangements within the tetrameric receptor (Zhao et al., 2019). AMPARs are composed of an NTD, LBD, TMD and CTD (Figure 1.2B1). AMPARs are widely expressed in the CNS and are the principle mediators of excitatory synaptic transmission.

C-terminal domain

The AMPAR CTD is a long sequence diverse polypeptide which extends into the intracellular space (García-Nafría et al., 2016a). AMPAR CTDs are involved in subunit-specific regulation of channel gating (Kristensen et al., 2011), synaptic trafficking (Shepherd and Huganir, 2007) and synaptic plasticity (Liu et al., 2020; Zhou et al., 2018). These functional roles are thought to be regulated by a number of different protein interactions (Figure 1.2B2) and post-translational modifications, such as phosphorylation (Figure 1.6; S831 and S845; Lee et al., 2003). A prevailing model suggests that CTD phosphorylated receptors are captured at postsynaptic sites during long-term potentiation (LTP; Hayashi et al., 2000; Shi et al., 2001). However, some reports suggest no functional requirement for the AMPAR CTD in synaptic trafficking and plasticity (Díaz-Alonso et al., 2020; Granger et al., 2013). It is likely however, that the CTD plays a modulatory role in shaping AMPAR-mediated synaptic transmission (Watson et al., 2020). A wealth of protein interactions have been identified with the AMPAR CTD, discussed in detail later in this chapter (see 1.3.2).

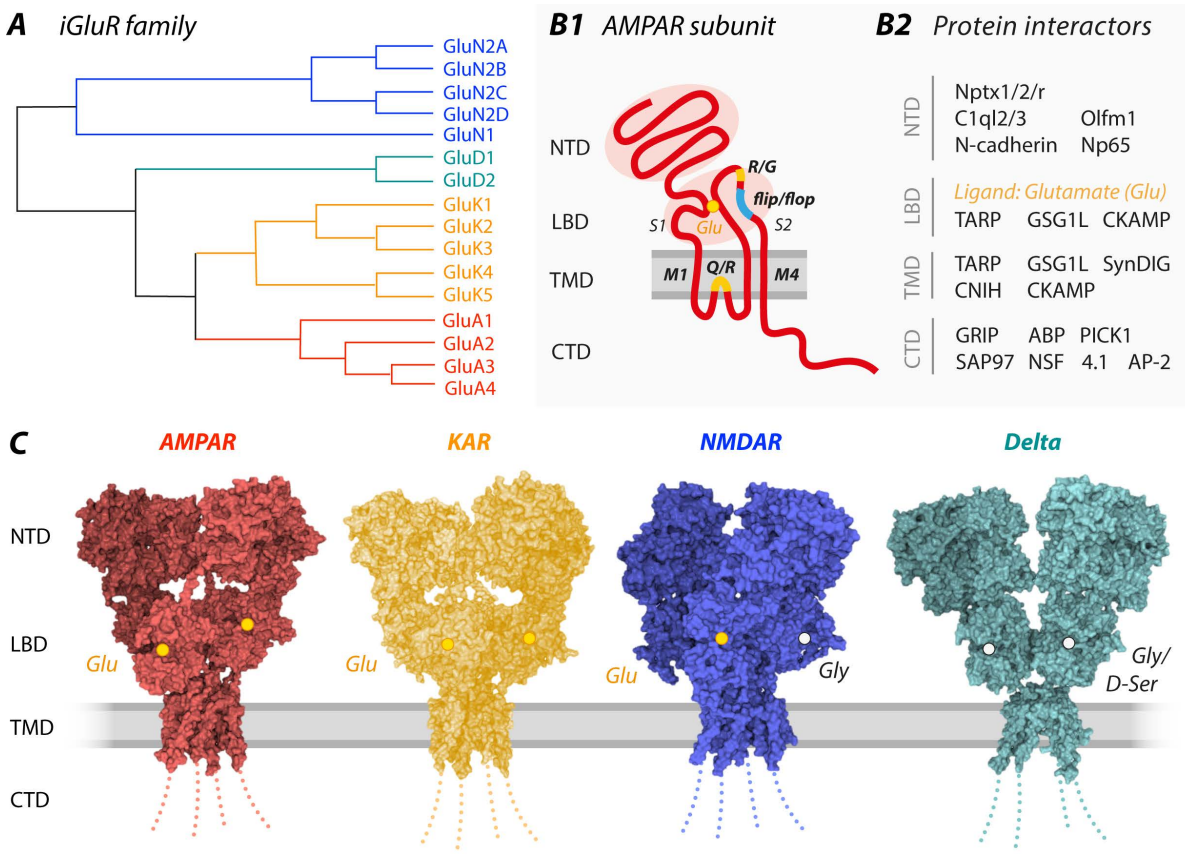

Figure 1.2 *AMPAR structure and known protein interaction sites.*

Figure 1.2 ***AMPAR structure and known protein interaction sites.*** *(**A**) Dendrogram of ionotropic glutamate receptor (iGluR) family based on amino acid sequence (constructed using Simple Phylogeny EMBL-EBI; www.ebi.ac.uk). iGluR subfamilies include NMDA receptors (NMDAR; GluN subunits; blue), delta receptors (GluD subunits; teal), kainate receptors (KARs; GluK subunits; orange) and AMPA receptors (AMPARs; GluA subunits; red). (**B1**) AMPAR subunit polypeptide schematic composed of an N-terminal domain (NTD), ligand binding domain (LBD), transmembrane domain (TMD) and C-terminal domain (CTD), with the plasma membrane coloured in grey. The NTD comprises 50% of the AMPAR projecting into the extracellular space. The LBD is composed of S1 and S2 loops forming the glutamate binding site. Key RNA editing and splice sites are indicated on the AMPAR subunit (R/G site and Q/R editing sites are shown in yellow and the flip/flop cassette is shown in blue). AMPAR subunits are composed of 4 TMDs labelled M1-M4. (**B2**) Known protein interactors with the AMPAR are listed, grouped by their published binding sites. (**C**) iGluR family members structures presented for comparison (CTDs depicted by dotted line). X-ray crystal structure of AMPAR subunit, GluA2 (PDB: 3KG2; Sobolevsky et al., 2009). X-ray crystal structure of NMDAR subunit, GluN1/2B (PDB: 4PE5; Karakas and Furukawa, 2014). Cryo-EM structure of KAR subunit, GluK2 (PDB: 5KUF; Meyerson et al., 2016) Cryo-EM structure of delta receptor subunit, GluD1 (PDB: 6KSS; Burada et al., 2020). 2 of a total 4 binding sites are illustrated for each iGluR. AMPARs and KARs bind glutamate (Glu; yellow). NMDARs bind glutamate and co-agonist glycine (white). Delta receptors bind glycine/D-serine (white).*

Transmembrane domain

The AMPAR transmembrane domain (TMD) forms the ion channel pore, allowing passage of Na^+ and in some cases, Ca^{2+}, to achieve membrane depolarisation. AMPAR subunits are formed from four TMD helices, three membrane spanning (M1, M3 and M4) and one re-entrant loop (M2), which forms the ion selectivity filter (Kuner et al., 2001; Sobolevsky et al., 2009). The M2 helix is responsible for dictating subunit-specific channel properties. A conserved glutamine (Q) residue is located within the M2 helix of all AMPAR subunits, however ribonucleic acid (RNA) editing of the GluA2 (but not GluA1/3/4) transcript results in selective alteration of glutamine (Q; encoded by CAG) to arginine (R; encoded by the non-canonical triplet CIG, translated as CGG) residue at site 586, referred to as the 'Q/R site' (Figure 1.2B1; Kuner et al., 2001; Sommer et al., 1991). GluA2 Q/R edited receptors are Ca^{2+}-impermeable (Hollmann et al., 1991), due to positively charged R residues projecting into the water-filled ion channel cavity, restricting cation flux (Herguedas et al., 2019). Other altered electrophysiological properties of Q/R edited receptors include the current-voltage (IV) relationship (Bowie and Mayer, 1995) and single channel conductance (Swanson et al., 1997). Moreover, the Q/R site affects the assembly and exit of AMPARs from the endoplasmic reticulum (ER) (Greger et al., 2003; 2002; Greger and Esteban, 2007).

Q/R edited receptors are permissive to intracellular polyamines, such as spermine, at positive membrane potentials. However, unedited Q-pore receptors bind spermine at the electronegative selectivity filter within the ion channel pore, preventing ion channel flow at positive membrane potentials (Figure 1.3A2; Q586-D590; Twomey et al., 2018). GluA2 Q-pore (GluA2Q) receptors therefore, have an inwardly recitifying IV relationship (Figure 1.3A3; Bowie and Mayer, 1995; Kamboj et al., 1995; Koh et al., 1995). GluA2 R-pore (GluA2R) subunits however, are permissive to spermine, due to repulsion of the positive charge on R-residues and spermine. Therefore, these receptors confer a linear IV relationship (Figure 1.3A3). This electrophysiological property has been harnessed to study the synaptic trafficking of exogenous Q-pore receptors against the linear IV relationship of an endogenous (R-pore) receptor population (Hayashi et al., 2000; Shi et al., 2001), and is used extensively throughout this study to determine the extent of AMPAR subunit synaptic trafficking.

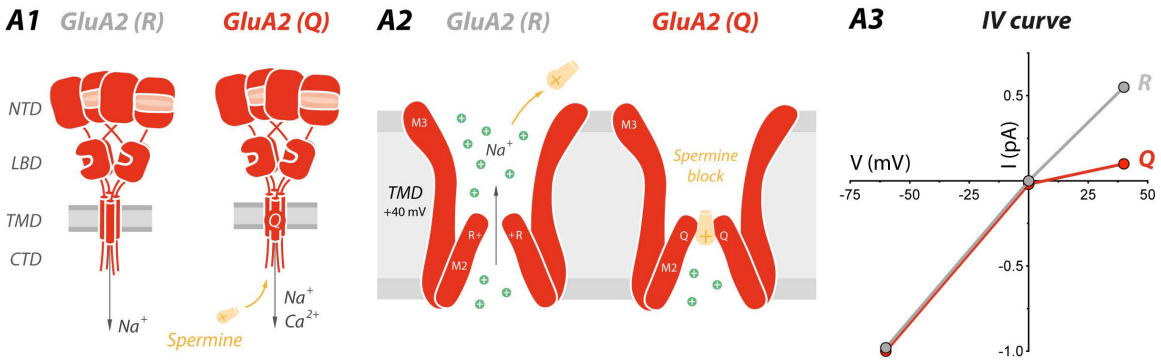

Figure 1.3 ***Inward rectification properties of Q/R edited AMPARs.*** *(**A1**) Endogenous GluA2 receptors are Q/R edited at residue 586, GluA2(R), rendering them Ca^{2+}-impermeable and permissive to intracellular polyamines, such as spermine. Exogenous GluA2 Q-pore containing receptors (GluA2Q) however, are Ca^{2+}-permeable and blocked by intracellular spermine at positive membrane potentials. (**A2**) Mechanism of polyamine (spermine) block at positive membrane potentials (+40 mV). Spermine permeates GluA2(R) receptors allowing an outward flux of Na^{+} ions through the channel at +40 mV. GluA2(Q) receptors however, are blocked by spermine at +40 mV, preventing an outward flux of Na^{+} ions. This is due to positively charged spermine directly interacting with neutral Q residues, but not positively charged R residues in the selectivity filter (Q586-D590) (Twomey et al., 2018). (**A3**) Endogenous GluA2(R) confers a linear current-voltage (IV) relationship, whereas exogenous GluA2(Q) is inwardly-rectifying at positive membrane potentials (+40 mV).*

Ligand binding domain

The AMPAR ligand binding domain (LBD) is a 'clam-shell'-like domain formed of two non-continuous polypeptides, S1 and S2, forming the glutamate binding site (Figure 1.2). AMPARs subunits GluA1-4 undergo alternative splicing at the flip/flop site, a 115 bp region that generates one of two alternative splice forms (9−11 amino acids) (Figure 1.2B1; Sommer et al., 1990). Flip splice variants have a faster activation and slower desensitisation relative to flop variants, with flop receptors showing reduced current responses to glutamate (Sommer et al., 1990), and reduced surface trafficking (Coleman et al., 2006). Changes in these splice forms are also thought to occur upon activity, affecting synaptic signalling (Penn et al., 2012). RNA editing also occurs at the 'R/G site' (Figure 1.2B1), where a codon switch from arginine (R) to glycine (G) changes channel gating kinetics (Lomeli et al., 1994), in an activity-dependent manner (Balik et al., 2013).

N-terminal domain

The AMPAR N-terminal domain comprises 50% of the receptor (Figure 1.2B1). The extracellular region of the AMPAR is a very flexible structure (Krieger et al., 2015), which may interact directly with proteins in the synaptic cleft (Biederer et al., 2017; Perez De Arce et al., 2015). The NTD, much like the CTD, is a very sequence diverse domain, raising the possibility of subunit-selective protein interactions (García-Nafría et al., 2016a). Until recently, very little was known about the functional role of this domain. The NTD is involved in AMPAR assembly (Ayalon et al., 2005), promoting formation of specific heteromeric or homomeric receptors (Rossmann et al., 2011). Additionally, the AMPAR NTD has also been implicated in surface trafficking (Möykkynen et al., 2014) and desensitisation (Bedoukian et al., 2006; Cais et al., 2014; Pasternack et al., 2002).

Recent reports suggest that the AMPAR NTD plays a subunit-specific role in maintaining excitatory synaptic transmission and plasticity (Díaz-Alonso et al., 2017; Jiang et al., 2021; Watson et al., 2020; 2017). In these reports, NTD-deleted (ΔNTD) receptors form functional channels, and even traffic to synaptic sites to a similar extent as wild-type (WT) AMPARs. However, the strength of the synaptic response is impaired with receptors lacking the NTD. Further evidence suggests that this is due to an anchoring of receptors at postsynaptic sites, potentially through NTD-synaptic cleft protein interactions (Watson et al., 2020). Given that the AMPAR NTD is exposed to the synaptic cleft, a protein-rich subcellular compartment (Perez De Arce et al., 2015), it is possible that it engages in protein interactions positioning receptors for effective signal transduction. Potential synaptic protein interactors (see 1.3.4) and mechanisms of sub-synaptic receptor positioning are discussed in further detail later in this chapter (see 1.4).

1.2.2 Kainate receptors

Kainate receptors (KARs) (subunits GluK1-5) have specific expression patterns across the brain, particularly in the hippocampal CA3 region and dentate gyrus (DG) (Wisden and Seeburg, 1993). KARs, like other iGluRs, form tetrameric receptors that respond to glutamate, but were orginially classified owing to their specific responsiveness to the compound kainate (Watkins and Evans, 1981). Similarly to AMPARs, KARs contain a Q/R editing site witin their M2 helix, affecting ion channel permeability and single channel conductance (Contractor et al., 2011). The physiological function of KARs is best described at hippocampal mossy fibre (MF) DG-CA3 synapses, where trains of electrical stimulation are required for their synaptic activation, suggestive of a postsynaptic localisation (Castillo et al., 1997; Vignes and Collingridge, 1997). Interestingly the temporal profile of the KAR EPSC at these synapses is surprisingly slow relative to AMPAR EPSCs recorded from the same synapse. This highlights the striking difference in synaptic function of different iGluRs, despite similar sequence homology and structural features (Figure 1.2A/C). KARs are thought to be additionally localised at presynaptic sites, where they contribute to the expression of MF long-term potentiation (LTP) (Lauri et al., 2001).

KARs, like AMPARs, function in concert with auxiliary proteins (see 1.3.3), namely neuropilin and tolloid-like proteins 1/2 (Neto1/2). Neto1/2 modulate KAR gating kinetics and synaptic trafficking (Copits et al., 2011; Sheng et al., 2015; Zhang et al., 2009) through CUB (complement C1r/C1s, Uegf, Bmp1)-domain interactions with the KAR NTD (Li et al., 2019; Sheng et al., 2017). In the context of the AMPAR, it is interesting to note that CUB-domain containing proteins, SOL-1/2 (Wang et al., 2012; Zheng et al., 2004; 2006) and neuropilin-2 (Wang et al., 2017) have been shown to directly interact with AMPAR subunits regulating their function. This suggests that CUB-domain containing proteins may serve as regulators of iGluR function.

The KAR NTD also engages in synaptic cleft protein interactions with complement C1q-like protein 2 (C1ql2) and 3 (C1ql3), forming a *trans*-synaptic complex with presynaptic neurexin (Matsuda et al., 2016; Straub et al., 2016). C1ql2/3 interactions are essential for maintaining hippocampal circuit function, with disruption of this complex resulting in the development of epileptiform activity (Matsuda et al., 2016). The role of this *trans*-synaptic tri-partite complex in synaptic anchoring of iGluRs is discussed in more detail later in this chapter (see 1.3.4).

1.2.3 Delta receptors

The delta receptor (subunits GluD1/2) is regarded as a subfamily of iGluRs based solely on its sequence homology (Figure 1.2A; Yamazaki et al., 1992). Historically, owing to the apparent lack of ionotropic activity (Schmid and Hollmann, 2008), functional studies were limited to studying the constitutively active lurcher mutant (Zuo et al., 1997), or by transplanting the LBD of AMPAR or KARs onto the delta receptor, permitting glutamate-gated currents (Orth et al., 2013; Schmid et al., 2009). The lurcher mutation, A654T, occurs in the pore-lining TMD and results in persistent ion flux in the absence of ligand, leading to excitotoxicity and neurodegeneration (Zuo et al., 1997). Recently however, specific pharmacological tools have uncovered an ionotropic role for wild-type GluD2, where metabotropic glutamate receptor 1 has been shown to trigger opening of the GluD2 channel (Lemoine et al., 2020).

GluD2 is expressed predominantly in purkinje cells of the cerebellum, where it functions through formation of a *trans* -synaptic complex with secreted cerebellin-1 (Cbln1) and presynaptic neurexin (Elegheert et al., 2016; Matsuda et al., 2010). Postsynaptic GluD2 mediates long-term depression (LTD) at cerebellar parallel fiber–Purkinje cell synapses through endocytosis of AMPARs (Elegheert et al., 2016; Kohda et al., 2013). Following complex formation and synaptic anchoring, GluD2 requires D-serine or glycine binding (Figure 1.2C; Naur et al., 2007), to exert its metabotropic postsynaptic signalling mechanisms. In contrast to GluD2 and other iGluRs, GluD1 is also expressed at inhibitory synapses in the cortex (Fossati et al., 2019). Here, GluD1 mediates synapse formation through *trans*-synaptic interactions with Cbln4, released from somatostatin-expressing interneurons, further emphasising the importance of synaptic protein interactions in shaping diverse iGluR physiology.

Cbln1/2/4 binding to GluD1/2 NTDs simultaneously induces synapse formation and metabotropic signalling mechanisms at different synapses (Elegheert et al., 2016; Fossati et al., 2019; Tao et al., 2018; Matsuda et al., 2010). As *trans*- synaptic protein complexes have been uncovered for both KARs and delta receptors, it remains possible that this type of interaction may also occur with the AMPAR NTD. However, to date no such *trans*-synaptic complex has been described (see 1.3.4).

1.2.4 NMDA receptors

NMDARs form heteromeric assemblies of two obligatory GluN1 subunits and two GluN2 (A-D) subunits. The biophysical properties of the NMDAR are remarkably distinct, relative to other iGluRs. The most stricking features are: voltage-dependent magnesium (Mg^{2+}) block, high Ca^{2+} permeability, co-agonist binding of glycine or D-serine, and remarkably slow channel gating kinetics relative to other iGluRs (Paoletti et al., 2013). NMDARs are widely expressed in the CNS existing in various heteromeric combinations.

Perhaps the most important biophysical feature of NMDARs, is their block by Mg^{2+} at resting membrane potentials (-70 mV). Crucially, Mg^{2+} block is relieved by membrane depolarisation (Mayer et al., 1984; Nowak et al., 1984). In the context of neuronal function, Mg^{2+} un-block is required for the expression of LTP (Bliss and Collingridge, 1993), observed as a long-lasting potentiation of the synaptic response (Bliss and Lømo, 1973). D-(-)-2-Amino-5-phosphonopentanoic acid (D-APV), synthesised by Jeffrey Watkins, is a selective NMDAR antagonist demonstrated to prevent the induction of LTP (Collingridge et al., 1983) and memory formation (Bannerman et al., 1995), highlighting the importance of the NMDAR in this physiological process.

Postsynaptic NMDARs are only activated when glutamate binds and membrane depolarisation relieves Mg^{2+} block, allowing the receptor to behave as a 'coincidence detector' for pre- and post-synaptic activation (Bliss and Collingridge, 1993). This discovery supports the ideas of Donald Hebb (1949), who proposed that 'neurons that fire together wire together'. This popular paraphrase is referred to as Hebb's law, and subsequently NMDAR-mediated LTP was termed 'Hebbian plasticity'. NMDARs therefore, play a vital role in this physiological process and have subsequently been the subject of intensive research to understand the molecular mechanism by which this occurs.

NMDAR have very long CTDs relative to other iGluRs, exposing these cytoplasmic elements to a wealth of intracellular signalling and scaffolding proteins. A number of NMDAR CTD-protein interactions have been identified, perhaps the most crucial of which, CaMKII, is required for the expression of LTP (Barria and Malinow, 2005). Analogously, the AMPAR CTD engages in a number of protein interactions, required for synaptic trafficking (see 1.3.2).

The NMDAR NTD also forms protein interactions modulating receptor function. NRAP-1 is a presynaptically-released protein that has auxiliary function through direct interactions with the NMDAR extracellular domain, potentially forming a *trans*-synaptic complex with an unknown presynaptic anchor (Lei et al., 2017). Another reported NMDAR NTD interactor Ephrin type-B receptor 2 (EphB2), interacts with the NMDAR NTD trapping receptors at the synapse for excitatory synaptic function (Dalva et al., 2000; Nolt et al., 2011; Washburn et al., 2020). Similarly, the AMPAR NTD appears to be required for successful trapping of receptors at postsynaptic sites (Watson et al., 2017), further emphasising the significance of iGluR NTD interactions (see 1.3.4) in sub-synaptic positioning (see 1.4).

1.3 AMPAR-protein interactors

1.3.1 ER biogenesis

AMPARs are assembled in the endoplasmic reticulum (ER) in a stepwise process, initiated by GluA monomers associating into dimers, and subsequently into dimer-of-dimers to build the tetrameric receptor. This process is supported by inter-subunit interactions (Greger et al., 2003; Greger and Esteban, 2007; Rossmann et al., 2011) and ER-residing proteins orchestrating the different steps of AMPAR biogenesis (Schwenk et al., 2019; Schwenk and Fakler, 2020). These protein interactions therefore, are crucial for the formation of tetrameric AMPARs for trafficking to synaptic sites.

AMPARs are translated in the ER and are first associated with widely expressed ER chaperones immunoglobulin binding protein (BiP) and calnexin (Figure 1.4A; Fukata et al., 2005; Rubio and Wenthold, 1999), thought to shield immature proteins from degradation (Hebert and Molinari, 2007). GluA monomers subsequently engage in protein interactions with α/ β- hydrolase domain-containing protein 6 (ABHD6) and porcupine O-acetyltransferase (PORCN) (Figure 1.4B; Schwenk et al., 2012), potentially stabilising AMPAR monomers and protecting them from ER-associated degredation (Schwenk and Fakler, 2020). These protein interactions accumulate GluA monomers, limiting surface trafficking of tetrameric AMPARs (Erlenhardt et al., 2016; Schwenk et al., 2019; Wei et al., 2020; 2016).

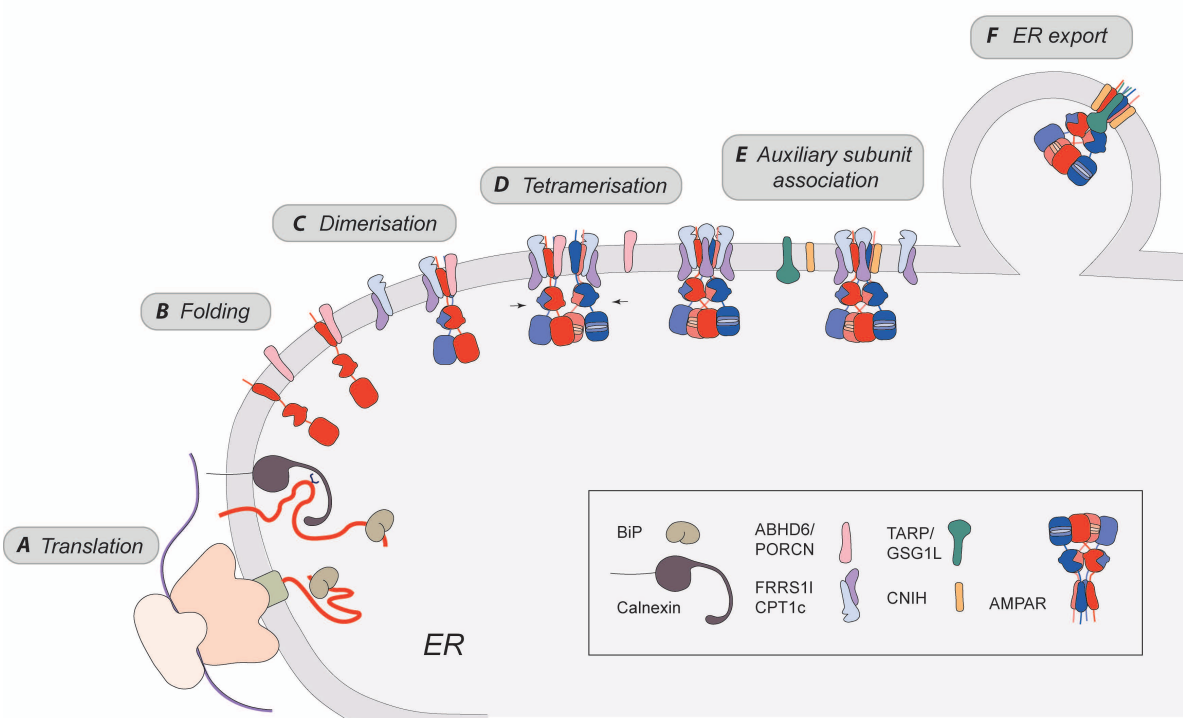

Figure 1.4 ***AMPAR-interacting proteins regulate assembly in the ER.*** *(**A**) AMPARs are first translated and inserted into the ER membrane. Widely expressed ER chaperones immunoglobulin binding protein (BiP) and calnexin are involved in the early stages of biogenesis, potentially shielding immature protein from degradation (Hebert and Molinari, 2007). (**B**) AMPARs are next folded into monomeric GluA subunits before association with ABHD6 and PORCN, trapping AMPAR subunits in a monomeric state and preventing them from ER-associated degradation (Schwenk et al., 2012; Schwenk and Fakler, 2020). (**C**) Next, dimerisation is promoted by association with FRRS1L and CPT1c (Brechet et al., 2017; Schwenk et al., 2019) and interactions at the level of the AMPAR TMD (Greger et al., 2003) and NTD (Rossmann et al., 2011). (**D**) The AMPAR tetramer is then formed as a dimer-of-dimers by the FRRS1L/CPT1c complex. (**E**) Finally, AMPARs associate with auxiliary proteins TARP/CNIH (Schwenk et al., 2019), before being (**F**) exported from the ER and trafficked to the cell surface. (schematic kindly provided by Dr Alexandra Pinggera).*

The next step in AMPAR biogenesis involves dimerisation of momomeric GluA subunits, through interactions at the level of the TMD (Greger et al., 2003) and NTD (Rossmann et al., 2011), assisted by additional ER-resident protein interactions. Ferric-chelate reductase 1-like (FRRS1L) and carnitine palmitoyl tranferase-1c (CPT1c) bind to AMPAR monomers dissociating ABHD6 from the complex (Figure 1.4C; Brechet et al., 2017; Schwenk et al., 2019; Schwenk and Fakler, 2020). Knockout of FRRS1L or CPT1c results in increased low molecular weight monomeric and dimeric AMPARs in the ER and decreased intracellular and surface AMPAR levels (Fadó et al., 2015; Gratacòs-Batlle et al., 2018; Schwenk et al., 2019). FRRS1L/CPT1c complexes therefore, promote the formation of dimers and subsequently tetramers (Figure 1.4D), regulating AMPAR surface trafficking and expression levels, ultimately shaping synaptic transmission and plasticity (Fadó et al., 2015; Gratacòs-Batlle et al., 2015; Han et al., 2017; Schwenk et al., 2019).

Finally, for tetrameric AMPARs to be trafficked to the cell surface, the FRRS1L/CPT1c complex is dissociated from the receptor by binding of auxiliary subunits, such as CNIH/TARP (Figure 1.4E/F; Schwenk et al., 2019). Auxiliary proteins modulate both channel function and trafficking properties of AMPARs (see 1.3.3). ER-resident protein interactors therefore, are crucial for the assembly of neuronal AMPARs and subsequent export to synaptic sites. Loss-of function mutations in FRRS1L results in a severe form of intellectual disability, highlighting the importance of ER AMPAR-protein interactors in brain function (Brechet et al., 2017).

1.3.2 Synaptic trafficking

Trafficking of AMPARs to the postsynaptic density (PSD), where receptors face presynaptic glutamate release, is a major determinant of synaptic strength. Following assembly in the ER, AMPARs are exported and trafficked to postsynaptic sites dependent on a number of protein interactions predominantly with the AMPAR CTD and TMD. Given that the AMPAR CTD varies considerably in amino acid sequence and length (Shepherd and Huganir, 2007), this domain has been the focus of intensive research to identify protein interactors that modulate synaptic trafficking in a sub-unit specific manner. CTD interactors have been shown to regulate intracellular transport (Figure 1.5A) and membrane fusion (Figure 1.5B/E) of AMPARs. Modulators of AMPAR trafficking are discussed below, detailing their binding sites on the CTD.

PDZ domain interactions

PDZ domains are common protein interaction modules named after their interaction with PSD-95/DLG/ZO-1 (PDZ) and play a key role in regulating AMPAR trafficking. GRIP/ABP are PDZ domain-containing proteins that interact specifically with the GluA2 CTD PDZ domain (*SVKI*; Figure 1.6B; Dong et al., 1997; Osten et al., 2000) and conventional kinesins, steering vesicles to dendrites (Setou et al., 2002). This suggests that GRIP/ABP serves as an adaptor to link AMPARs to kinesins and promote dendritic transport (Figure 1.5A). Functionally, GRIP1 interactions are required for synaptic plasticity and learning and memory (Tan et al., 2020). PICK1 interactions are also thought to form part of the GRIP/ABP complex, regulating AMPAR trafficking (Lu and Ziff, 2005; Perez et al., 2001). Interestingly, PICK1 is essential for NMDAR-mediated LTD, by removal of surface GluA2 receptors (Citri et al., 2010; Perez et al., 2001). Similarly, synapse-associated protein 97 (SAP97) interacts with CTD PDZ domains, but specifically with GluA1 (*ATGL*; Figure 1.6A; Wu et al., 2002). These interactions occur simultaneously with actin-based motor protein, myosin VI, likely playing a key role in trafficking of AMPARs to the plasma membrane (Osterweil et al., 2005; Wu et al., 2002). Functionally, SAP97 interactions are sufficient, but not individually necessary for AMPAR trafficking to synapses (Howard et al., 2010).

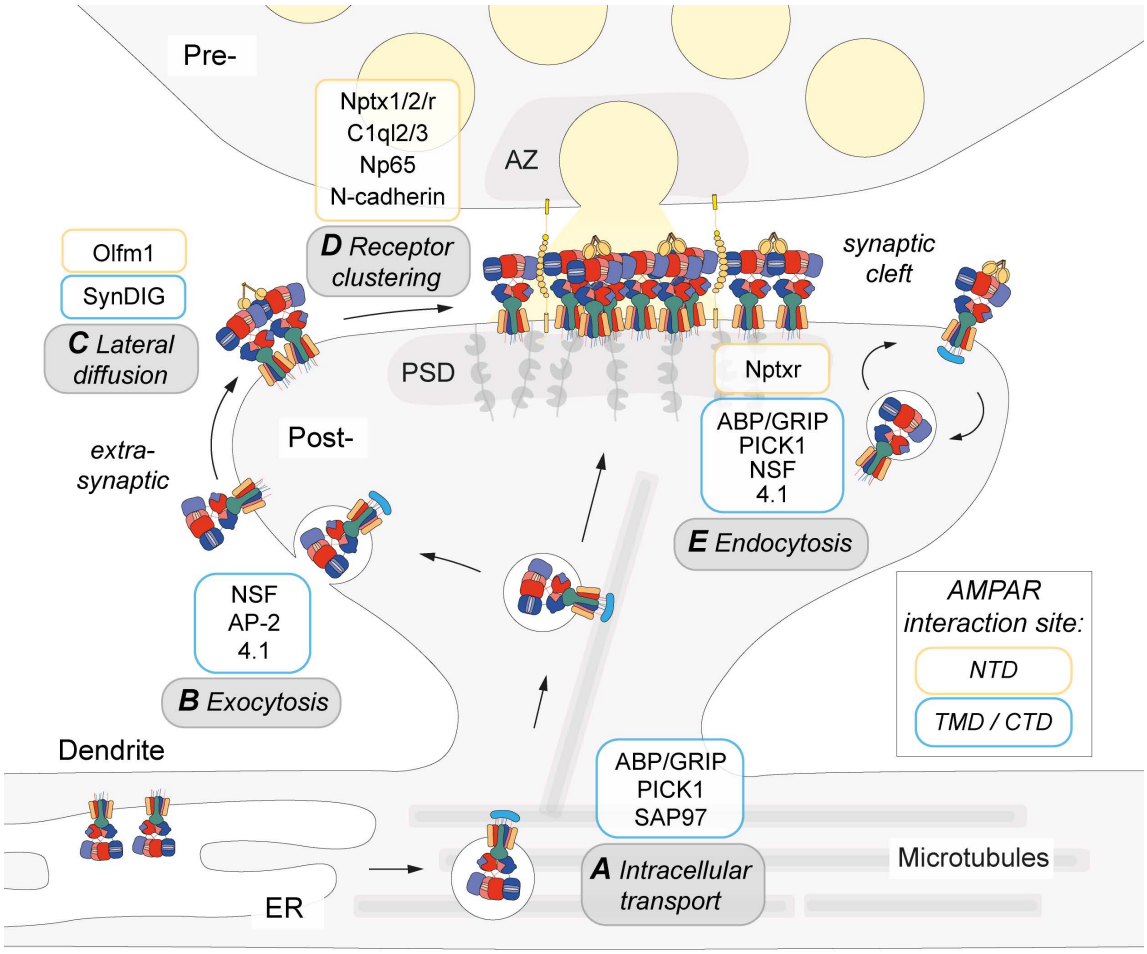

Figure 1.5 ***Trafficking of AMPARs to postsynaptic sites.*** *(**A**) AMPARs are subject to secretory trafficking along microtubules by intracellular transport (Hangen et al., 2018). (**B**) Receptors are then exocytosed into the surface of the plasma membrane by membrane fusion events (Araki et al., 2010). (**C**) AMPARs are subsequently inserted into the synapse by lateral diffusion (Penn et al., 2017). (**D**) Finally, receptors are accumulated and clustered at the postsynaptic density (PSD) (Opazo and Choquet, 2011), for efficacious synaptic transmission (Lisman and Raghavachari, 2006). (**E**) The number of synaptic receptors is then controlled by endocytic recycling of AMPARs within the dendritic spine. These molecular processes are tightly controlled by direct protein interactions with the AMPAR at the level of the CTD, TMD and NTD. Known protein interactors are indicated next to each trafficking event. Broadly, CTD/TMD protein interactors appear to regulate intracellular transport and membrane fusion events (blue; Jackson and Nicoll, 2011; Shepherd and Huganir, 2007), whereas NTD interactors modulate lateral diffusion and trapping (yellow; Pandya et al., 2018; Watson et al., 2017).*

non-PDZ domain interactions

CTD protein interactors also influence membrane fusion events (Figure 1.5B/E), regulating surface AMPAR content. *N*-ethylmaleimide–sensitive fusion protein (NSF) binds directly to the GluA2 CTD (Figure 1.6B; Osten et al., 1998), regulating membrane fusion and the strength of AMPAR-mediated synaptic transmission (Araki et al., 2010; Nishimune et al., 1998). Similarly, clathrin adaptor, AP-2, interacts with the GluA2 CTD at a site that overlaps with NSF binding and is required for NMDAR-mediated LTD (Figure 1.6B; Lee et al., 2002). Finally, actin adaptor, protein 4.1, associates with the AMPAR CTD stabilising GluA1 surface expression (Figure 1.6A; Shen et al., 2000), by inhibiting AMPAR endocytosis (Hayashi et al., 2005). Although the precise function of protein 4.1 during excitatory synaptic transmission and plasticity is unclear (Wozny et al., 2009).

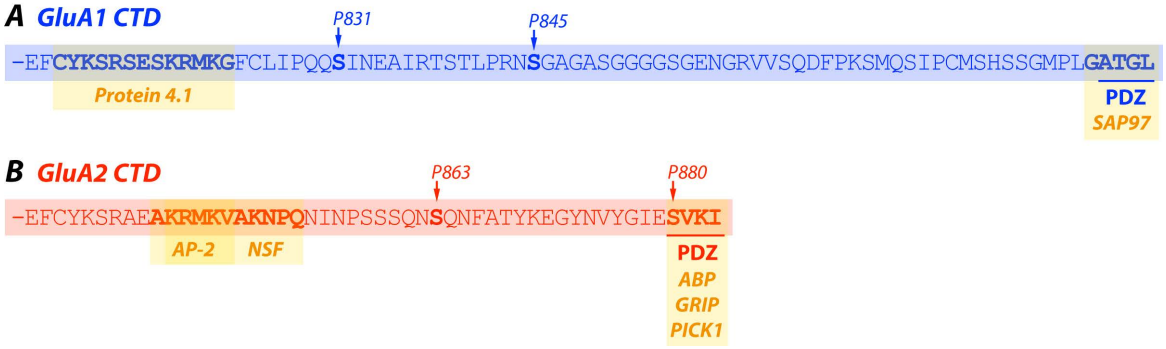

Figure 1.6 ***AMPAR C-terminal domain protein interaction sites.*** *AMPAR CTDs differ in their amino acid sequence and length, depicted by an amino acid sequence alignment of rat GluA1/2 CTDs. (**A**) GluA1 CTD interacts with protein 4.1 (Shen et al., 2000) and SAP97 (Osterweil et al., 2005; Wu et al., 2002). Phosphorylation sites P831 and P845 are highlighted (Diering et al., 2016). GluA1 PDZ binding motif 'ATGL'. (**B**) GluA2 CTD interacts with AP-2 (Lee et al., 2002), NSF (Osten et al., 1998) and ABP (Osten et al., 2000), GRIP (Dong et al., 1997) and PICK1 (Perez et al., 2001). Phosphorylation sites P863 and P880 are highlighted (Matsuda et al., 2000). GluA2 PDZ binding motif 'SVKI'. Figure adapted from Shepherd and Huganir, (2007).*

1.3.3 Auxiliary proteins

AMPAR gating kinetics are modulated by a number of different mechanisms, including RNA-editing (see 1.2.1), subunit composition (Coombs et al., 2012) and subunit placement (He et al., 2016; Herguedas et al., 2019). Furthermore, direct protein interactors with the AMPAR have the capability to modulate channel function, known as auxiliary proteins. Protein interactors are considered auxiliary proteins if, they selectively bind to iGluRs forming a stable complex at the cell surface, and modulate the functional characteristics and trafficking of the receptor (Jackson and Nicoll, 2011). Auxiliary proteins are expressed in different isoforms and have distinct expression patterns in the brain, enabling spatio-temporal control over AMPAR function. Our appreciation of how these proteins bind and modulate AMPAR gating kinetics, has been greatly improved by recent advances in structural biology (Herguedas et al., 2019; Nakagawa et al., 2019; Zhang et al., 2021).

TARPs

Transmembrane AMPAR regulatory proteins (TARPs) were the first AMPAR-interacting protein to be identified as an auxiliary subunit (Chen et al., 2000). The TARP family has 6 members including γ2 (stargazin), γ3 , γ4 , γ5 , γ7 and γ8 (Tomita et al., 2003), subdivided into type I and type II TARPs depending on their PDZ binding motif (Figure 1.7; Kato et al., 2008). TARPs bind to all AMPAR subunits, forming part of the native macromolecular complex (Tomita et al., 2003; Schwenk et al., 2012). TARP protein interactions occur predominantly at the level of the AMPAR TMD, and in some cases (TARP-γ8) their extracellular loop region interacts with the AMPAR LBD (Figure 1.7B1; Herguedas et al., 2019; Zhang et al., 2021). TARPs are capable of modulating not only receptor gating, but also trafficking to the cell-surface and positioning at synaptic sites (Chen et al., 2000; Sheng et al., 2018).

TARP interactions generally slow AMPAR gating kinetics, prolonging receptor activation (Figure 1.7C1; Tomita et al., 2005). The first TARP to be identified, stargazin (TARP-γ2), is predominantly expressed in the cerebellum and is essential for synaptic AMPAR function and motor coordination (Chen et al., 2000; Yamazaki et al., 2010). Crucially, TARP binding to PSD-95 through its C-terminal PDZ domain permits retention of AMPARs at postsynaptic sites for efficacious synaptic transmission to occur (Watson et al., 2020; Zheng et al., 2019).

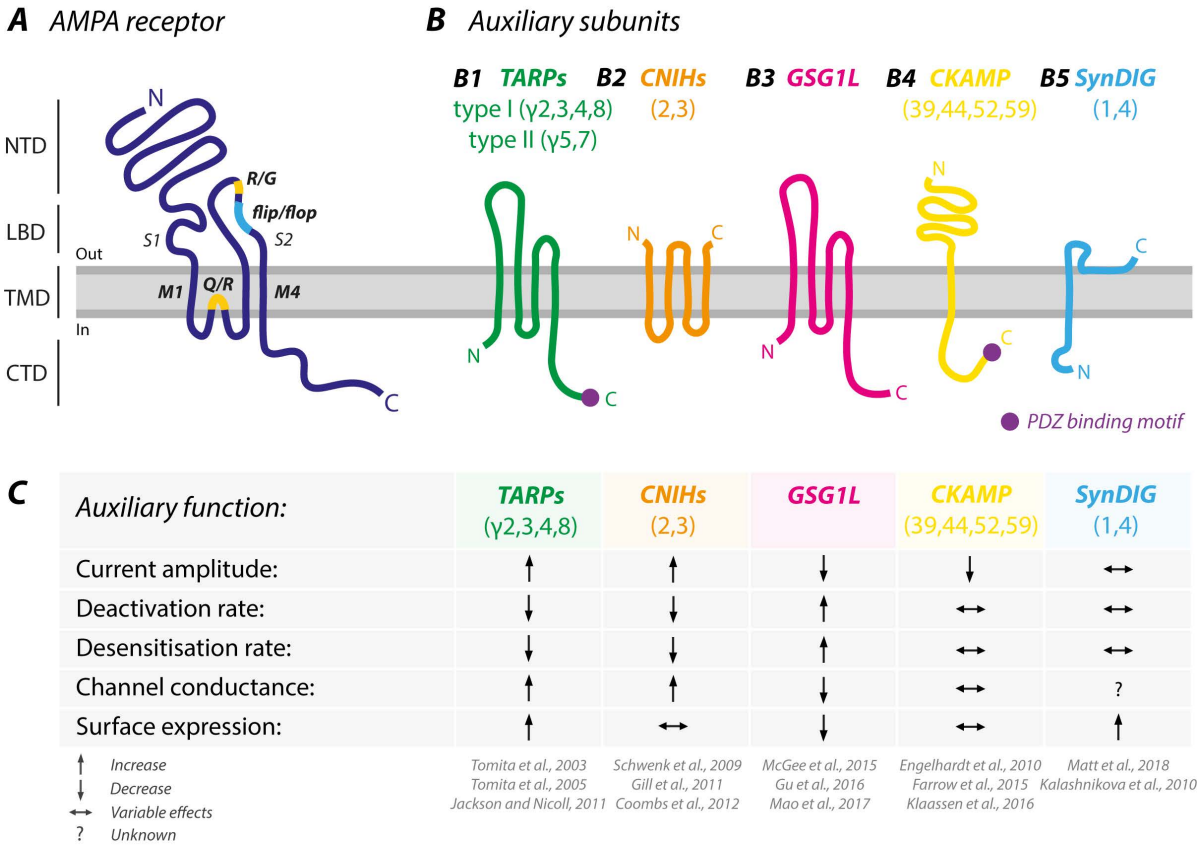

Figure 1.7 ***AMPAR and auxiliary subunit topology and function.*** *(**A**) AMPAR subunit polypeptide schematic (navy) depicting the four domain layers: N-terminal domain (NTD), ligand binding domain (LBD), transmembrane domain (TMD) and C-terminal domain (CTD), with the plasma membrane coloured in grey. (**B**) Known AMPAR auxiliary subunit polypeptide schematics. (**B1**) TARPs (green; topology based on Herguedas et al., 2019; Zhang et al., 2021), (**B2**) CNIHs (orange; topology based on Nakagawa et al., 2019; Zhang et al., 2021), (**B3**) GSG1L (pink; topology based on Twomey et al., 2017), (**B4**) CKAMP (yellow; predicted topology) and (**B5**) SynDIG (blue; predicted topology) all associate with the AMPAR modulating its function. Type I TARPs (γ2 ,3,4,8) and SynDIGs contain a canonical PDZ binding motif (purple circle). Type II TARPs (γ5 ,7) have an atypical PDZ binding motif. (**C**) Table of functional consequences of auxiliary protein modulation. (**C1**) TARPs (type I) positively modulate channel gating. CNIHs are positive regulators of AMPAR function. Conversely, GSG1L is a negative regulator of AMPAR function. CKAMP proteins have varied effects on channel gating depending on subtype. SynDIG auxiliary proteins have varied effects on deactivation and desensitisation kinetics depending on AMPAR subunit expression.*

TARP-γ8 is required for the maintenance of basal synaptic transmission and the expression of LTP at CA1 synapses (Rouach et al., 2008; Sheng et al., 2018). TARP-γ8 is expressed specifically in the hippocampus (Rouach et al., 2008; Yamasaki et al., 2016), making it an attractive target to alleviate diseases such as temporal lobe epilepsy, which is characterised by hippocampal hyperexcitability (Maher et al., 2017). Recently, a number of negative allosteric modulators have been produced with high specificity for TARP-γ8 -containing AMPARs (Kato et al., 2016; Maher et al., 2016; Savall et al., 2019). These ligands are capable of functionally uncoupling TARP-γ8 from the receptor by binding at the interface of TARP-AMPAR interactions in the TMD (Dohrke et al., 2020). Interestingly, modest changes in receptor kinetics recorded in recombinant systems translate to profound attenuation of the synaptic response and alleviation of seizure-like activity (Kato et al., 2016). This demonstrates the remarkable influence TARP auxiliary proteins have on brain-wide activity under physiological conditions and their clinical relevance.

CNIHs

Cornichon proteins 2/3 (CNIH2/3) are auxiliary proteins, that alter AMPAR function by profoundly slowing gating kinetics (Coombs et al., 2012; Gill et al., 2011; Schwenk et al., 2009). CNIHs are composed of 4 transmembrane domains and occupy up to 4 binding sites on the AMPAR TMD (Nakagawa et al., 2019; Zhang et al., 2021). CNIH2/3 are essential for AMPAR-mediated synaptic transmission in the hippocampus (Boudkkazi et al., 2014; Herring et al., 2013). The predominant auxiliary proteins present in the hippocampus are CNIH2 and TARP-γ8 (Schwenk et al., 2014). Interestingly, these proteins simultaneously dock at the 4 binding sites on the AMPAR TMD, further modulating gating kinetics (Zhang et al., 2021). It is likely that in neurons an assortment of auxiliary proteins occupy the 4 TMD binding sites, fine tuning AMPAR function.

GSG1L

GSG1L was identified as an AMPAR-interacting protein by affinity purification mass spectrometry (AP-MS) (Schwenk et al., 2012; Shanks et al., 2012). GSG1L is structurally related to TARP auxiliary proteins, as claudin homologs, although they lack a PDZ binding motif (Figure 1.7B3; Twomey et al., 2017). While most auxiliary proteins positively modulate AMPAR gating and synaptic trafficking (Jackson and Nicoll, 2011), GSG1L has a strong negative modulatory effect on AMPAR function (Figure 1.7C; Gu et al., 2016; Mao et al., 2017; McGee et al., 2015).

In the context of circuit function, GSG1L is crucial for suppressing short-term facilitation, dampening neuronal excitability at cortical synapses (Kamalova et al., 2020).

CKAMPs

Cysteine-knot AMPAR modulatory proteins (CKAMP44/39/52/59; also known as Shisa9/8/6/7; Figure 1.7B4) were first identified as auxiliary proteins that modulate AMPAR desensitisation and attenuate short-term plasticity at hippocampal synapses (von Engelhardt et al., 2010). CKAMP44/39/52 are single transmembrane proteins that contain a PDZ type II motif (Farrow et al., 2015), permitting protein interactions with PSD-95 and trapping receptors at postsynaptic sites (Khodosevich et al., 2014; Klaassen et al., 2016). CKAMP proteins therefore, modulate AMPAR trafficking, gating and synaptic localisation, thus are defined as auxiliary proteins. CKAMP59 (Shisa7) has also been suggested to act as an AMPAR auxiliary protein (Schmitz et al., 2017), although recent data indicates that this protein also modulates $GABA_A$ receptor function (Han et al., 2019).

SynDIGs

SynDIG (synapse differentiation-induced gene) proteins are repeatedly identified as constituents of the AMPAR proteome by AP-MS (Schwenk et al., 2012; 2014; Shanks et al., 2012; von Engelhardt et al., 2010; Figure 1.7B5). SynDIG1 associates with the AMPAR reducing excitatory synapse density in an activity-dependent manner (Kalashnikova et al., 2010). Additionally, SynDIG4 modulates AMPAR localisation by trapping AMPARs at extra-synaptic sites (Matt et al., 2018). Furthermore, Matt et al., (2018) found that SynDIG4 modulates channel gating in a subunit-specific manner, suggestive of auxiliary function (Figure 1.7C). SynDIG1 however, does not appear to modulate AMPAR biophysical properties (Lovero et al., 2013). Further characterisation is required to conclusively determine the role of SynDIG as an AMPAR auxiliary protein.

Another notable iGluR auxiliary protein is SOL-1, a C1r/C1s-Uegf-BMP (CUB)-domain containing protein that regulates channel gating of GLR-1 glutamate receptors in *C. elegans.* (Zheng et al., 2004; 2006). Interestingly, KAR auxiliary proteins Neto1/2 also modulate receptor gating through their CUB-domains (Li et al., 2019; see 1.2.2). It is possible that other AMPAR auxiliary proteins exist, but are yet to be identified using current proteomic methods.

1.3.4 Synaptic interactions

Following successful incorporation into synaptic sites, AMPARs are positioned within the PSD and contribute to excitatory synaptic transmission. AMPARs are inserted into the synapse by exocytosis (Figure 1.5B) and lateral diffusion (Figure 1.5C), and can be retained through protein interactions (Figure 1.5D; Opazo and Choquet, 2011; Penn et al., 2017), for more efficacious synaptic transmission (Lisman and Raghavachari, 2006). Proteins in the synaptic cleft form *trans*- synaptic interactions, regulating various aspects of synaptic function, including synapse formation, maintenance and elimination (Südhof, 2017; Yuzaki, 2018). A number of these *trans*- synaptic interactions influence iGluR synaptic function through direct or indirect mechanisms (Figure 1.8).

C1q-like proteins

Complement C1q-like protein 2 (C1ql2) and 3 (C1ql3) both directly interact with the KAR NTD and presynaptic neurexin forming a *trans*- synaptic complex, capable of regulating hippocampal circuit function (Figure 1.8A1; Matsuda et al., 2016; Straub et al., 2016). Secreted C1ql2/3 proteins accumulate KARs at MF DG-CA3 synapses through its NTD, for effective synaptic function. Interestingly, C1ql2/3 also directly interact with the GluA1 NTD (Matsuda et al., 2016). Given the requirement of the GluA1 NTD for maintenance of long-term potentiation at CA1 synapses (Díaz-Alonso et al., 2017; Jiang et al., 2021; Watson et al., 2017) and activity-dependent release of C1ql3 in the hippocampus (Martinelli et al., 2016), it would be interesting to explore the physiology of this protein interaction further. This *trans*- synaptic interaction highlights the importance of iGluR NTDs in shaping neuronal function.

Cerebellins

Cerebellins (Cblns) are secreted glycoproteins that bind to presynaptic neurexin and postsynaptic delta receptors (Figure 1.8A2; Südhof, 2017; Yuzaki, 2018). Cbln1 interacts directly with the NTD of GluD2, forming a *trans*- synaptic complex with presynaptic neurexin (Elegheert et al., 2016; Matsuda et al., 2010). This tri-partite complex bears a remarkable similarity to that of C1ql2/3 *trans*- synaptic interactions (Figure 1.8A1). Functionally, Cbln1 interactions are required for the formation and maintenance of synapses and LTD at purkinje cell synapses in the cerebellum, and ultimately motor coordination (Elegheert et al., 2016; Hirai et al., 2005; Matsuda et al., 2010).

More recently, the role of Cblns has also been extended to the hippocampus (Tao et al., 2018) and cerebral cortex (Fossati et al., 2019). Cbln2 forms a *trans*-synaptic complex with postsynaptic GluD1 and presynaptic neurexin to regulate hippocampal synapse formation and maintenance (Tao et al., 2018). Interestingly, Cbln4 interactions occur at inhibitory synapses in the cerebral cortex, where its secretion is regulated by somatostatin-expressing inhibitory interneurons, eliciting metabotropic cascades in the postsynaptic neuron (Fossati et al., 2019). This demonstrates the diversity in function achieved by *trans*- synaptic signalling with the Cbln protein family.

Neuronal pentraxins

Neuronal pentraxins (Nptx) are a family of secreted (Nptx1 and Nptx2) and type-II transmembrane-bound (Nptxr) proteins that bind to postsynaptic AMPAR NTDs through their pentraxin (PTX) domain (Figure 1.8A3; Lee et al., 2017; O'Brien et al., 1999; Sia et al., 2007; Xu et al., 2003). Nptxs are predominantly axonally-released from presynaptic sites (O'Brien et al., 2002; 1999; Reti et al., 2008), induced by glypican-4 (Gpc4) interactions with presynaptic RPTPδ (Farhy-Tselnicker et al., 2017). Physiologically, Nptx2 (also known as neuronal activity-regulated pentraxin; NARP) recruits GluA4-containing AMPARs to increase synaptic strength onto aspiny parvalbumin-positive interneurons (PV-INs) in the hippocampus (Chang et al., 2010; Gu et al., 2013; Pelkey et al., 2015).

Nptxs also localise to dendritic spines in the hippocampus (O'Brien et al., 1999; Xu et al., 2003; Cho et al., 2008), where their synaptic function is not as well understood. Nptxr is thought to regulate mGluR1/5-dependent LTD through binding to postsynaptic AMPARs, capturing them for endocytosis (Cho et al., 2008), and Nptx1 may act as a negative regulator of excitatory synaptic transmission (Figueiro-Silva et al., 2015). However, further investigation is required to deduce the role of Nptxs in shaping synaptic AMPAR function through NTD interactions. Moreover, it is unknown if Nptxs also bind to presynaptic proteins forming a *trans*-synaptic complex.

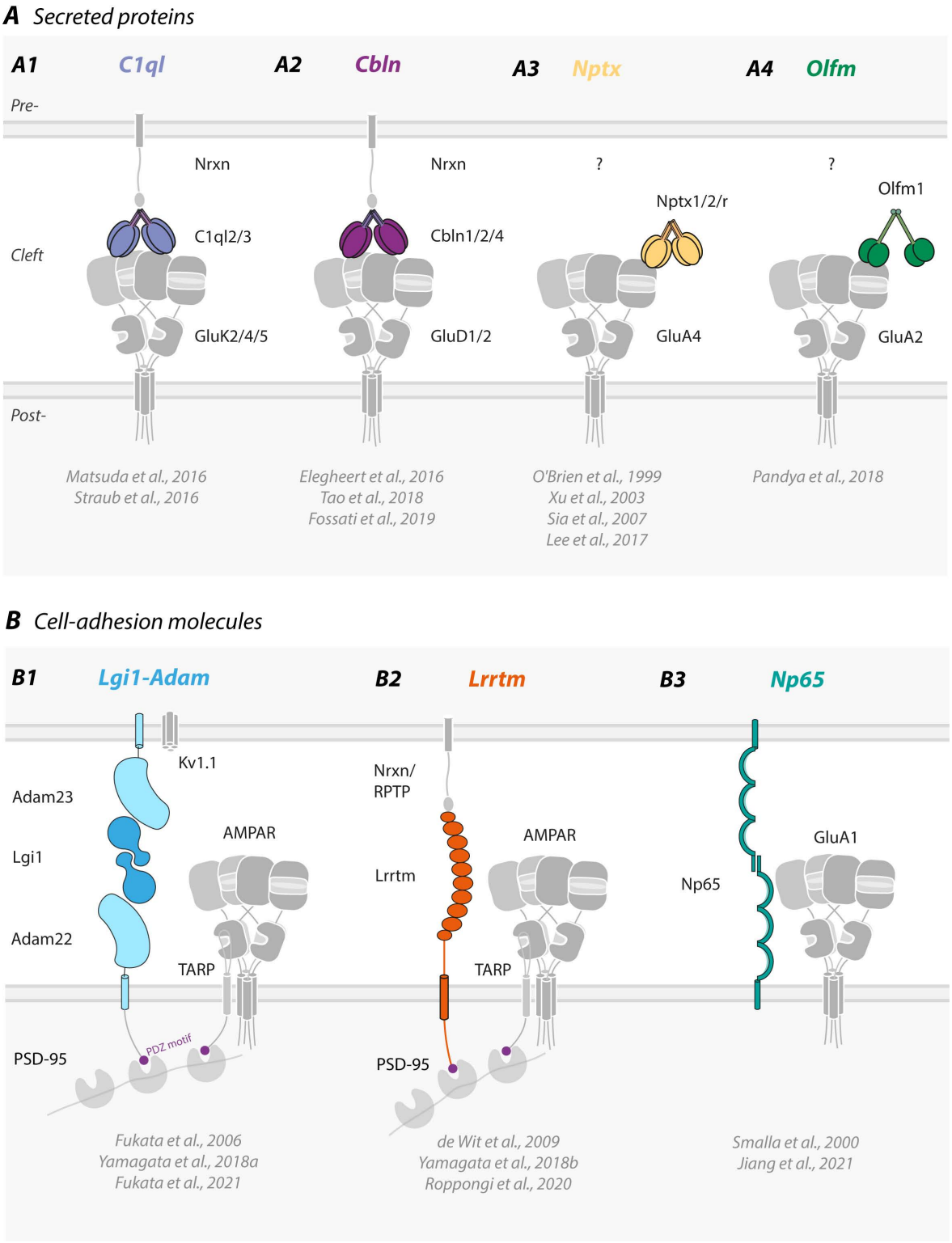

Figure 1.8 *Known trans-synaptic protein complexes.*

Figure 1.8 ***Known trans-synaptic protein complexes.*** *(**A**) Secreted proteins participating in trans-synaptic complexes. (**A1**) Complement C1q-like protein 2/3 (C1ql2/3) interact with the NTD of postsynaptic KAR subunits GluK2/4/5 and presynaptic neurexin (Nrxn), forming a trans-synaptic complex, crucial for regulation of hippocampal circuit function (Straub et al., 2016; Matsuda et al., 2016). (**A2**) Cerebellin-1/2/4 (Cbln1/2/4) bind to postsynaptic delta receptor subunits GluD1/2 and presynaptic neurexin, forming a transsynaptic complex, critical for synapse formation and maintenance (Elegheert et al., 2016; Fossati et al., 2019; Matsuda et al., 2010; Tao et al., 2018). (**A3**) Neuronal pentraxin-1/2/receptor (Nptx1/2/r) interact with the NTD of GluA4 subunits promoting postsynaptic receptor clustering at excitatory and inhibitory synapses (Lee et al., 2017; O'Brien et al., 1999; Sia et al., 2007; Xu et al., 2003). (**A4**) Olfactomedin-1 (Olfm1) binds to the NTD of GluA2-containing AMPARs regulating lateral diffusion of AMPARs into hippocampal synapses (Pandya et al., 2018). (**B**) Cell-adhesion molecules engaging in trans-synaptic complexes. (**B1**) Leucine-rich glioma-inactivated protein (Lgi1) forms a trans-synaptic complex with presynaptic disintegrin and metalloproteinase domain-containing protein 23 (Adam23) associated with Kv1.1, and postsynaptic Adam22, associated with TARP-containing AMPARs through PSD-95 interactions (Fukata et al., 2006; 2021; Yamagata et al., 2018a). (**B2**) Leucine-rich repeat transmembrane proteins (Lrrtms) bind to presynaptic Nrxn or receptor-type protein tyrosine phosphatases (RPTPs) in a trans-synaptic complex (de Wit et al., 2009; Roppongi et al., 2020; Yamagata et al., 2018b). (**B3**) Neuroplastin-65 (Np65) is an Ig superfamily glycoprotein that engages in homophilic trans-synaptic interactions required for long-term potentiation at CA1 synapses through direct GluA1 NTD interactions (Jiang et al., 2021; Smalla et al., 2000).*

Olfactomedin

Olfactomedin domain-containing proteins 1-4 (Olfm1-4; also known as Noelin or Pancortin) are secreted glycoproteins identified repeatedly by AP-MS as part of the AMPAR proteome (Brechet et al., 2017; Schwenk et al., 2014; 2012; Shanks et al., 2012; von Engelhardt et al., 2010). Proximity-labelling proteomics has confirmed Olfm1 localisation at synapses (Cijsouw et al., 2018; Loh et al., 2016), where direct interactions with the AMPAR NTD have been postulated (Figure 1.8A4; Pandya et al., 2018). A reduction in the synaptic AMPAR content is observed with reduced expression of Olfm1 (Nakaya et al., 2017), Olfm2 (Sultana et al., 2014) and Olfm3 (Tang et al., 2020). Olfm1 is thought to limit receptor mobility, trapping AMPARs at the synapse (Pandya et al., 2018). Functionally, Olfm3 has been shown to interact directly with GluA1/2 AMPAR subunits enhancing excitatory synaptic transmission at CA1 synapses (Tang et al., 2020). Further studies are required to first to resolve the molecular features of direct interactions between Olfm and the AMPAR and if *trans*- synaptic interactions take place. Secondly, the physiological importance of this protein interaction at excitatory synapses should be investigated in further detail.

Leucine-rich glioma-inactivated protein 1

Leucine-rich glioma-inactivated protein 1 (Lgi1) is a secreted protein that forms a *trans*-synaptic complex with presynaptic disintegrin and metalloproteinase domain-containing protein 23 (Adam23), which interacts with presynaptic voltage-gated potassium channels Kv1.1 (Figure 1.8B1; Boillot et al., 2016; Schulte et al., 2006; Seagar et al., 2017), and postsynaptic Adam22, which regulates postsynaptic AMPARs through interactions with PSD-95 (Figure 1.8B1; Fukata et al., 2006; Lovero et al., 2015). Lgi1 forms tight interactions with the metalloprotease-like domain of Adam22/23 and the Adam22-Lgi1-Adam23 complex is formed with a stoichiometry of 1:2:1 (Figure 1.8B1; Yamagata et al., 2018a).

Patients with epilepsy possess mutations in Adam22 (Chabrol et al., 2007), or produce auto-antibodies to Lgi1 (Irani et al., 2010), this ruptures the *trans*-synaptic complex and decreases the synaptic expression of both presynaptic Kv1.1 and postsynaptic AMPARs (Ohkawa et al., 2013; Petit-Pedrol et al., 2018). Functionally, this results in defective AMPAR-mediated synaptic transmission (Fukata et al., 2006; 2010; Lovero et al., 2015), increased presynaptic glutamate release (Boillot et al., 2016; Petit-Pedrol et al., 2018), and increased neuronal excitability (Seagar et al., 2017). Ultimately leading to the

development of lethal epileptic seizures *in vivo* (Chabrol et al., 2010; Fukata et al., 2010). Recent data suggests that this complex is responsible for the arrangement of postsynaptic AMPARs on a nanometer scale, ensuring receptors are positioned in direct apposition to presynaptic release sites (Fukata et al., 2021). This highlights the importance of *trans*-synaptic protein interactions in arranging pre- and post-synaptic proteins to achieve effective AMPAR-mediated synaptic transmission.

Leucine-rich repeat transmembrane proteins

Leucine-rich repeat transmembrane proteins (Lrrtms) are postsynaptic cell-adhesion molecules (CAMs) that promote the formation and maintenance of excitatory synaptic connections (Lauren et al., 2003; Lindoff et al., 2009). Lrrtms bind to presynaptic neurexin and receptor-type protein tyrosine phosphatases (de Wit et al., 2013; Ko et al., 2009; 2015; Roppongi et al., 2020; Siddiqui et al., 2013), through their N-terminal leucine-rich repeat region (Yamagata et al., 2018b), and to PSD-95 through their type I PDZ-binding motif (Figure 1.8B2; de Wit et al., 2009). Interactions between Lrrtms and AMPARs have also been reported for Lrrtm2 (de Wit et al., 2009), Lrrtm3 (Shanks et al., 2012) and Lrrtm4 (Schwenk et al., 2012). Although the precise nature of these interactions remain unresolved. Lrrtm1/2 are critical for the maintenance of basal synaptic transmission and long-term potentiation at CA1 synapses (Bhouri et al., 2018; Soler-Llavina et al., 2011; 2013). Whereas Lrrtm3/4 are required for excitatory synaptic function on DG cells (Siddiqui et al., 2013; Um et al., 2016). Lrrtm likely tunes AMPAR-mediated synaptic function via indirect mechanisms, by maintaining synaptic stability through interactions with presynaptic proteins and retaining AMPARs at the postsynapse through interactions with PSD-95 (Figure 1.8B2).

N-cadherin

Synaptic CAM, N-Cadherin, has been shown to interact directly with the GluA2 NTD (Saglietti et al., 2007). This interaction is thought to potently induce synapse formation (Passafaro et al., 2003), critical for the maintenance of mGluR-mediated LTD (Zhou et al., 2011). However, other reports were unable to reproduce the synaptogenic effect of the GluA2 NTD (Biou et al., 2008; Lu et al., 2009; Watson et al., 2017). Therefore, the reported direct interaction and synaptogenic function of the GluA2 NTD-N-Cadherin complex (Saglietti et al., 2007), requires further exploration.

Neuroplastin-65

Neuroplastin-65 (Np65) is a synaptogenic CAM part of the immunoglobulin superfamily, thought to directly interact with the GluA1 NTD (Figure 1.8B3; Jiang et al., 2021; Vemula et al., 2020). Np65 is essential for the expression of long-term potentiation (LTP) at CA1 synapses (Smalla et al., 2000). Recently, this function has been attributed to direct interactions with the GluA1 NTD (Jiang et al., 2021), although the precise details of this protein interaction remain unknown.

Trans- synaptic protein interactions are crucial for the maintenance of synaptic AMPAR function. A number of iGluR NTD interactors are emerging in the literature (Figure 1.8A). It is likely that other protein interactions remain unresolved, given the difficulty in capturing these weak and transient interactions. In this study, a novel proteomic method is developed for the AMPAR, to detect direct protein interactions with the NTD. Next, the physiology of AMPAR NTD interactions is determined using patch-clamp electrophysiology.

1.4 AMPAR sub-synaptic positioning

AMPARs have a relatively low-affinity for glutamate (0.1-1 mM; Traynelis et al., 2010) and are not saturated by vesicular glutamate release during transmission. Therefore, their postsynaptic localisation must be precisely controlled to achieve efficacious synaptic transmission (Franks et al., 2003; Raghavachari and Lisman, 2004). Quantal glutamate release activates a 'hotspot' of ~10 synaptic glutamate receptors (Figure 1.9; Lisman et al., 2017; Raghavachari and Lisman, 2004). Indeed, not all synaptic AMPARs response to every glutamate release event (Liu et al., 1999; McAllister and Stevens, 2000). Therefore, sub-synaptic clustering of receptors on a nanometer scale profoundly enhances the size of the postsynaptic response (Savtchenko and Rusakov, 2014).

AMPARs are inserted into the synapse via lateral diffusion (Figure 1.9A; Opazo and Choquet, 2011; Penn et al., 2017), and are thought to arrange in to nanocolumns (Figure 1.9B; Biederer et al., 2017; Tang et al., 2016), facilitating efficient excitatory synaptic transmission (Diering and Huganir, 2018; Lisman and Raghavachari, 2006). The PDZ binding motifs on the AMPAR or auxiliary protein CTDs likely regulate AMPAR organisation into these slots (Hayashi et al., 2000; Sheng et al., 2018), however recent evidence also supports a role for the AMPAR NTD (Díaz-Alonso et al., 2017; Jiang et al., 2021; Watson et al., 2020; 2017). It is possible that the AMPAR NTD may be guided into synaptic 'slots' by synaptic cleft protein interactions (Watson et al., 2020). The synaptic cleft is a protein-rich environment made up of a number of *trans*-synaptic complexes composed of CAMs, secreted proteins and even iGluRs NTDs (Chamma et al., 2016; Elegheert et al., 2016; Fossati et al., 2019; Fukata et al., 2021). Currently however, no *trans*-synaptic complexes have been described involving protein interactions with the AMPAR NTD.

This study aims to identify previously undetermined synaptic AMPAR NTD interactors and characterise their function using electrophysiology. The AMPAR NTD is required for efficacious synaptic transmission and plasticity, however potential protein interactors responsible for this functional effect remain unresolved. Ultimately, this study aims to further our understanding of the molecular mechanisms of information transfer and storage at neuronal connections in the mammalian brain.

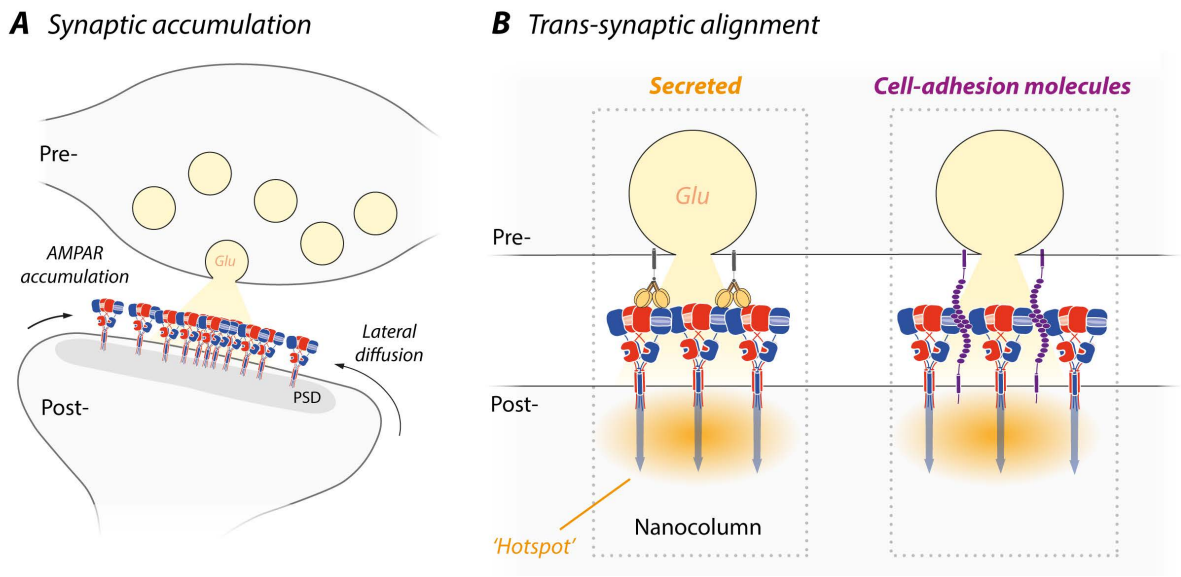

Figure 1.9 ***Trans-synaptic alignment of postsynaptic AMPARs and presynaptic glutamate release.*** *(**A**) AMPARs accumulate at postsynaptic sites where they respond to presynaptically released glutamate (Glu). Arrows indicate insertion of receptors via lateral diffusion. (**B**) Hypothetical mechanisms of AMPAR trans-synaptic alignment. 'Hotspots' of glutamate release are thought to activate only a small proportion of synaptic AMPARs, requiring sub-synaptic receptor positioning for efficacious synaptic transmission (Lisman et al., 2017; Raghavachari and Lisman, 2006). Secreted proteins (orange) and cell-adhesion molecules (purple) may position the AMPAR within 'nanocolumns' (Tang et al., 2016) or 'slots' (Diering and Huganir, 2018) for faithful signal transduction. Synaptic protein interactions may occur through with AMPAR NTD, anchoring the receptor for efficient signal transduction (Watson et al., 2020; 2017).*

Chapter 2

Methods

Statistics and data analysis

Data are presented as mean ± SEM. Mass spectrometry data are presented as mean fold enrichment (Log_2) and *P* values ($-Log_{10}$) from three independent experiments. Statistical analyses were carried out using Prism 8 software as paired or unpaired two-tailed students t-test or using a one-way ANOVA as stated. Statistical significance was considered if $*P < 0.05$, $**P < 0.01$, or $***P < 0.001$.

2.1 Molecular biology

Molecular cloning was performed using either *In Vivo* Assembly (IVA) cloning (García-Nafría et al., 2016b; Watson et al., 2019), Gibson Assembly (Gibson et al., 2009; Gibson et al., 2010) or restriction cloning. BirA* tags were subcloned from the following plasmids: BioID2 (Kim et al., 2016; Addgene: 74223), MiniTurbo (Branon et al., 2018; Addgene: 107174) and TurboID (Branon et al., 2018; Addgene: 107173). Rat sequence DNA was used for AMPAR subunits GluA1 and GluA2 (flip and R/G edited) with GluA2 NTD-deletion (ΔNTD) of amino acid residues 1–377 and GluA1 ΔNTD deletion of amino acid residues 1–373 as reported previously (Watson et al., 2017). GluA2 R586Q mutation was used throughout (GluA2Q) to permit block by intracellular polyamines and subsequent rectification of current-voltage relationship (Bowie and Mayer, 1995; Kamboj et al., 1995; Koh et al., 1995). GFP-P2A-AMPAR vectors were constructed by fusing GFP with a downstream P2A sequence (*GSGATNFSLLKQAGDVEENPGP*) to the native signal sequence of AMPAR subunits. P2A self-cleavage leaves a proline residue on the native signal sequence (Liu et al., 2017), which is subsequently cleaved in the ER to reveal the mature protein. Backbones of all pAAV transfer plasmids were based on pAAV-CW3SL-EGFP (Addgene, 61463) with the CaMKIIα promoter and a shortened woodchuck hepatitis post transcriptional regulatory element to maximise construct expression (Choi et al., 2014). Each construct was PCR amplified and inserted into the pAAV vector between two unique restriction sites, NheI and XhoI. All AAVs were produced by triple transfection of the transfer plasmid with pAAV-Rep/Cap stereotype 2/9, to provide AAV replication and capsid genes, and pAAV-pHGTI-adeno1, to provide AAV

helper function. pAAV transfer plasmids were screened for ITR recombination by SmaI digestion to ensure ITR deletion did not occur. For the cell-based binding assay candidate interactors were cloned into the pHL-avitag3 vector using AgeI and KpnI unique restriction sites and an AviTag was positioned on the N- or C-terminus (Aricescu et al., 2006; Addgene, 99847). All constructs were verified by restriction enzyme digestion and Sanger DNA sequencing.

2.2 Neuronal culture preparation

Animal use

All procedures were carried out under PPL P81248620 in accordance with UK Home Office regulations. Experiments conducted in the UK are licensed under the UK Animals (Scientific Procedures) Act, 1986 following local ethical approval (MRC AWERB, University of Cambridge). C57/BL6 mice were used throughout from a mixture of male and female pups.

Dissociated hippocampal cultures

Dissociated hippocampal cultures were prepared as described previously (Beaudoin et al., 2012). Briefly, the hippocampus was isolated from P0-1 C57Bl/6 mice in ice-cold dissection medium containing the following: 97.5% Hank's Balanced Salt Solution (HBSS; Ca^{2+} and Mg^{2+}-free, Gibco, #14175095), 1 mM Sodium Pyruvate (Gibco, #11360070), 0.1% glucose and 10 mM HEPES (Gibco, #11560496). Hippocampal cells were then dissociated using 0.25% trypsin (Gibco, #15090046) and plated on poly-L-lysine coated 12 mm glass coverslips (Corning, 354085) in plating medium containing: 86.55% Minimum Essential Medium (MEM; Gibco, 11550556), 10% heat-inactivated fetal bovine serum (Gibco, #10091148), 0.45% glucose, 1 mM Sodium Pyruvate (Gibco, #11360070) and 2 mM GlutaMAX (Gibco, #35050061). Cultures were then maintained in equilibrated dissociated culture medium (37°C/5% CO_2) containing: 96% Neurobasal medium (Gibco, #21103049), 2% B-27 Plus Supplement (Gibco, #A3582801) and 2 mM GlutaMAX (Gibco, #35050061). Cultures were half-fed with fresh dissociated medium every 5-7 days. Dissociated cultures were transduced with AAV at day *in vitro* (DIV) 7 and used for immunofluorescence experiments at day post infection (DPI) 7. Dissociated hippocampal neurons were transfected with 2 µl lipofectamine 2000 (Thermo Scientific; #11668019) and 0.5 µg DNA per well. Cultures were incubated with lipofectamine-DNA mixture for 20 mins before half-feeding with fresh medium.

Organotypic hippocampal slices

Organotypic slice cultures were prepared as described previously (Stoppini et al., 1991). Briefly, the hippocampus was isolated from P6-8 C57Bl/6 mice in high-sucrose Gey's Balanced Salt Solution (GBSS) containing (in mM): 175 Sucrose, 50 NaCl, 2.5 KCl, 0.85 NaH_2PO_4, 0.66 KH_2PO_4, 2.7 $NaHCO_3$, 0.28 $MgSO_4$, 2 $MgCl_2$, 0.5 $CaCl_2$ and 25 glucose at pH 7.3. Hippocampi were cut into 300 µm slices using a McIlwain Tissue Chopper and cultured on Millicell Cell Culture Inserts (Merk-Millipore, PICM0RG50) in equilibrated organotypic slice culture medium (37°C/ 5% CO_2). Organotypic medium contained the following: 78.5% Minimum Essential Medium (Gibco, 21090), 15% Heat Inactivated Horse Serum (Gibco, 26050), 2% B27 Plus Supplement (Gibco, A3582801), 2.5% 1 M HEPES, 1.5% 0.2 M GlutaMax supplement, 0.5% 0.05 M ascorbic acid, 1 mM $CaCl_2$ and 1 mM $MgSO_4$. Organotypic medium was refreshed every 3.5 days. Slices were either transfected at DIV5 by SCE with electrophysiological recordings performed at day post-transection (DPT) 4, or transduced by AAV at DIV3 with electrophysiological recordings performed at DPI 5-7 for microinjected slices or DPI 4-13 for globally infected slices.

Single-cell electroporation

Organotypic slices were transfected using single-cell electroporation (SCE) based on the method described by Rathenberg et al., (2003) and Wiegert et al., (2017b). Endotoxin-free plasmid DNA in TE buffer (pH 7.4) was diluted to 33 ng/µl in a potassium-based intracellular solution containing (in mM): 135 CH_3SO_3H, 135 KOH, 4 NaCl, 2 $MgCl_2$, 10 HEPES, 2 Na_2-ATP, 0.3 Na-GTP, 0.06 EGTA and 0.01 $CaCl_2$ at pH 7.3. To visualise successful electroporation, 20 µM Alexa Fluor-594 (Invitrogen, A33082) was added to the solution and to visualise successful expression, pN1-EGFP (Clontech, 6085-1) was included at a ratio of 1:7 (EGFP:AMPAR). Organotypic hippocampal slices were submerged in HEPES-based artificial cerebrospinal fluid (ACSF) containing (in mM): 140 NaCl, 3.5 KCl, 1 $MgCl_2$, 2.5 $CaCl_2$, 10 HEPES, 10 Glucose, 1 sodium pyruvate and 2 $NaHCO_3$, at pH 7.3. Borosilicate pipettes (Science Products; GB150F-8P; Dimensions: 0.86 x 1.5 x 80 mm) with a resistance of 3-5 MΩ were backfilled with the transduction solution containing plasmid DNA. Neurons were electroporated by obtaining a loose seal in cell-attached mode followed by delivery of a pulse train (14 V at 200 Hz for 60 pulses, 0.50 ms pulse width). 20 cells were electroporated per slice, with a typical success rate of ~25% .

AAV global transduction

For global transduction of organotypic slice culture, AAV stock solutions constituted in PBS were diluted in organotypic media to a concentration of 1.0 x10^{13} GC/ml. Individual DIV 3 organotypic hippocampal slices were then submerged in 2 µl of diluted virus and placed back in the incubator. Electrophysiological recordings were performed at DPI 4, 7 and 13 and immunofluorescence experiments were performed at DPI 13. Dissociated hippocampal cultures were infected with AAV by application 2 µl of 1.0 x10^{13} GC/ml virus at DIV 7. Immunofluorescence experiments were subsequently performed at DPI 7. A face mask was worn during this procedure and all instruments were washed thoroughly with 70% ethanol.

AAV microinjection

For selective expression in the CA1 region of organotypic hippocampal slices, high titer AAV (1.0 x10^{13} GC/ml) was injected into the extracellular space of the CA1 pyramidal layer (Ehrengruber et al., 1999; Wiegert et al., 2017a). Injection pipettes were prepared from borosilicate glass capillaries pulled using a single-step heating protocol with a tip diameter of ~50 µm. To inject organotypic hippocampal slices, pressure was applied through a 1 ml syringe for a total of 5 times per injection site, with 3 injection sites per slice. GFP fluorescence was observed from DPI 3 onwards, with subsequent electrophysiological recordings performed at DPI 5-7.

P0 stereotactic injection

Mice were bred with floxed loci at *Gria1* ,*2* and *3* genes (*Gria1*$^{lox/lox}$;*Gria2*$^{lox/lox}$;*Gria3*$^{lox/lox}$) referred to as *Gria1-3*$^{fl/fl}$. 0.5 µl of AAV-Cre-GFP (Penn Vector Core) was injected into each hippocampus of postnatal day 0-1 (P0/1) pups at a titer of 2.0 x10^{12} GC/ml using injection pipettes made of borosilicate glass. Pups were anaesthetised using 4% isoflurance throughout the procedure before performing intracerebral injection, as described previously (Ho et al., 2020). Following recovery pups were used for the preparation of organotypic slices at P6-8.

2.3 AAV production, purification and titration

AAV serotype 2/9 viral vectors were produced and purified in a Biosafety Level 2 containment suite (Biological Safety Committee, MRC LMB). Recombinant AAVs were generated by triple transfection of HEK 293T cells (ATCC) using polyethylenimine (Gray et al., 2011). Viral particles were harvested from the cells and media at 72 hours. 40% polyethylene glycol 8000 (Sigma-Aldrich, P2139) in 500 mM NaCl was used to precipitate viral particles from the cell media to ensure recovery of high titer virus (Chan et al., 2017; Deverman et al., 2016). Cell pellets were resuspended in 150 mM NaCl with 20 mM Tris pH 8.0, freeze-thawed three times, and treated with 250 U/ml Benzonase (Sigma-Aldrich, E8263) and 1 mM $MgCl_2$ at 37°C for 15 mins. Precipitated virus was then resuspended and added to the cell lysates before incubation at 37°C for 15 mins and clarified by centrifugation at 3,900 rpm. The clarified stocks were purified over iodixanol (Optiprep, Sigma-Aldrich, D1556) step gradients (15%, 25%, 40% and 60%) (Zolotukhin et al., 1999) and then subjected to ultracentrifugation at 50,000 rpm for 1.5 hours (Beckman, VTi50 rotor). 3 ml of the 40% layer was collected post-ultracentrifugation and concentrated to 150 µl in PBS using centrifugal filters (100K, Amicon, Merck-Millipore, UFC910024). AAV titer was measured using quantitative RT-PCR (qPCR) (Zolotukhin et al., 1999). The purified viral stock was treated with 10 U DNase I (Takara, 2270A) and 10 mg/ml Proteinase K to remove contaminating DNA. Plasmid DNA was used to construct a standard curve with a range of 100 pg/ml to 1000 ng/ml. Two samples were prepared for each standard concentration of DNA and the viral stock to improve the accuracy of qPCR measurement. qPCRs were run with Rotor-Gene SYBR Green PCR Kit (Qiagen, 204074).

2.4 Electrophysiology

Recordings were made from hippocampal CA1 pyramidal neurons visually identified using a 60x water immersion objective on an upright microscope (Scientifica, SliceScope). Electrical responses were measured using a Multiclamp 700B amplifier and pClamp 10 acquisition software (Molecular Devices). Signals were low-pass filtered at 4 kHz and digitised at 25-50 kHz (Digidata 1550B). Series resistance (Rs), measured by the instantaneous current response to a −5 mV step was <20 MΩ. Rs was compensated to remain less than 10 MΩ and was monitored throughout the recording. Recordings were discarded if Rs changed significantly (>20%) and cells from dual recordings differed by >8 MΩ. Organotypic hippocampal slices were submerged in ACSF containing (in mM): 125 NaCl, 2.5 KCl, 1.25 NaH_2PO_4, 25 $NaHCO_3$, 10 glucose, 1 sodium pyruvate, 4 $MgCl_2$, 4 $CaCl_2$ at pH 7.3 (95% O_2 / 5% CO_2). For spontaneous EPSC (sEPSC) recordings, 4 mM $CaCl_2$ was substituted with 4 mM $SrCl_2$ and for miniature EPSC (mEPSC) recordings, 1 µM TTX was included in the ACSF solution. All recordings were conducted at 26°C, maintained with an in-line Peltier heater (Scientifica).

Excitatory postsynaptic currents (EPSCs) were evoked by stimulation of Schaffer collaterals in the stratum radiatum of CA1 using a monopolar glass electrode, filled with ACSF, at a test pulse frequency of 0.2 Hz. For synaptic rectification index (RI) experiments, AMPAR currents were isolated by the addition of 100 µM D-AP5 (NMDAR antagonist; Tocris-Bioscience, Cat No. 0106), 10 µM SR 95531 hydrobromide ($GABA_AR$ antagonist; Tocris-Bioscience, Cat No. 1262) and 2-Chloroadenosine (Adenosine receptor agonist; Tocris-Bioscience, Cat No. 3136) to prevent epileptiform activity. 3-5 MΩ borosilicate pipettes were filled with intracellular solution containing (in mM): 135 CH_3SO_3H, 135 CsOH, 4 NaCl, 2 $MgCl_2$, 10 HEPES, 4 Na_2-ATP, 0.4 Na-GTP, 0.15 spermine, 0.6 EGTA, 0.1 $CaCl_2$, adjusted to pH 7.3 with CsOH. Simultaneous dual whole-cell voltage clamp recordings were obtained from untransfected (GFP-) and neighbouring transfected (GFP+) CA1 pyramidal neurons, visualised by epifluorescence.

RI was calculated by recording AMPAR currents from cells held at a membrane potential of –60, 0 and +40 mV and calculated using the following equation:

$$RI = -(I_{+40} - I_0) / (I_{-60} - I_0)$$

The paired pulse ratio (PPR) was calculated using the following equation:

$$PPR = EPSC_2 / EPSC_1$$

The coefficient of variation (CV) was calculated using the following equation:

$$CV = EPSC_{SD} / EPSC_{Mean}$$

Recombinant AMPAR recordings were performed by pulling outside-out patches of membrane from GFP+ AMPAR expressing HEK293 cells. AMPAR currents were recorded from the peak response to 200 ms 10 mM glutamate application. The weighted tau (τw) decay was calculated using the following equation, where A_1 and A_2 are the relative amplitudes of the two exponentials:

$$\tau w = \tau_1 (A_1 / A_1+A_2) + \tau_2 (A_2 / A_1+A_2)$$

To study neuronal excitability, measurements were performed in current-clamp mode using the whole-cell configuration. Spike number was measured from the response to a 2 s +350 pA depolarising current injection. The action potential threshold was determined from +50 pA current injection steps and the resting membrane potential was measured from the baseline response.

2.5 Mass spectrometry

Biotinylation in organotypic slices

Biotin-depleted media was prepared by incubating organotypic medium with streptavidin agarose beads (Pierce™ Streptavidin Agarose; Thermo Scientific; #20353) overnight, before spinning down and collecting the supernatant. Biotinylation was induced in DPI 13 BirA*-AMPAR expressing organotypic slices by a combination of media replacement and submersion in 2 µl organotypic media containing 200 µM biotin (Sigma; #B4501) and 2 mM ATP (Sigma; #A2383) for a total of 48, 18 or 2 hrs, for BioID2-, MiniTurbo- and TurboID-AMPARs respectively. For APEX2- organotypic media was supplemented with 500 µM biotin-phenol (Sigma; #SML2135) and H_2O_2 (Sigma #H1009) to initiate biotinylation for a total of 10 mins. 50 slices were processed per condition from a litter of 6x C57/Bl6 mice and each preparation was performed independently 3 times. Following biotinylation, slices were submerged in ice-cold PBS containing 1x Protease Inhibitor cocktail (Roche; #5056489001) and 1 mM PMSF (phenylmethylsulfonyl fluoride) and lifted from the culture membrane using a sterilised micro spatula (Fischer Scientific; #11523482). Slices were then collected in Protein LoBind microcentrifuge tubes (Eppendorf; #0030108116), snap frozen and stored at -80°C. Subsequent sample processing was performed in triplicate, to limit the variability of downstream sample handling steps.

Lysis of organotypic slices

Slices were lysed in 500 µl RIPA buffer, containing (in mM): 150 NaCl, 50 Tris-HCl, 1% Triton X-100, 0.5% Sodium deoxycholate, 1% sodium dodecyl sulfate (SDS), 1 PMSF and 1x Protease Inhibitor cocktail at pH 7.4. Samples were dounce homogenised 15 times, probe sonicated twice for 10 sec and heated to 95˚C for 5 min to denature the postsynaptic density (Loh et al., 2016). 500 µl SDS-free RIPA buffer was added to the samples before rotation for 1 hour at 4˚C. Lysed samples were then centrifuged at 15,000 rpm for 10 min at 4°C and 1 ml of the clarified lysate was carefully collected and kept on ice. The protein concentration of each sample was then determined using the BCA assay (Thermo Scientific; #23225) and adjusted to 1 mg/ml using RIPA buffer. 100 µl organotypic slice lysate was reserved for western blotting and 900 µl was used for isolation of biotinylated proteins.

Enrichment of biotinylated proteins

Streptavidin magnetic beads (Invitrogen; Dynabeads™ MyOne™ Streptavidin C1, 65002) were used to isolate biotinylated proteins from slice lysates. For each experimental condition, 500 µl streptavidin magnetic beads were pre-washed three times in RIPA buffer and then incubated with 900 µl of 1 mg/ml clarified lysate on rotation at 4˚C overnight. Beads were then subjected to the following wash steps by collection and 10 min re-suspension using a magnetic bead rack (GE Healthcare; 28-9489-64) and rotor: 3 washes in Wash Buffer 1, containing (in mM): 150 NaCl, 1 EDTA, 2% SDS, 50 Tris-HCl; 3 washes in Wash Buffer 2, containing (in mM): 500 NaCl, 1 EDTA, 1% Triton X-100, 50 Tris-HCl; and 3 washes in Wash Buffer 3, containing (in mM): 150 NaCl, 50 Tris-HCl, all wash buffers were supplemented with 1 PMSF and 1x Protease Inhibitor cocktail at pH 7.4. Biotinylated proteins were eluted by re-suspending washed streptavidin magnetic beads in 50 µl Elution buffer containing (in mM): 1x SDS-PAGE loading buffer (Invitrogen; NP0007), 10 mM dithiothreitol (DTT), biotin added to saturation and heating to 95˚C for 10 mins. Elution samples were then run on a 60 µl capacity Bolt 4-12% Bis-Tris Plus gel (Invitrogen; NW04120BOX) in 1X Bolt MES SDS running buffer (Invitrogen; B0002) stained with Coomassie blue and cut into 1 mm^3 gel pieces re-suspended in 10 µl H_2O and stored at -20° C.

In-Gel digestion and nano-LC-MS/MS analysis

SDS-PAGE separated protein gel bands were excised, destained, reduced with DTT and alkylated with iodoacetamide. They were then digested overnight with trypsin (Promega) in ammonium bicarbonate at 37°C. Extracted peptide mixtures were separated using an Ultimate 3000 RSLC nano System (Thermo Scientific), with an acetonitrile gradient, consisting of Buffer A (2% MeCN, 0.1% formic acid) and Buffer B (80% MeCN, 0.1% formic acid) at a flow rate of 300 nl/ min. Eluted peptides were introduced directly via a nanospray ion source into a Q Exactive Plus hybrid quardrupole-Orbitrap mass spectrometer (Thermo Fisher Scientific). The mass spectrometer was operated in standard data dependent mode, performed survey full-scan (MS, m/ z = 380-1600) with a resolution of 70000, followed by MS2 acquisitions of the 15 most intense ions with a resolution of 17500 and NCE of 27%. MS target values of 1 $x10^6$ and MS2 target values of 1 $x10^5$ were used. The isolation window was set as 1.5 m/z and dynamic exclusion was enabled for 30 seconds.

Protein quantification

The acquired MSMS raw files were processed using MaxQuant (Cox and Mann) with the integrated Andromeda search engine (v.1.6.6.0). MSMS spectra were searched against *Mus muculus*, UniProt Fasta database (Mar 2019). Carbamidomethylation of cysteines was set as fixed modification, while oxidation of methionine, N-terminal protein acetylation and deamination of glutamine as variable modifications. Enzyme specificity was set to trypsin/p and maximum two missed cleavages were allowed. Obtained label-free quantification (LFQ) intensities were used for relative quantification of enriched proteins. Protein quantification requires 1 (unique+ razor) peptide. MaxQuant output file, proteinGroups.txt was then processed with Perseus software (v 1.6.6.0). After uploading the matrix, the data was filtered, to remove identifications from reverse database and modified peptide only, and common contaminants. Also filtered razor plus unique peptides, at least greater or equal to 2. Inclusion criteria was set to include only proteins present in at least 2 out of 3 repeats for each condition in the dataset. Missing values were replaced from normal distribution after filtered row based on valid values.

Proteomic analysis

Fold-enrichment between experimental conditions was calculated from the difference in biotinylation intensity (LFQ) between two experimental conditions and Log_2 transformed. Statistical significance was calculated using the P value from a paired t-test of triplicate datasets and $-Log_{10}$ transformed. Volcano plots were subsequently constructed by plotting fold-enrichment (x-axis) against significance (y-axis) for each given comparison. Reproducibility plots were constructed by plotting the biotinylation intensity of the 1st and 2nd replicate of a given condition and calculating the R^2 value of a simple linear regression in Prism 8 (GraphPad). BirA* enrichment was determined by constructing volcano plots of GluA2 full-length (WT)/ ΔNTD against Uninfected control. NTD enrichment was determined by constructing volcano plots of GluA2 against GluA2 ΔNTD. Proteins were considered AMPAR NTD candidates if they passed through the following filters: Filter 1: 2-fold enrichment for BirA*-AMPARs relative to Uninfected control. Filter 2: 2-fold enrichment for TurboID-GluA2 WT relative to TurboID-GluA2 ΔNTD. Filter 3: P value < 0.05 for TurboID NTD-enrichment. Final ranking was based on overall NTD-enrichment value across all three BirA* tags and APEX2. Cellular component and biological function enrichment analysis was performed using the Synapse Gene Ontology (SynGO) database (Koopmans et al., 2019; www.syngoportal.org). Synaptic coverage was calculated by calculating the number of synaptic genes identified by SynGO divided by the total number of identified genes (SynGO/ Total) and expressed as a percentage. Subcellular locations of non-synaptic proteins were deduced using the Gene Ontology (GO) database (www.geneontology.org). Candidates were defined as secreted or transmembrane-bound and protein boundaries were defined using the UNIPROT database (www.uniprot.org).

Western blotting

Western blotting of HEK293 cells or organotypic slices was performed by combining 26 µl cell lysate with 4 µl 100 mM DTT and 10 µl 4x NuPAGE LDS Sample Buffer (Invitrogen, #NP0007) before protein denaturation at 95°C for 5 min. Samples were run on Bolt 4-12% Bis-Tris gels (Invitrogen, #NW04122BOX) alongside a molecular weight marker (GE Healthcare, #RPN800E). Proteins were then transferred to a nitrocellulose membrane using an iBlot (Invitrogen, #IB1001) and incubated in blocking buffer containing 5% milk powder or 0.5% BSA for blots to be probed with streptavidin-HRP, as the free biotin present in milk competes with biotinylated proteins binding to streptavidin-HRP. Blots were incubated for 1 hr in

anti-BioID2 (1:5000) or anti-GluA2 (Sigma, #AB10529; 1:1000) followed by incubation with respective secondary antibodies anti-chicken- HRP (Abcam, #ab97135; 1:10,000), anti-rabbit-HRP (Abcam, #ab6721; 1:1000) or streptavidin- HRP (Abcam, #ab7403; 1:12,000) for 1 hr at RT. All blots were washed 3x 10 min in tween PBS before exposure with ECL Prime detection reagent (GE Healthcare, #RPN2232) for imaging.

2.6 Fluorescence imaging

Immunostaining neuronal cultures

Immunostaining of organotypic hippocampal slices was performed using an adapted protocol from Gogolla et al., (2006). Briefly, DPI 13 organotypic hippocampal slices were fixed in 4% paraformaldehyde (PFA), 4% sucrose in PBS for 10 min at room temperature (RT). Slices were then washed 3x briefly and 3x for 10 min in PBS and permeabilised with 0.5% Triton X-100 (Fisher Bioreagents, #BP151-500) in blocking solution containing 20% bovine serum albumin (BSA) (Fisher Bioreagents, #BP1605-100) for 12 hrs at 4°C. Slices were then incubated in primary anti-BioID2 (Kim et al., 2016; BioFront Technologies; #BID2-CP-100; 1:1000) prepared in 5% BSA in PBS overnight at 4°C followed by incubation in secondary antibody anti-chicken Alexa Fluor-568 (AF^{568}) (Invitrogen, #A-11041; 1:500) and streptavidin AF^{647}-conjugate (Molecular Probes, 10654043; 1:300) at RT for 4 hrs. Slices were then washed 3x briefly and 3x 10 min in PBS on a horizontal shaker and incubated with Hoechst 33258 (Invitrogen, H3569) for 1 min on the penultimate wash. Slices were stored in PBS at 4°C until imaging, where they were transferred onto a glass coverslip, submerged in PBS and imaged using a 10x/0.40 dry objective, 40x/1.10 water-immersion objective or 63x/1.40 oil-immersion objective on a Leica TCS SP8 confocal microscope using LAS X software. DPI 7 dissociated hippocampal cultures were fixed in 4% PFA, 4% sucrose in PBS for 10 min at RT. Cells were then washed 3x briefly and 3x for 10 min with PBS and permeabilised with 0.1% Triton X-100 in blocking solution containing 1% BSA and 10% normal goat serum (NGS) (Sigma-Aldrich, #NS02L) in PBS for 30 min. Neurons were then incubated with primary antibody anti-BioID2 for 2-4 hrs followed by secondary antibodies for 1 hr with *anti-chicken* AF^{568} and streptavidin AF^{647}-conjugate in 10% BSA and 1% NGS. Neurons were washed 3x briefly and 3x 10 min in PBS following primary and secondary antibody incubations.

The following primary antibodies were used to stain for candidate proteins: Olfm1 (Neuromab; Cat# 75-042; 1:500), Np65 (R&D systems; Cat# AF5360; 1:500) and Nptx1 (kindly provided by Dr Kunimichi Suzuki). Nptx1 was stained for in organotypic slice cultures by treating PFA fixed slices with 100 mg/ml pepsin for 3 min at 37°C, to improve antibody penetration. Live-labelling of surface HA-AMPARs was performed at 4 DPT by incubation with rabbit anti-HA (Sigma, Cat# H6908; 1:200) for 20 min at room temperature. Total HA-AMPAR was detected using mouse anti-HA (BioLegend, Cat# 901501; 1:500), followed by incubation in corresponding secondary antibodies: goat anti-rabbit IgG AF^{568} (Invitrogen, Cat# A - 11036; 1:500), goat anti-mouse IgG AF^{488} (Invitrogen, Cat# A - 11029; 1:500). Coverslips were mounted in ProLong Diamond Antifade Mountant (Invitrogen, #P36961) and cured in the dark at RT for 48 hrs.

Cell-based binding assay

Direct interactions between candidate proteins and iGluR NTDs were assessed in a cell-based binding assay using a protocol adapted from Matsuda et al., (2016) and Suzuki et al., (2020). HEK293T cells (ATCC, #CRL-11268) were transfected with NTD-myc-pDisplay constructs displaying iGluR NTDs with an extracellular myc tag. Candidates were co-transfected in a different subset of HEK293 cells with pDisplay-BirA-ER at a ratio of 3:1 and biotin was added to the media to permit *in vivo* biotinylation and secretion of candidates into the culture media for 60 hrs. NTD displaying HEK293 cells were plated on poly-L-lysine coated 12 mm glass coverslips (Corning, #354085) and allowed to settle overnight before incubation with secreted candidates for 4 hrs. Cells were then fixed in PFA for 10 min at RT and stained with primary antibodies: anti-myc (1:500; Sigma, #M4439) and respective secondary antibodies: *anti-mouse* AF^{555} and Streptavidin AF^{647}-conjugate (1:300; Molecular Probes, #10654043). Coverslips were then mounted in ProLong Diamond Antifade Mountant (Invitrogen, #P36961) and cured in the dark at RT for 48 hrs. Images were taken using a 63x oil-immersion objective on a Leica TCS SP8 confocal microscope using LAS X software. Equivalent laser power settings were applied across all experimental conditions. 6 images were taken per coverslip at a resolution of 512 x 512 from at least 3 independent preparations. Fluorescence intensity (FI) of NTD expression (myc; AF^{555}) and candidate binding (streptavidin; AF^{647}) was quantified using ImageJ and calculated using the following equation:

$$\text{Candidate binding (AU)} = (\text{FI } AF^{647}) / (\text{FI } AF^{555}) \times 100$$

Chapter 3

AMPAR sub-synaptic positioning through its N-terminal domain

3.1 Introduction

The molecular organisation of the presynaptic active zone (AZ) and postsynaptic density (PSD) ensure efficacious synaptic transmission can occur. AMPARs are localised predominantly within the PSD where they contribute to the fast component of the excitatory postsynaptic current (EPSC) (Figure 3.1; Bekkers and Stevens, 1989). On a sub-synaptic scale, AMPARs are not uniformly distributed within the PSD, instead assembling themselves within 'nanodomains' (Nair et al., 2013; MacGillavry et al., 2013). Due to the relatively low-affinity of AMPARs for glutamate (0.1-1 mM; Traynelis et al., 2010) and localised release of vesicular glutamate, receptors must be positioned sub-synaptically near vesicle release sites to achieve full activation (Franks et al., 2003; Raghavachari and Lisman, 2004). It is thought that not all synaptic AMPARs respond to every release event (Liu et al., 1999; McAllister and Stevens, 2000), therefore, clustering of synaptic AMPARs on a nanometer scale profoundly increases the synaptic efficacy (Xie et al., 1997; Franks et al., 2003; Lisman et al., 2007; Raghavachari and Lisman, 2004; Savtchenko and Rusakov, 2014). Furthermore, recent evidence suggests that alignment of the AZ and PSD in *trans* -synaptic 'nanocolumns' increases synaptic strength (Tang et al., 2016; Biederer et al., 2017), with a number of synaptic proteins facilitating this process (Chamma et al., 2016; Fukata et al., 2021). Evidence for the functional importance of sub-synaptic receptor positioning however, remains entirely computational. This chapter aims to resolve the physiological importance of AMPAR positioning at CA1 synapses using glutamate spillover and electrophysiology.

The AMPAR N-terminal domain (NTD) is required to maintain excitatory synaptic transmission and plasticity (Watson et al., 2017; Díaz-Alonso et al., 2017; Watson et al., 2020; Jiang et al., 2021). NTD-deleted (ΔNTD) AMPARs exhibit increased mobility at hippocampal synapses, as measured by fluorescence recovery after photobleaching (Watson et al., 2017). This suggests that ΔNTD receptors are unable to anchor at postsynaptic sites, likely being omitted from the PSD and instead localising at the 'peri-synaptic' region (Figure 3.1; within ~100 nm of the PSD; Hardingham and Bading, 2010). An emerging hypothesis is that the AMPAR NTD engages in interactions with synaptic proteins, positioning receptors within nanocolumns for effective synaptic transmission (Watson et al., 2020). Previous studies have relied on electrophysiological assays to detect the incorporation or exclusion of AMPARs from CA1 synapses, however direct functional evidence for AMPAR sub-synaptic positioning remains elusive. To directly measure activation of peri-synaptic AMPARs, glutamate spillover experiments were designed to investigate the requirement of the AMPAR NTD for sub-synaptic positioning.

The synaptic cleft is a protein-rich environment (Perez de Arce et al., 2015; Biederer et al., 2017), composed of a number of *trans*-synaptic interactions responsible for orchestrating alignment of pre- and post-synaptic sites (Chamma et al., 2016; Fukata et al., 2021). A number of secreted cleft proteins have been shown to simultaneously influence postsynaptic ionotropic glutamate receptor (iGluR) function and presynaptic differentiation (Matsuda et al., 2010; Matsuda et al., 2016; Elegheert et al., 2016). The AMPAR NTD appears to maintain synaptic transmission in a subunit-specific manner at CA1 synapses (Watson et al., 2017; Díaz-Alonso et al., 2017; Watson et al., 2020). Given that the NTD protrudes mid-way into the synaptic cleft exposing it to a protein-rich environment, it is possible that the AMPAR NTD may engage in subunit-specific interactions with synaptic proteins. Cleft protein interactions with the AMPAR NTD are hypothesised to influence receptor mobility (Watson et al., 2017) and sub-synaptic positioning (Watson et al., 2020). However, despite numerous computational studies (Xie et al., 1997; Franks et al., 2003; Lisman et al., 2007; Raghavachari and Lisman, 2004; Savtchenko and Rusakov, 2014), there is currently no direct evidence for the physiological consequence of sub-synaptic AMPAR positioning.

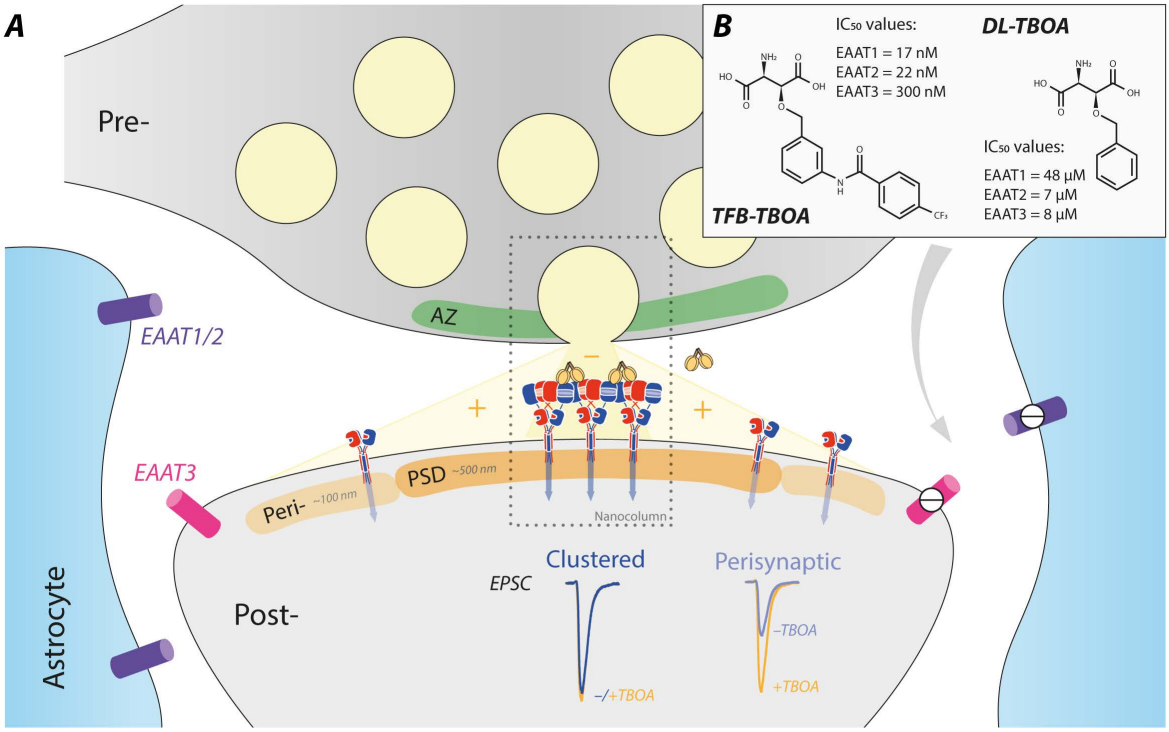

Figure 3.1 ***Hypothesised sub-synaptic positioning of WT and NTD-deleted AMPARs.*** *(**A**) Hypothesised synaptic arrangement of WT and ΔNTD AMPARs. WT receptors are positioned within the postsynaptic density (PSD, ~1000 nm size; Hruska et al., 2018; Sun et al., 2019) in direct apposition to presynaptic glutamate release from the active zone (AZ). Postsynaptic AMPARs are thought to be aligned with presynaptic release sites in nanocolumns (dashed box) (Tang et al., 2016), potentially through direct interactions with proteins in the synaptic cleft. A robust postsynaptic EPSC is hypothesised with receptors clustered in nanocolumns. ΔNTD receptors however, may be excluded from the PSD residing in the peri-synaptic region (peri-synapse, within 100 nm of the PSD; Hardingham and Bading, 2010). Subsequently, the postsynaptic EPSC may be decreased, due to the relatively low affinity of AMPARs for glutamate and distal positioning from glutamate release sites. Excitatory amino acid transporters (EAATs) 1-3 are expressed in the hippocampus. EAAT1/2 are located on astrocytes and EAAT3 is located on neurons. (**B**) DL-TBOA and TFB-TBOA are non-transportable inhibitors of EAAT1-3 (Shimamoto et al., 1998; Shimamoto et al., 2000; Shimamoto et al., 2004). Blockade of glutamate uptake into astrocytes results in a 'spillover' in the synaptic cleft. Glutamate spillover (+) can be used to activate receptors in the peri-synaptic region, which would otherwise not be activated during basal conditions (-).*

Excitatory amino-acid transporters (EAATs) rapidly uptake glutamate from the synaptic cleft. Of the five glutamate transporters, EAAT1-3 are expressed in the hippocampus. EAAT1 and EAAT2 are predominantly expressed in astrocytes and EAAT3 in neurons (Tzingounis and Wadiche, 2007). DL-threo-β-Benzyloxyaspartic acid (DL-TBOA) is a selective glutamate uptake inhibitor of EAAT 1-3 (Figure 3.1B; IC_{50} in μM: EAAT1 = 48, EAAT2 = 7.0, EAAT3 = 8.0; Shimamoto et al., 1998; Shimamoto et al., 2000), and (3S)-3-[[3-[[4-(Trifluoromethyl)benzoyl]amino]phenyl]methoxy]-L-aspartic acid (TFB-TBOA) is a selective glutamate uptake inhibitor of EAAT 1/2 (Figure 3.1B; IC_{50} in nM: EAAT1 = 17, EAAT2 = 22, EAAT3 = 300; Shimamoto et al., 2004). Glutamate transporters tightly control the spatio-temporal release of glutamate in the synaptic cleft minimising the concentration at extra-synaptic sites and cross-talk with neighbouring synapses (Asztely et al., 1997; Tzingounis and Wadiche, 2007). Under physiological conditions the concentration of glutamate is thought to rise above 1 mM in the synaptic cleft and is cleared within 10 ms (Dzubay and Jahr, 1999; Reiner and Levitz, 2018). Comparitively, extra-synaptic sites see low nM range concentrations of glutamate (Herman and Jahr, 2007). Pharmacological blockade of EAAT1-3 with TBOA however, results in a spillover of glutamate from the synapse increasing the concentration and time-course of glutamate at extra-synaptic sites (Hires et al., 2008; Armbruster et al., 2016; Pinky et al., 2018).

TBOA application has been used extensively to activate receptors outside the PSD (peri- and extra-synaptic) and even those on neighbouring synapses (DiGregorio et al., 2002; Nietz et al., 2017), demonstrating the synaptic localisation of extra-synaptic NMDARs (Chen and Diamond, 2002; Clark and Cully-Candy, 2002), peri-synaptic AMPARs (He et al., 2009; Yang et al., 2008; Yang et al., 2010) and peri-synaptic mGluRs (Huang et al., 2004; Sheng et al., 2017b). This study utilises TBOA-induced glutamate spillover to study the sub-synaptic localisation of GluA1/2 WT and ΔNTD receptors at CA1 synapses. Ultimately determining the physiological importance of the AMPAR NTD in sub-synaptic receptor positioning.

3.2 Results

3.2.1 AMPAR subunit composition at CA1 synapses

To determine the AMPAR subunit composition at hippocampal CA1 synapses, AMPAR excitatory postsynaptic currents (EPSCs) were recorded from CA1 synapses lacking GluA1-3 subunits. To achieve GluA1-3 knockout, Cre-GFP was expressed in CA1 pyramidal neurons of conditional AMPAR knockout mice (Gria1-3$^{fl/fl}$; Lu et al., 2009) via neonatal injection of AAV-Cre-GFP (Ho et al., 2020). Organotypic hippocampal slices were prepared from AAV-Cre-GFP injected Gria1-3$^{fl/fl}$ pups and electrophysiological recordings were performed at day in vitro (DIV) 10. These experiments were performed to establish dual whole-cell recording of pairs of CA1 pyramidal neurons, the principle experimental technique used throughout this study.

AMPAR and NMDAR EPSCs were recorded at membrane potentials of -60 and +40 mV respectively, measuring the AMPAR EPSC from the peak amplitude of responses at -60 mV, and the NMDAR EPSC from the amplitude 50 ms after the stimulus to avoid contamination by AMPAR currents (Figure 3.2A2). Pairs of untransfected (GFP-) and infected (GFP+) CA1 pyramidal neurons were recorded simultaneously to determine the effect of Cre-GFP expression on excitatory synaptic transmission. The AMPAR EPSC of Cre-GFP expressing cells was significantly reduced relative to paired untransfected cells (Figure 3.2A3), as reported previously (Lu et al., 2009; Ho et al., 2020). AMPAR EPSC responses were reduced to ~5-10%, likely mediated by residual AMPARs or NMDAR-contaminating currents. This suggests that GluA1-3 subunits mediate the majority of AMPAR-mediated synaptic transmission at CA1 synapses in organotypic hippocampal slices. Cre-GFP NMDAR EPSCs were unchanged relative to paired untransfected cells (Figure 3.2A4), suggesting no compensatory change in NMDAR content, and no change in spine density (Lu et al., 2009). These experiments confirm that GluA1-3 subunits mediate the majority of AMPAR-mediated synaptic transmission at CA1 synapses (Lu et al., 2009) and establish the use of dual whole-cell electrophysiology for use throughout this study. Furthermore, Lu et al., (2009) found that ~80% of AMPARs at CA1 synapses were composed of GluA1/2 subunits. Therefore, this study predominantly investigates the role of GluA1/2 subunits on AMPAR-mediated synaptic transmission.

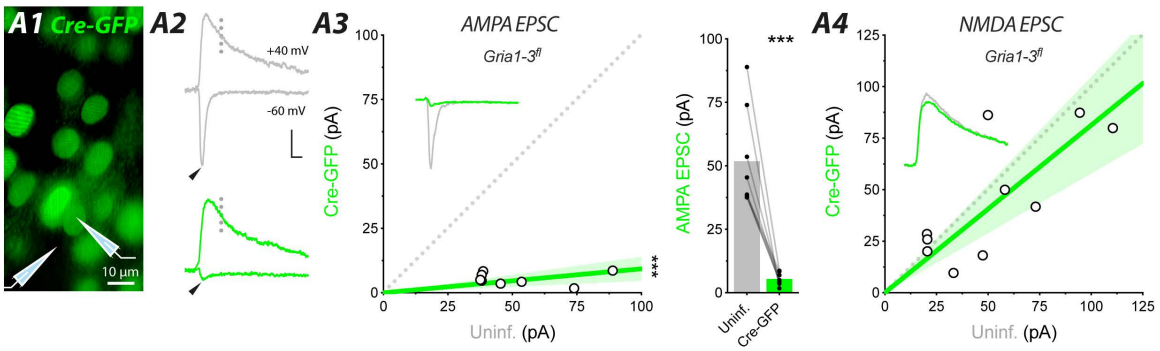

Figure 3.2 ***GluA1-3 knockout abolishes AMPAR currents at CA1 synapses*** *(**A1**) Cre-GFP expressing CA1 pyramidal neurons were detectable by nuclear GFP expression in CA1 pyramidal neurons of infected organotypic hippocampal slices preparared from Gria1-3$^{fl/fl}$ pups (kindly provided by Dr Alexandra Pinggera). Dual whole-cell recordings were performed from Uninf. (GFP-) and neighbouring Cre-GFP infected (GFP+) cells. (**A2**) AMPAR EPSCs were recorded from cells held at -60 mV and measured from the peak amplitude response. NMDAR EPSCs were recorded from cells held at + 40 mV and measured from the amplitude response 50 ms after the stimulus to avoid contamination by AMPAR currents. Uninf. (grey) and Cre-GFP (green) cells were recorded simultaneously using dual whole-cell patch clamp electrophysiology (scale bar = 20 pA; 20 ms). (**A3**) Cre-GFP AMPAR EPSC amplitude was significantly reduced relative to Uninf. (Uninf. = 51.8 ± 6.9 pA; Cre-GFP = 5.4 ± 0.9 pA; n = 8; paired t-test, p < 0.001). (**A4**) Cre-GFP NMDAR EPSC amplitude was unchanged relative to Uninf. (Uninf. = 52.8 ± 10.0 pA; Cre-GFP = 44.8 ± 9.4 pA; n = 10; paired t-test, p = 0.27).*

3.2.2 The AMPAR NTD is required for excitatory synaptic transmission

The AMPAR NTD is involved in the maintenance of synaptic transmission and plasticity at CA1 synapses (Watson et al., 2017; Díaz-Alonso et al., 2017; Watson et al., 2020; Jiang et al., 2021). To confirm these findings, electrophysiology experiments were first performed using overexpression (OE) of full-length (WT) and NTD-deleted (ΔNTD) AMPAR subunits in CA1 pyramidal neurons (Figure 3.3). Next, the role of endogenous AMPAR NTD-protein interactions was investigated by applying exogenous purified GluA1-3 NTDs to organotypic hippocampal slices whilst recording basal transmission and synaptic potentiation (Figure 3.4).

Overexpression of NTD-deleted AMPARs

OE of exogenous WT and ΔNTD receptors revealed a subunit-specific role for the AMPAR NTD in synaptic incorporation, determined by measurement of the synaptic rectification index (RI) (Watson et al., 2017; Díaz-Alonso et al., 2017). To corroborate these findings, GluA1/2 WT and ΔNTD receptors were introduced into CA1 pyramidal neurons of organotypic hippocampal slices via single-cell electroporation (SCE) transfection (Figure 3.3A). Subsequently the AMPAR EPSC amplitude was recorded from pairs of untransfected and transfected cells using dual whole-cell electrophysiology (Figure 3.3A3).

The synaptic RI is commonly used as a measure of AMPAR synaptic trafficking (Hayashi et al., 2000; Shi et al., 2001). This assay exploits the inwardly-rectifying current-voltage (IV) relationship of calcium-permeable AMPARs (Bowie and Mayer, 1995; Kamboj et al., 1995; Koh et al., 1995), owing to RNA editing at the Q/R site for GluA2 (Sommer et al., 1991). The synaptic RI serves as a measure of exogenous receptor (Q pore-containing) trafficking and positioning at CA1 synapses during this Chapter, calculated from AMPAR EPSC amplitudes (current; I) at different membrane potentials (-60, 0, +40 mV) using the following equation:

$$RI = -(I_{+40} - I_0) / (I_{-60} - I_0)$$

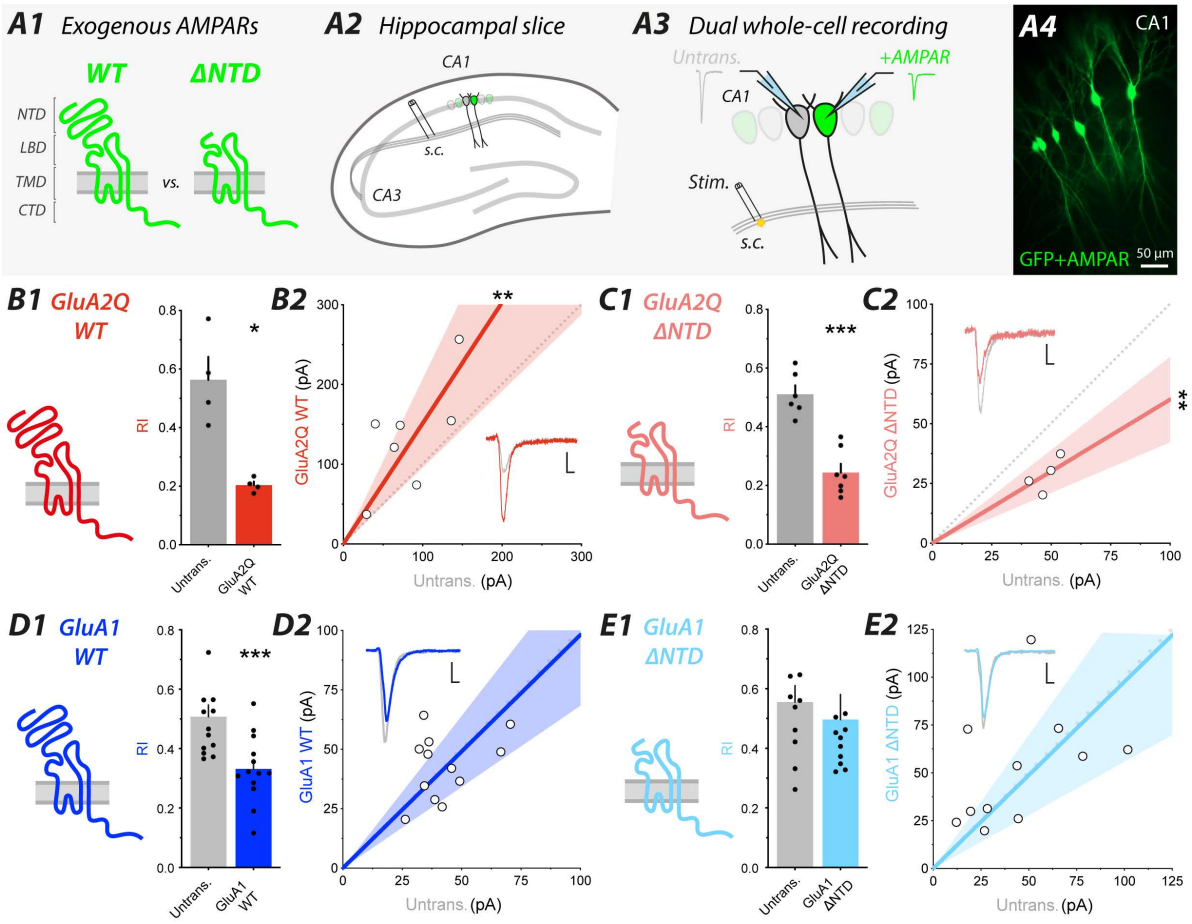

Figure 3.3 *Subunit-specific role for the AMPAR NTD in synaptic incorporation*

Figure 3.3 ***Subunit-specific role for the AMPAR NTD in synaptic incorporation*** *(**A1**) Exogenous full-length (WT) and NTD-deleted (ΔNTD) AMPAR subunits. (**A2**) Organotypic hippocampal slice preparation expressing GFP + AMPAR subunits. (**A3**) Dual whole-cell recording was performed from untransfected (GFP-) and transfected (GFP+) CA1 pyramidal neurons. AMPAR EPSCs were recorded in reponse to electrical stimulation of Schaffer collateral presynaptic inputs at a basal stimulation frequency of 0.2 Hz. (**A4**) GFP+ CA1 pyramidal neurons were transfected by single-cell electroporation (SCE) of AMPAR subunits. (**B1**) Synaptic RI of GluA2Q WT was significantly reduced relative to Untrans. (Untrans. = 0.56 ± 0.079; GluA2Q WT = 0.20 ± 0.012; n = 4; p < 0.05). (**B2**) AMPAR EPSC amplitude of GluA2Q WT was significantly increased relative to Untrans. (Untrans. = 46.2 ± 10.9 pA; GluA2Q WT = 75.2 ± 9.9 pA; n = 8; p < 0.001). (**C1**) Synaptic RI of GluA2Q ΔNTD was significantly reduced relative to Untrans. (Untrans. = 0.51 ± 0.074; GluA2Q ΔNTD = 0.25 ± 0.032; n = 6; p < 0.001). (**C2**) AMPAR EPSC amplitude of GluA2Q ΔNTD was significantly reduced relative to Untrans. (Untrans. = 47.7 ± 2.8 pA; GluA2Q ΔNTD = 28.5 ± 3.6 pA; n = 4; p < 0.001). (**D1**) Synaptic RI of GluA1 WT was significantly decreased relative to Untrans. (Untrans. = 0.51 ± 0.04; GluA1 WT = 0.33 ± 0.03; n = 13; paired t-test, P < 0.001). (**D2**) GluA1 WT EPSC amplitude was unchanged relative to Untrans. (Untrans. = 65.0 ± 12.6 pA; GluA1 WT = 74.6 ± 14.2 pA; n = 18; paired t-test, P = 0.42). (**E1**) Synaptic RI of GluA1 ΔNTD was unchanged relative to Untrans. (Untrans. = 0.56 ± 0.06; GluA1 ΔNTD = 0.50 ± 0.08; n = 11; paired t-test, P = 0.43). (**E2**) GluA1 ΔNTD EPSC amplitude was unchanged relative to Untrans. (Untrans. = 44.6 ± 8.45 pA; GluA1 ΔNTD = 52.0 ± 9.05 pA; n = 11; paired t-test, P = 0.45). (Scale bars: 20 pA; 20 ms).*

GluA2Q WT expressing cells have a significantly reduced synaptic RI relative to paired untransfected cells (Figure 3.3B1). This suggests that exogenous Q pore-containing receptors are incorporated into CA1 synapses where they contribute to synaptic transmission. Furthermore, the AMPAR EPSC amplitude of GluA2Q WT was significantly increased by ~50% relative to untransfected cells (Figure 3.3B2). GluA2Q ΔNTD expressing cells also have a significantly reduced synaptic RI relative to paired untransfected cells (Figure 3.3C1), indicative of successful synaptic incorporation. However, GluA2Q ΔNTD receptors have a significantly reduced AMPAR EPSC amplitude by ~50% relative to paired untransfected cells (Figure 3.3C2). These findings support previous publications (Watson et al., 2017; Díaz-Alonso et al., 2017; Watson et al., 2020), suggesting the GluA2 NTD is required for efficacious AMPAR-mediated synaptic transmission.

Exogenous expression of GluA1 WT resulted in significant rectification of the synaptic response relative to paired untransfected cells (Figure 3.3D1). This suggests that GluA1 WT receptors are incorporated into CA1 synapses where they contribute to the synaptic response. The AMPAR EPSC amplitude however, remained unchanged relative to paired untransfected cells (Figure 3.3D2). GluA1 ΔNTD receptors, however, had no effect on the extent of synaptic rectification (Figure 3.3E1) or AMPAR EPSC amplitude (Figure 3.3E2) relative to paired untransfected cells. This indicates that deletion of the GluA1 NTD results in a reduction in the number of synaptic receptors contributing to the AMPAR EPSC. These findings support previous publications (Watson et al., 2017; Díaz-Alonso et al., 2017; Watson et al., 2020), suggesting the GluA1 NTD is required for synaptic incorporation to maintain effective excitatory synaptic transmission.

Taken together, OE of GluA1/2 WT and ΔNTD receptors demonstrates the subunit-specific role of the AMPAR NTD in ensuring effective AMPAR-mediated synaptic transmission. A developing hypothesis in the field is that synaptic protein interactions with the AMPAR NTD may position receptors at the synapse for optimal signal transduction (Watson et al., 2017; Díaz-Alonso et al., 2017; Watson et al., 2020). To investigate the subunit-specific effect of the AMPAR NTD on excitatory synaptic transmission, experiments were performed with exogenous GluA1-3 NTD application to compete with endogenous synaptic protein interactions (Figure 3.4).

Application of exogenous AMPAR NTDs

The AMPAR NTD is a very sequence diverse region of the receptor (Figure 3.4A; García-Nafría et al., 2016a), suggesting it may engage in subunit-specific protein interactions. Here, it was hypothesised that application of exogenous purified AMPAR NTDs might compete with endogenous NTD-cleft protein interactions, thereby decreasing AMPAR-mediated synaptic transmission, as observed with OE of NTD-deleted receptors (Figure 3.3). This alternative approach enables assessment of the functional effect of AMPAR NTD interactions on endogenous receptors. Organotypic hippocampal slices were treated with 100 nM GluA1-3 NTDs, forming predominantly NTD dimers (Rossmann et al., 2011). Slices were pre-incubated with purified NTDs or buffer solution for 12 hrs to ensure sufficient penetration of protein through the slice before recording. Additionally, 100 nM NTDs were included in the recording solution to prevent wash-out. Due to the large perfusion system volume (20 ml) required for electrophysiological recordings, a relatively low working concentration of 100 nM was chosen, as this was the maximal concentration achievable with the attained quantities of purified protein. To assess changes in excitatory synaptic transmission, AMPAR and NMDAR EPSCs were recorded at -60 mV and +40 mV respectively, recorded at a basal stimulation frequency of 0.2 Hz.

AMPAR/NMDAR (A/N) ratio was measured by recording the AMPAR and NMDAR EPSC, as described previously (Figure 3.2). Application of GluA1 NTDs had no significant effect on the AMPAR or NMDAR EPSC amplitude relative to buffer control (Figure 3.4B1). Similarly, GluA3 NTD application had no significant effect on the size of the AMPAR or NMDAR EPSC (Figure 3.4B3). This suggests that exogenous GluA1 and GluA3 NTDs do not interfere with excitatory synaptic transmission. In contrast however, GluA2 NTD application significantly reduced the AMPAR EPSC amplitude by ~50% relative to buffer control (Figure 3.3B2). With no change detected in the size of the NMDAR EPSC, this effect is measured as a ~50% reduction in the A/N ratio. This suggests that exogenous GluA2 NTDs interfere with endogenous AMPAR-mediated synaptic transmission, potentially by binding to, and occluding, protein interactions with endogenous AMPAR NTDs. Interestingly, these data support findings with OE of NTD-deleted AMPARs, as GluA2Q ΔNTD receptors depress the size of the AMPAR EPSC by ~50% (Figure 3.3).

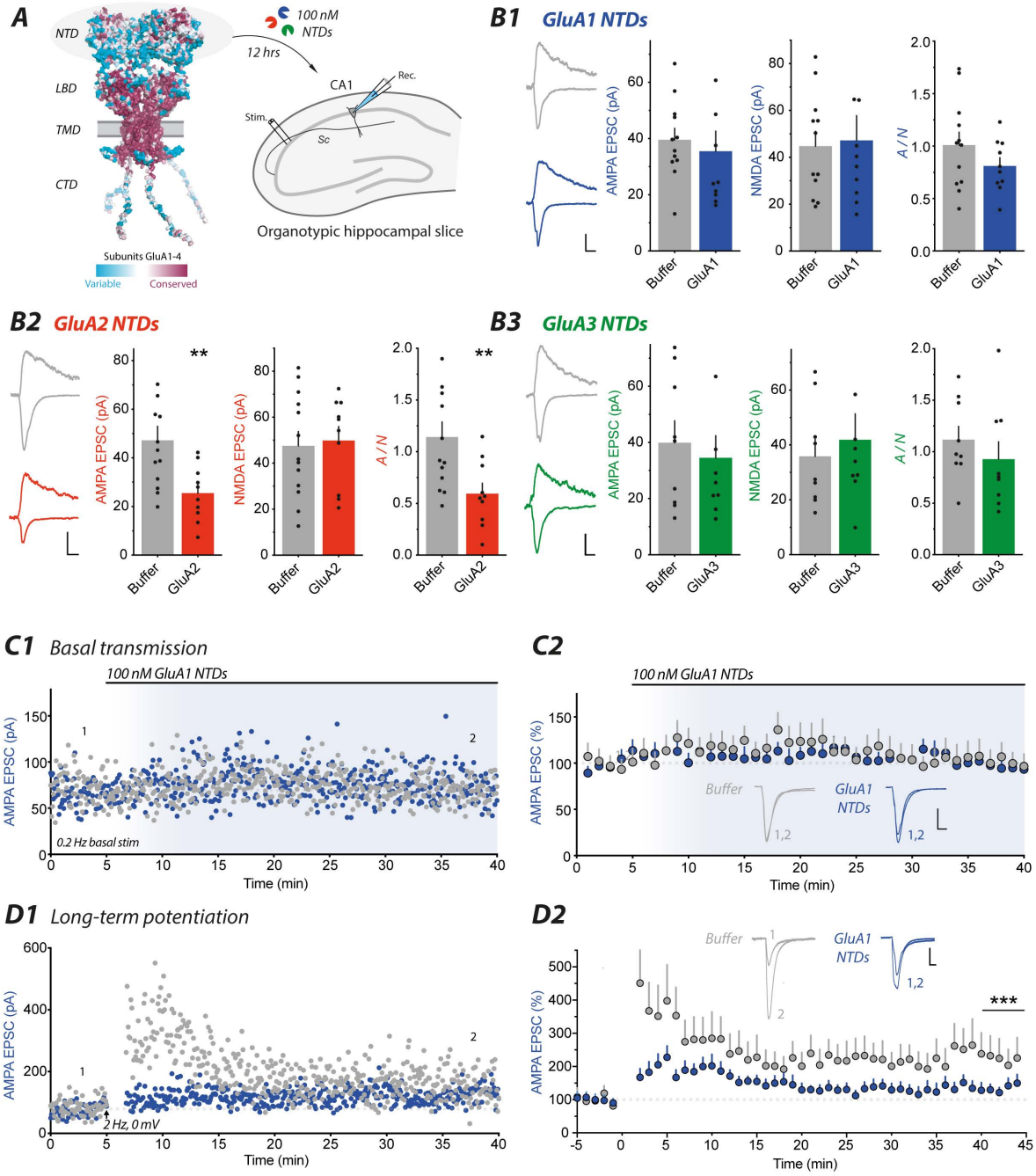

Figure 3.4 *Exogenous application of AMPAR NTDs perturbs excitatory synaptic transmission and plasticity.*

Figure 3.4 ***Exogenous application of AMPAR NTDs perturbs excitatory synaptic transmission and plasticity.*** *(**A**) The AMPAR NTD has a high sequence diversity across AMPAR subunits (sequence conservation map kindly provided by Dr James Krieger). 100 nM purified GluA1-3 NTDs were applied to organotypic hippocampal slices and incubated for 12 hrs before recording in ACSF solution also containing 100 nM NTDs (purified NTDs kindly provided by Dr Veronica Chang). (**B1**) 100 nM GluA1 NTDs had no effect on the amplitude of AMPAR (Buffer = 39.6 ± 4.06 pA; n = 12; GluA1 = 35.5 ± 7.14 pA; n = 10; unpaired t-test, P = 0.61), or NMDAR (Buffer = 44.8 ± 6.3 pA; n = 12; GluA1 = 47.2 ± 10.6 pA; n = 10, unpaired t-test, P = 0.84) EPSCs. GluA1 A/N ratio was unchanged relative to buffer control (Buffer = 1.01 ± 0.13; n = 12 cells; GluA1 = 0.81 ± 0.08; n = 10 cells; n = 3 preparations; unpaired t-test, P = 0.21). (**B2**) 100 nM GluA2 NTDs significantly reduced the amplitude of AMPAR (Buffer = 47.2 ± 5.73 pA; n = 13; GluA2 = 25.5 ± 3.60 pA; n = 10; unpaired t-test, P < 0.01), but not NMDAR EPSCs (Buffer = 47.6 ± 6.24 pA; n = 13; GluA2 = 49.9 ± 6.09 pA; n = 10; unpaired t-test, P = 0.80). GluA2 NTDs significantly reduced the A/N ratio (Buffer = 1.14 ± 0.15; n = 13 cells; GluA2 = 0.59 ± 0.10; n = 10 cells; n = 3 preparations; unpaired t-test, P < 0.01). (**B3**) 100 nM GluA3 NTDs had no effect on the amplitude of AMPAR (Buffer = 39.9 ± 7.8 pA; n = 9; GluA3 = 34.5 ± 7.9; n = 9; unpaired t-test, P = 0.64), or NMDAR (Buffer = 35.8 ± 6.22 pA; n = 9; GluA3 = 41.9 ± 9.47 pA; n = 9; unpaired t-test, P = 0.60) EPSCs. GluA3 A/N ratio was unchanged relative to buffer control (Buffer = 1.11 ± 0.13; n = 9 cells; GluA3 = 0.93 ± 0.17; n = 9 cells; n = 3 preparations; unpaired t-test, P = 0.39). (**C1**) Representative AMPAR EPSC amplitude data. AMPAR EPSC amplitude remained unchanged following 100 nM GluA1 NTDs application recorded at a basal stimulation frequency of 0.2 Hz. (**C2**) Normalised AMPAR EPSC combined data. AMPAR EPSC amplitude in GluA1 NTDs was unchanged relative to buffer control (Buffer = 99.5 ±5.88 %; n = 5; GluA1 = 98.3 ± 2.68 %; n = 3; unpaired t-test, P = 0.89). (**D1**) Representative AMPAR EPSC amplitude data. Long-term potentiation (LTP) was induced by a pairing protocol (2 Hz, 0 mV, 100 s) following a 5 min baseline. AMPAR EPSC amplitude was increased for buffer control slices, but not GluA1 NTD-treated slices. (**D2**) Normalised AMPAR EPSC combined data. LTP was impaired in 100 nM GluA1 NTDs relative to buffer control (Buffer = 221 ± 34.5 %; n = 8 cells; GluA1 = 115 ± 19.4 %; n = 7 cells; n = 3 preparations; unpaired t-test, P < 0.05).*

GluA1 ΔNTD receptors fail to incorporate into CA1 synapses with OE (Figure 3.3E) and GluA1 NTD application has no effect on basal AMPAR-mediated synaptic transmission (Figure 3.4B1). Suggesting the GluA1 NTD has no role in the maintenance of basal synaptic transmission. Interestingly however, the GluA1 NTD appears to be essential for the maintenance of synaptic potentiation (Watson et al., 2017; Díaz-Alonso et al., 2017; Jiang et al., 2021). An interpretation of these results is that the GluA1 NTD positions the receptor at CA1 synapses during synaptic potentiation through direct cleft protein interactions. If this were the case, application of exogenous GluA1 NTDs may compete with NTD interactors, displacing receptor anchoring mechanisms specifically during potentiation. To investigate this hypothesis further, 100 nM GluA1 NTDs were applied to organotypic hippocampal slices during basal transmission (0.2 Hz stimulation) and before the induction of long-term potentiation (LTP) (2 Hz, 0 mV, 100 s induction) (Figure 3.3C/D).

The AMPAR EPSC amplitude of acutely applied buffer and GluA1 NTD-treated slices were unchanged over 30-35 min incubation relative to baseline (Figure 3.4C). These data support those determined using 12 hrs exogenous GluA1 NTD incubation (Figure 3.4B1) and GluA1 ΔNTD receptor OE (Figure 3.3E). Taken together these data indicate that synaptic cleft proteins do not engage the GluA1 NTD during basal transmission at CA1 synapses. To test whether GluA1 NTD interactions were disrupted during synaptic potentiation, LTP was induced in slices pre-treated GluA1 NTDs or buffer (Figure 3.4D). LTP induction resulted in a robust potentiation of the AMPAR EPSC of buffer-treated slices, with responses at ~200% of baseline 40-45 min after stimulation. In the presence of GluA1 NTDs however, initiation and maintenance of LTP was attenuated. These data support findings with OE (Watson et al., 2017) and knockout and replacement (Díaz-Alonso et al., 2017; Jiang et al., 2021) of GluA1 WT and ΔNTD receptors. This suggests that GluA1 NTD interactions may engage with the receptor selectively upon synaptic potentiation.

Collectively these data suggest that the GluA2 NTD is required for basal synaptic transmission and the GluA1 NTD is required for synaptic potentiation at CA1 synapses. This is likely mediated by direct synaptic protein interactions with the AMPAR NTD, influencing receptor positioning at the synapse. To further investigate the influence of GluA1/2 NTDs on sub-synaptic receptor positioning, glutamate spillover experiments were conducted on GluA1/2 WT and ΔNTD expressing cells.

3.2.3 TBOA-induced glutamate spillover at CA1 synapses

To elicit a spillover of glutamate at excitatory synapses, EAAT uptake of neurotransmitter can be prevented using selective pharmacological blockade. EAATs, located on neurons and astrocytes, regulate the uptake of extra-synaptic glutamate and therefore control spillover-mediated activation of extra-synaptic receptors even receptors on neighbouring synapses (Rusakov and Kullmann, 1998; Arnth-Jensen et al., 2002; DiGregorio et al., 2002). To assess glutamate spillover at CA1 synapses a number of electrophysiological parameters were measured in the presence (+TBOA) and absence (-TBOA) of 50 μM DL-TBOA, using a basal stimulation frequency of 0.2 Hz (Figure 3.5).

AMPAR EPSC

Throughout this study, numerous stimulation protocols and TBOA concentrations were applied in an attempt to control the extent of glutamate spillover. In the presence of 50 μM TBOA, the AMPAR EPSC amplitude was increased by ~50% (Figure 3.5A1). This suggests that glutamate spillover elicited by TBOA application results in the activation of AMPARs positioned outside of the PSD (peri- or extra-synaptic), or even on neighbouring synapses. TBOA-induced glutamate spillover exposes synaptic AMPARs to higher concentrations of glutamate over a longer timescale (Hires et al., 2008). As a result, synaptic receptors are more likely to become desensitised in the presence of TBOA. To test this hypothesis, the decay time of AMPAR EPSCs was determined from +TBOA and -TBOA treated slices, however no significant change was detected (Figure 3.5A2). This indicates no change in AMPAR desensitisation with glutamate spillover, consistent with previous reports studying evoked EPSCs (eEPSCs) (Christie and Jahr, 2006). Next, changes in the presynaptic release machinery were assessed using the paired pulse ratio (PPR) and the coefficient of variation (CV). Glutamate spillover and pooling has been shown to activate presynaptic metabotropic glutamate receptors (Scanziani et al., 1997; Sheng et al., 2017b; Mitchell and Silver, 2000), leading to changes in the probability of glutamate release, reflected by a change in the PPR and CV (Malinow and Tsien, 1990; McAllister and Stevens, 2000). To ensure that the presynaptic release machinery is unaltered with 50 μM TBOA application, the PPR was determined by recording two EPSCs with an inter-stimulus interval of 50 ms. The PPR was then calculated using the following equation:

$$PPR = EPSC_2 / EPSC_1$$

CA1 synapses reveal a classical paired pulse facilitation (Figure 3.5A; Zucker et al., 1989; Dobrunz and Stevens, 1997), with no significant changes in PPR of +TBOA relative to -TBOA treated slices (Figure 3.5A3). This suggests that there is no change in the probability of glutamate release with TBOA application. To further confirm these findings, the CV of AMPAR EPSCs was measured in the presence and absence of TBOA. The CV provides a measure of the variability of the synaptic response, dependent on the probabilistic nature of presynaptic glutamate release (Huijstee et al., 2020). The CV measured in 50 μM TBOA was unchanged relative to -TBOA (Figure 3.5A4), indicating no effect of glutamate spillover on the variability of the synaptic response. Taken together, this indicates that the presynaptic release machinery is unaffected by 50 μM DL-TBOA application and 0.2 Hz frequency stimulation.

NMDAR EPSC

TBOA application is commonly used to study the synaptic localisation of NMDARs, where glutamate spillover is required for extra-synaptic NMDAR activation (Diamond et al., 2001; Clark and Cully-Candy, 2002). To confirm these findings in organotypic hippocampal slices, NMDAR EPSCs were recorded in the presence and absence of 50 μM TBOA. The NMDAR EPSC decay time (Figure 3.5C1) and overall synaptic charge (Figure 3.5C2) was significantly increased by ~40% in +TBOA relative to -TBOA. Interestingly, no change was observed in the peak current (measured at 50 ms after the stimulus) of NMDAR EPSCs, consistent with previous reports (Christie and Jahr, 2006). However, delivery of stimulation trains further enhances the significant increase in NMDAR EPSC decay time and synaptic charge (Figure 3.5C3), suggesting glutamate spillover activates extra-synaptic NMDARs. Crucially, this indicates that TBOA application to organotypic hippocampal slices induces robust glutamate spillover at CA1 synapses using both single and pulse-train stimulation to activate extra-synaptic glutamate receptors.

Rectification index

The synaptic rectification index (RI) is commonly used as a measure of AMPAR synaptic trafficking (Hayashi et al., 2000; Shi et al., 2001), as established with AMPAR subunit OE (Figure 3.3). Before measuring the synaptic RI of exogenously expressed AMPARs in the presence of TBOA, the synaptic RI was first determined from endogenous receptors in the absence and presence of

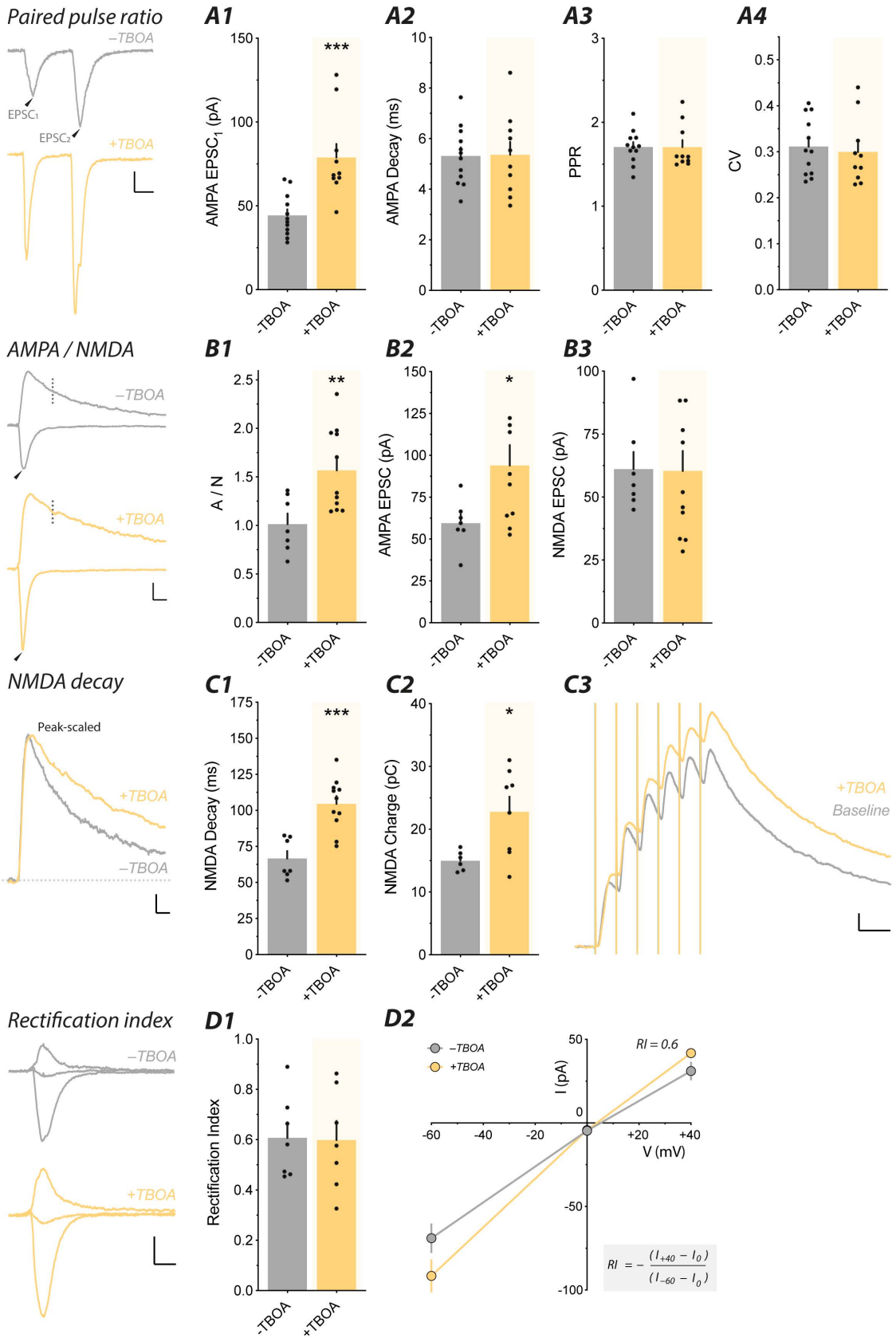

Figure 3.5 *Application of 50 µM DL-TBOA causes glutamate spillover at CA1 synapses.*

Figure 3.5 ***Application of 50 μM DL-TBOA causes glutamate spillover at CA1 synapses.*** *(**A**) PPR measured from slices in the presence and absence of TBOA indicates no change in presynaptic release machinery with glutamate spillover. (**A1**) AMPAR EPSCs were increased in +TBOA relative to -TBOA (-TBOA = 44.3 ± 3.6 pA; n = 12; +TBOA = 78.9 ± 8.1 pA; n = 10; unpaired t-test, P < 0.001). (**A2**) AMPAR EPSC decay time was unchanged (-TBOA = 5.32 ± 0.34 ms; n = 12; +TBOA = 5.36 ± 0.51 ms; n = 10; unpaired t-test, P = 0.94). (**A3**) PPR was unchanged (-TBOA = 1.71 ± 0.05; n = 12; +TBOA = 1.70 ± 0.08; n = 10; unpaired t-test, P = 0.99). (**A4**) Coefficient of variation (CV) was unchanged (-TBOA = 0.30 ± 0.02; n = 12; +TBOA = 1.70 ± 0.08; n = 10; unpaired t-test, P = 0.69). Example traces shown on the left (scale bar = 20 ms; 25 pA). (-TBOA: grey; +TBOA: gold). (**B**) AMPAR EPSCs (arrow; peak amplitude) were selectively increased with glutamate spillover, with no change in NMDAR EPSCs (dotted line; 50 ms after stimulus). (**B1**) AMPAR/NMDAR (A/N) ratio was increased in +TBOA relative to -TBOA (-TBOA = 1.01 ± 0.11; n = 7; +TBOA = 1.57 ± 0.13; n = 11; unpaired t-test, P < 0.01). (**B2**) AMPAR EPSCs were increased in +TBOA relative to -TBOA (-TBOA = 59.5 ± 5.4 pA; n = 7; +TBOA = 93.9 ± 12.2 pA; n = 10; unpaired t-test, P < 0.05). (**B3**) NMDAR EPSCs amplitude was unchanged (-TBOA = 61.1 ± 6.8 pA; n = 7; +TBOA = 60.4 ± 7.9 pA; n = 11; unpaired t-test, P = 0.95). AMPAR EPSC amplitude derived from peak inward current (arrow) recorded at -60 mV. NMDAR EPSC amplitude derived from the outward current at 50 ms post-stimulation (dotted line) recorded at +40 mV (scale bar = 20 ms; 25 pA). (**C**) The overall NMDAR EPSC charge was increased with glutamate spillover. (**C1**) NMDAR EPSC decay time was increased in +TBOA relative to -TBOA (-TBOA = 66.6 ± 5.2 ms; n = 7; +TBOA = 104.5 ± 5.4 ms; n = 11; unpaired t-test, P < 0.001). (**C2**) NMDAR EPSC charge was increased in +TBOA relative to -TBOA (-TBOA = 15.0 ± 0.6 pC; n = 6; +TBOA = 22.7 ± 2.4 pC; n = 8; unpaired t-test, P < 0.05). (**C3**) NMDAR EPSC pulse train (scale bar = 50 ms; 50 pA). Example trace shown on left of peak scaled NMDAR EPSC (scale bar = 10 ms; 20 pA). (**D**) The synaptic RI was unchanged with glutamate spillover. (**D1**) RI was unchanged (-TBOA = 0.61 ± 0.06; n = 7; +TBOA = 0.60 ± 0.08; n = 7; unpaired t-test, P = 0.93). (**D2**) Current-voltage relationship indicates no inward rectification of the synaptic response. Example traces shown on left recorded at -60, 0 and +40 mV (scale bar = 10 ms; 20 pA).*

(-/+TBOA). A concern is that endogenous peri-synaptic calcium-permeable AMPARs may alter the RI at CA1 synapses upon glutamate spillover (He et al., 2009; Yang et al., 2008; Yang et al., 2010), confounding interpretations from this assay. The synaptic RI was recorded from untransfected CA1 pyramidal neurons -/+TBOA, indicating no change in the RI in +TBOA relative to -TBOA (Figure 3.5D). This suggests there is no change in the contribution of calcium-permeable and calcium-impermeable AMPARs to the synaptic response with glutamate spillover. This permits the use of the RI to study TBOA-induced glutamate spillover on exogenous GluA2Q and GluA1 expressing cells.

These parameters validate the use of TBOA as a pharmacological agent to induce glutamate spillover at CA1 synapses, resulting predominantly in the activation of extra-synaptic NMDARs and likely AMPARs on neighbouring synapses. Crucially, the synaptic RI is unchanged in the presence of TBOA, permitting the use of this assay to study the synaptic localisation of exogenous WT and ΔNTD AMPARs.

TBOA wash-in

Following characterisation of synaptic parameters from slices recorded in ACSF continually perfused with -/+TBOA (Figure 3.5), the effect of drug application was then assessed in naïve slices to permit comparison of baseline and drug-perfused responses. As glutamate spillover is sensitive to changes in electrical stimulation intensity of presynaptic fibres (Carter and Regehr, 2000), these experiments were designed to retain the same intensity of stimulation for the duration of the experiment in a paired experimental design, limiting the variability of stimulation intensity experienced across recorded slices. Furthermore, the efficacy of two EAAT transporter inhibitors, DL-TBOA and TFB-TBOA were compared at different concentrations to deduce optimal spillover conditions for studying AMPAR EPSCs. These compounds differ in their selectivity and potency for EAAT 1-3, likely resulting distinct spatio-temporal spillover of glutamate from the synaptic cleft. Bath concentrations were selected based on experimental protocols and IC_{50} values published in the literature (Shimamoto et al., 1998; Shimamoto et al., 2000; Shimamoto et al., 2004).

AMPAR EPSCs were recorded for a baseline of 5 mins before bath application of DL-TBOA using a basal stimulation frequency of 0.2 Hz. A trend wise 5% increase in AMPAR EPSC amplitude was observed with 10 μM DL-TBOA, however no statistical significance was detected

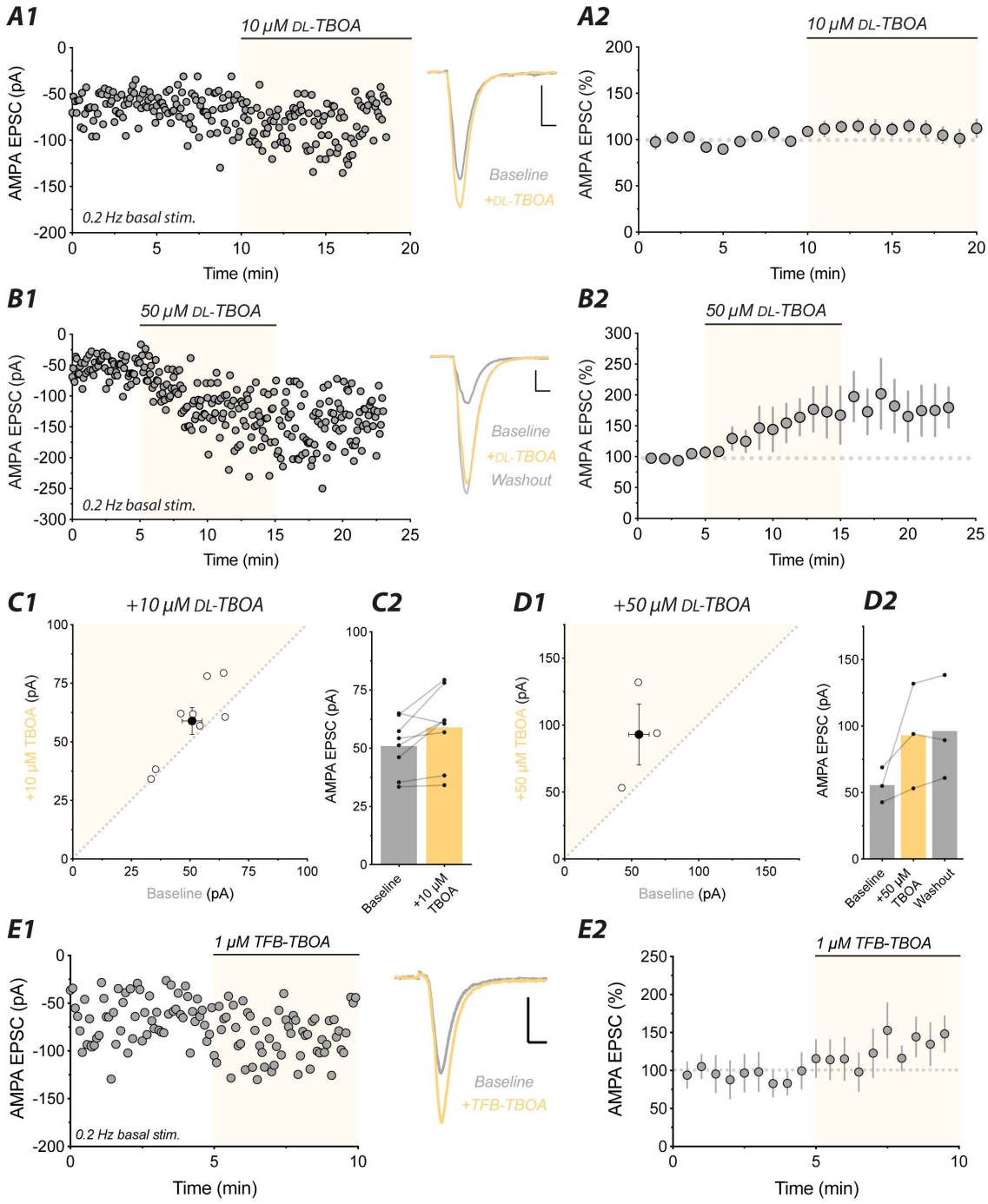

Figure 3.6 *TBOA causes a concentration-dependent increase in AMPAR EPSCs.*

Figure 3.6 ***TBOA causes a concentration-dependent increase in AMPAR EPSCs.*** *(**A**) 10 μM TBOA application had no significant effect on the amplitude of AMPAR EPSCs over time. (**A1**) Representative AMPAR EPSCs recorded at a basal stimulation frequency of 0.2 Hz showed a modest increase in amplitude in 10 μM TBOA relative to baseline. Example average traces shown on the right (scale bar = 10 ms; 20 pA) (Baseline: grey; +TBOA: gold). (**A2**) Normalised AMPAR EPSC combined data. AMPAR EPSC amplitude remained unchanged in the presence of 10 μM TBOA (10-20 min) relative to baseline (0-10 min). AMPAR EPSCs remained unchanged relative to baseline (Baseline: 50.9 ± 4.2 pA; +10 μM TBOA: 54.2 ± 4.9 pA; n = 8; paired t-test, P = 0.37). (**B**) 50 μM TBOA application caused a dramatic increase in the amplitude of AMPAR EPSCs over time. (**B1**). Representative AMPAR EPSCs recorded at a basal stimulation frequency of 0.2 Hz showed an increase in the presence of 50 μM TBOA, which persisted during washout of TBOA relative to baseline. Example average traces shown on the right. (scale bar = 10 ms; 20 pA). (**B2**) Normalised AMPAR EPSC combined data. Average AMPAR EPSC amplitude increased in the presence of 50 μM TBOA (5-15 min) relative to baseline (0-5 min) and persisted during washout of drug (15-20 min). AMPAR EPSCs increased trend wise compared to baseline (Baseline: 55.5 ± 7.6 pA; +50 μM TBOA: ± 7.6 pA; Washout: 96.3 ± 22.6 pA; n = 3; one-way ANOVA, P = 0.19). (**C1**) Scatter plot of AMPAR EPSC amplitude in 10 μM TBOA against baseline indicates no change. (**C2**) AMPAR EPSC amplitude remained unchanged in the presence of 10 μM TBOA relative to baseline. (**D1**) Scatter plot of AMPAR EPSC amplitude in 50 μM TBOA against baseline indicates a trend wise increase. (**D2**) AMPAR EPSC amplitude was increased in 50 μM TBOA and persisted with washout of drug. (**E1**) Representative AMPAR EPSCs recorded in 1 μM TFB-TBOA. TFB-TBOA caused no significant change in AMPAR EPSC amplitude. (**E2**) TFB-TBOA had no effect on AMPAR EPSCs over time (n = 6). (**E2**) Normalised AMPAR EPSC combined data indicates no significant change in the AMPAR EPSC amplitude over time with 1 μM TFB-TBOA application.*

in DL-TBOA (10-20 min) relative to baseline (0-10 min) (Figure 3.6C2). This suggests that 10 μM TBOA-induced glutamate spillover was not sufficient to activate AMPARs outside of the PSD. It has been reported that 10 μM TBOA application produces a 10% increase in the AMPAR EPSC, through activation of peri-synaptic AMPARs (He et al., 2009). The discrepancy between these findings is most likely explained by the use of different basal stimulation frequencies. He et al., (2009) used a lower basal stimulation frequency of 0.033 Hz, thought to only activate a fraction of synaptic AMPARs during basal conditions (Papouin and Oliet, 2014). Thus upon 10 μM TBOA application, AMPARs outside of the PSD (peri- or extra-synaptic) are activated. Higher stimulation frequencies (0.2 Hz) employed in these experiments however, likely activate a proportion of peri-synaptic receptors before drug application, therefore reducing the effect size (~5% increase) observed in the presence of 10 μM TBOA (Figure 3.6C).

To increase the extent of glutamate spillover from the synaptic cleft, 50 μM DL-TBOA was applied to organotypic hippocampal slices and the AMPAR EPSC amplitude was compared relative to baseline. 50 μM TBOA increased the AMPAR EPSC amplitude by 50% following bath application (10-15 min) relative to baseline (0-5 min) (Figure 3.6B2), reaching maximal effect after 10 mins, supporting findings using an unpaired experimental design (Figure 3.5A1). This robust increase persists following 10 mins wash-out of the drug, suggesting EAAT block is irreversible in this slice preparation (Figure 3.6D2). Taken together this suggests that additional peri- or extra-synaptic AMPARs are activated during 50 μM TBOA-induced glutamate spillover. These data support previous reports of peri-synaptic AMPAR activation with glutamate spillover (He et al., 2009; Yang et al., 2008; Yang et al., 2010). Glutamate spillover and subsequent extra- or peri-synaptic AMPAR activation therefore, is concentration-dependent (Figure 3.6).

Finally, selective EAAT 1/2 inhibitor TFB-TBOA was applied at a concentration of 1 μM to elicit glutamate spillover, based on published concentrations (Balmer et al., 2021). Despite reports of a higher potency for EAAT 1/2 (Shimamoto et al., 2004), no significant change in the AMPAR EPSC amplitude was observed (Figure 3.6E). This suggests that glutamate spillover induced by TFB-TBOA (1 μM) is not as extensive as that of DL-TBOA (50 μM). To permit a direct comparison of the extent of glutamate spillover with these two compounds, the same, or IC_{50} concentration must be used for both drugs. However, based on these findings, DL-TBOA (hereafter referred to as TBOA) was used in all experiments at a concentration of 10 or 50 μM, as stated in the text.

Spontaneous EPSCs

A concern with recording evoked EPSCs (eEPSCs) is that glutamate spillover is elicited even before the application of TBOA. Electrical stimulation of eEPSCs at frequencies >0.05 Hz can result in activation of extra-synaptic glutamate receptors (Papouin and Oliet, 2014). Therefore, to activate solely synaptic AMPARs, spontaneous EPSCs (sEPSCs) were recorded, where single quantas of glutamate are released. Substituting Ca^{2+} with Sr^{2+} in the ACSF recording solution induces asynchronous quantal release of glutamate (Oliet et al., 1999), this permits study of synaptic events without the spillover of glutamate onto extra-synaptic AMPARs under basal conditions (-TBOA) (Clark and Cully-Candy, 2002).

In the absence of TBOA, substitution of 4 mM Ca^{2+} with 4 mM Sr^{2+} results in the generation of asynchronous sEPSCs following artificial stimulation at 0.05 Hz (Figure 3.7A1). These events are detected using a template search and analysed for sEPSC amplitude, frequency and decay time. eEPSCs have an amplitude of ~35 pA, whereas sEPSCs have an amplitude of ~10 pA, similar to previous reports (Oliet et al., 1999). Having established recording of sEPSCs, the effect of glutamate spillover was then assessed by addition of 50 μM TBOA into the recording solution.

Slices perfused with 50 μM TBOA similarly, display eEPSCs (~35 pA) and sEPSCs (~11 pA), detectable above a noise level of ~6 pA. Interestingly, 50 μM TBOA application has no effect on the eEPSC amplitude recorded at a basal stimulation frequency of 0.05 Hz (Figure 3.7B2), whereas it produced a ~50% increase in the AMPAR eEPSC amplitude with 0.2 Hz stimulation frequency (Figure 3.5A1; Figure 3.6D2). This suggests that lower stimulation frequencies decrease the extent of glutamate spillover, likely due to an increased amount of time for glutamate to be cleared from the synaptic cleft. These data support the hypothesis that stimulation frequencies of > 0.05 Hz are sufficient to activate extra-synaptic receptors (Papouin and Oliet, 2014). By recording sEPSCs, fewer AMPARs are activated outside of the PSD before TBOA application, allowing for a larger effect size upon drug application.

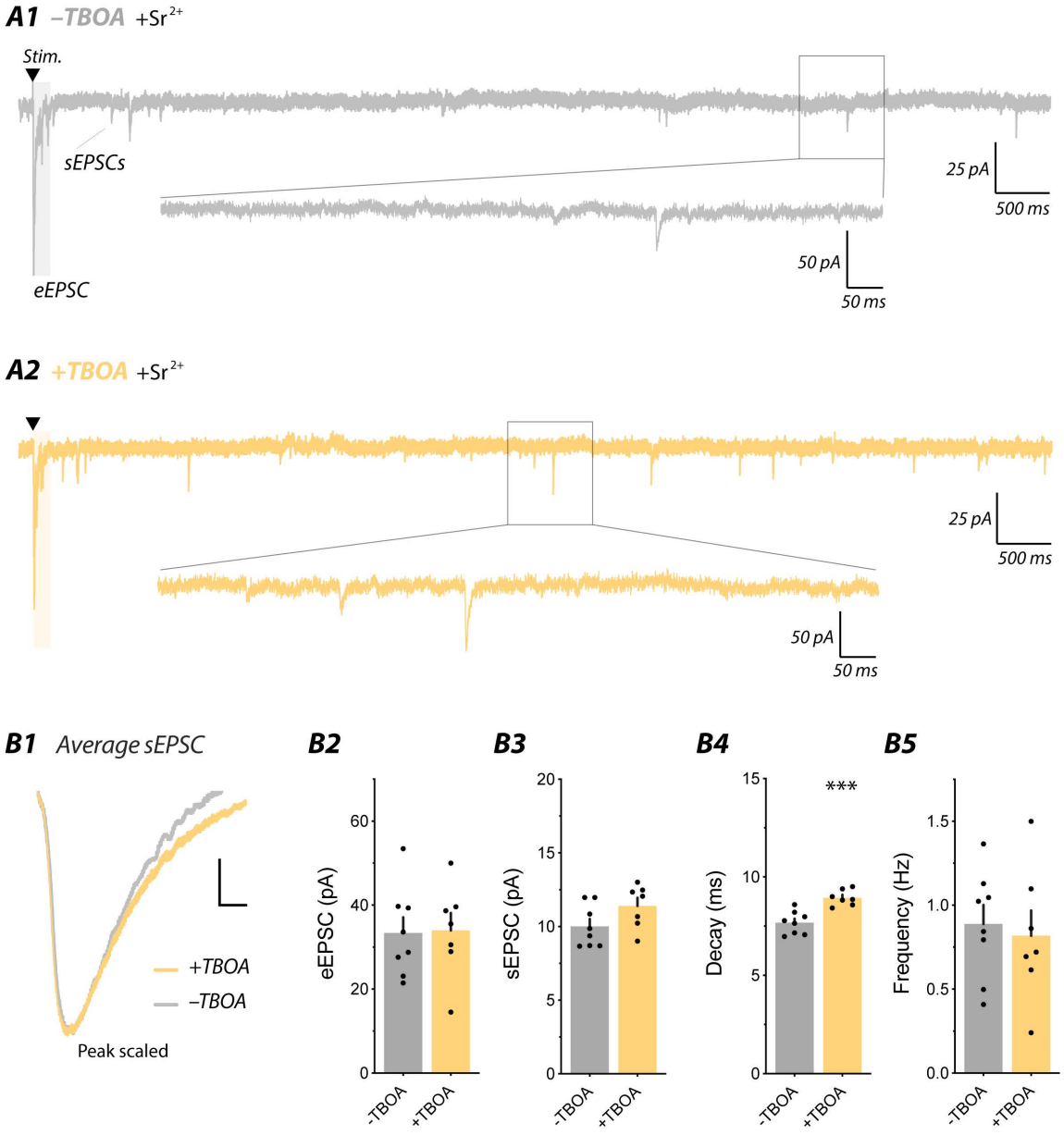

Figure 3.7 *TBOA-induced glutamate spillover increases spontaneous EPSC decay.*

Figure 3.7 ***TBOA-induced glutamate spillover increases spontaneous EPSC decay.*** *(**A**) AMPAR evoked EPSC (eEPSC) and spontaneous EPSC (sEPSC) were elicited by electrical stimulation at a frequency of 0.05 Hz in the presence of ACSF containing 4 mM Mg^{2+} and 4 mM Sr^{2+}. eEPSC amplitude was deduced from the the peak EPSC after the stimulus (black triangle). sEPSCs are detected using a template search of EPSCs occurring 10 ms after the stimulus. (**A1**) -TBOA (grey) and (**A2**) +TBOA (gold) eEPSC and sEPSC example traces from 5 sec sweeps (scale bar = 500 ms; 25 pA) reveal AMPAR EPSCs in zoomed panel (box) (scale bar = 50 ms; 20 pA). (**B1**) Peak scaled average sEPSC from -TBOA and +TBOA conditions (scale bar = 2 ms; 2 pA). (**B2**) eEPSC amplitude was unchanged in +TBOA relative to -TBOA (-TBOA = 33.4 ± 3.7 pA; n = 8; +TBOA = 34.0 ± 4.2 pA; n = 7; unpaired t-test, p = 0.92). (**B3**) sEPSC amplitude was unchanged in +TBOA relative to -TBOA (-TBOA = 10.0 ± 0.50 pA; n = 8; +TBOA = 11.4 ± 0.55 pA; n = 7; unpaired t-test, p = 0.08). (**B4**) sEPSC decay time was significantly increased in +TBOA relative to -TBOA (-TBOA = 7.67 ± 0.21; n = 8; +TBOA = 8.94 ± 0.15; n = 7; unpaired t-test, p < 0.001). (**B5**) sEPSC frequency was unchanged in +TBOA relative to -TBOA (-TBOA = 0.89 ± 0.11 Hz; n = 8; +TBOA = 0.82 ± 0.15 Hz; n = 7; unpaired t-test, p = 0.71).*

Analysis of sEPSCs reveals no significant change in +TBOA sEPSC amplitude relative to -TBOA (Figure 3.7B3). This indicates that spillover of quantal glutamate release does not activate additional receptors more distal to release sites. The frequency of +TBOA events was also found to be unchanged relative to -TBOA (Figure 3.7B5), suggesting no change in the presynaptic release machinery, further to PPR (Figure 3.5A3) and CV (Figure 3.5A4) experiments. However, interestingly the AMPAR EPSC decay time of +TBOA was significantly increased relative to -TBOA (Figure 3.7B4), in line with previous reports studying +TBOA miniature EPSCs (Sanderson et al., 2018). This raises the possibility of an increase in the desensitisation of synaptic AMPARs, likely due to an increased concentration and time-course of glutamate in the synaptic cleft. To test this hypothesis, experiments should be repeated in the presence of desensitisation blocker, cyclothiazide, to assess if the increase in AMPAR EPSC decay time can be abolished. These results further highlight the physiological importance of glutamate uptake transporters in shaping the time-course of synaptic transmission (Overstreet et al., 1999).

In these experiments, TBOA-induced glutamate spillover resulted in a broadening of the sEPSC waveform, likely due to increased desensitisation of synaptic AMPARs. sEPSCs permit recording of AMPARs within the PSD only, beneficial for detecting changes in sub-synaptic receptor positioning. However, the effect size on decay time induced by glutamate spillover is marginal, making it difficult to detect changes with WT and ΔNTD receptor expression using this assay.

3.2.4 Pulse train-evoked glutamate spillover

To test the limits of glutamate spillover at CA1 synapses in the hippocampus, continuous 50 μM TBOA perfusion was combined with delivery of trains of electrical stimulation (Figure 3.8). Pulse-train stimulation in combination with TBOA application greatly increases the spatio-temporal spillover of glutamate (Hires et al., 2008; Armbruster et al., 2016; Pinky et al., 2018). The intention of these experiments was to elicit maximal spillover of glutamate onto extra-synaptic receptors (Anderson et al., 2015) and neighbouring synapses (DiGregorio et al., 2002; Nietz et al., 2017), before applying this protocol to cells expressing exogenous AMPARs. Therefore, testing the hypothesis of ‘mis-placed’ exogenous NTD-deleted AMPARs.

Endogenous AMPARs

To determine the effect of glutamate spillover induced by pulse-train stimulation, 6 pulses were delivered to schaffer collateral fibers at a pulse-train frequency of 30 and 50 Hz in combination with 10 μM TBOA. This protocol was based on previous publications, where pulse-trains significantly increase the spatio-temporal spillover of glutamate (Hires et al., 2008; Armbruster et al., 2016; Pinky et al., 2018). The resultant EPSC amplitudes were then plotted against pulse number in the absence and presence of TBOA (Figure 3.8). -TBOA slices exhibited a paired pulse facilitation of AMPAR EPSCs in response to 30 Hz train stimulation, attributed to short-term plasticity mechanisms (Jackman and Regehr, 2017). Interestingly, +TBOA AMPAR EPSC amplitude was significantly increased relative to -TBOA (Figure 3.8A3), and these responses were completely abolished in the presence of AMPAR antagonist, NBQX (Figure 3.8A; black trace). The increase in AMPAR EPSC amplitude observed with +TBOA was further accentuated with 50 Hz train stimulation (Figure 3.8B). These data suggest that pulse-train stimulation in combination with TBOA application activates additional AMPARs localised at extra-synaptic sites or on neighbouring synapses. Normalised EPSC versus pulse number scatter plots provide a measure of the extent of receptor activation with increasing glutamate spillover (Figure 3.8). Therefore, the resultant profile of these plots can be used to detect the sub-synaptic distribution of receptors, with more distal receptors being activated after increasing pulse numbers. This validates the use of this protocol for inducing glutamate spillover onto extra-synaptic or neighbouring synaptic AMPARs. The purpose of this protocol is to test the limit of exogenous receptor localisation, as it is possible that NTD-deleted AMPARs are positioned extra-synaptically on hippocampal dendrites.

Increasing the stimulation intensity of presynaptic inputs resulted in a significant increase in the AMPAR EPSC, changing the profile of the normalised EPSC response (Figure 3.8C). This suggests that pulse-train stimulation-induced glutamate spillover experiments are sensitive to changes in stimulation intensity, as previously reported (Carter and Regehr, 2000). These findings are imperative for the study of exogenously expressed AMPARs, as the response of transfected cells must therefore be directly compared to a pairwise untransfected cell. This will ensure comparable levels of stimulation input to each CA1 pyramidal neuron.

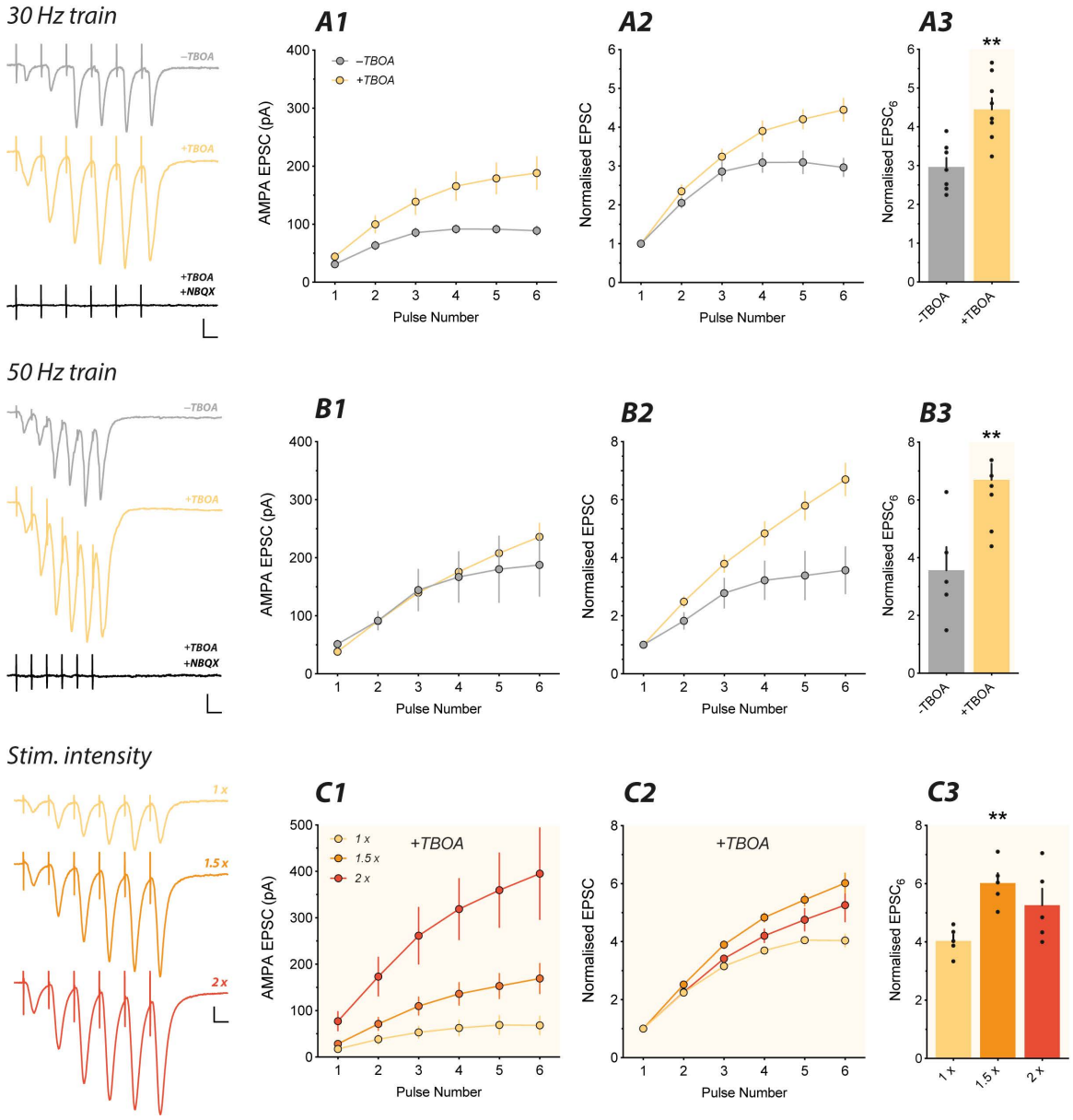

Figure 3.8 *Pulse-train stimulation enhances TBOA-induced glutamate spillover.*

Figure 3.8 ***Pulse-train stimulation enhances TBOA-induced glutamate spillover.*** *(**A**) AMPAR EPSCs were dramatically increased in the presence of 10 μM TBOA with 30 Hz train stimulation. Pulse-train responses were abolished in the presence of AMPAR antagonist, NBQX (black). (**A1**) AMPAR EPSC amplitude increased with pulse number (-TBOA: $EPSC_1$ = 31.0 ± 3.2 pA; $EPSC_6$ = 88.9 ± 7.5 pA; n = 7; +TBOA: $EPSC_1$= 44.1 ± 6.7 pA; $EPSC_6$ = 188.2 ± 26.3 pA; n = 8). (**A2**) Normalised EPSC indicates a greater increase in the AMPAR EPSC with +TBOA relative to -TBOA (-TBOA: 2-fold increase; +TBOA: 3.5-fold increase). (**A3**) Summary of normalised AMPAR EPSC indicates a greater increase in +TBOA relative to -TBOA (-TBOA: 2.97 ± 0.23; n = 7; +TBOA: 4.45 ± 0.29; n = 8; unpaired t-test, P < 0.001). Example 30 Hz train stimulation traces shown on the left (scale bar = 20 ms; 50 pA) (-TBOA: grey; +TBOA: gold; +TBOA +NBQX: black). (**B**) AMPAR EPSCs were vastly increased in the presence of 10 μM TBOA with 50 Hz train stimulation. (**B1**) AMPAR EPSC amplitude increased with pulse number (-TBOA: $EPSC_1$ = 51.2 ± 6.1 pA; $EPSC_6$ = 187.6 ± 48.1 pA; n = 5; +TBOA: $EPSC_1$ = 38.3 ± 6.2 pA; $EPSC_6$ = 235.9 ± 21.9 pA; n = 8). (**B2**) Normalised EPSC indicates a greater increase in the AMPAR EPSC with +TBOA relative to -TBOA (-TBOA: 2.5-fold increase; +TBOA: 6-fold increase). (**B3**) Summary of normalised AMPAR EPSC indicates a greater increase in +TBOA relative to -TBOA (-TBOA: 3.57 ± 0.80; n = 5; +TBOA: 6.70 ± 0.56; n = 8; unpaired t-test, P < 0.001). Example 50 Hz train stimulation traces shown on the left (scale bar = 20 ms; 50 pA) (-TBOA: grey; +TBOA: gold; +TBOA +NBQX: black). (**C**) Electrical stimulation intensity affected AMPAR EPSC amplitude with increasing pulse number. (**C1**) AMPAR EPSC amplitude was increased with increasing stimulation intensity and pulse number (1x: $EPSC_1$ = 17.2 ± 2.4 pA; $EPSC_6$ = 68.4 ± 8.8 pA; 1.5x: $EPSC_1$ = 28.3 ± 2.5 pA; $EPSC_6$ = 169.2 ± 14.4 pA 2x: $EPSC_1$ = 77.1 ± 9.2 pA; $EPSC_6$ = 395.2 ± 44.0 pA ; n = 5). (**C2**) Normalised EPSC indicates a greater increase with 1.5x stimulation intensity relative to 1x (1x: 3-fold increase; 1.5x: 5-fold increase; 2x: 4.5-fold increase). (**C3**) Summary of normalised AMPAR EPSC indicates a greater increase with 1.5x stimulation intensity relative to 1x (1x: 4.04 ± 0.22; 1.5x: 6.02 ± 0.34; 2x: 5.26 ± 0.57; n = 5; one-way ANOVA, P < 0.01). Example 30 Hz train stimulation traces shown on the left (scale bar = 20 ms; 50 pA) (1x: gold; 1.5x: organge; 2x: red).*

GluA2Q WT and ΔNTD receptors

Single recording

Having established the compound (DL-TBOA), concentration (10 and 50 μM) and electrical stimulation protocols (single or pulse-train) on endogenous receptors, experiments were then performed on CA1 pyramidal neurons expressing exogenous GluA2Q receptors. GluA2Q full-length (WT) and NTD-deleted (ΔNTD) receptors were introduced into CA1 pyramidal neurons by SCE transfection.

30 Hz pulse-train stimulation in combination with 10 μM TBOA application was first utilised on GluA2Q WT and ΔNTD expressing cells. Interestingly, the normalised AMPAR EPSC amplitude of GluA2Q WT was decreased with increasing pulse number relative to untransfected slices (Figure 3.9A2), although statistical significance was not observed at $EPSC_6$ (Figure 3.9A3). Conversely, GluA2Q ΔNTD expressing cells exhibited an increased normalised AMPAR EPSC amplitude with increasing pulse number relative to untransfected control slices (Figure 3.9A2), although not statistically significant (Figure 3.9A3). These trend wise effects were further emphasised using 50 Hz pulse-train stimulation, where the extent of glutamate spillover is increased (Figure 3.8B). These effects are intriguing, as they suggest that a larger spillover of glutamate induced by increasing pulse-train frequency increases the number of GluA2Q ΔNTD receptors activated, whereas GluA2Q WT activation decreases. This fits with the hypothesis of GluA2Q ΔNTD receptors being localised more distally on the postsynaptic neuron (Figure 3.1A).

However, these recordings should be interpreted with caution, as the stimulation intensity can profoundly affect the extent of glutamate spillover (Figure 3.8C). Therefore, variation in the stimulation intensity used between slices in this unpaired experimental design has the potential to affect the outcome of these results. To overcome this limitation, these experiments were repeated using dual whole-cell recording of untransfected (GFP-) and transfected (GFP+) CA1 pyramidal neurons (established in Figure 3.2), to ensure comparable levels of stimulation intensity input, permitting paired experimental design and statistics (Figure 3.10).

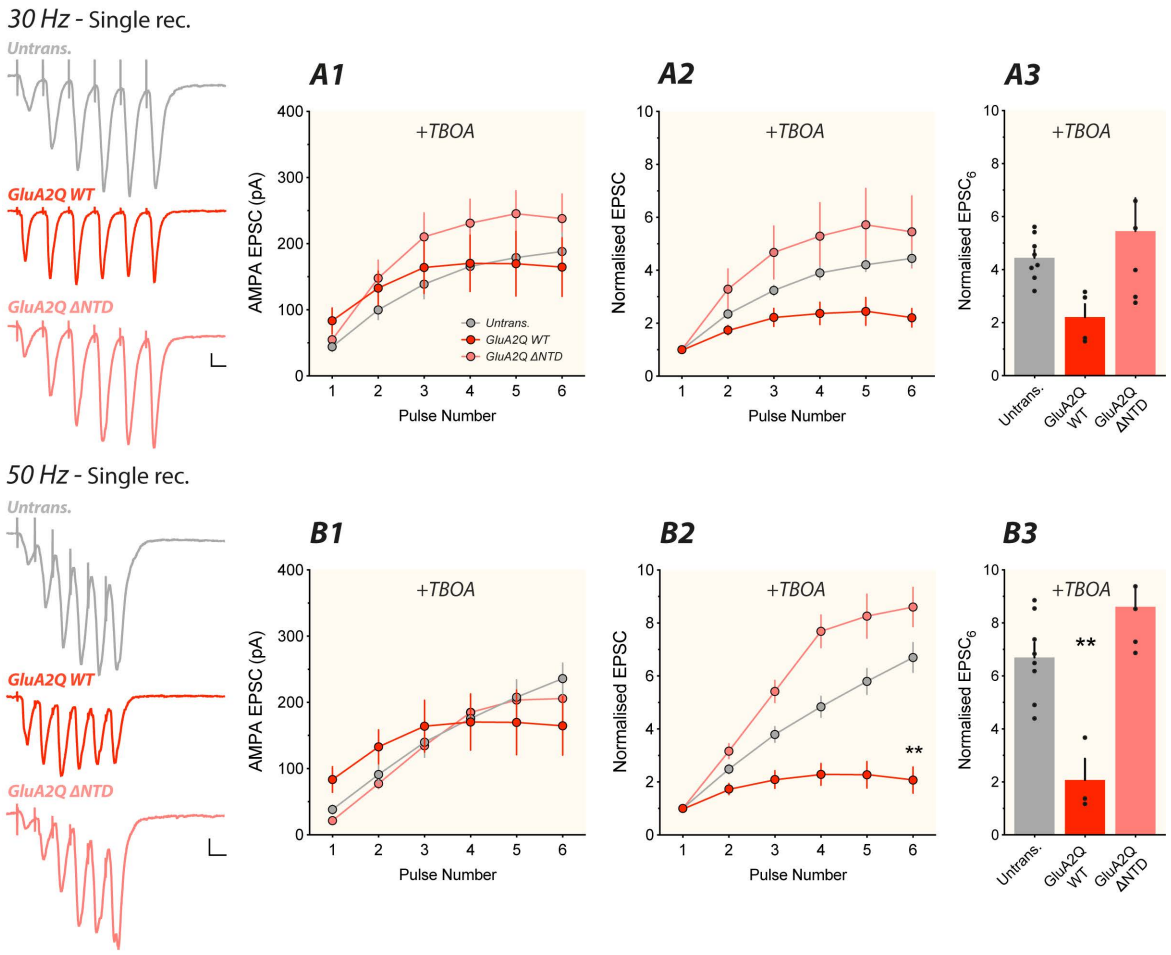

Figure 3.9 *Single recording indicates NTD-dependent sub-synaptic positioning with pulse train-evoked glutamate spillover.*

Figure 3.9 ***Single recording indicates NTD-dependent sub-synaptic positioning with pulse train-evoked glutamate spillover.*** *(**A**) GluA2Q WT receptors were saturated whereas GluA2Q ΔNTD receptors were activated by 30 Hz glutamate spillover. (**A1**) GluA2Q WT, GluA2Q ΔNTD and Untrans. AMPAR EPSCs were all increased with increasing pulse number. (**A2**) GluA2Q WT and GluA2Q ΔNTD AMPAR EPSCs were decreased and increased respectively relative to Untrans. (**A3**) Summary of normalised AMPAR EPSC indicates a modest increase in GluA2Q ΔNTD and a modest decrease in GluA2Q relative to Untrans. cells (Untrans. = 4.45 ± 0.29; n = 8; GluA2Q = 2.21 ± 0.49; n = 4; GluA2Q ΔNTD = 5.46 ± 1.24; n = 6; one-way ANOVA, P = 0.13). (**B**) GluA2Q WT receptors were saturated while GluA2Q ΔNTD receptors were activated by 50 Hz glutamate spillover. (**B1**) GluA2Q WT AMPAR EPSCs were saturated by 50 Hz glutamate spillover (Untrans. = $EPSC_1$ = 38.3 ± 6.2 pA; $EPSC_6$ = 235.9 ± 21.9 pA; n = 8; GluA2Q = $EPSC_1$ = 83.6 ± 16.7 pA; $EPSC_6$ = 164.7 ± 38.4 pA; n = 3; GluA2Q ΔNTD = $EPSC_1$ = 22.0 ± 4.1 pA; $EPSC_6$ = 213.1 ± 11.7 pA; n = 6). (**B2**) GluA2Q WT AMPAR EPSCs were decreased and GluA2Q ΔNTD AMPAR EPSCs were increased relative to Untrans. cells (GluA2Q WT: 3-fold decrease; GluA2Q ΔNTD: 2-fold increase). (**B3**) Summary of normalised AMPAR EPSC indicates a modest increase in GluA2Q ΔNTD and a significant decrease in GluA2Q WT relative to Untrans. cells (Untrans. = 6.70 ± 0.56; n = 8; GluA2Q WT = 2.07 ± 0.80; n = 3; GluA2Q ΔNTD = 8.60 ± 0.74; n = 5; one-way ANOVA, P < 0.01).*

Dual recording

Exogenous GluA2Q WT and ΔNTD receptors were expressed in CA1 pyramidal neurons using SCE transfection and the functional output was recorded by dual whole-cell recording in response to 30 and 50 Hz pulse-train stimulation +10 μM TBOA (Figure 3.10).

30 and 50 Hz pulse-train stimulation significantly increased GluA2Q WT AMPAR EPSC amplitude with increasing pulse number (Figure 3.10A/B). The normalised AMPAR EPSC amplitude was increased trend wise by $EPSC_6$ relative to untransfected cells, however, no statistical significance was observed (Figure 3.10A3/B3). Similarly, GluA2Q ΔNTD AMPAR EPSC amplitude was modestly increased relative to paired untransfected cells (Figure 3.10C/D), however no statistical significance was detected (Figure 3.10C3/D3). Surprisingly, these findings differ to those observed using single recording (Figure 3.9). The most apparent explanation for the discrepancy between these data is the variability in stimulation intensity experienced with single whole-cell recording across different slices (Figure 3.8C). Whilst dual whole-cell recording permits similar stimulation intensity input to pairs of cells (Figure 3.10), single recording results in differential stimulation intensity across conditions. Whilst the stimulation intensity can be controlled to an extent on the stimulator (Digitimer DS3 Constant Current Stimulator), this level must be adjusted depending on exogenous AMPAR expression levels across slices and conditions.

These findings therefore, suggest that extensive glutamate spillover with pulse-train stimulation +TBOA does not activate additional GluA2Q WT or ΔNTD receptors at extra-synaptic sites.

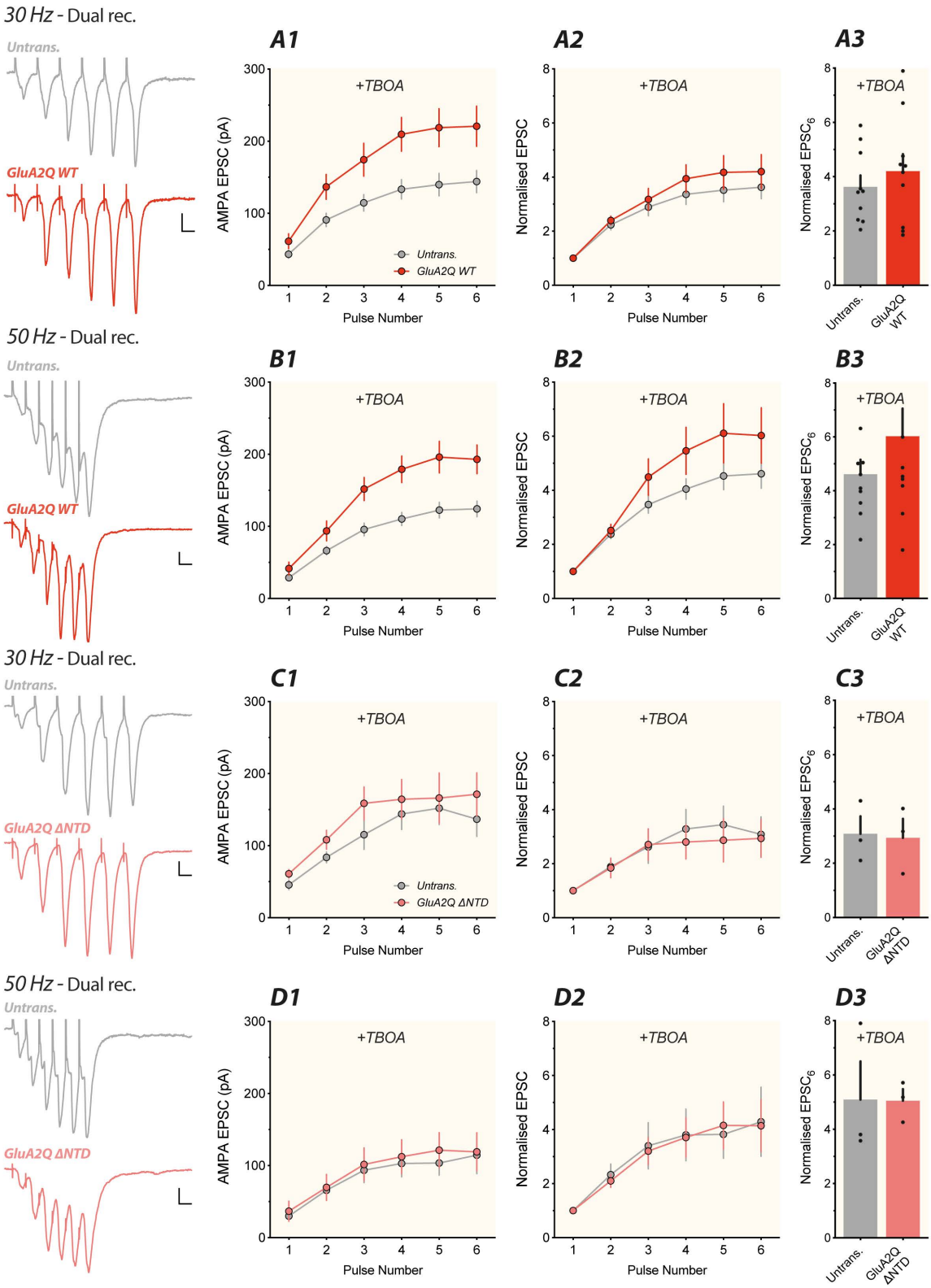

Figure 3.10 *Dual recordings indicate no change in GluA2Q AMPAR EPSCs with pulse train-evoked glutamate spillover.*

Figure 3.10 ***Dual recordings indicate no change in GluA2Q AMPAR EPSCs with pulse train-evoked glutamate spillover.*** *(**A**) 30 Hz glutamate spillover resulted in no change in GluA2Q WT AMPAR EPSCs relative to Untrans. (**A1**) GluA2Q WT AMPAR EPSCs were increased to a greater extent relative to Untrans. with increasing pulse number (Untrans. = $EPSC_1$ = 43.2 ± 5.5 pA; $EPSC_6$ = 144.0 ± 15.4 pA; GluA2Q = $EPSC_1$ = 61.2 ± 10.3 pA; $EPSC_6$ = 220.7 ± 27.8 pA; n = 10 pairs). (**A2**) 30 Hz normalised EPSC amplitudes remained unchanged from GluA2Q WT relative to Untrans. (**A3**) Summary of normalised AMPAR EPSC indicates no change in GluA2Q WT compared to Untrans. (Untrans. = 3.63 ± 0.42; GluA2Q WT = 4.20 ± 0.63; n = 10; paired t-test; P = 0.30). (**B**) 50 Hz glutamate spillover resulted in no change in GluA2Q WT AMPAR EPSCs relative to Untrans. (**B1**) GluA2Q WT AMPAR EPSCs were increased to a greater extent than Untrans. (Untrans. = $EPSC_1$ = 28.9 ± 2.8 pA; $EPSC_6$ = 124.2 ± 10.9 pA; GluA2Q WT = $EPSC_1$ = 41.6 ± 8.8; $EPSC_6$ = 192.9 ± 19.9; n = 10 pairs). (**B2**) 50 Hz normalised EPSC amplitude of GluA2Q WT remained unchanged relative to Untrans. (**B3**) Summary of normalised AMPAR EPSC indicates no change in GluA2Q WT relative to Untrans. cells (Untrans. = 4.61 ± 0.53; GluA2Q WT = 6.03 ± 1.03; n = 10; paired t-test; P = 0.22). (**C**) 30 Hz glutamate spillover had no significant effect on GluA2Q ΔNTD AMPAR EPSCs relative to Untrans. (**C1**) GluA2Q ΔNTD AMPAR EPSCs remain unchanged relative to Untrans. (Untrans. = $EPSC_1$ = 45.6 ± 6.6 pA; $EPSC_6$ = 136.7 ± 23.8 pA; GluA2Q ΔNTD = $EPSC_1$ = 60.9 ± 5.9 pA; $EPSC_6$ = 171.3 ± 29.8 pA; n = 3 pairs). (**C2**) 30 Hz normalised EPSC amplitudes were unchanged from Untrans. (**C3**) Summary of normalised AMPAR EPSC indicates no significant change (Untrans. = 3.08 ± 0.65; GluA2Q ΔNTD = 2.94 ± 0.70; n = 3; paired t-test; P = 0.85). (**D**) 50 Hz glutamate spillover had no significant effect on GluA2Q ΔNTD AMPAR EPSCs. (**D1**) GluA2Q ΔNTD AMPAR EPSCs remain unchanged compared to Untrans. (Untrans. = $EPSC_1$ = 24.6 ± 3.6 pA; $EPSC_6$ = 124.1 ± 33.7 pA; GluA2Q ΔNTD = $EPSC_1$ = 23.5 ± 6.1 pA; $EPSC_6$ = 122.9 ± 37.0 pA; n = 3 pairs). (**D2**) 50 Hz normalised EPSC amplitudes were unchanged from Untrans. (**D3**) Summary of normalised AMPAR EPSC indicates no significant change (Untrans. = 5.10 ± 1.4; GluA2Q ΔNTD = 5.05 ± 0.43; n = 3; paired t-test; P = 0.98).*

Glutamate spillover induced by pulse-train stimulation did not affect the AMPAR EPSC of GluA2Q WT or GluA2Q ΔNTD receptors with increasing pulse number (Figure 3.10). Additionally, the PPR of GluA2Q WT and GluA2Q ΔNTD remained unchanged relative to paired untransfected cells (Figure 3.11A). However, an curious observation was made during these recordings. In the presence of TBOA, $EPSC_1$ of GluA2Q ΔNTD expressing cells was increased trend wise (Figure 3.11C1), opposed to decreased, as observed in -TBOA in this study (Figure 3.2A2) and other publications (Watson et al., 2017; Díaz-Alonso et al., 2017; Watson et al., 2020). This lead to the hypothesis that single pulse stimulation +TBOA causes sufficient glutamate spillover onto peri-synaptic GluA2Q ΔNTD receptors. To investigate this further, experiments were then conducted using 0.2 Hz basal stimulation in the presence of 50 μM TBOA to further increase glutamate spillover (Figure 3.12).

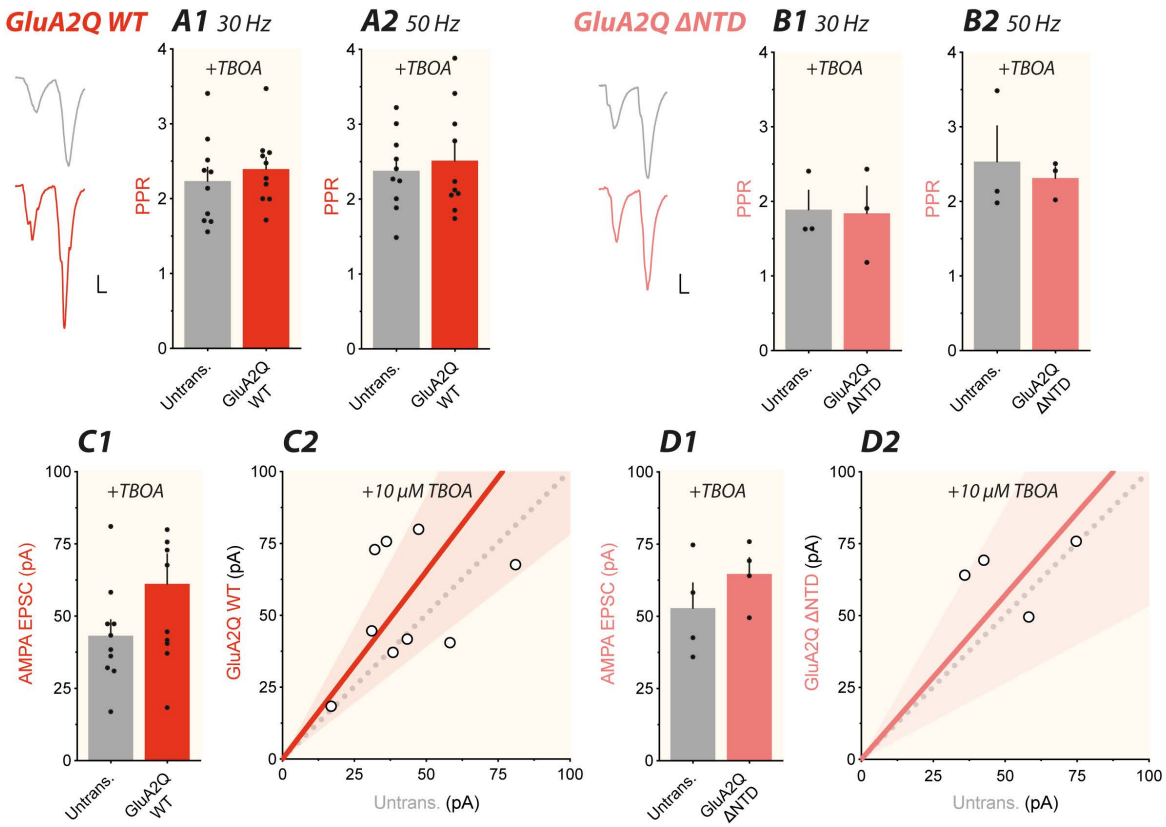

Figure 3.11 ***10 μM TBOA-induced glutamate spillover enhances NTD-deleted GluA2Q EPSC$_1$ amplitude.*** *(**A**) GluA2Q WT paired pulse ratio was unchanged relative to Untrans. (**A1**) GluA2Q WT PPR was unchanged with 30 Hz stimulation (Untrans. = 2.24 ± 0.18; GluA2Q WT = 2.40 ± 0.15; n = 10; paired t-test; P = 0.27) and (**A2**) 50 Hz stimulation (Untrans. = 2.38 ± 0.17; GluA2Q ΔNTD = 2.52 ± 0.23; n = 10; paired t-test; P = 0.55). Example traces of Untrans. (grey) and GluA2Q WT (red) shown on the left (scale bar = 10 ms; 20 pA). (**B**) GluA2Q ΔNTD paired pulse ratio was unchanged relative to Untrans. indicating no change in presynaptic release machinery in 10 μM +TBOA. (B1) GluA2Q ΔNTD PPR was unchanged with 30 Hz stimulation (Untrans. = 3.08 ± 0.65; GluA2Q ΔNTD = 2.94 ± 0.70; n = 3; paired t-test; P = 0.85) and (**B2**) 50 Hz stimulation (Untrans. = 5.10 ± 1.41; GluA2Q ΔNTD = 5.05 ± 0.43; n = 3; paired t-test; P = 0.98). Example traces shown on the left (scale bar = 10 ms; 20 pA) (Untrans.: grey; GluA2Q ΔNTD: pink). (**C1**) GluA2Q WT and (**D1**) GluA2Q ΔNTD AMPAR EPSCs were modestly increased in 10 μM TBOA. (**C2**) Scatter plot of GluA2Q WT versus Untrans. and (**D2**) GluA2Q ΔNTD versus Untrans. indicate a modest increase in the AMPAR EPSC.*

3.2.5 Single stimulation-evoked glutamate spillover

GluA2Q WT and ΔNTD receptors

To further investigate the trend wise increase in AMPAR EPSC amplitude observed with GluA2Q ΔNTD in 10 μM TBOA (Figure 3.11), further experiments were performed using a concentration of 50 μM TBOA, to increase the extent of glutamate spillover. Experiments were designed by blinding both construct expression (GluA2Q WT and ΔNTD) and ACSF solutions (-TBOA and +TBOA). These 4 experimental conditions were then recorded from 6 independent preparations and analysed before unblinding conditions.

The synaptic RI of GluA2Q WT and GluA2Q ΔNTD was significantly reduced relative to untransfected cells indicating successful synaptic trafficking of GluA2Q homomers and remained unchanged in +TBOA perfused slices (Figure 3.12A1/B1). GluA2Q ΔNTD AMPAR EPSC amplitude was however, not reduced by ~50%, as reported previously (Watson et al., 2017). An explanation for this discrepancy is that the SCE transfection efficiency was variable in these experiments. However, the RI indicates that the receptor is successfully incorporated into CA1 synapses (Figure 3.12B1). Experiments should be repeated with robust construct expression to accurately assess the effect of glutamate spillover onto GluA2Q WT and ΔNTD receptors.

The AMPAR EPSC amplitude of GluA2Q WT expressing cells was increased by ~50% in -TBOA and +TBOA relative to paired untransfected cells (Figure 3.12C1). This indicates no peri-synaptic GluA2Q WT receptor activation with glutamate spillover, as hypothesised (Figure 3.1A). GluA2Q ΔNTD AMPAR EPSC amplitude however, is modestly decreased in -TBOA and increased in +TBOA relative to paired untransfected cells (Figure 3.12C2). No statistical significance is observed in these experiments, but trend of these results fits the hypothesis of peri-synaptic ΔNTD receptor activation with glutamate spillover (Figure 3.1A).

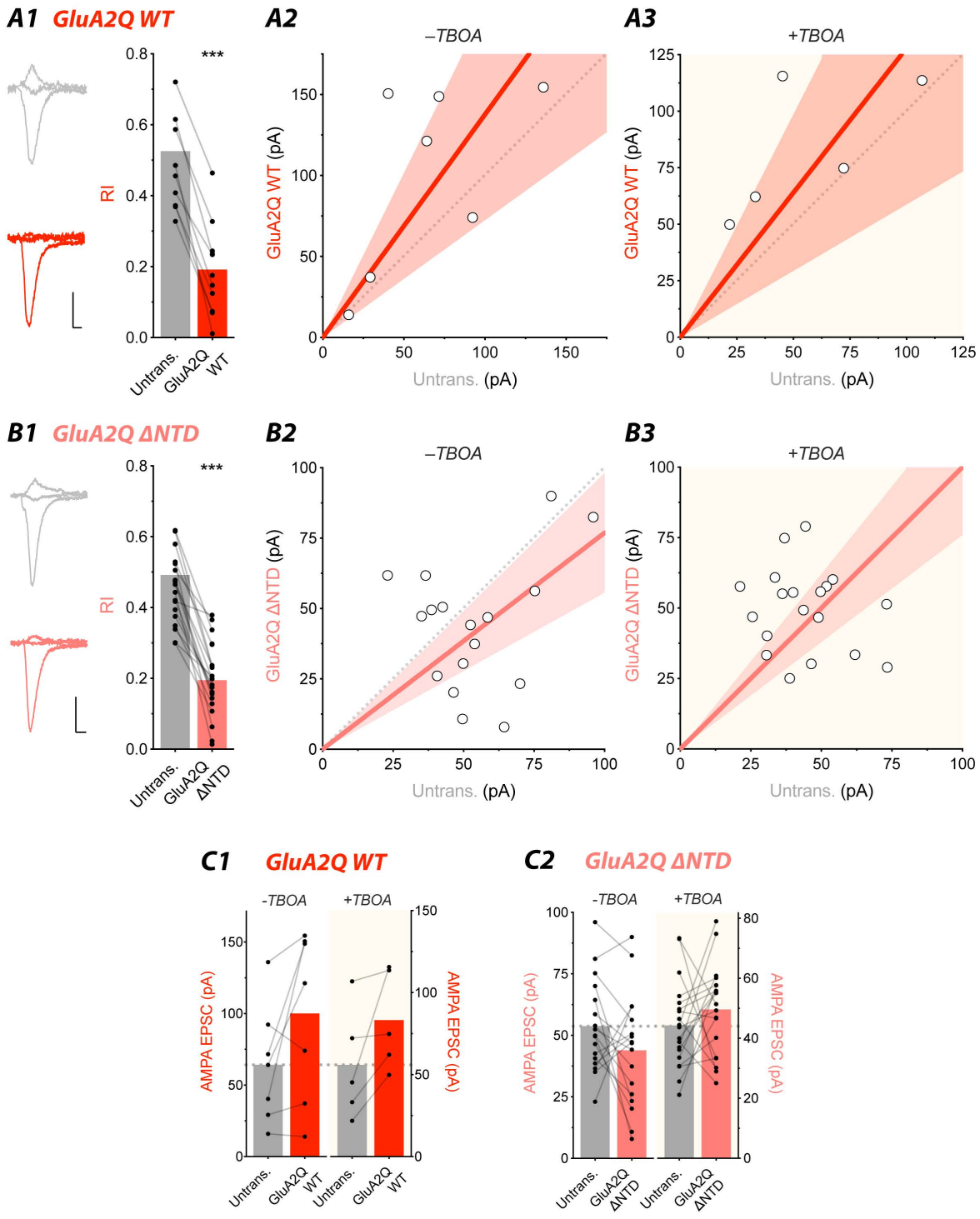

Figure 3.12 *50 µM TBOA-induced glutamate spillover has no effect on WT or NTD-deleted GluA2Q EPSC amplitude.*

Figure 3.12 ***50 μM TBOA-induced glutamate spillover has no effect on WT or NTD-deleted GluA2Q EPSC amplitude.*** *(**A**) GluA2Q incorporates into CA1 synapses and enhances the AMPAR EPSC in the absence and presence of 50 μM +TBOA. (**A1**) Synaptic RI of GluA2Q WT was significantly reduced relative to Untrans. (Untrans. = 0.53 ± 0.06; GluA2Q WT = 0.19 ± 0.04; n = 10; paired t-test; P < 0.001). Example traces shown on the left, recorded at -60, 0 and +40 mV. (scale bar = 10 ms; 20 pA) (Untrans.: grey; GluA2Q WT: red). (**A2**) GluA2Q WT EPSCs were modestly increased in -TBOA (Untrans. = 64.2 ± 15.5 pA; GluA2Q WT = 100.1 ± 22.0 pA; n = 7; paired t-test; P = 0.09) and +TBOA (Untrans. = 55.9 ± 15.3 pA; GluA2Q WT = 83.2 ± 13.4 pA; n = 5; paired t-test; P = 0.09). (**A3**) Scatter plots indicate GluA2Q WT AMPAR EPSCs were increased relative to Untrans. in -TBOA and +TBOA. (**B**) GluA2Q ΔNTD incorporates into CA1 synapses and causes a modest change in the AMPAR EPSC amplitude. (**B1**) RI of GluA2Q ΔNTD was significantly lower than Untrans. cells indicating synaptic incorporation (Untrans. = 0.49 ± 0.03; GluA2Q ΔNTD = 0.19 ± 0.02; n = 21; paired t-test; P < 0.001). Example traces shown on the left, recorded at -60, 0 and +40 mV. (scale bar = 10 ms; 20 pA) (Untrans.: grey; GluA2Q ΔNTD: pink). GluA2Q ΔNTD EPSCs were modestly decreased in -TBOA (Untrans.: 53.8 ± 4.5 pA; GluA2Q ΔNTD: 43.9 ± 5.6 pA; n = 17; paired t-test; P = 0.12) and modestly increased in +TBOA (Untrans. = 44.3 ± 3.3 pA; GluA2Q ΔNTD = 49.6 ± 3.4 pA; n = 19; paired t-test; P = 0.32). (**B3**) Scatter plots indicate GluA2Q ΔNTD AMPAR EPSCs were modestly decreased in -TBOA and increased in +TBOA. (**C**) AMPAR EPSC summary. (**C1**) GluA2Q WT AMPAR EPSC amplitude was increased trend wise in -TBOA and +TBOA relative to paired untransfected cells. (**C2**) GluA2Q ΔNTD AMPAR EPSC amplitude was trend wise decreased in -TBOA and increased in +TBOA relative to paired untransfected cells.*

GluA1 WT and ΔNTD receptors

Next, a similar approach was applied to test for peri-synaptic localisation of GluA1 ΔNTD receptors. First, in -TBOA, the synaptic RI for GluA1 WT and ΔNTD receptors was determined (Figure 3.13A). GluA1 WT receptors had a significantly reduced RI relative to paired untransfected cells (Figure 3.13A1), suggesting GluA1 WT incorporates into CA1 synapses where it contributes to synaptic transmission. However, the synaptic RI of GluA1 ΔNTD was unchanged relative to paired untransfected cells (Figure 3.13A2), confirming previous findings (Watson et al., 2017; Díaz-Alonso et al., 2017). Interestingly, despite the lack of GluA1 ΔNTD synaptic rectification, these receptors were localised at synaptic sites, as determined by confocal microscopy (Watson et al., 2020). This suggests that GluA1 ΔNTD receptors position at the synapse, but are unable to contribute effectively to synaptic transmission, possibly due to a 'mis-alignment' of postsynaptic receptors with presynaptic glutamate release sites (Biederer et al., 2017; Watson et al., 2020). It is hypothesised that receptors lacking the AMPAR NTD are positioned at peri-synaptic sites, due to a loss of NTD interactions with proteins in the synaptic cleft (Figure 3.1A). To deduce the sub-synaptic arrangement of GluA1 receptors, glutamate spillover was induced whilst recording the synaptic RI of GluA1 WT and ΔNTD receptors (Figure 3.13).

In -TBOA, GluA1 WT but not ΔNTD receptors are able to contribute to effective synaptic transmission (Figure 3.13A). Building on this hypothesis, an experimental protocol was designed to deduce if TBOA-induced glutamate spillover is able to activate peri-synaptic GluA1 ΔNTD receptors. AMPAR EPSCs were recorded at -60, +40 and 0 mV in baseline (-TBOA) and 50 μM TBOA (+TBOA) ACSF to measure the synaptic RI (Figure 3.13B1). It was hypothesised that if GluA1 ΔNTD receptors are positioned at peri-synaptic sites, then TBOA-induced glutamate spillover would activate these receptors, reflected by a significantly reduced synaptic RI relative to baseline. Unlike experiments conducted on GluA2Q receptors (Figure 3.12), the experimental protocol described here permits a pairwise comparison of the synaptic RI before and after TBOA application, improving the statistical power of this experiment.

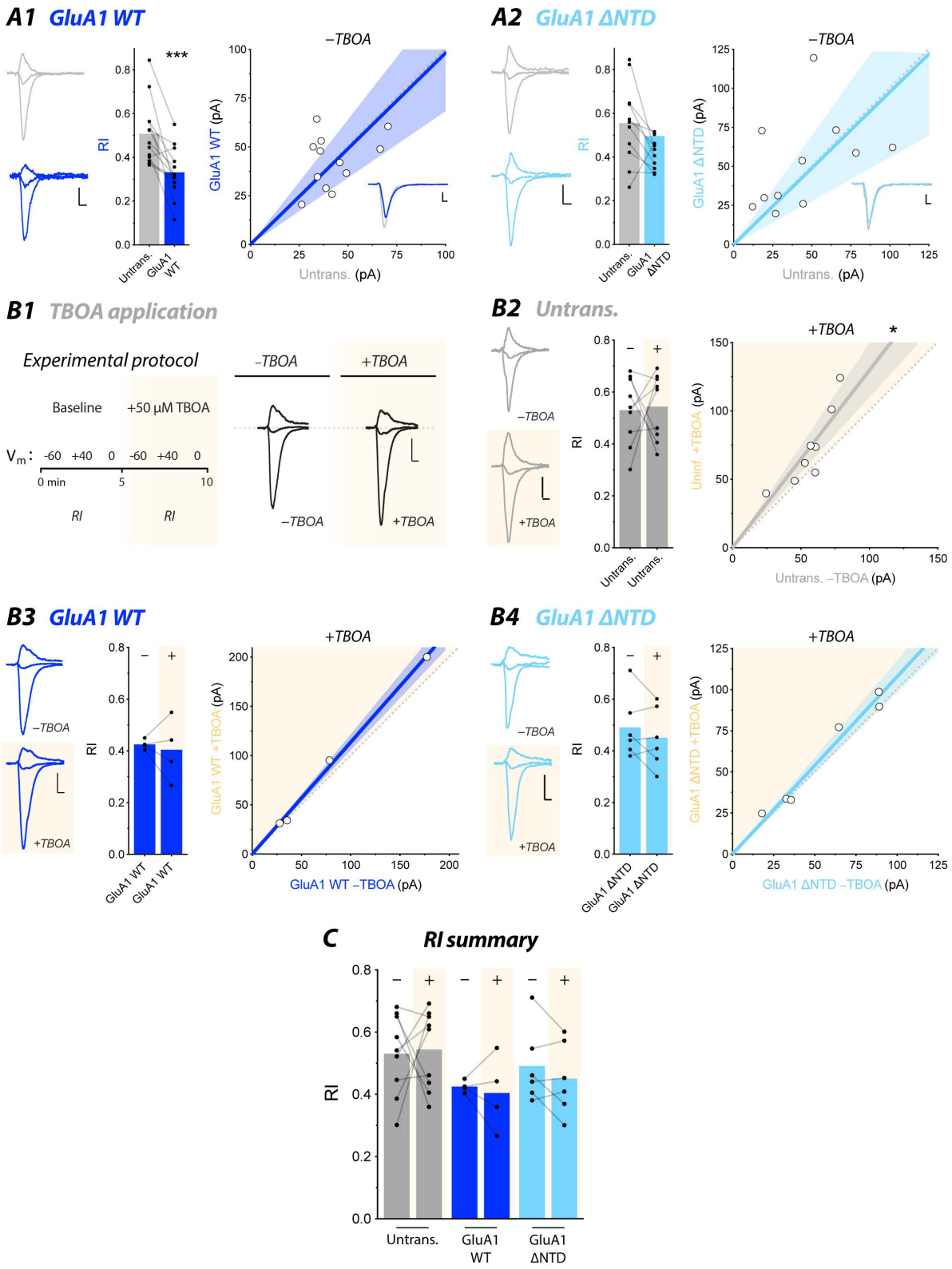

Figure 3.13 *50 µM TBOA-induced glutamate spillover has no effect on WT or NTD-deleted GluA1 synaptic rectification.*

Figure 3.13 ***50 μM TBOA-induced glutamate spillover has no effect on WT or NTD-deleted GluA1 synaptic rectification.*** *(**A1**) Representative synaptic RI traces of Untrans. (grey) and GluA1 WT (blue) held at -60, 0 and + 40 mV (scale bar = 20 pA; 10 ms). Synaptic RI of GluA1 WT was significantly decreased relative to Untrans. (Untrans. = 0.51 ± 0.04; GluA1 WT = 0.33 ± 0.03; n = 13; paired t-test, P < 0.001). GluA1 WT EPSC amplitude was unchanged relative to Untrans. (Untrans. = 65.0 ± 12.6 pA; GluA1 WT = 74.6 ± 14.2 pA; n = 18; paired t-test, P = 0.42). Representative synaptic RI traces of Untrans. (grey) and GluA1 ΔNTD (light blue) (scale bar = 20 pA; 10 ms). (Data re-presented from Figure 3.3). (**A2**) Synaptic RI of GluA1 ΔNTD was unchanged relative to Untrans. (Untrans. = 0.56 ± 0.06; GluA1 ΔNTD = 0.50 ± 0.08; n = 11; paired t-test, P = 0.43). GluA1 ΔNTD EPSC amplitude was unchanged relative to Untrans. (Untrans. = 44.6 ± 8.45 pA; GluA1 ΔNTD = 52.0 ± 9.05 pA; n = 11; paired t-test, P = 0.45). (**B1**) Experimental protocol for TBOA application and synaptic rectification. EPSCs were recorded at -60, +40 and 0 mV during baseline and 50 μM TBOA application. (**B2**) Untrans. representative traces (scale bar = 20 pA; 10 ms). Untrans. synaptic RI was unchanged following TBOA application (Untrans. -TBOA = 0.53 ± 0.04; Untrans. +TBOA = 0.54 ± 0.04; n = 9; paired t-test, P = 0.86). Untrans. EPSC amplitude was significantly increased following TBOA application (Untrans. -TBOA = 56.5 ± 5.87 pA; Untrans. +TBOA = 72.4 ± 9.95 pA; n = 8; paired t-test, P < 0.05). (**B3**) GluA1 WT representative traces (Scale bar = 20 pA; 10 ms). GluA1 WT synaptic RI was unchanged following TBOA application (GluA1 WT -TBOA = 0.42 ± 0.01; GluA1 WT +TBOA = 0.40 ± 0.06; n = 4; paired t-test, P = 0.71). GluA1 WT EPSC amplitude was unchanged following TBOA application (GluA1 WT -TBOA = 79.7 ± 34.4 pA; GluA1 WT +TBOA = 90.2 ± 39.5 pA; n = 4; paired t-test, P = 0.16). (**B4**) GluA1 ΔNTD representative traces (scale bar = 20 pA; 10 ms). GluA1 ΔNTD synaptic RI was unchanged following TBOA application (GluA1 ΔNTD -TBOA = 0.49 ± 0.05; GluA1 ΔNTD +TBOA = 0.45 ± 0.05; n = 6; paired t-test, P = 0.21). GluA1 ΔNTD EPSC amplitude was unchanged following TBOA application (GluA1 ΔNTD -TBOA = 54.8 ± 12.5 pA; GluA1 ΔNTD +TBOA = 59.5 ± 13.3 pA; n = 6; paired t-test, P = 0.11). (**C**) Synaptic RI summary of Untrans., GluA1 WT and GluA1 ΔNTD expressing cells perfused with -/+ TBOA (ANOVA, p > 0.05).*

Initial experiments deduced the synaptic RI from untransfected slices in baseline and 50 μM TBOA (Figure 3.13B2). The synaptic RI in +TBOA was unchanged relative to -TBOA, with a read-out of ~0.55, confirming measurements from previous experiments (3.13A1/2). The AMPAR EPSC amplitude of untransfected cells was significantly increased by ~10% in +TBOA relative to -TBOA (Figure 3.13B2), supporting findings from TBOA wash-in experiments (Figure 3.6D). This indicates that glutamate spillover is successfully induced using this experimental design. Importantly, the synaptic RI, although variable, remains unchanged. This permits use of this assay to study glutamate spillover onto GluA1 WT and ΔNTD expressing cells.

GluA1 WT synaptic RI is unchanged in +TBOA relative to -TBOA (Figure 3.13B3). The extent of synaptic rectification, ~0.4, is similar to that observed in previous experiments (Figure 3.13A1) and publications (Watson et al., Díaz-Alonso et al., 2017). Additionally, no significant change is observed in the AMPAR EPSC amplitude of GluA1 WT in 50 μM TBOA relative to baseline (Figure 3.13B3). This suggests that glutamate spillover has no effect on the contribution of GluA1 WT receptors to the synaptic response, in line with the hypothesis outlined in Figure 3.1. This implies that GluA1 WT receptors are positioned within the PSD, effectively responding to presynaptically released glutamate and do not require spillover of glutamate to be activated.

Finally, the synaptic RI of GluA1 ΔNTD expressing cells was measured in baseline and 50 μM TBOA. No significant change was observed in +TBOA relative to -TBOA for GluA1 ΔNTD expressing cells (Figure 3.13B4). Similarly, no significant change in the size of the AMPAR EPSC was observed. This indicates that TBOA-induced glutamate spillover has no effect on the contribution of GluA1 ΔNTD receptors to the synaptic response. These findings indicate that GluA1 ΔNTD receptors are not positioned at peri- or extra-synaptic sites. These results raise questions over the mechanism underlying a lack of synaptic rectification with GluA1 ΔNTD during basal conditions. It remains possible that the functional difference between GluA1 WT and ΔNTD is alternatively due to a trafficking defect, as observed with AMPAR NTD deletion in heterologous cells by western blotting (Möykkynen et al., 2014) and reduced synaptic enrichment in neurons by confocal imaging (Watson et al., 2020).

3.3 Discussion

The synaptic RI can be used as a measure of synaptic incorporation of exogenous AMPARs. In combination with expression of AMPAR mutants, this assay has been used extensively to answer a number of questions about synaptic trafficking in basal ACSF (Hayashi et al., 2000; Shi et al., 2001). However, in order to address questions about the sub-synaptic arrangement of AMPARs this assay alone will not suffice. Therefore, the RI was used in combination with TBOA-induced glutamate spillover. A number of protocols were tested throughout this chapter to address if the AMPAR NTD is required for sub-synaptic receptor positioning.

The AMPAR NTD maintains excitatory synaptic transmission and plasticity

AMPAR subunits GluA1-3 are responsible for mediating the majority of AMPAR-mediated synaptic transmission at CA1 synapses in the hippocampus (Figure 3.2). Furthermore, GluA1/2 heteromers are the most abundant AMPAR subunits in the hippocampus (Schwenk et al., 2014) and mediate the bulk of CA1 synaptic transmission (Lu et al., 2009). Therefore, the synaptic function of GluA1/2 NTDs was determined using exogenous expression of WT and ΔNTD receptors, highlighting the importance of the GluA1/2 NTD in maintaining effective synaptic transmission (Figure 3.3; Watson et al., 2017; Díaz-Alonso et al., 2017; Watson et al., 2020). Moreover, application of exogenous AMPAR NTDs interferes selectively with GluA2-mediated synaptic transmission and GluA1-mediated synaptic potentiation (Figure 3.4). This is potentially mediated by exogenous NTDs competing with endogenous AMPAR NTD-protein interactions, reflected by a loss of synaptic function. Ultimately, the AMPAR NTD appears to regulate excitatory synaptic transmission in a subunit-specific manner, potentially through directly interacting with proteins in the synaptic cleft.

AMPARs are non-uniformally distributed at postsynaptic sites, organising into nanodomains (Nair et al., 2013; MacGillavry et al., 2013). These nanodomains have also been shown to align with presynaptic vesicle release sites, in nanocolumns (Tang et al., 2016; Biederer et al., 2017). Computer modelling suggests that clustering of AMPARs on a nanometer scale, can profoundly enhance the strength of the synaptic response (Franks et al., 2003; Raghavachari and Lisman, 2004; Savtchenko and Rusakov, 2014). Sub-synaptic positioning of AMPARs therefore, is crucial to achieve efficient synaptic transmission, particularly as not all AMPARs are saturated by glutamate at CA1 synapses (McAllister and

Stevens, 2000). Recent reports suggest that the AMPAR NTD is required for positioning AMPARs within nanodomains for effective synaptic transmission (Watson et al., 2020). To test this hypothesis physiologically, glutamate spillover experiments were performed using application predominantly of selective EAAT1-3 inhibitor DL-TBOA (Shimamoto et al., 1998; Shimamoto et al., 2000). Glutamate spillover has greatly improved our understanding of peri-synaptic mGluR (Huang et al., 2004; Sheng et al., 2017b) and extra-synaptic NMDAR distribution (Chen and Diamond, 2002; Clark and Cully-Candy, 2002). A spillover of glutamate in this study therefore, is expected to activate potentially mis-aligned NTD-deleted receptors.

TBOA-induced glutamate spillover

One of the key difficulties with addressing the sub-synaptic positioning of AMPARs using electrophysiology alone, is not knowing the true extent of glutamate spillover. Different drugs (TFB-TBOA and DL-TBOA), concentrations (1 μM, 10 μM and 50 μM) and stimulation protocols (single pulse and pulse-train stimulation) were used throughout these experiments in an attempt to vary the extent of glutamate spillover at pyramidal CA1 synapses. Lower TBOA concentrations and single pulse stimulation was used to limit glutamate spillover onto extra-synaptic sites and neighbouring synapses, ensuring activation of peri-synaptic receptors. Having confirmed successful spillover of glutamate with single pulse stimulation (Figure 3.6) and pulse-train stimulation (Figure 3.8) on endogenous receptors, these established protocols were then extended to study exogenous GluA1/2 WT and ΔNTD expressing cells to assess the sub-synaptic positioning of these receptors (Figure 3.12/13).

Pulse-train stimulation

TBOA application in combination with pulse-train stimulation was used to maximise the spatio-temporal extent of glutamate spillover (Hires et al., 2008; Armbruster et al., 2016; Pinky et al., 2018) in an attempt to detect extra-synaptic receptors. Application of TBOA significantly enhances glutamate spillover at CA1 synapses in untransfected slices (Figure 3.8), suggesting successful spillover onto extra-synaptic receptors or neighbouring synapses. However, no change in the AMPAR EPSC amplitude of GluA2Q WT and ΔNTD expressing cells is detected using dual whole-cell recording of paired untransfected and transfected cells (Figure 3.10). This suggests that both GluA2Q WT and ΔNTD receptors are not positioned at extra-synaptic sites.

Significant effects observed with unpaired experimental design (Figure 3.9) are thought to be due to differences in stimulation intensity input affecting the extent of glutamate spillover (Figure 3.8C) across different slices and conditions.

Single-stimulation

Extensive glutamate spillover onto extra-synaptic receptors did not reveal a difference in the localisation of GluA2Q WT and ΔNTD receptors. However, an interesting observation was made from these experiments, where the first EPSC of GluA2Q ΔNTD expressing cells was found to be trend wise increased in 10 μM TBOA (Figure 3.11). In contrast, GluA2Q ΔNTD expression in -TBOA is depressed by ~50% relative to untransfected cells (Figure 3.3C; Watson et al., 2017; Díaz-Alonso et al., 2017; Watson et al., 2020). Therefore, single stimulation (frequency 0.2 Hz) was employed to study this effect in further detail. Despite a trend wise increase in the AMPAR EPSC recorded from GluA2Q ΔNTD expressing cells in the presence of 50 μM TBOA (Figure 3.12), the AMPAR EPSC was not significantly decreased in -TBOA. These results conflict with those reported previously using SCE transfection (Figure 3.3C), thought to be due to variable expression levels.

GluA1 WT receptors incorporate into CA1 synapses, whereas GluA1 ΔNTD receptors do not (Figure 3.13A). The lack of synaptic incorporation with GluA1 ΔNTD is thought to be due to a loss of synaptic anchoring (Watson et al., 2017). Here, it was hypothesised that GluA1 ΔNTD receptors are excluded from the PSD at peri-synaptic sites (Figure 3.1A) and spillover of glutamate onto these receptors will activate them, increasing the extent of synaptic rectification to WT levels. Using a paired experimental design, the synaptic RI was recorded during basal conditions and following TBOA application (Figure 3.13B1). However, the synaptic RI was found to be unchanged in both GluA1 WT and ΔNTD expressing cells (Figure 3.13B3/4). This indicates that GluA1 ΔNTD receptors are not positioned peri-synaptically, and therefore another mechanism may explain the lack of synaptic rectification. For example, decreased surface expression or distribution, observed in both heterologous and neuronal cells (Möykkynen et al., 2014; Watson et al., 2020).

Sub-synaptic AMPAR positioning cannot be studied using electrophysiology alone. In addition to glutamate spillover experiments, super-resolution imaging will permit determination of GluA1/2 WT and ΔNTD localisation. Recently, super-resolution has also been used to study the AMPAR NTD, suggesting it is not required for nanodomain formation (Watson et al., 2020). Using STORM microscopy, the authors show that nanodomain of postsynaptic AMPARs are formed with both GluA1/2 WT and ΔNTD receptors. Similarly, experiments in this chapter using glutamate spillover onto peri- and extra-synaptic sites, suggest no difference in the sub-synaptic distribution of GluA1/2 WT and ΔNTD receptors. It remains possible that a nanometer difference in sub-synaptic receptor positioning exists, however if this is the case, it is undetectable by glutamate spillover and super-resolution microscopy.

Regardless, the AMPAR NTD appears to be crucial for the maintenance of synaptic transmission and plasticity (Figure 3.3/4), but how this functional phenotype manifests remains elusive. It is also possible, that synaptic protein interactions with the AMPAR NTD may have various functional effects. Identification (Chapter 4) and functional characterisation (Chapter 5) of AMPAR-interacting proteins is investigated further in this study.

Chapter 4

Identifying synaptic protein interactions with the AMPAR N-terminal domain

4.1 Introduction

The AMPAR N-terminal domain (NTD) is required for synaptic transmission and plasticity (Chapter 3; Watson et al., 2017; Díaz-Alonso et al., 2017, Watson et al., 2020; Jiang et al., 2021). Given that the synaptic cleft is a protein-rich environment (Perez de Arce et al., 2015), an emerging theory is that cleft protein interactions with the NTD influence synaptic AMPAR positioning and consequently synaptic strength (Watson et al., 2020). Extracellular protein interactions have been identified with the NTD of other ionotropic glutamate receptors (iGluRs), including complement C1q-like protein 2/3 (C1ql2/3) binding to kainate subunit GluK2/4/5 NTDs (Matsuda et al., 2016; Straub et al., 2016) and Cerebellin-1/2/4 (Cbln1/2/4) binding to delta subunit GluD1/2 NTDs (Matsuda et al., 2010; Elegheert et al., 2016; Tao et al., 2018; Fossati et al., 2019). These protein interactions are essential for hippocampal circuit function and cerebellar long-term depression respectively. Additionally, a growing number of AMPAR NTD interactors are being described, for example neuronal pentraxin-1/2/receptor (Nptx1/2/r) binding to GluA4 NTDs (O'Brien et al., 1999; Xu et al., 2003; Sia et al., 2007; Lee et al., 2017) and more recently olfactomedin-1 (Olfm1) binding to GluA2 NTDs (Pandya et al., 2018). These secreted proteins represent all currently known direct iGluR NTD interactors (Figure 4.1). However, it is likely that numerous proteins that interact with the AMPAR NTD remain unresolved.

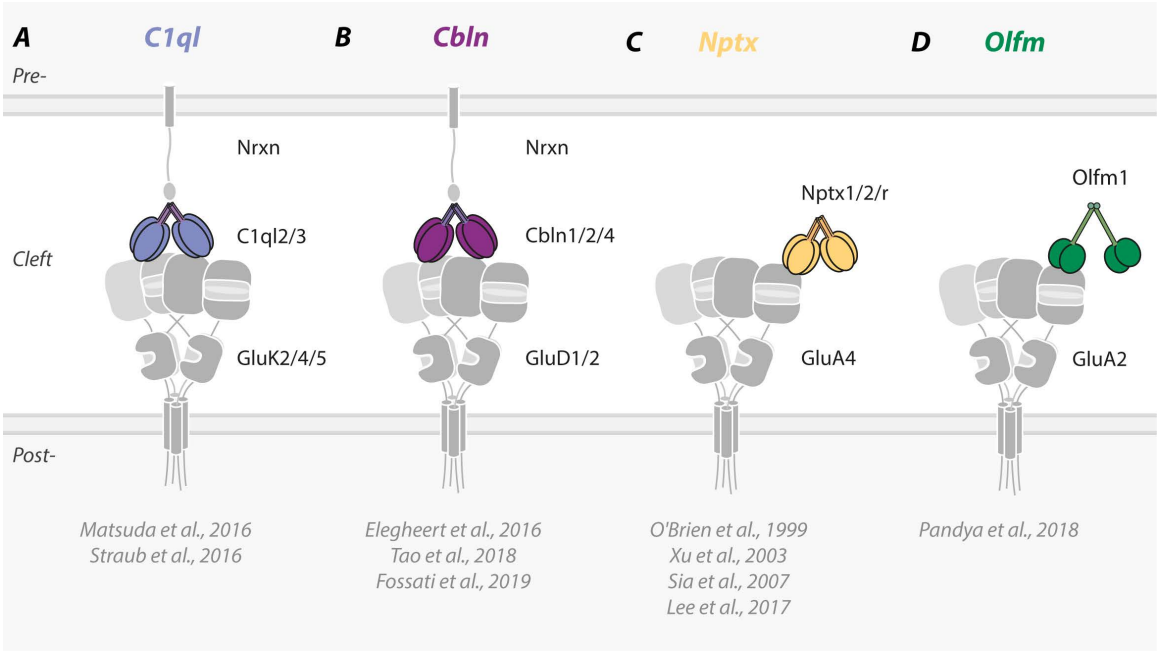

Figure 4.1 ***Known ionotropic glutamate receptor NTD interactors.*** *(**A**) Complement C1q-like protein 2/3 (C1ql2/3) interact with the NTD of postsynaptic kainate receptor subunits GluK2/4/5 and presynaptic neurexin (Nrxn), forming a trans-synaptic complex. This interaction is required to regulate circuit function at hippocampal mossy fibre synapses (Matsuda et al., 2016; Straub et al., 2016). (**B**) Cerebellin-1/2/4 (Cbln1/2/4) bind to postsynaptic delta receptor subunits GluD1/2 and presynaptic neurexin, forming a trans-synaptic complex. This interaction is critical for the expression of long-term depression at cerebellar climbing fibre synapses and hippocampal synapse formation and maintenance (Matsuda et al., 2010; Elegheert et al., 2016; Tao et al., 2018; Fossati et al., 2019). (**C**) Neuronal pentraxin-1/2/receptor (Nptx1/2/r) interact with the NTD of GluA4 subunits promoting postsynaptic receptor clustering at excitatory and inhibitory synapses (O'Brien et al., 1999; Xu et al., 2003; Sia et al., 2007; Lee et al., 2017). (**D**) Olfactomedin-1 (Olfm1) binds to the NTD of GluA2-containing AMPARs regulating lateral diffusion of AMPARs into hippocampal synapses (Pandya et al., 2018).*

Secreted proteins form low-affinity interactions with iGluR NTDs in the μM range (Matsuda et al., 2010; Matsuda et al., 2016; Elegheert et al., 2016; Suzuki et al., 2020), and therefore are not amenable for identification by classical affinity-purification mass spectrometry. (AP-MS; Schwenk et al., 2012; Schwenk et al., 2014; Shanks et al., 2012). In order to identify AMPAR NTD interactions, proximity-labelling (PL) proteomics was employed as a means of capturing weak and transient synaptic cleft protein interactions. This was implemented by fusing promiscuous biotin ligase (BirA*) and ascorbate peroxidase (APEX) tags to the N-terminus of AMPAR subunits (BirA*-AMPAR) and expressing these constructs in organotypic slice culture by adeno-associated virus (AAV) transduction.

Proximity-labelling (PL) proteomics is gaining momentum as a technique used to detect interactions with a protein of interest. This method relies on proximity-dependent biotinylation of neighbouring proteins by fusion with BirA* (Choi-Rhee et al., 2004; Cronan, 2005). In the presence of biotin + ATP, BirA* generates a biotin derivative which diffuses from the active site and labels lysine residues on neighbouring proteins within a 10-35 nm radius (Figure 4.2A1; Kim et al., 2014; May et al., 2020). Proteins covalently labelled by biotin are biochemically captured, isolated and identified by nanoscale liquid chromatography with tandem mass spectrometry (nano-LC-MS/MS). Since the advent of BioID (35 kD; Roux et al., 2012), a number of variants have been developed to improve the enzymatic biotinylation efficiency and to reduce the overall size of the enzyme. Namely, BioID2, derived from *A. Aeolicus* BirA* with enhanced labelling and reduced size (27 kD; Kim et al., 2016; Figure 4.2B1), and more recently MiniTurbo (28 kD) and TurboID (35 kD), the product of directed evolution of *E. Coli* BirA* (Branon et al., 2018, Figure 4.2B2 and 4.2B3). TurboID has a significantly improved labelling efficiency, rivalling that of engineered APEX tags (Martell et al., 2012; Lam et al., 2015; Hung et al., 2016) APEX (27 kD) and APEX2 (27 kD), and horse radish peroxidase (HRP) (44 kD; Jiang et al., 2012). The labelling efficiency of PL tags varies (Figure 4.1), differing in their spatio-temporal labelling capabilities, with some tags more suitable than others for the identification of proteins from different subcellular compartments. The improved temporal resolution (2-fold relative to BioID using 3 hrs reaction time; Branon et al., 2018) and non-toxicity of biotin application makes TurboID an ideal tag for capturing dynamic protein interactions in intact tissue preparations. Successful capture of protein interactions with BioID2, MiniTurbo, TurboID and APEX2 was directly compared to determine the most effective PL tag.

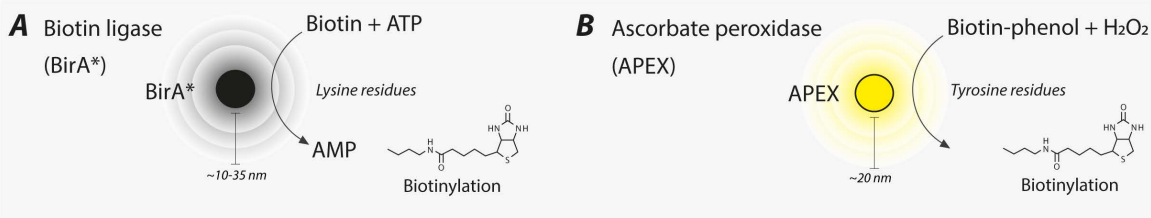

Tag	Enzyme activity	Source	Size (kD)	Reaction time	Ligand	Mutations
BioID	Biotin ligase	*E. Coli*	35	48 hrs	Biotin + ATP	R118G
BioID2	Biotin ligase	*A. Aeolicus*	27	48 hrs	Biotin + ATP	R40G
BASU	Biotin ligase	*B. Subtilis*	28	48 hrs	Biotin + ATP	ΔN-ter 3 mut
MiniTurbo	Biotin ligase	*E. Coli*	28	18 hrs	Biotin + ATP	ΔN-ter 12 mut
TurboID	Biotin ligase	*E. Coli*	35	1 hr	Biotin + ATP	14 mut
APEX	Ascorbate peroxidase	Synthetic	27	10 mins	Biotin-P + H_2O_2	3 mut
APEX2	Ascorbate peroxidase	Synthetic	27	10 mins	Biotin-P + H_2O_2	4 mut
HRP	Ascorbate peroxidase	*A. Rusticana*	44	10 mins	Biotin-P + H_2O_2	0 mut

Figure 4.2 ***Proximity-labelling tag size and labelling efficiency.*** *(**A**) Biotin ligase (BirA*) tags require biotin + ATP to initiate biotinylation of proximal lysine residues on neighbouring proteins. BirA* tags vary in size (kD) and labelling efficiency, requiring different reaction times for sufficient biotinylation. BioID (Roux et al., 2012), BioID2 (Kim et al., 2016), BASU (Ramanathan et al., 2018), MiniTurbo (Branon et al., 2018) and TurboID (Branon et al., 2018) all permit labelling and identification of proximal proteins within a ~10-35 nm radius (Kim et al., 2014; May et al., 2020). (**B**) Ascorbate peroxidase (APEX) tags require biotin phenol (biotin-p) and H_2O_2 to initiate biotinylation of proximal tyrosine residues on neighbouring proteins. APEX (Martell et al., 2012), APEX2 (Lam et al., 2015; Hung et al., 2016) and HRP (Jiang et al., 2012) all permit labelling and identification of proximal proteins within a ~20 nm radius (Martell et al., 2012). Considerably shorter labelling times are required for APEX tags relative to BirA*.*

Organotypic slice cultures provide a versatile tool for studying synapses using electrophysiology, light microscopy and biochemistry (Gähwiler et al., 1997). This culturing method provides an intact physiological network easily manipulated by changing the experimental conditions *in vitro*. As a synaptic role for the AMPAR NTD has been determined in organotypic hippocampal slices (Watson et al., 2017; Díaz-Alonso et al., 2017, Watson et al., 2020), this experimental system was chosen to probe for candidate NTD cleft protein interactions. PL proteomics was implemented by AAV-mediated BirA*-AMPAR expression, labelling and identification of proximal proteins in organotypic slice culture. This system offers considerable advantages over PL proteomics performed in dissociated cortical cultures (Loh et al., 2016; Cijsouw et al., 2018), where hippocampal anatomy is lost during neuronal dissociation, and *in vivo* (Uezu et al., 2016; Spence et al., 2019; Takano et al., 2020), which requires numerous subcutaneous biotin injections. Additionally, BirA* tags label vicinal proteins under physiological conditions, without the requirement for toxic H_2O_2 application or 4˚C recovery conditions necessary for APEX and HRP (Loh et al., 2016; Cijsouw et al., 2018; Li et al., 2020).

In this chapter, candidate AMPAR NTD interactors were identified in organotypic slice culture, with the ability of three BirA* tags (BioID2, MiniTurbo and TurboID) and APEX2 to successfully identify direct AMPAR NTD interactors compared in parallel. Subsequently, direct protein interactions were confirmed by high-throughput screening of candidate interactors in a cell-based binding assay. Candidate binding and localisation was then further characterised using co-immunoprecipitation (co-IP) experiments and immunofluorescence microscopy. These findings describe the identification and confirmation of direct synaptic protein interactions with the AMPAR NTD and describe novel methodology for identification of AMPAR NTD interactors in organotypic slice culture.

4.2 Results

4.2.1 Establishing proximity-labelling in organotypic slices

Cell-permeable biotin application used to initiate proximity-dependent biotinylation is expected to result in protein labelling at all stages of the AMPAR life cycle. Proximal proteins will be identified from the ER during AMPAR biogenesis (eg. Frrs1l; Schwenk et al., 2019) and at the synaptic cleft during synaptic transmission (eg. Nptx1; Xu et al., 2003) (Figure 4.3C). To identify synaptic AMPAR-interacting proteins, the following BirA*-AMPAR constructs were chosen based on their successful incorporation into CA1 synapses, GluA2Q WT, GluA2Q ΔNTD and GluA1 WT (Chapter 3; Watson et al., 2017). GluA1 ΔNTD receptors however, fail to incorporate into CA1 synapses, therefore this construct was deemed unsuitable as a control bait for the identification of synaptic AMPAR NTD interactors. To assess enrichment of proteins for the AMPAR NTD, PL proteomics of GluA2Q WT and ΔNTD receptors were compared extensively throughout this chapter fused to 4 different PL tags (BioID2, MiniTurbo, TurboID and APEX2).

Experimental conditions were first optimised before detailing the finalised PL protocol in Figure 4.8. Briefly, once robust BirA*-AMPAR expression is achieved at day post infection (DPI) 13 using AAV-mediated transduction, biotinylation is initiated by applying biotin for 48, 18 or 2 hrs, for BioID2, MiniTurbo or TurboID respectively, or 10 mins for APEX2. Following biotinylation, slices were harvested and solubilised in lysis buffer before isolating biotinylated proteins using streptavidin magnetic beads. Finally, streptavidin-isolated proteins were eluted and identified by MS for multiple experimental conditions to enable comparison of proximity-proteomes.

To establish this protocol (Figure 4.8), experimental conditions were first optimised during pilot experiments with BirA*-AMPAR expression in heterologous and neuronal cells (see 4.2.1).

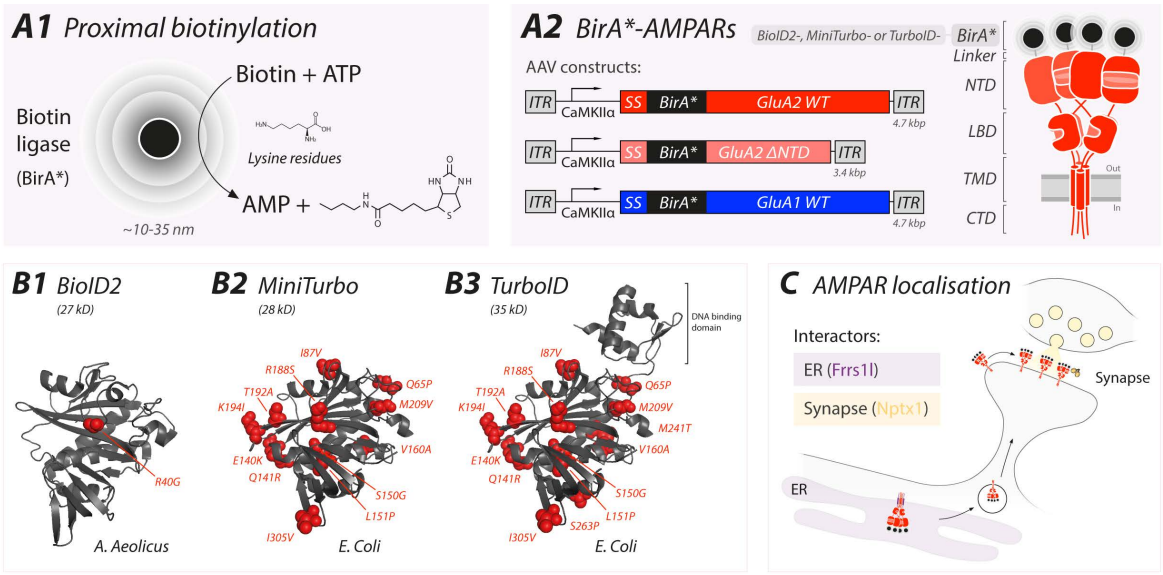

Figure 4.3 ***Proximity-labelling of AMPAR interactors in organotypic slice culture.*** *(**A1**) Proximity-dependent biotinylation reaction mediated by a promiscuous biotin ligase (BirA*) tag. (**A2**) (Left) BirA*-AMPAR subunit constructs packaged into AAV vectors under the CaMKIIα promoter containing the native AMPAR signal sequence (SS). (**A2**) (Right) BirA* is fused to the extreme N-terminus of the AMPAR using a flexible amino acid linker. AMPARs are composed of a large extracellular N-terminal domain (NTD), ligand binding domain (LBD), transmembrane domain (TMD) and C-terminal domain (CTD). (**B**) BirA* tags employed in PL experiments. (**B1**) BioID2, derived from A. Aeolicus, contains a single mutation to permit promiscuous biotinylation (Kim et al., 2016). (**B2**) MiniTurbo, derived from E. Coli, contains 12 mutations introduced to improve the efficiency of biotinylation and lacks the BirA* DNA binding domain to reduce tag size (Branon et al., 2018). (**B3**) TurboID contains 14 mutations and includes the E. Coli DNA binding domain, producing the highest efficiency of biotinylation (Branon et al., 2018). (**C**) AMPAR biogenesis and synaptic localisation exposes BirA* tags to both ER and synaptic protein interactors. Known AMPAR constituents from the ER (Frrs1l) and synapse (Nptx1) should be identified using PL proteomics.*

Optimisation of BirA*-AMPAR labelling conditions

The following experiments were conducted to validate the use of BirA*-AMPARs to label and isolate proximal proteins. Experimental conditions for biotinylation were first optimised in a recombinant setting by transfection of HEK293 cells with BirA*-AMPARs. BioID2-, MiniTurbo- and TurboID-AMPAR constructs were built by fusing tags to the N-terminus of AMPAR subunits using a '*Gly-Lys-Ser-Ser-Gly-Ser*' amino acid linker inserted after the native signal sequence (Figure 4.3A2).

First, to ensure that proximal proteins labelled by BirA*-AMPARs can be isolated by streptavidin magnetic beads, BioID2-tagged GluA2Q WT and NTD-deleted (ΔNTD) receptors were co-expressed in HEK293 cells alongside GluA1 (Figure 4.4A1). BioID2-GluA2Q WT (~135 kD) and BioID2-GluA2Q ΔNTD (~85 kD) were expressed at the expected molecular weights compared to un-tagged GluA2Q WT (~100 kD) indicated by western-blotting (WB) with antibodies directed at the GluA2 CTD. The intensity of streptavidin-HRP staining observed was greater from the cell lysate of BioID2-GluA2Q WT and BioID2-GluA2Q ΔNTD in the presence of 200 μM biotin, demonstrating that biotin supplementation into the media for 48 hrs enhances the extent of protein biotinylation. Bands at molecular weights of ~80 and 150 kD in untransfected cells represent endogenously biotinylated proteins (Chapman-Smith and Cronan, 1999). Most importantly, biotinylated GluA1 could be isolated with streptavidin magnetic beads selectively from cells expressing BioID2-tagged receptors in the presence of biotin (Figure 4.4A1). This demonstrates that BioID2-AMPARs successfully biotinylate proximal GluA1 and streptavidin magnetic beads are able to effectively capture biotinylated GluA1 receptors.

Enzymatic biotinylation requires both biotin + ATP to covalently attach biotin to neighbouring lysine residues. Whilst 200 μM biotin supplementation is sufficient to initiate proximal biotinylation, ATP was additionally supplemented to ensure a greater coverage of the proximal environment. The ATP concentration differs across the intracellular (~3-10 mM) and extracellular environment (~10 nM) (Schwiebert and Zsembery, 2003). Consequently, BirA* enzymatic activity may also differ in the intra- and extra-cellular space. To account for these differences, the extracellular concentration of ATP was increased and together with 200 μM

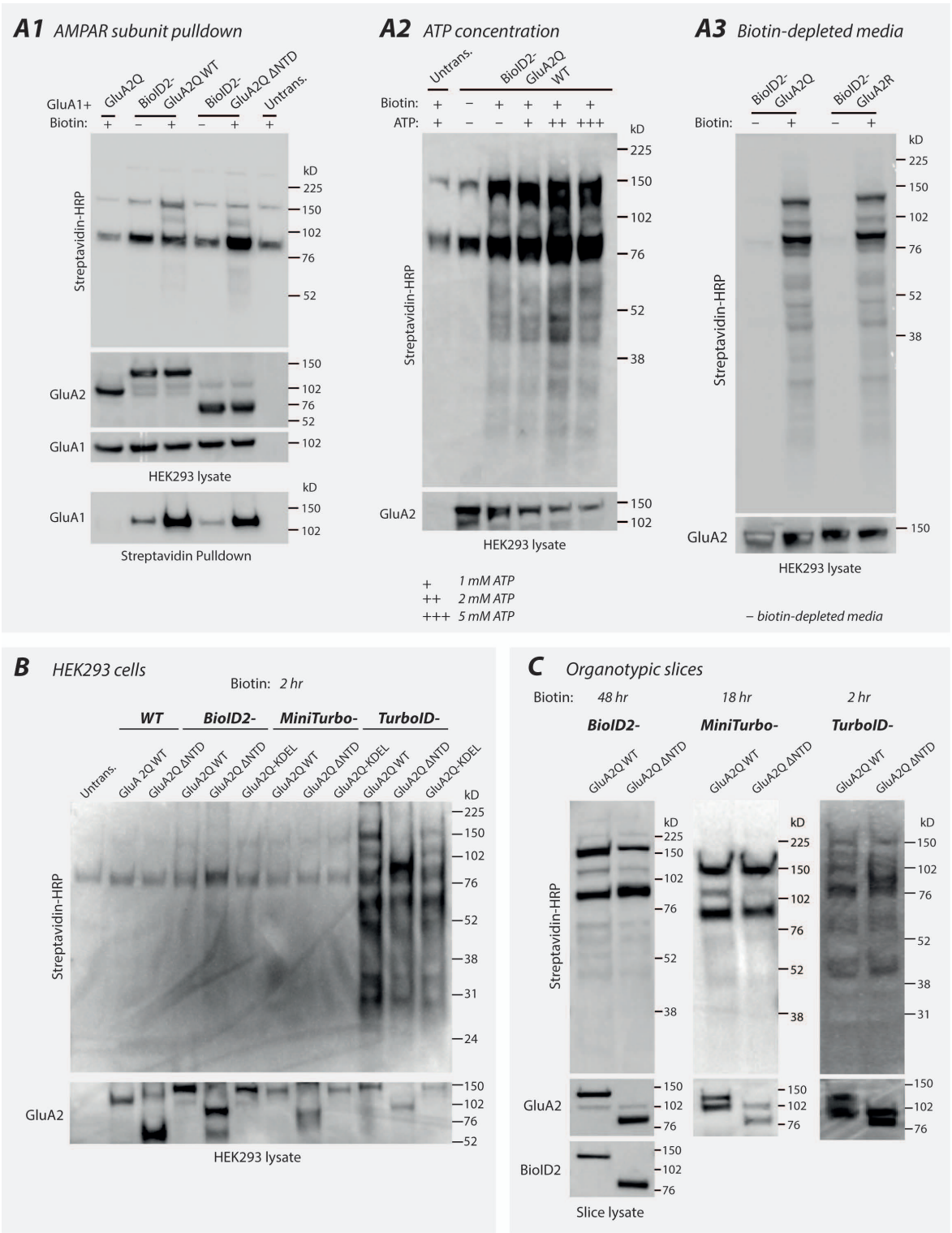

Figure 4.4 *Optimisation of BirA*-AMPAR experimental conditions.*

Figure 4.4 ***Optimisation of BirA*-AMPAR experimental conditions.*** *(**A1**) AMPAR subunit GluA1 can be labelled and isolated successfully by neighbouring subunits BioID2-GluA2Q WT and ΔNTD. Co-expression of BioID2-GluA2Q WT or ΔNTD and GluA1 receptors elicited biotinylation in the presence of 200 μM biotin. Biotinylated GluA1 was successfully isolated following a streptavidin pulldown selectively for BioID2-GluA2Q WT and BioID2-GluA2Q ΔNTD conditions in the presence of biotin. (**A2**) The intensity of biotin-induced biotinylation was increased in the presence of 2 mM ATP. Increasing concentrations of ATP were applied to cells expressing BioID2-GluA2Q in the presence of 200 μM biotin (n = 3 independent preparations). Biotinylation intensity was greatest for 200 μM biotin + 2 mM ATP media conditions. Of note, cell health was compromised at ATP concentrations of 5 mM. (**A3**) Biotin-depleted media had a drastically reduced level of background biotinylation in control conditions. With endogenously biotinylated proteins (Chapman-Smith and Cronan, 1999) undetectable by WB. (**B**) Biotinylation intensity was greatest for TurboID-AMPARs following 2 hrs biotin + ATP application (n = 3 independent preparations). Of note, 10 mins labelling time was insufficient to produce biotinylation in BioID2- and MiniTurbo-GluA2Q expressing cells, as detected by WB. (**C**) BioID2-, MiniTurbo- and TurboID- GluA2Q WT and ΔNTD receptors produce similar levels of proximal biotinylation when expressed in organotypic hippocampal slices via AAV-mediated transduction (titer = 1.0 x 10^{13} GC/mL). BioID2-, MiniTurbo and TurboID- GluA2Q WT and ΔNTD receptors were detected in the slice lysate using primary antibodies direct at the GluA2 CTD. Additionally, anti-BioID2 was used to specifically probe for the BioID2 tag on WB.*

biotin applied to HEK293 cells expressing BioID2-GluA2Q for 48 hrs (Figure 4.4A2). The intensity of streptavidin-HRP blotting is increased in a concentration-dependent manner from 0 mM ATP to 2 mM ATP, reaching maximal biotinylation intensity (Figure 4.4A2). Increasing the ATP concentration to 5 mM did not result in further increases in biotinylation and cell health at this concentration was compromised. Therefore, application of 200 μM biotin + 2 mM ATP was selected for all organotypic hippocampal slice PL proteomics experiments.

Endogenous biotinylation can be observed in BioID2-GluA2Q expressing cells in the absence of biotin application, likely due to very low levels of biotin being present in the media (Figure 4.4A2). It is important to reduce the level of background biotinylation in order to retain temporal control over the labelling time-window. Lower levels of background biotinylation will also ensure a reduction in the noise level of mass spectrometry (MS) data. To reduce endogenous and background biotinylation, biotin-depleted media was prepared by isolating biotin from HEK293 media with streptavidin agarose beads. This successfully abolished background biotinylation (Figure 4.4A3), enabling strict control over the labelling time-window and reducing levels of noise for PL proteomics.

To deduce the time-window required for sufficient biotinylation by different BirA* tags, a direct comparison of streptavidin-HRP staining intensity was performed. Un-tagged-, BioID2-, MiniTurbo- and TurboID-tagged GluA2Q WT and GluA2Q ΔNTD were expressed in HEK293 cells and supplemented with biotin + ATP for 2 hrs. The level of biotinylation observed was significantly higher for TurboID- relative to MiniTurbo- and BioID2- expressing cells (Figure 4.4B). This suggests that the temporal efficiency of TurboID is significantly greater than that of MiniTurbo and BioID2. This experiment was performed in parallel with cells treated with biotin + ATP for 10 mins, as the intensity of biotinylation by TurboID is reported to be sufficient within this time (Branon et al., 2018). However, the intensity of biotinylation by TurboID-GluA2Q receptors was undetectable with 10 mins labelling. This is likely due to the previous characterisation of TurboID (Branon et al., 2018) by fusion to single transmembrane domains (pDisplay; Howarth et al., 2008), which are expressed in higher quantities than AMPARs. The difference in labelling intensity observed here compared to the literature therefore, is most likely due to a difference in expression levels of different TurboID fusion constructs.

Finally, BirA*-AMPARs were expressed in organotypic hippocampal slices by transduction with high titer (1.0 x 10^{13} GC/mL) AAV (Figure 4.4C). Having validated construct expression and labelling in recombinant cells, encoding DNA was packaged into AAVs for transduction of post-mitotic neurons (Figure 4.3A2). BirA*-AMPAR expression was driven by the CaMKIIα promoter to ensure selective expression in excitatory hippocampal neurons (Wang et al., 2013; Choi et al., 2014) and AAV serotype 2/9 vectors were selected given their low toxicity and stable long-term expression in cultured hippocampal neurons (Royo et al., 2008). BirA*-tagged WT and ΔNTD receptors are expressed in slices indicated by higher (~135 kD) and lower (~85 kD) molecular weights respectively, compared to endogenous GluA2 (~100 kD). Biotin + ATP was supplemented into the media for 48, 18 and 2 hrs, (BioID2, MiniTurbo and TurboID respectively) depending on the BirA* tag used. These labelling times were selected based on published timings (Kim et al., 2016; Branon et al., 2018) and streptavidin-HRP staining intensity from WB of organotypic slice culture lysate (Figure 4.4C). BirA*-GluA2Q WT and BirA*-GluA2Q ΔNTD biotinylated proteins, were subsequently isolated from the slice lysate and identified by nano-LC-MS/MS. These experiments establish the experimental conditions for PL proteomics conducted throughout this chapter (Figure 4.8).

4.2.2 BirA*-AMPARs traffic to CA1 synapses

Fusion of BirA* tags (27-35 kD; Figure 4.3B) to the N-terminus of the AMPAR may hinder synaptic expression and physiological function in organotypic hippocampal slices. Therefore, to ensure that BirA*-AMPARs express and function equivalent to WT receptors, excitatory postsynaptic currents (EPSCs) were recorded from CA1 pyramidal neurons expressing BirA*-tagged (BioID2) and un-tagged AMPAR subunits. The rectification index (RI) was used as a measure of AMPAR synaptic trafficking (Hayashi et al., 2000; Shi et al., 2001) and the AMPAR EPSC amplitude was used to determine synaptic strength. Initial screening was performed with BioID2 as this is the most well-characterised tag for identification of synaptic proteins in intact tissue preparations (Uezu et al., 2016; Spence et al., 2019).

Single-cell electroporation (SCE) transfection of un-tagged AMPAR subunits all resulted in significant rectification of the synaptic response (Figure 4.5C1). This indicates that GluA2Q WT, GluA2Q ΔNTD and GluA1 WT receptors are expressed at CA1 synapses, as previously reported (Watson et al., 2017). Crucially, BioID2-AMPAR subunits also caused a significant rectification of the synaptic response, implying fusion of BioID2 to the N-terminus of AMPAR subunits does not occlude synaptic trafficking. Additionally, changes in EPSC amplitude observed with un-tagged AMPARs are mirrored by BioID2-AMPAR subunit expression (Figure 4.5C2). Whilst GluA2Q WT increased the EPSC, GluA2Q ΔNTD expression resulted in a decrease in EPSC amplitude, with no significant change observed for GluA1, as previously reported for untagged receptors (Watson et al., 2017). This demonstrates that synaptic expression and function is independent of the BioID2 tag, validating the use of this construct for the identification of synaptic AMPAR interactors.

SCE permits sparse transfection of AMPARs in organotypic slice culture (Figure 4.5A3). However, nano-LC-MS/MS experiments require expression of BirA*-AMPARs in a large proportion of excitatory neurons to increase the quantity of biotinylated material. Therefore, AAV transduction of organotypic slice cultures was implemented to increase the proportion of expressing cells (Figure 4.5A3). To determine the time-course of BioID2-AMPAR synaptic expression in CA1 pyramidal neurons following AAV transduction, the synaptic RI was measured at three different time points post infection. The RI of BioID2-AMPARs was unchanged at day post infection (DPI) 4 and 7, but significantly reduced relative to uninfected slices at DPI 13 (Figure 4.5D1). The extent of synaptic rectification observed at DPI 13 was

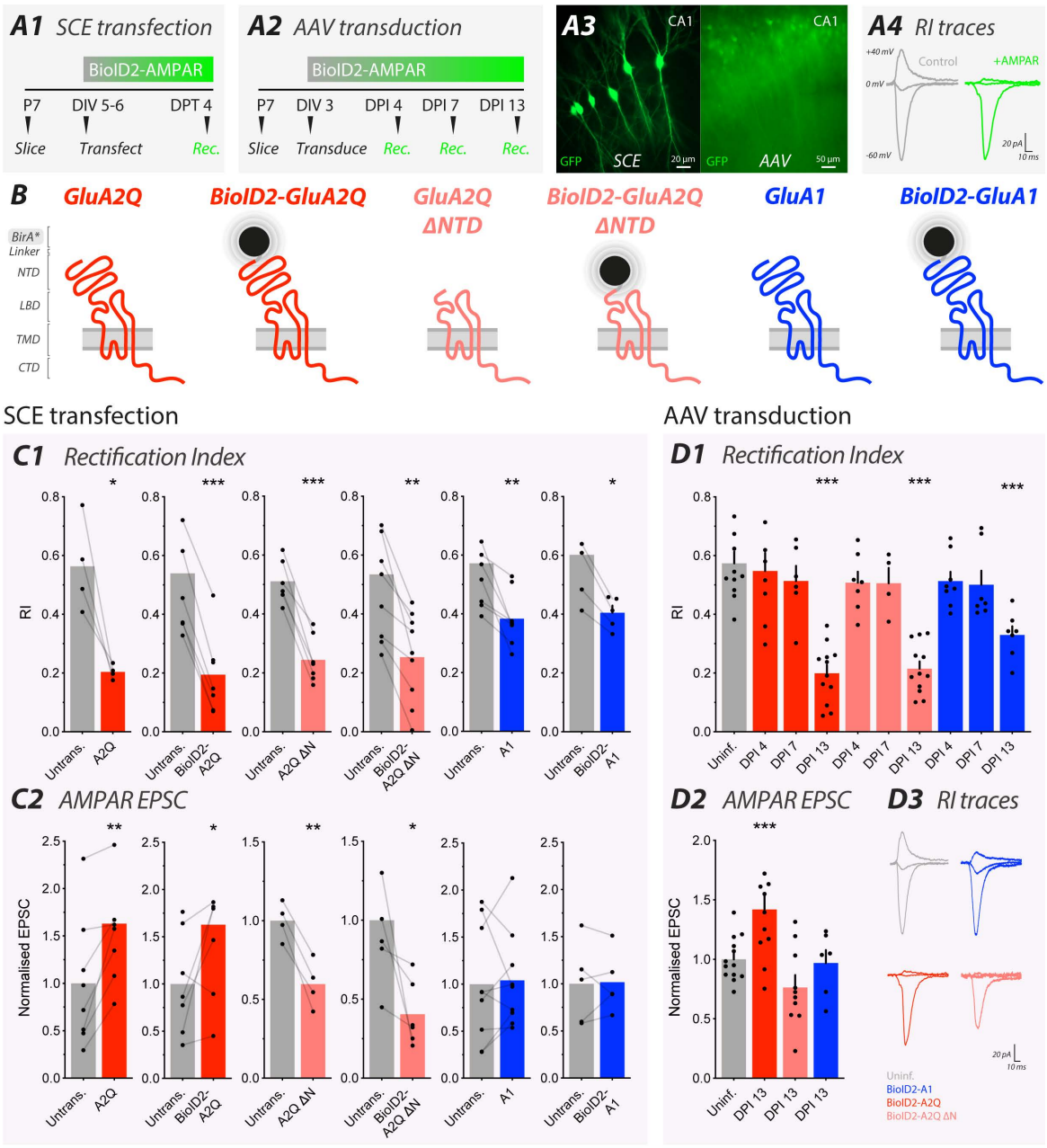

Figure 4.5 *BioID2-AMPARs traffic to CA1 synapses.*

Figure 4.5 ***BioID2-AMPARs traffic to CA1 synapses.*** *(**A1**) Protocol for SCE transfection of organotypic hippocampal slices. (**A2**) Protocol for AAV transduction of organotypic hippocampal slices. (**A3**) Left, SCE transfection of CA1 pyramidal neurons resulted in sparse GFP expression. Right, AAV transduction of CA1 pyramidal neurons resulted in global GFP expression. (**A4**) Rectification index (RI) traces were recorded at membrane potentials of -60, 0 and +40 mV from untransfected (Left, Control) and transfected (Right, +AMPAR) cells. Intracellular spermine blocks Q-pore containing AMPARs at positive potentials, reflected by a decrease in the +40 mV current in cells with synaptic expression of exogenous AMPARs. (**B**) Un-tagged and BioID2-tagged AMPAR subunits expressed in CA1 pyramidal neurons. (**C**) Synaptic RI and EPSC amplitude from cells transfected by SCE. (**C1**) A2Q (Untrans.: 0.56 ± 0.079; A2Q: 0.20 ± 0.012; n = 4; p < 0.05), BioID2-A2Q (Untrans.: 0.54 ± 0.083; BioID2-A2Q: 0.19 ± 0.052; n = 7; p < 0.001), A2Q ΔNTD (Untrans.: 0.51 ± 0.074; A2Q ΔNTD: 0.25 ± 0.032; n = 6; p < 0.001), BioID2-A2Q ΔNTD (Untrans.: 0.53 ± 0.079; BioID2-A2Q ΔNTD: 0.25 ± 0.050; n = 9; p < 0.05), A1 (Untrans.: 0.57 ± 0.066; A1: 0.38 ± 0.033; n = 8; p < 0.01), BioID2-A1 (Untrans.: 0.60 ± 0.078; BioID2-A1: 0.40 ± 0.024; n = 5; p < 0.05) all caused significant rectification of the synaptic response. (**C2**) A2Q (Untrans.: 46.2 ± 10.9 pA; A2Q: 75.2 ± 9.9 pA; n = 8; p < 0.001) and BioID2-A2Q (Untrans.: 82.8 ± 17.0 pA; BioID2-A2Q: 134.7 ± 26.3 pA; n = 7; p < 0.05) significantly increased the size of the EPSC. A2Q ΔNTD (Untrans.: 47.7 ± 2.8 pA; A2Q ΔNTD: 28.5 ± 3.6 pA; n = 4; p < 0.001) and BioID2-A2Q ΔNTD (Untrans.: 47.6 ± 7.5 pA; BioID2-A2Q ΔNTD: 19.3 ± 4.0 pA; n = 6; p < 0.05) significantly decreased the size of the EPSC. A1 (Untrans.: 57.0 ± 11.7 pA; A1: 59.3 ± 9.8 pA; n = 9; p < 0.79) and BioID2-A1 (Untrans.: 94.2 ± 18.2 pA; BioID2-A1: 95.9 ± 13.5 pA; n = 5; p < 0.86) had no effect on the size of the EPSC. (**D**) Synaptic RI and EPSC amplitude of cells transduced by AAV. (**D1**) BioID2-A2Q, BioID2-A2Q ΔNTD and BioID2-A1 all caused significant rectification of the synaptic response at DPI 13 relative to Uninf. slices (Uninf: 0.57 ± 0.040; BioID2-A2Q: 0.20 ± 0.028; BioID2-A2Q ΔNTD: 0.22 ± 0.025; BioID2-A1: 0.33 ± 0.030; p < 0.001). (**D2**) BioID2-A2Q significantly increased the size of the ESPC (Uninf: 53.3 ± 2.8 pA; BioID2-A2Q: 75.7 ± 7.4 pA; BioID2-A2Q ΔNTD: 40.7 ± 5.6 pA; BioID2-A1: 51.7 ± 5.3 pA; p < 0.05). (**D3**) Representative RI traces recorded at DPI 13.*

similar to that of SCE transfected cells at day post transfection (DPT) 4. Changes observed in the EPSC amplitude recorded at DPI 13 showed a similar trend to that of SCE transfected cells (Figure 4.5D2). This demonstrates that AAV transduction permits synaptic expression of functional BioID2-AMPARs at DPI 13 in a large proportion of cells.

Construct optimisation

A concern with placing BirA* tags at the N-terminus of the AMPAR is that synaptic protein interactions with the NTD may be occluded. In an attempt to overcome this issue, other variations of this construct were made by fusing BioID2 (27 kD) within an amino acid loop region of the AMPAR NTD (Figure 4.6A; Dutta et al., 2012; Krieger et al., 2015). This loop region is positioned on the 'side' of the NTD, therefore inclusion of the BioID2 tag at this site would permit protein interactions to occur with the 'top' of the AMPAR NTD. BioID2 was fused within the NTD loop region (Loop-BioID2-GluA1) at a site previously shown to be permissible by GFP (27 kD) fusion (D259-T261; Sheridan et al., 2006). BioID2 was flanked by two 9 amino acid '*Gly-Ser-Ser*' linkers before testing the surface expression and gating kinetics of Loop-BioID2-GluA1 in recombinant cells (Figure 4.6). Loop-BioID2-GluA1 however, displayed significantly smaller peak current amplitudes relative to N-terminally tagged GluA1 (N-BioID2-GluA1) (Figure 4.6B). Although total expression and labelling efficiency of Loop-BioID2-GluA1 appeared similar to N-BioID2-GluA1 (Figure 4.6C), the surface expression and/ or gating kinetics of this construct were severely hampered. Therefore, Loop-BioID2-GluA1 was deemed unsuitable for identification of AMPAR NTD interactors, as surface expression levels of receptors must be comparable for reliable PL proteomics experiments. Although direct protein interactions with the 'top' of the NTD may be occluded using exogenous N-terminally tagged BirA*-AMPARs, these proteins can still interact with neighbouring endogenous receptors and thus will be identified using PL proteomics owing to the 10-35 nm labelling radius of BirA* tags (Kim et al., 2014; May et al., 2020).

Taken together, these results indicate that N-terminally tagged BioID2-AMPARs are expressed as functional receptors and incorporate into CA1 synapses to the same extent as WT using both SCE transfection and AAV transduction (Figure 4.5). These data validate BirA*-AMPAR constructs for the identification of proximal synaptic proteins during excitatory synaptic transmission.

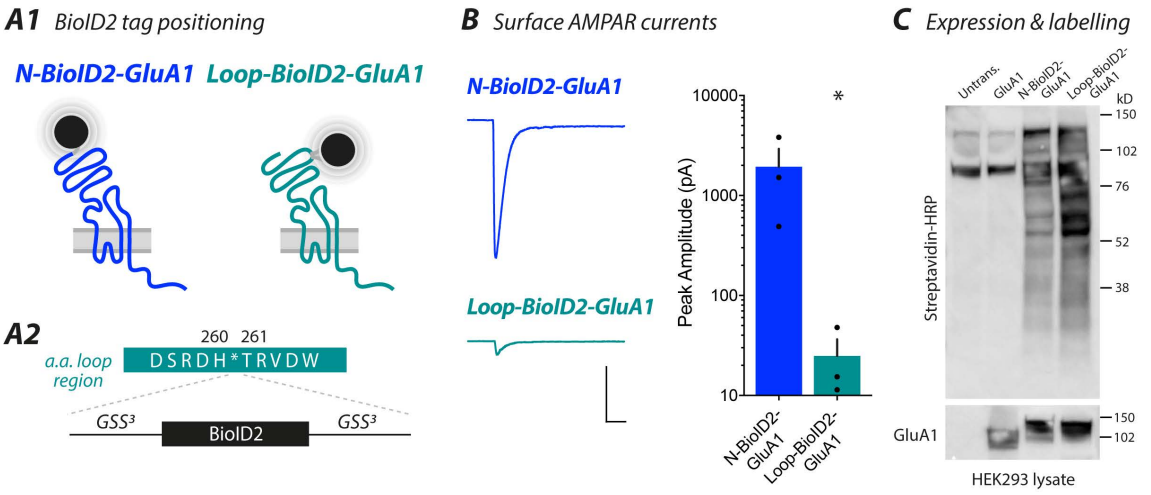

Figure 4.6 ***BioID2 tag positioning at the N-terminus but not NTD loop region permits surface expression of functional receptors.*** *(**A1**) N-terminal BioID2-GluA1 (N-BioID2-GluA1) was constructed by fusing BioID2 to the N-terminus of GluA1 following the native signal sequence using a 6 amino acid linker. Amino acid loop BioID2-GluA1 (Loop-BioID2-GluA1) was constructed by fusing BioID2 within a permissible amino acid loop region of the GluA1 NTD (H260-T261; Sheridan et al., 2006). (**A2**) Loop-BioID2-GluA1 was inserted within the GluA1 NTD at H260-T261, flanked by two GSS³ linkers. (**B**) Outside-out patches were pulled from HEK293 cells expressing N-BioID2-GluA1 and Loop-BioID2-GluA1 and subjected to fast application of 10 mM glutamate (electrophysiology data kindly provided by Mr Hinze Ho). AMPAR current peak amplitude of Loop-BioID2-GluA1 was significantly reduced relative to N-BioID2-GluA1 (N-BioID2-GluA1 = 2233 ± 792 pA; n = 3; Loop-BioID2-GluA1 = 24.8 ± 11 pA; n = 4; unpaired t-test, $p < 0.05$). (**C**) WB of biotinylated proteins probed for with streptavidin-HRP and GluA1 construct expression probed for with anti-GluA1 CTD.*

4.2.3 BirA*-AMPARs label in organotypic slice culture

To further confirm expression and proper localisation of BirA*-AMPARs, immunostaining was performed on organotypic hippocampal slices following transduction with AAV at DPI 13 (Figure 4.7A1). Transduction of excitatory neurons was achieved by application of high titer AAV (1.0 x 10^{13} GC/mL) with BirA*-AMPAR subunits under the CaMKIIα promoter. BioID2-AMPAR expression was observed in a high proportion of excitatory neurons using a selective antibody for the BioID2 tag (Figure 4.7A3). In slices treated with biotin for 48 hrs, streptavidin co-localised with BioID2 indicating biotinylation of proximal proteins in slice culture. Expression and labelling occurred globally across the hippocampal slice in CA1 and CA3 pyramidal and dentate gyrus (DG) cells (Figure 4.7B). PL proteomics therefore, will identify proteins from all these hippocampal cell types. Neurons expressing BioID2-AMPARs were positive for biotinylation in the soma and at dendritic spines (Figure 4.7A4). This demonstrates that at DPI 13 BioID2-AMPARs are localised in the ER and at hippocampal synapses and upon the application of biotin + ATP label their proximal environment.

Crucially, BioID2-GluA2Q localised to hippocampal dendritic spines, in-line with functional evidence for synaptic trafficking to CA1 synapses (Figure 4.5D1). Here, BioID2-GluA2Q extensively biotinylated proximal proteins (Figure 4.7A4), showing enrichment for dendritic protrusions. Thus, BioID2-GluA2Q permits unbiased labelling of potential synaptic protein interactors with the AMPAR NTD.

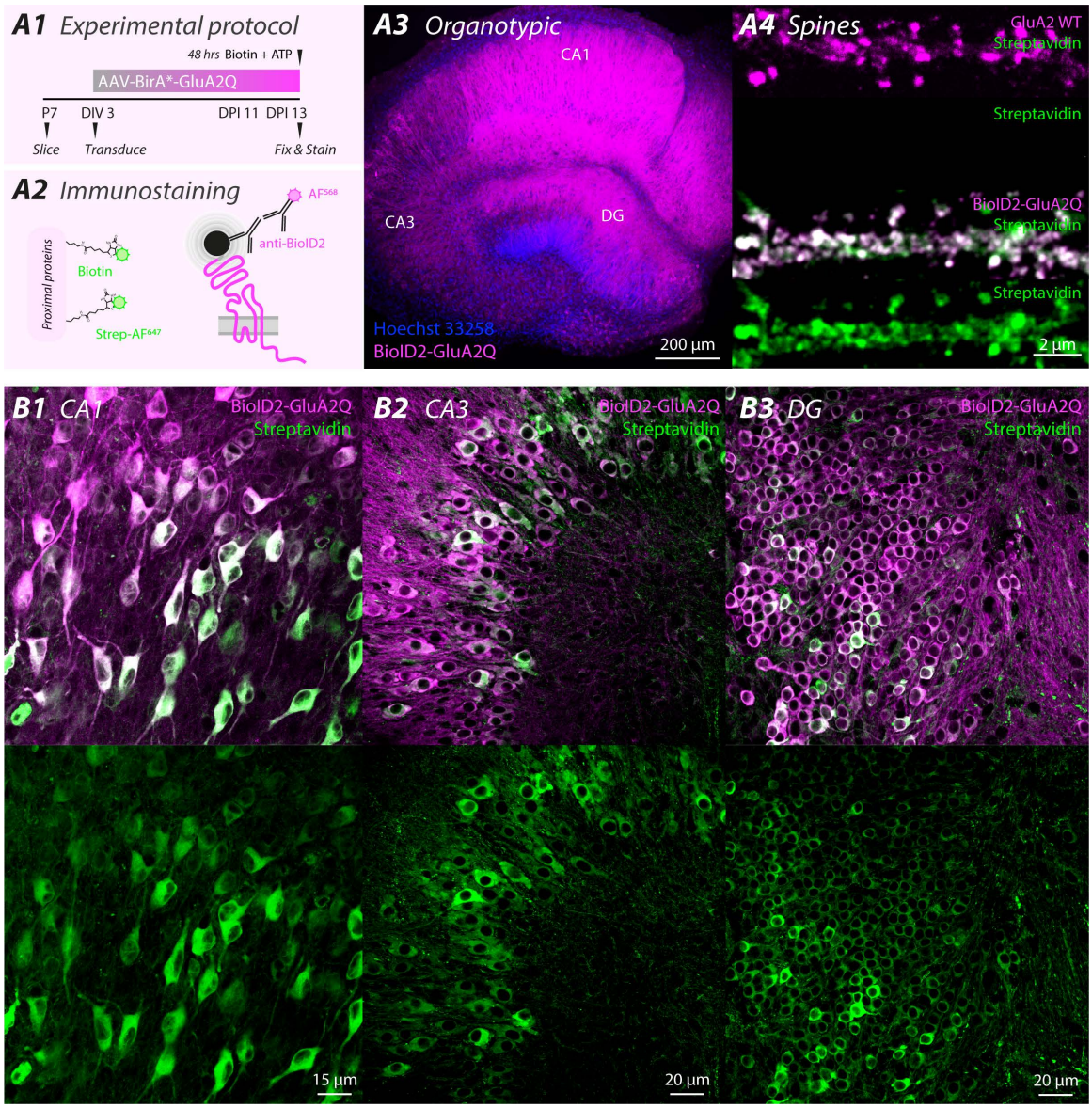

Figure 4.7 *BioID2-AMPARs express and label in hippocampal neurons.*

Figure 4.7 ***BioID2-AMPARs express and label in hippocampal neurons.*** *(**A1**) Experimental protocol for immunostaining of BioID2-AMPARs and biotinylated proteins in hippocampal neurons. (**A2**) BioID2-AMPAR expression was detected using primary anti-BioID2 and secondary AF^{568} antibodies. PL was initiated by 48 hrs biotin + ATP application. Biotinylated proteins were detected using streptavidin AF^{647}-conjugate. (**A3**) Organotypic hippocampal slices transduced by AAV expressed BioID2-AMPARs in excitatory neurons throughout the slice. Global expression includes hippocampal CA1, CA3 and DG neurons at DPI 13. (**A4**) Exogenous BioID2-GluA2Q and endogenous GluA2 localised to dendritic spines. However, BioID2- but not endogenous GluA2, labelled extensively throughout the dendrite and in dendritic spines. (**B1**) Co-localisation of BioID2-GluA2Q expression and biotinylated proteins indicated robust exogenous expression and labelling of excitatory neurons in hippocampal (**B1**) CA1, (**B2**) CA3 and (**B3**) DG regions.*

4.2.4 Proximity-labelling proteomics protocol

Initial BirA* characterisation was performed using BioID2, demonstrating successful expression (Figure 4.4), function (Figure 4.5), localisation and labelling (Figure 4.7) of BioID2-AMPARs. Experimental characterisation was performed with BioID2 due to its well documented use in neuronal tissue (Uezu et al., 2016; Spence et al., 2019). These experiments permitted establishment of an experimental timeline outline below (Figure 4.8). This PL protocol was then applied to higher labelling efficiency tags, MiniTurbo and TurboID (Branon et al., 2018), and subsequently APEX2 (Lam et al., 2015; Hung et al., 2016).

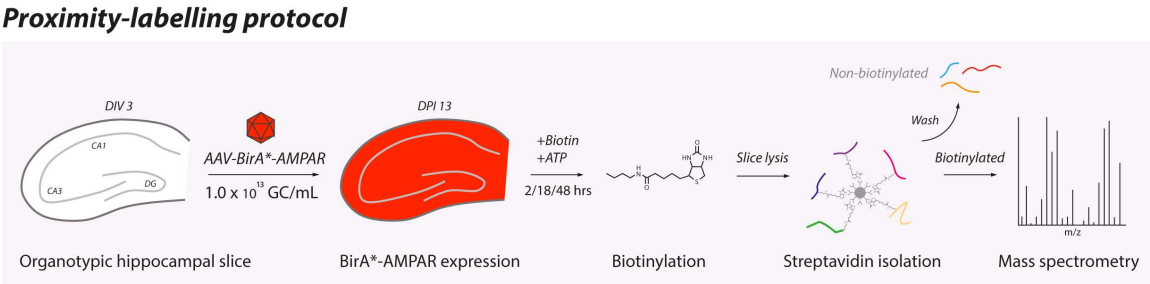

Figure 4.8 ***Proximity-labelling protocol for BirA*-AMPARs.*** *Experimental protocol for BirA*-AMPAR PL proteomics in organotypic slice culture. BirA*-AMPARs were expressed in hippocampal slices by transduction with 1.0 x 10^{13} GC/mL AAV. BirA*-AMPARs were expressed selectively in principle excitatory neurons of the hippocampal slice up until day post infection (DPI) 13. Biotinylation was induced by application of 200 µM biotin + 2 mM ATP for 2 hrs (BioID2), 18 hrs (MiniTurbo) or 48 hrs (TurboID). For APEX2, biotinylation was induced by application of 500 µM biotin-phenol and H_2O_2 for 10 mins (Lam et al., 2015; Hung et al., 2016). Biotinylated proteins were then solubilised by slice lysis and isolated using streptavidin magnetic beads before identification by mass spectrometry (MS).*

Proximity-labelling proteomics data filtering

50 organotypic hippocampal slices were prepared and AAV-transduced per experimental condition, to maximise the amount of biotinylated material for MS. Experiments were performed separately using the same protocol for BioID2-, MiniTurbo- and TurboID-AMPARs, and all conditions were produced in triplicate to reduce the chance of identifying false positive hits. Following labelling initiated by biotin + ATP, slices were harvested and solubilised in lysis buffer before isolating biotinylated proteins with streptavidin. Slice lysates were probed using WB (Figure 4.9A3) to confirm expression and labelling before processing samples for MS. Biotinylated proteins were subjected to trypsin digestion and the peptide mixtures were then analysed by nano-LC-MS/MS. Raw files were analysed using MaxQuant and processed by Perseus to obtain label-free quantification (LFQ) intensities used for relative quantification of enriched proteins.

LFQ data indicates a higher biotinylation intensity of BirA*-AMPAR expressing slices relative to uninfected slices (Figure 4.9B), further confirming successful labelling with BirA*-AMPAR probes. Reproducibility plots were produced by plotting the biotinylation intensity detected from the 1^{st} versus 2^{nd} biological replicate for each given protein (Figure 4.9C). An R^2 value of 0.95 indicates that TurboID produces MS data with the highest reproducibility, as the biotinylation intensity for a given protein remains consistent across biological replicates. Volcano plots indicating the statistical significance (y-axis; p value; $-\text{Log}_{10}$) versus fold-enrichment (x-axis; Log_2 show an enrichment of biotinylated proteins for BirA*-GluA2Q WT and ΔNTD relative to uninfected control (Figure 4.9D). This demonstrates successful labelling and identification of enriched proximal proteins with BirA*-AMPARs. Furthermore, it suggests that TurboID has the highest degree of specificity, possibly due to its shorter required labelling time and higher efficiency (Figure 4.4; Branon et al., 2018).

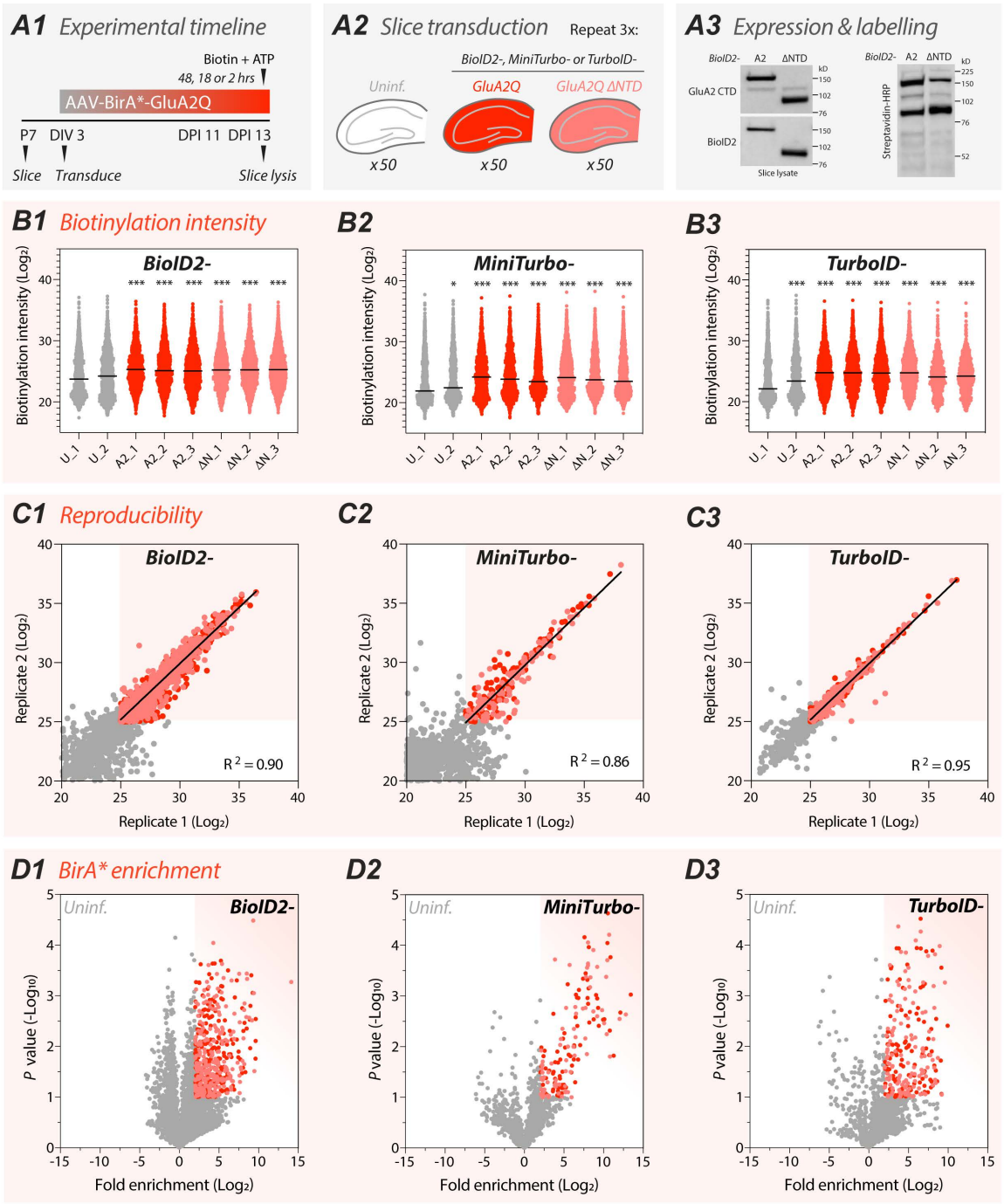

Figure 4.9 *Proximity-labelling proteomics with BirA* tags.*

Figure 4.9 ***Proximity-labelling proteomics with BirA* tags.*** *(**A1**) Experimental timeline for PL in organotypic slice culture. Slices were treated with biotin + ATP for 48, 18 or 2 hrs for BioID2-, MiniTurbo- and TurboID-AMPARs respectively. (**A2**) 50 organotypic hippocampal slices were cultured and AAV transduced per condition, repeated in triplicate for BioID2-, MiniTurbo- and TurboID-AMPARs. (**A3**) Left, Expression of BioID2-GluA2 and BioID2-GluA2ΔNTD in organotypic hippocampal slices indicated by anti-GluA2 and anti-BioID2 antibodies probing of slice lysate. Right, Biotinylation in organotypic hippocampal slices was indicated by streptavidin-HRP probing of slice lysate. (**B**) Biotinylation intensity, indicated by MS label free quantification values (Log_2). is greater for that of BioID2-GluA2 and GluA2Q ΔNTD expressing slices relative to Uninf. for (**B1**) BioID2-, (**B2**) MiniTurbo- and (**B3**) TurboID-. (**C**) Scatter plot indicating the reproducibility of biotinylated hits from replicate 1 versus replicate 2. Reproducibility between sample replicates was highest for TurboID- data. (**C1**) BioID2- reproducibility plot (simple linear regression; $R^2 = 0.90$), (**C2**) MiniTurbo- reproducibility plot (simple linear regression; $R^2 = 0.86$) and (**C3**) TurboID- reproducibility plot (simple linear regression; $R^2 = 0.95$) for GluA2Q WT and ΔNTD. WT (red) and ΔNTD (pink) data is overlayed. Datapoints outside the threshold cut-off (grey) represent non-specific proteins. (**D1**) Volcano plot of BirA*-enrichment relative to Uninf. for (**D1**) BioID2-, (**D2**) MiniTurbo- and (**D3**) TurboID- GluA2Q WT and ΔNTD. WT (red) and ΔNTD (pink) data is overlayed. Datapoints outside the threshold cut-off (grey) represent non-specific proteins.*

AMPAR NTD-enriched proteins

Having established BirA* PL proteomics in organotypic slice culture, this study next examined the proteomes of GluA2Q WT and ΔNTD receptors relative to uninfected control slices (Appendix Figure A.1/2/3). Volcano plots were produced for data from BioID2-, MiniTurbo- and TurboID-, providing a robust statistical comparison of WT versus ΔNTD acquired in triplicate (Figure 4.10A). Proteins were considered enriched for a given condition if their fold enrichment was > 2 and their P value was < 0.05. This ensures that candidate proteins are reliably enriched for a given condition. In this case, proteins that showed significant enrichment for WT over ΔNTD receptors were considered candidate AMPAR NTD interactors.

One of the most NTD-enriched proteins detected is neuronal pentraxin-1 (Nptx1), observed across all triplicate BirA* datasets (Figure 4.10B). The relative capability of BirA* tags to capture this interaction is as follows: TurboID > MiniTurbo > BioID2. Nptx1 has been shown to bind to and cluster postsynaptic AMPARs through their NTD (O'Brien et al., 1999; Xu et al., 2003; Sia et al., 2007), validating this as a method to identify AMPAR NTD interactors. TurboID also captured other known constituents of the AMPAR proteome, including, Nptxr (Lee et al., 2017) and Olfm1 (Pandya et al., 2018), proposed direct AMPAR NTD interactors, and Frrs1l, a positive regulator of AMPAR assembly in the ER (Schwenk et al., 2019). PL proteomics identifies both known AMPAR constituents and a number of novel candidate interactors that influence glutamatergic synaptic transmission. A complete list of GluA2Q NTD- enriched proteins is listed in Appendix A (Figure A.1) and the relevance of these proteins in the literature is explored further in the discussion (see 4.3).

To assess the coverage of the synaptic cleft by BirA* tags, identified proteins were entered into the synaptic gene ontology (SynGO) database (Koopmans et al., 2019; www.syngoportal.org). SynGO enrichment analysis identified protein components of the pre- and post-synaptic membrane involved in synaptic signaling mechanisms (Figure 4.10C1). Interestingly, TurboID-GluA2Q WT receptors identified the highest percentage of synaptic proteins, ~40% (Figure 4.10C2), suggesting TurboID is the most effective tag at labelling this subcellular compartment.

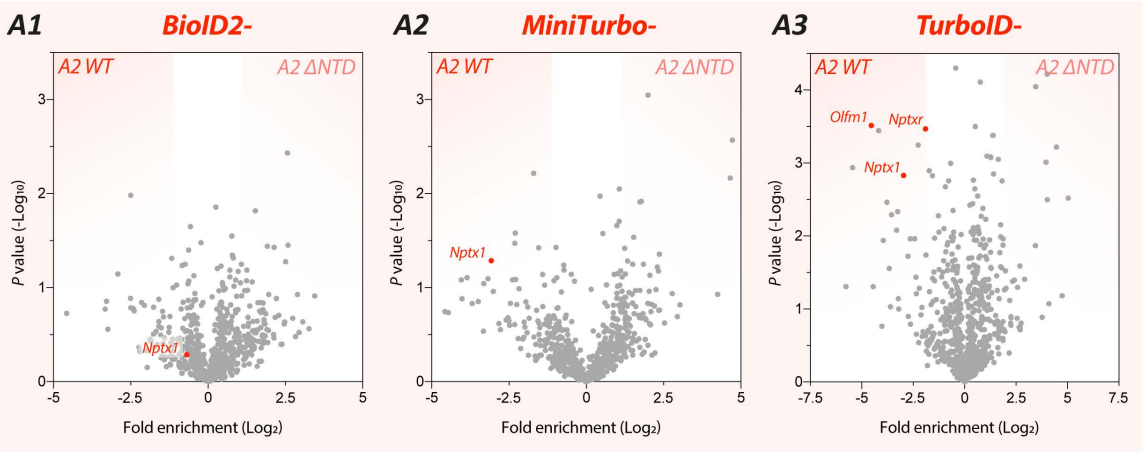

B *NTD enrichment (Log₂)*

BioID2_1	BioID2_2	BioID2_3	BioID2_Avg.	MiniTurbo_1	MiniTurbo_2	MiniTurbo_3	MiniTurbo_Avg.	TurboID_1	TurboID_2	TurboID_3	Turbo_Average	Overall	Uniprot	Gene names	Protein names
0.0	0.0	0.0	0.0	0.5	-0.4	-0.6	-0.1	5.0	6.3	5.1	5.4	2.7	CA2D1_MOUSE	Cacna2d1	Voltage-dependent calcium channel subunit alpha-2/delta-1
0.0	0.0	0.0	0.0	-0.7	-2.1	-0.7	-1.2	3.2	7.4	6.7	5.8	2.6	VTM2L_MOUSE	Vstm2l	V-set and transmembrane domain-containing protein 2-like protein
1.4	0.1	0.4	0.6	2.0	4.1	3.1	3.1	2.7	3.4	2.8	3.0	2.4	NPTX1_MOUSE	Nptx1	Neuronal pentraxin-1
0.0	0.0	0.0	0.0	0.0	0.0	0.0	0.0	4.4	3.8	5.4	4.5	2.3	NOE1_MOUSE	Olfm1	Olfactomedin-1/ Noelin-1
0.7	-1.5	-0.1	-0.3	0.7	6.1	6.9	4.6	-1.7	4.3	4.1	2.2	2.2	FRS1L_MOUSE	Frrs1l	DOMON domain-containing protein FRRS1L
0.0	0.0	0.0	0.0	-1.0	0.0	0.4	-0.2	2.5	5.7	5.2	4.4	2.2	NELL2_MOUSE	Nell2	Protein kinase C-binding protein NELL2
-0.1	-0.9	-0.5	-0.5	1.1	1.0	-0.8	0.4	3.9	4.4	4.2	4.2	2.1	STIM2_MOUSE	Stim2	Stromal interaction molecule 2
0.0	0.0	0.0	0.0	0.0	0.0	0.0	0.0	0.9	4.1	7.1	4.0	2.0	DYN2_MOUSE	Dnm2	Dynamin-2
0.0	0.0	0.0	0.0	-1.0	1.5	1.9	0.8	3.3	3.2	4.2	3.6	2.0	TMX4_MOUSE	Tmx4	Thioredoxin-related transmembrane protein 4
-0.1	-0.3	-0.9	-0.5	1.7	1.5	0.9	1.4	2.9	3.1	3.9	3.3	1.9	CHID1_MOUSE	Chid1	Chitinase domain-containing protein 1
0.2	0.3	-0.3	0.1	0.0	0.9	-0.4	0.2	1.0	4.8	5.0	3.6	1.9	PPIB_MOUSE	Ppib	Peptidyl-prolyl cis-trans isomerase B;Peptidyl-prolyl cis-trans isomerase
0.0	0.0	0.0	0.0	0.4	5.0	5.6	3.7	1.7	2.0	2.0	1.9	1.9	NPTXR_MOUSE	Nptxr	Neuronal pentraxin receptor
0.0	0.0	0.0	0.0	0.6	0.0	2.2	0.9	5.0	2.0	2.6	3.2	1.8	ABCA2_MOUSE	Abca2	ATP-binding cassette sub-family A member 2
0.0	0.0	0.0	0.0	0.5	-1.5	-1.0	-0.6	3.4	3.8	4.1	3.8	1.7	Q6ZQ56_MOUSE	mKIAA0743	Neurexin-3
-0.1	-0.2	-1.1	-0.4	-1.3	0.0	-0.9	-0.8	3.4	3.2	5.3	4.0	1.7	RYR2_MOUSE	Ryr2	Ryanodine receptor 2
0.0	0.0	0.0	0.0	0.7	-0.1	-0.2	0.1	4.3	4.0	1.3	3.2	1.6	EXTL2_MOUSE	Extl2	Exostosin-like 2
-0.1	-1.6	-0.8	-0.8	3.0	2.2	2.1	2.5	2.3	2.4	2.1	2.3	1.5	CNTP1_MOUSE	Cntnap1	Contactin-associated protein 1
-0.2	1.1	0.8	0.6	0.0	0.0	0.0	0.0	3.1	0.5	4.6	2.7	1.5	SYPH_MOUSE	Syp	Synaptophysin
0.0	0.0	0.0	0.0	0.9	1.7	0.8	1.1	0.6	1.6	4.8	2.3	1.5	NCAN_MOUSE	Ncan	Neurocan core protein
0.0	0.0	0.0	0.0	-0.3	3.7	2.5	2.0	2.6	1.2	1.8	1.9	1.4	P4HA1_MOUSE	P4ha1	Prolyl 4-hydroxylase subunit alpha-1
0.1	0.9	0.7	0.5	0.3	6.5	0.7	2.5	-0.3	0.8	3.4	1.3	1.4	EFTU_MOUSE	Tufm	Elongation factor Tu, mitochondrial
0.0	0.0	0.0	0.0	0.3	0.1	-0.1	0.1	2.3	2.8	3.2	2.8	1.4	L1CAM_MOUSE	L1cam	Neural cell adhesion molecule L1
0.9	0.1	-0.5	0.2	1.3	4.6	7.5	4.5	0.4	0.0	0.9	0.4	1.4	CNPY3_MOUSE	Cnpy3	Protein canopy homolog 3
0.0	-0.1	0.5	0.2	0.0	0.0	0.0	0.0	3.4	4.1	0.4	2.6	1.4	SHSA6_MOUSE	Shisa6	Protein shisa-6 homolog
1.0	0.2	-0.6	0.2	2.6	0.4	1.1	1.3	1.0	0.4	4.1	1.8	1.3	LGI1_MOUSE	Lgi1	Leucine-rich glioma-inactivated protein 1
0.0	0.0	0.0	0.0	-0.5	3.5	4.6	2.5	0.6	1.3	1.4	1.1	1.2	TICN2_MOUSE	Spock2	SPARC/ Osteonectin
0.0	0.0	0.0	0.0	0.1	2.5	0.2	0.9	2.0	-1.8	5.1	1.7	1.1	ALDH2_MOUSE	Aldh2	Aldehyde dehydrogenase, mitochondrial
0.0	0.0	0.0	0.0	-1.4	0.3	1.6	0.2	1.2	3.7	1.5	2.1	1.1	PP2BA_MOUSE	Ppp3ca	Serine/threonine-protein phosphatase 2B catalytic subunit alpha isoform
0.5	-0.3	0.5	0.2	0.0	0.0	0.0	0.0	-1.2	2.9	4.4	2.1	1.1	1433F_MOUSE	Ywhah	14-3-3 protein eta
2.9	0.4	-1.6	0.6	1.1	1.6	2.4	1.7	1.0	1.2	0.8	1.0	1.1	ERO1A_MOUSE	Ero1l	ERO1-like protein alpha

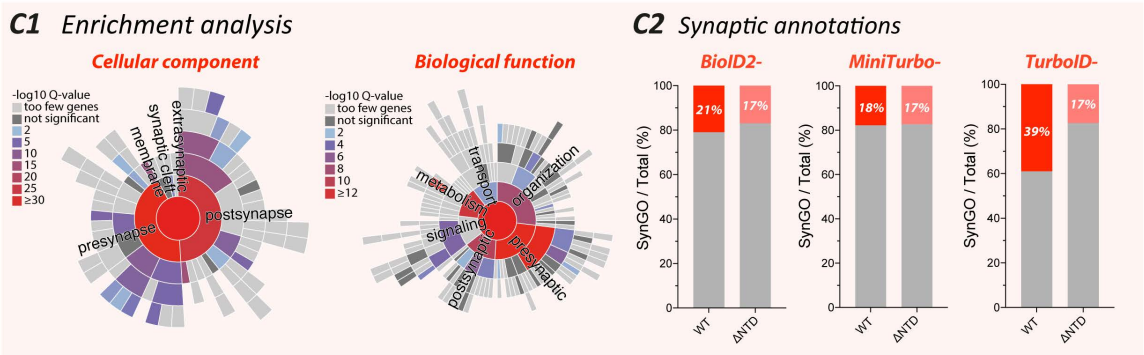

Figure 4.10 *BirA*-GluA2 proximity-dependent proteome.*

Figure 4.10 ***BirA*-GluA2 proximity-dependent proteome.*** *(**A1**) Volcano plot of triplicate data for GluA2Q WT versus ΔNTD acquired using BioID2-. Enrichment for WT (left; red box) or NTD-deleted (ΔNTD) (right; pink box) GluA2Q receptors was considered significant if fold enrichment (Log_2) > 2 and P value ($-Log_{10}$) > 1. Nptx1 showed a trend towards NTD-enrichment, but no statistical significance was detected. (**A2**) Volcano plot of triplicate data for GluA2Q WT versus ΔNTD acquired using MiniTurbo-. Nptx1 was significantly enriched for GluA2Q WT versus ΔNTD using MiniTurbo. (**A3**) Volcano plot of triplicate data for GluA2Q WT versus ΔNTD acquired using TurboID-. Nptx1 was significantly enriched for WT GluA2 along with other candidate NTD interactors, Olfm1 and Nptxr, using TurboID. Note the increased x and y axis of TurboID, the greatest extent of NTD-enrichment for Nptx1 was detected with TurboID relative to MiniTurbo and BioID2. (**B**) Table of ranked GluA2Q NTD-enriched proteins. Nptx1 NTD enrichment values averages among the highest across all three triplicate BirA* datasets. (**C1**) SynGO cellular component and biological function terms visualised in a sunburst plot with the number of terms represented by heat-mapping (Koopmans et al., 2019). (**C2**) Proportion of synaptic SynGO annotations identified using BioID2-, MiniTurbo- and TurboID-. TurboID-GluA2Q WT identified the greatest proportion of synaptic genes (~40%) relative to MiniTurbo- and BioID2-.*

Extracellular labelling efficiency

As with any experimental method, there are a number of limitations to be considered. BirA* PL proteomics relies on the biotinylation of surface lysine residues (Figure 4.2A) on neighbouring proteins, it is possible therefore that proteins interactors without surface-exposed lysine residues cannot be biotinylated and go undetected. To overcome this limitation, PL proteomics was repeated using an APEX tag. In contrast to BirA*, APEX biotinylates surface tyrosine residues on proximal proteins (Figure 4.2B). Therefore, by combining the proteomes of BirA* and APEX, the chance of missing protein interactors will be greatly reduced.

In addition to the differential amino acids biotinylated by BirA* and APEX, the enzymatic efficiency of these PL tags has been reported to differ considerably. Although vast improvements in the temporal labelling efficiency of BirA* tags have been achieved with the development of MiniTurbo and TurboID (Branon et al., 2018), APEX2 has a superior labelling efficiency with a reaction time of 1 min (Lam et al., 2015; Hung et al., 2016), opposed to 3 hrs with TurboID (Branon et al., 2018). Furthermore, the relative efficiency of these enzymes varies in different subcellular compartments, where APEX2 is thought to be superior at labelling extracellular proteins at the cell surface, but not in the reducing environment of the cytosol (Trinkle-Mulcahy, 2019). In the context of this study, APEX2 would therefore permit a higher labelling efficiency of synaptic proteins enabling capture of dynamic cleft protein interactions with the AMPAR NTD, on a timescale of mins rather than hrs.

To compare the relative surface biotinylation efficiency of PL tags, BioID2-, MiniTurbo, TurboID and APEX2-tagged GluA2Q receptors were expressed recombinantly in HEK293 cells and biotinylation was initiated by 10 min application of biotin. Cells were subsequently live-stained for surface biotinylation using a streptavidin AF^{647}-conjugate and imaged to quantify fluorescence intensity of biotinylated proteins at the cell surface (Figure 4.11A). The level of surface biotinylation was significantly higher for APEX2- relative to other BirA*-tagged GluA2Q receptors using a 10 min reaction time (Figure 4.11B). This suggests that APEX2- has a significantly higher surface labelling efficiency over BirA*- GluA2Q receptors, therefore PL proteomics was repeated using with APEX2-GluA2Q WT and ΔNTD using the established PL protocol (Figure 4.8).

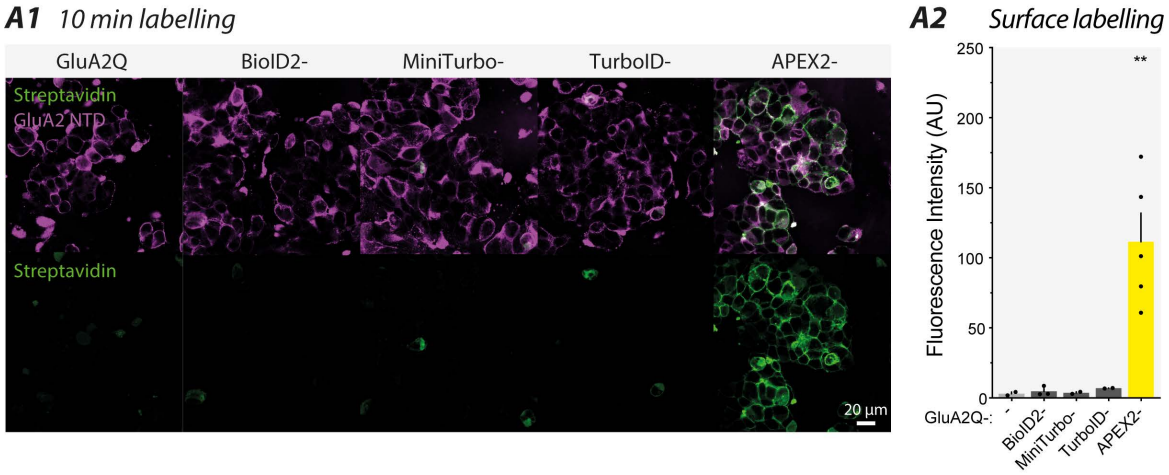

Figure 4.11 ***APEX2- has the highest surface labelling efficiency in 10 mins.*** *(**A1**) BioID2, MiniTurbo, TurboID and APEX2 tagged GluA2Q homomers were expressed in HEK293 cells (GluA2 NTD; magenta). 200 µM biotin + 2 mM ATP was applied to BirA*-AMPARs and 500 µM biotin-phenol + H_2O_2 was applied to APEX2-AMPARs for a total of 10 mins before PFA fixation. proximal surface proteins with 10 mins biotin application, whereas BioID2, MiniTurbo and TurboID -GluA2Q did not (streptavidin; green). Surface biotinylation was detected by live-staining with streptavidin AF^{647}-conjugate. (**A2**) Surface labelling fluorescence intensity (AU) was significantly higher for APEX2- expressing cells, relative to BirA*- and untagged- expressing cells (GluA2Q = 2.1 ± 0.1; n = 2; BioID2 = 3.5 ± 1.4; n = 3; MiniTurbo = 2.9 ± 0.5; n = 2; TurboID = 5.9 ± 0.3; n = 2; APEX2 = 109.5 ± 24.6; n = 5; ANOVA, ** p < 0.01).*

APEX2 PL proteomics

Using the experimental protocol (Figure 4.8) and data filtering (Figure 4.9) established with BirA* tags, APEX2 PL proteomics was performed in organotypic slice culture (Figure 4.12). APEX2-GluA2Q WT and ΔNTD fusion constructs (Figure 4.12A3) were introduced into organotypic hippocampal slices by transduction with high-titer AAV. To initiate biotinylation, APEX2 requires 500 μM biotin-phenol and H_2O_2 supplementation into the culture media for 10 mins (Figure 4.12A1), permitting biotinylation of sufficient protein material for identification by nano-LC-MS/MS. The extent of GluA2 NTD-enrichment was calculated as the fold-enrichment for WT versus ΔNTD receptors, visualised by a volcano plot (Figure 4.12B3) and table of NTD-enrichment (Figure 4.12C).

APEX2 PL proteomics identifies all top-ranked candidates identified using BirA* proteomics, illustrated in a combined NTD-enrichment table of all 4 PL tags (Appendix A.3). Additionally, APEX2 uncovers a number of novel candidate synaptic protein interactors unidentified using BirA*. New candidate proteins are potentially identified as a consequence of labelling surface tyrosine, opposed to lysine residues, and/or an increased temporal labelling efficiency over BirA*. These proteins were then screened for direct AMPAR NTD interactions in the cell-based binding assay (Figure 4.13)

The greatest extent of GluA2 NTD-enrichment with APEX2 PL proteomics is detected for neuropilin-1 (Nrp1; Figure 4.12C). Nrp1 localises at dendritic spines through direct PSD-95 interactions through its PDZ domain (Cai et al., 1999). Interestingly, neuropilin-2 (Nrp2) directly interacts with GluA1/2 through its CUB domain (Wang et al., 2017). Of note, CUB-domain containing proteins SOL-1/2 regulate synaptic AMPAR content (Zheng et al., 2004; Wang et al., 2012), and the CUB-domain of Neto1/2 binds the GluK2 NTD (Li et al., 2019), regulating synaptic trafficking (Sheng et al., 2017a), suggestive of a theme in the regulation of iGluR synaptic function by CUB-domain containing proteins. A complete list of GluA2 NTD-enriched proteins identified by APEX2 is listed in Appendix A (Figure A.2), with their significance explored further in the discussion (see 4.3).

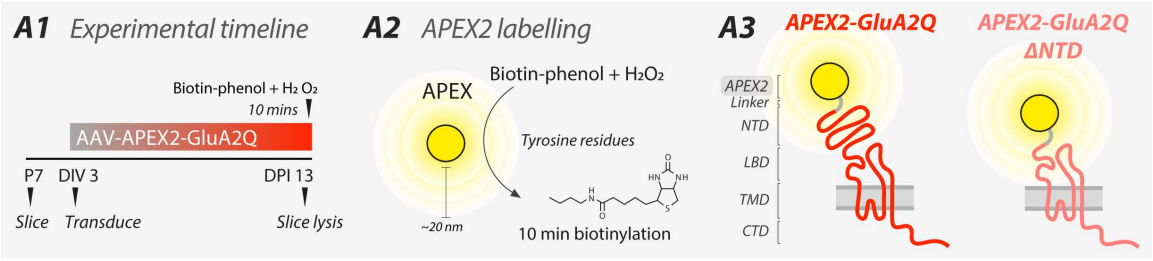

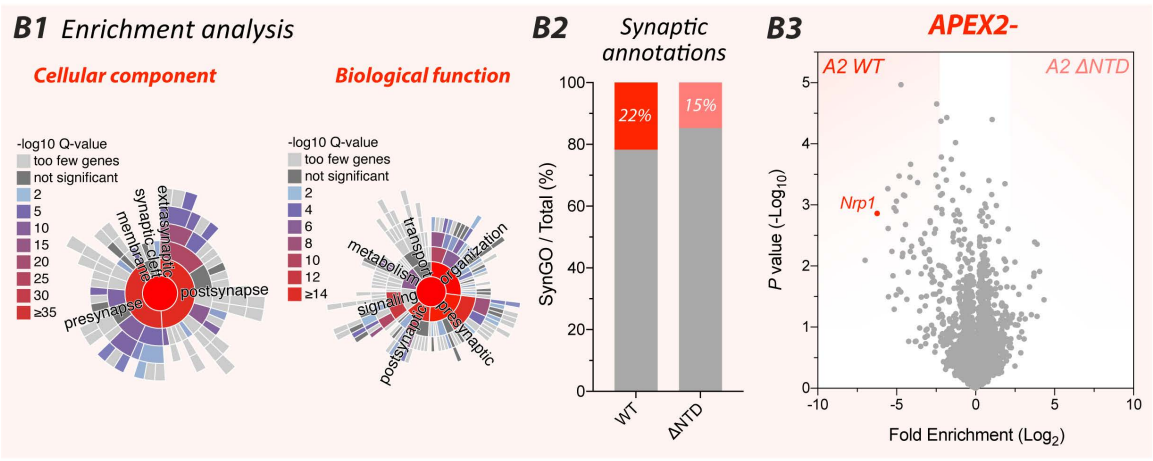

C NTD enrichment (Log_2)

Apex2_1	Apex2_2	Apex2_3	Apex2_Average	Uniprot	Gene names	Protein names
6.9	8.2	5.9	7.0	NRP1_MOUSE	Nrp1	Neuropilin-1
5.3	6.9	6.5	6.2	NECT1_MOUSE	Nectin1	Nectin-1
5.2	5.8	5.8	5.6	NEO1_MOUSE	Neo1	Neogenin
5.7	4.7	6.2	5.5	CXAR_MOUSE	Cxadr	Coxsackievirus and adenovirus receptor homolog
3.9	5.4	7.2	5.5	Q6ZQ56_MOUSE	mKIAA0743	Neurexin-3
6.0	5.1	4.8	5.3	GRM2_MOUSE	Grm2	Metabotropic glutamate receptor 2
4.5	6.6	4.5	5.2	PGCA_MOUSE	Acan	Aggrecan core protein
6.2	4.9	4.4	5.2	OMGP_MOUSE	Omg	Oligodendrocyte-myelin glycoprotein
4.0	3.7	7.8	5.2	NEGR1_MOUSE	Negr1	Neuronal growth regulator 1
4.7	5.0	5.4	5.0	CD166_MOUSE	Alcam	CD166 antigen
3.1	5.8	6.2	5.0	LIGO1_MOUSE	Lingo1	Leucine-rich repeat and immunoglobulin-like domain-containing nogo receptor-interacting protein 1
5.1	4.7	5.2	5.0	CSMD1_MOUSE	Csmd1	CUB and sushi domain-containing protein 1
5.1	3.4	6.1	4.9	AT1B3_MOUSE	Atp1b3	Sodium/potassium-transporting ATPase subunit beta-3
4.9	4.6	5.1	4.8	ITIH2_MOUSE	Itih2	Inter-alpha-trypsin inhibitor heavy chain H2
4.1	3.9	6.2	4.7	LGI1_MOUSE	Lgi1	Leucine-rich glioma-inactivated protein 1
5.1	4.4	4.6	4.7	CADM2_MOUSE	Cadm2	Cell adhesion molecule 2
5.7	4.2	4.0	4.6	EPHB2_MOUSE	Ephb2	Ephrin type-B receptor 2
5.4	4.3	4.2	4.6	GRM7_MOUSE	Grm7	Metabotropic glutamate receptor 7
4.6	3.9	5.2	4.6	MDGA1_MOUSE	Mdga1	MAM domain-containing glycosylphosphatidylinositol anchor protein 1
3.7	5.0	5.0	4.6	CRAC1_MOUSE	Crtac1	Cartilage acidic protein 1
4.2	5.2	4.0	4.5	MAG_MOUSE	Mag	Myelin-associated glycoprotein
4.1	5.3	3.9	4.4	NGAL_MOUSE	Lcn2	Neutrophil gelatinase-associated lipocalin
3.8	3.3	5.9	4.4	NTRI_MOUSE	Ntm	Neurotrimin
3.1	5.3	4.4	4.3	CADM3_MOUSE	Cadm3	Cell adhesion molecule 3

Figure 4.12 *APEX2-GluA2 proximity-dependent proteome.*

Figure 4.12 ***APEX2-GluA2 proximity-dependent proteome.*** *(**A1**) Experimental timeline for PL proteomics with APEX2-GluA2Q. Biotin-phenol and H_2O_2 were applied to slices expressing APEX-GluA2Q at DPI 13 for 10 mins before slice lysis. (**A2**) APEX2 biotinylates proximal tyrosine residues within a ~20 nm radius upon application of biotin-phenol and H_2O_2. (**A3**) APEX2-GluA2Q and APEX2-GluA2Q ΔNTD fusion constructs contained a 6 amino acid linker and were expressed under the native signal sequence, as with BirA*-AMPARs. (**B1**) SynGO cellular component and biological function terms visualised in a sunburst plot with the number of terms represented by heat-mapping (Koopmans et al., 2019). (**B2**) Proportion of synaptic annotations with APEX2-GluA2Q WT and ΔNTD. WT identified the greatest proportion of synaptic genes relative to ΔNTD. (**B3**) Volcano plot of GluA2Q WT versus ΔNTD reveals NTD-enriched proteins and top-ranked candidate neuropilin-1, Nrp1. (**C**) GluA2 NTD-enrichment table presented as a heat-map (Log_2) listing the top-ranked candidates identified by APEX2 PL proteomics.*

4.2.5 Cell-based binding assay validation

Candidate AMPAR NTD interactors identified by PL proteomics of GluA2Q receptors were subsequently studied for direct NTD interactions. A cell-based binding assay was developed to assess direct interactions between extracellular secreted proteins and the AMPAR NTD. Variations on the enzyme-linked immunosorbent assay have been used to identify low-affinity extracellular protein-protein interactions (Bushell et al., 2008; Ranaivoson et al., 2019). However, these screens require laborious protein purification of individual candidates, which often requires optimisation for each protein produced. The cell-based binding assay described in this chapter was performed using small-scale production of candidate proteins, improving assay efficiency and enabling high-throughput screening. Similar assays have been performed using iGluR NTDs to identify direct protein interactors: Cbln1, C1ql2/3 and CPTX permitting detection of μM affinity interactions, as determined using surface plasmon resonance (SPR; Matsuda et al., 2010; Elegheert et al., 2016; Matsuda et al., 2016; Suzuki et al., 2020).

The top 33 NTD-enriched proteins identified from PL proteomics (Figure 4.10B) and 8 identified from the literature were subjected to study in the cell-based binding assay (Figure 4.13D1). Several known iGluR NTD interactors were further used to validate the binding assay as detailed below. *Mus musculus* DNA encoding candidate proteins was cloned into the pHLsec vector to permit a high level of expression and secretion into the cell culture media (Aricescu et al., 2006). Candidates were C-terminally AviTagged and co-transfected with an ER-retained biotin ligase (BirA) to permit *in vivo* biotinylation in the presence of biotin. All candidate proteins were verified for production (Figure 4.13B1) and secretion (Figure 4.13B3) 60 hrs post-transfection before screening for direct NTD interactions. In another subset of HEK293 cells, NTDs were surface expressed using a modified pDisplay construct (adapted from Howarth et al., 2008), containing an extracellular myc tag. Secreted candidates were then applied to NTD-displaying cells and incubated for 4 hrs. Coverslips were subsequently processed for immunostaining, where co-localisation of NTD and candidate protein fluorescence can be used as a measure of direct protein interactions. Fluorescence intensity was then used as a measure of binding preference for different iGluR subunit NTDs.

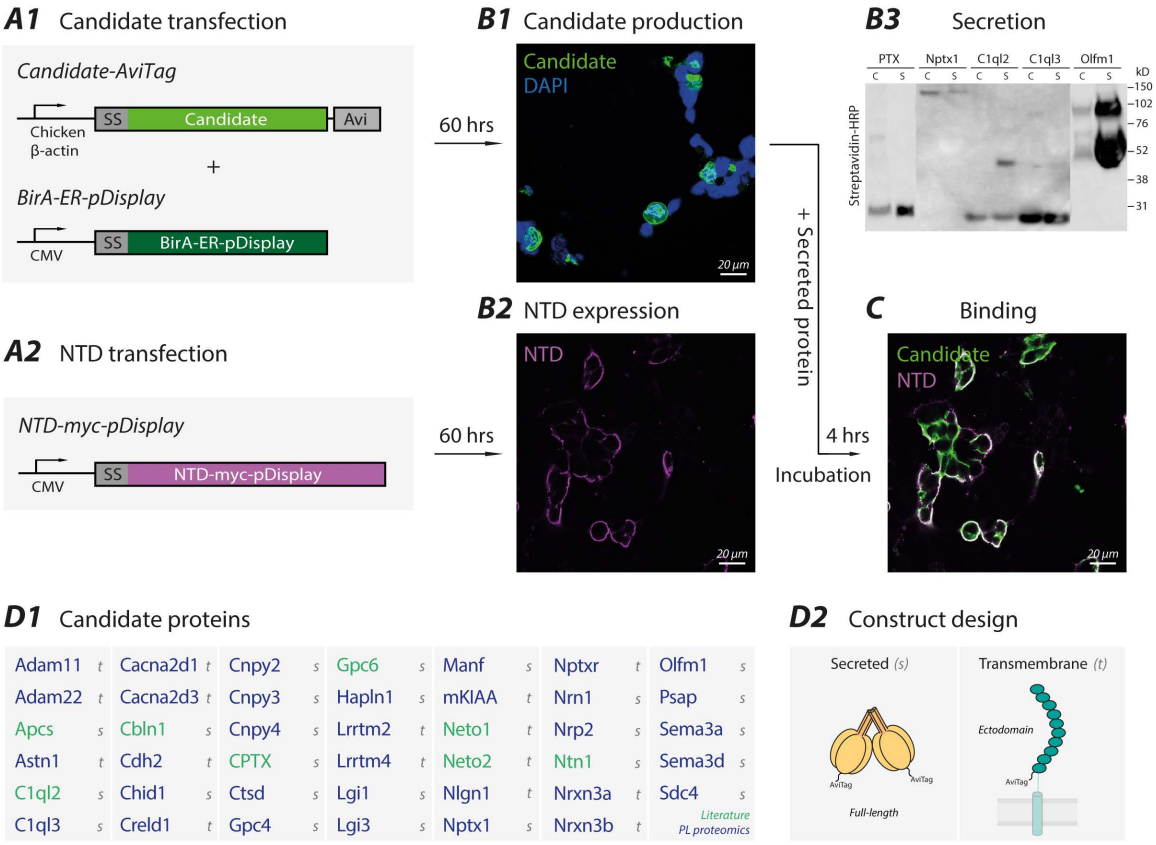

Figure 4.13 *Cell-based binding assay for detecting synaptic protein interactors.*

Figure 4.13 ***Cell-based binding assay for detecting synaptic protein interactors.*** *(**A1**) HEK293 cells were transfected with plasmids containing candidate proteins under the chicken β-actin promoter containing an AviTag and an ER-retained biotin ligase (BirA) to permit in vivo biotinylation (BirA-ER-pDisplay). (**A2**) Another subset of HEK293 cells were transfected with pDisplay constructs displaying iGluR subunit NTDs with an extracellular myc tag (NTD-myc-pDisplay). (**B1**) Biotinylated candidate synaptic proteins were produced for 60 hrs. (**B2**) NTD-myc-pDisplay constructs were expressed for 60 hrs, confirmed by non-permeabilised staining for myc. (**B3**) Protein biotinylation and secretion was confirmed by streptavidin-HRP WB of the cell lysate, C, and supernatant, S, before incubation with NTD-displaying cells. (**C**) The conditioned media containing candidate secreted proteins was incubated with NTD-displaying cells for 4 hrs before fixation with PFA and immunostaining with myc- and streptavidin-directed antibodies. (**D**) Candidate NTD interactors screened in the cell-based binding assay identified by PL proteomics (navy) and identified from the literature (green). (**D2**) Construct design for full-length secreted proteins (s) and secreted 'ectodomains' (first amino acid after signal sequence and last amino acid before TMD) of transmembrane-bound proteins (t).*

Cbln and C1ql directly interact with iGluR NTDs

To test the suitability of this assay, direct protein interactions were first evaluated with known iGluR NTD interactors; cerebellins (Cblns) and complement C1q-like proteins (C1ql). Cblns directly interact with the NTD of delta receptors (GluD1/2/4) (Elegheert et al., 2016; Tao et al., 2018; Fossati et al., 2019). Cbln1-GluD2 NTD interactions occur with an affinity of ~150 nM measured by SPR (Matsuda et al., 2010; Elegheert et al., 2016). Physiologically, direct Cbln interactions are crucial for long-term depression at cerebellar parallel fiber–purkinje cell synapses (Elegheert et al., 2016), hippocampal synapse formation and maintenance (Tao et al., 2018) and inhibitory synapse formation on cortical pyramidal neurons (Fossati et al., 2019). Interactions with postsynaptic iGluR NTDs occur in parallel with binding to presynaptic neurexins, mediated through their coiled coil domain (Suzuki et al., 2020).

C1ql-2 (Clql2) and -3 (C1ql3) form direct interactions with the NTD of GluK2/4/5 regulating postsynaptic kainate receptor (KAR) recruitment at CA3 synapses and neuronal circuit function (Figure 4.1; Matsuda et al., 2016; Straub et al., 2016). C1ql2/3 have an affinity of 5.6 μM and 3.4 μM respectively, for the GluK2 NTD (Matsuda et al., 2016). To confirm direct interactions between C1ql2/3 and iGluR NTDs, the C1q domain of C1ql2 and C1ql3 were evaluated in the cell-based binding assay against different iGluR subunit NTDs (Figure 4.15).

A direct interaction between Cbln1 and the GluD2 NTD was confirmed in the cell-based binding assay (Figure 4.14), with no binding observed to other iGluR subunit NTDs confirming the suitability of the assay. In this experiment fluorescence intensity was compared between two different epitope tags, 6xHis (Figure 4.14A) and AviTag (Figure 4.14B). The fluorescence intensity from GluD2 binding was 3-fold higher for Cbln1-AviTag relative to Cbln1-6xHis (Figure 4.14). The apparent higher sensitivity of the AviTag for detecting Cbln1 binding is most likely due to the high-affinity of streptavidin for biotin (K_D = 10^{-14} - 10^{-15} M). Use of streptavidin AF^{647}-conjugate likely permits a greater level of detection than lower-affinity 6xHis antibodies. Therefore, all subsequent candidate proteins were assayed using the AviTag to improve the sensitivity of this assay for weak protein interactions.

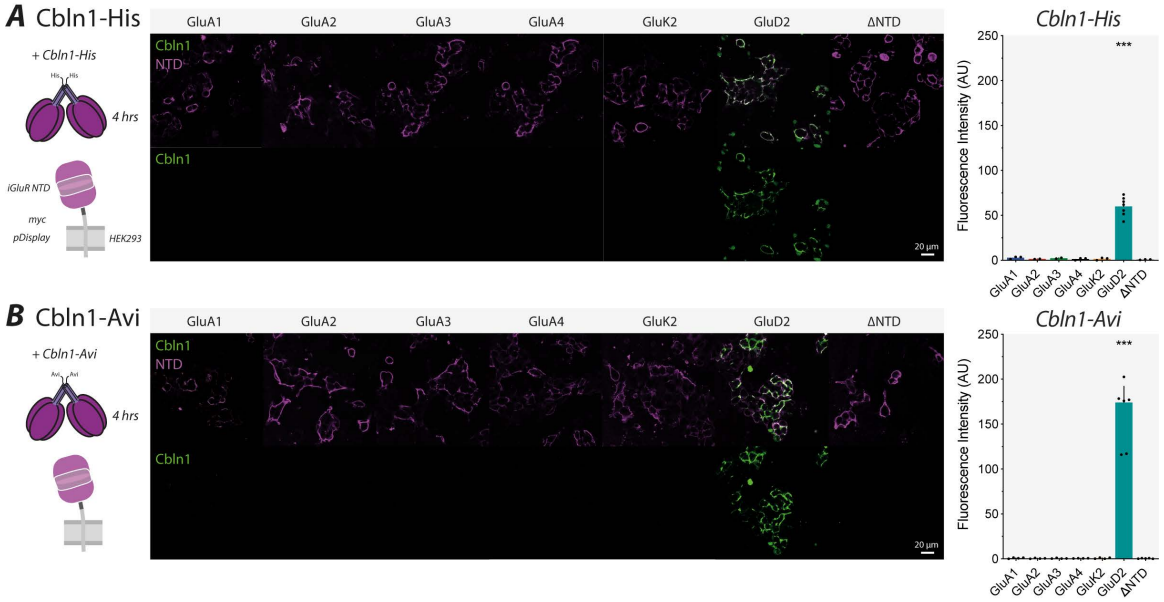

Figure 4.14 ***Cbln1 directly interacts with the GluD2 NTD.*** *(**A**) Cbln1-His interacts directly with the GluD2 NTD. Cbln1-His was secreted for 60 hrs before incubation with iGluR NTD-displaying cells for 4 hrs. Representative images indicate selective co-localisation of Cbln1-His (streptavidin, green) with GluD2 NTD-displaying cells (myc, magenta). Fluorescence intensity (AU) indicates binding exclusively to GluD2 NTDs (GluA1 = 2.93 ± 0.8; GluA2 = 1.46 ± 0.2; GluA3 = 2.33 ± 0.5; GluA4 = 1.43 ± 0.7; GluK2 = 1.63 ± 0.8; GluD2 = 60.0 ± 4.0; ΔNTD = 0.80 ± 0.2; n = 3 preparations; ANOVA, *** p < 0.001). (**B**) Cbn1-Avi interacts directly with the GluD2 NTD. Cbln1-Avi was biotinylated and secreted for 60 hrs before incubation with iGluR NTD-displaying cells for 4 hrs. Representative images indicate selective co-localisation of Cbln1-Avi (streptavidin, green) with GluD2 NTD-displaying cells (myc, magenta). Fluorescence intensity (AU) was significantly greater for GluD2 NTD-displaying cells relative to other iGluR NTDs (GluA1 = 0.80 ± 0.3; GluA2 = 0.47 ± 0.2; GluA3 = 0.49 ± 0.2; GluA4 = 0.57 ± 0.1; GluK2 = 0.72 ± 0.3; GluD2 = 174.1 ± 17.9; ΔNTD = 0.45 ± 0.2; n = 3 preparations; ANOVA, *** p < 0.001).*

Incubation of secreted C1ql2 with HEK293 cells displaying iGluR NTDs results in direct GluA1 and GluK2 NTD interactions, reflected by a robust increase in fluorescence intensity relative to ΔNTD control (Figure 4.15A). C1ql2 and C1ql3 binding occurs specifically with GluA1 and GluK2, but not with other iGluR subunit NTDs (Figure 4.15B), binding with the following subunit preference: GluA1 > GluK2. These findings are consistent with those reported previously (Matsuda et al., 2016). These results indicate that C1ql2/3 are direct GluA1/K2 NTD interactors, validating use of this assay to test candidates identified by PL proteomics for direct NTD interactions.

Functionally, Clql2/3 binding to the NTD of GluK2 controls postsynaptic KAR content at CA3 synapses. However, GluA1 does not appear to serve as an endogenous receptor for C1ql2/3 at these synapses (Matsuda et al., 2016). It would be interesting to see if direct interactions between the GluA1 NTD and C1ql2/3 (Figure 4.15) are engaged at CA1 synapses during synaptic potentiation, or at synapses in other brain regions. This is a particularly interesting hypothesis, as the GluA1 NTD is required for synaptic potentiation at CA1 synapses (Díaz-Alonso et al., 2017; Jiang et al., 2021; Watson et al., 2017), and C1ql3 is released in the hippocampus in an activity-dependent manner (Martinelli et al., 2016).

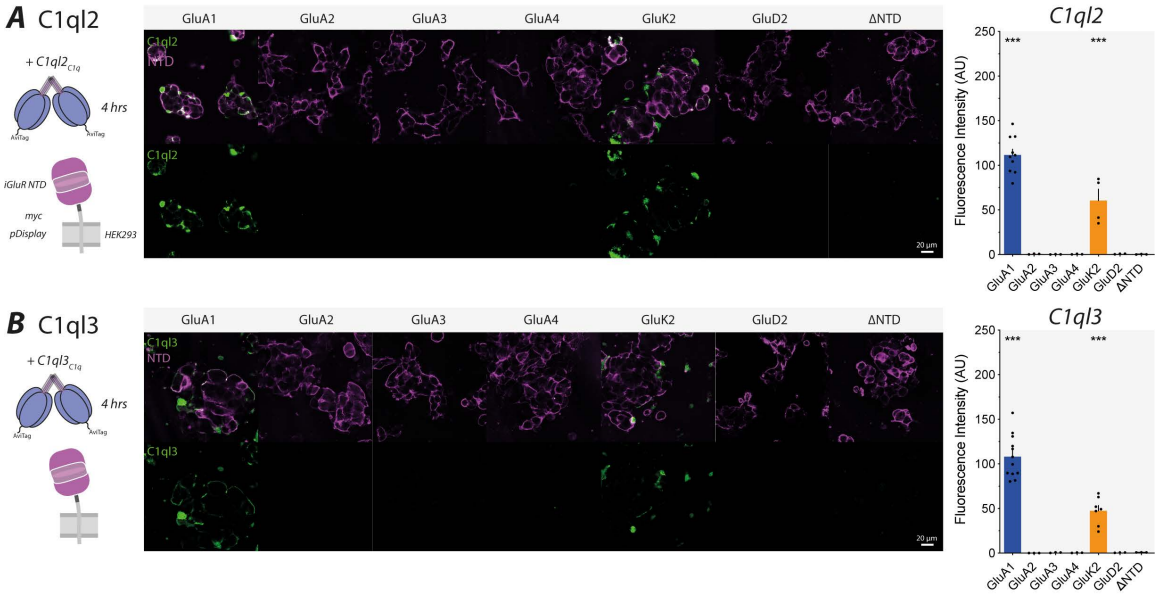

Figure 4.15 ***C1ql2/3 directly interacts with GluA1 and GluK2 NTDs.*** *(**A**) C1ql2 interacts directly with the GluA1 and GluK2 NTD. C1ql2 was biotinylated and secreted for 60 hrs before incubation with HEK293 cells displaying iGluR NTDs for 4 hrs. Representative images indicate selective co-localisation of C1ql2 (streptavidin, green) with GluA1 and GluK2 NTDs (myc, magenta). Fluorescence intensity (AU) demonstrates reproducibility of binding to GluA1 and GluK2 NTDs with a binding preference of GluA1 > GluK2 (GluA1 = 96.5 ± 6.6; GluA2 = 0.56 ± 0.3; GluA3 = 0.44 ± 0.1; GluA4 = 0.22 ± 0.1; GluK2 = 38.2 ± 3.1; GluD2 = 0.63 ± 0.3; ΔNTD = 0.30 ± 0.2; n = 3 preparations; ANOVA, *** p < 0.001). (**B**) C1ql3 interacts directly with the GluA1 and GluK2 NTD. C1ql3 was biotinylated and secreted for 60 hrs before incubation with iGluR NTD-displaying cells for 4 hrs. Representative images indicate co-localisation of C1ql3 (streptavidin, green) with GluA1 and GluK2 NTDs (myc, magenta). Fluorescence intensity (AU) indicates binding to GluA1 and GluK2 NTDs with a binding preference of GluA1 > GluK2 (GluA1 = 95.0 ± 8.5; GluA2 = 0.01 ± 0.0; GluA3 = 0.59 ± 0.2; GluA4 = 0.31 ± 0.1; GluK2 = 27.1 ± 3.0; GluD2 = 0.63 ± 0.0; ΔNTD = 0.86 ± 0.1; n = 3 preparations; ANOVA, *** p < 0.001).*

Nptx1 directly interacts with the GluA1-4 NTD

Neuronal pentraxin-1, -2 and -receptor (Nptx1, Nptx2 and Nptxr) bind and cluster AMPARs through PTX domain (PTX) interactions with the AMPAR NTD (O'Brien et al., 1999; Xu et al., 2003; Sia et al., 2007; Lee et al., 2017). The Nptx1 PTX domain ($Nptx1_{PTX}$) interacts with GluA4 NTDs (Sia et al., 2007) with μM affinity (Suzuki et al., 2020). The physiology of the Nptxs is best described for Nptx2 at excitatory synapses onto parvalbumin-positive interneurons (PV-INs), where recruitment of GluA4-containing AMPARs results in an increased inhibitory drive, modulating neuronal circuit activity (Chang et al., 2010; Gu et al., 2013; Pelkey et al., 2015). Current evidence of Nptx function at excitatory synapses onto pyramidal neurons, indicate a negative modulatory role in synaptic transmission and plasticity (Cho et al., 2008; Figueiro-Silva et al., 2015), although further investigation is required.

Nptx1 appears reproducibly in PL proteomics experiments, with a high candidate ranking based on GluA2 NTD-enrichment (Figure 4.10B). This suggests that Nptx1 comes within proximity of the GluA2 NTD. However, confirmation of direct Nptx1 interactions with the AMPAR NTD must be further investigated. Cell-based binding assays were performed by incubating iGluR NTD-displaying cells with N- (N-ter Nptx1) or C-terminally (C-ter Nptx1) tagged Nptx1 for 4 hrs. N-ter Nptx1 binds to GluA1-4 NTDs (Figure 4.16A), with the following binding preference: GluA4 > GluA3 > GluA1 > GluA2.

To ensure that N- or C-terminal positioning of the AviTag tag has no effect on Nptx1 GluA1-4 NTD binding, this experiment was repeated in parallel with C-ter Nptx1. C-ter Nptx1 binds to GluA1-4 NTDs with the same binding preference: GluA4 > GluA3 > GluA1 > GluA2 (Figure 4.16B). Showing that binding preference is independent of tag positioning in this assay. Interestingly, the apparent binding affinity (fluorescence intensity; AU) of C-ter Nptx1 is higher than that of N-ter Nptx1. This is somewhat surprising as the PTX domain, which engages in this interaction, may be masked by the C-terminal AviTag, however this appears not to be the case. An alternate explanation for this difference in binding affinity is that the N-terminal AviTag prevents formation of hexa-mers (Xu et al., 2003), therefore reducing the avidity of this protein interaction (Elegheert et al., 2016). This hypothesis is further supported by experiments performed with $Nptx1_{PTX}$, which yielded no binding unless purified and concentrated to 1 μM (Figure 4.18).

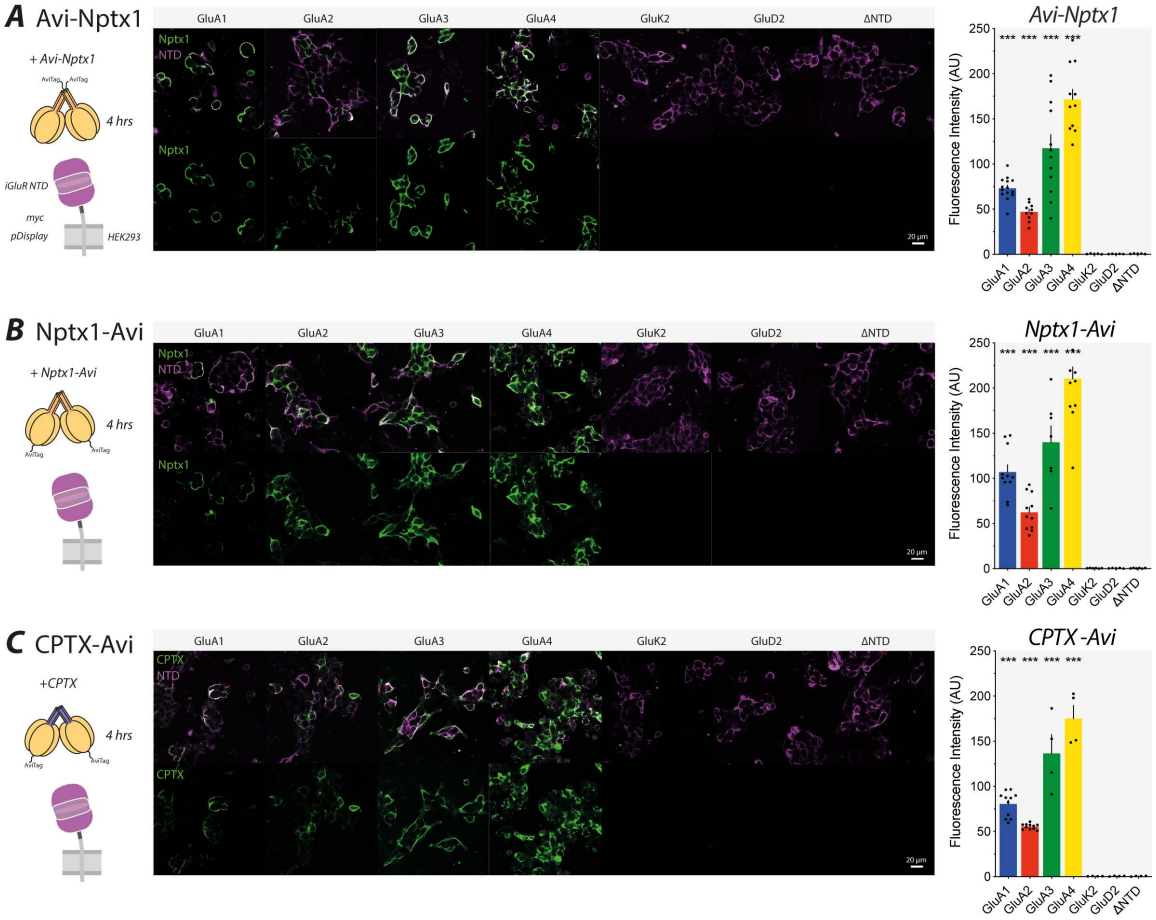

Figure 4.16 ***Nptx1 directly interacts with the GluA1-4 NTD.*** *(**A**) Fluorescence intensity (AU) indicates binding of N-ter Nptx1 (Avi-Nptx1) to GluA1-4 NTDs (GluA1 = 73.1 ± 3.4; GluA2 = 46.9 ± 3.1; GluA3 = 117.5 ± 15.0; GluA4 = 171.6 ± 11.1; GluK2 = 0.49 ± 0.15; GluD2 = 0.40 ± 0.05; ΔNTD = 0.61 ± 0.11; n = 6 independent preparations; ANOVA , *** p < 0.001). (**B**) Fluorescence intensity (AU) indicates binding of C-ter Nptx1 (Nptx1-Avi) to GluA1-4 NTDs (GluA1 = 107.0 ± 8.0; GluA2 = 62.3 ± 6.0; GluA3 = 140.1 ± 18.1; GluA4 = 210.2 ± 13.0; GluK2 = 0.50 ± 0.09; GluD2 = 0.47 ± 0.15; ΔNTD = 0.53 ± 0.15; n = 6 independent preparations; ANOVA, *** p < 0.001). (**C**) Fluorescence intensity (AU) indicates binding of CPTX to GluA1-4 NTDs (GluA1 = 80.4 ± 4.2; GluA2 = 55.5 ± 0.93; GluA3 = 136.4 ± 20.9; GluA4 = 175.0 ± 14.6; GluK2 = 0.51 ± 0.08; GluD2 = 0.60 ± 0.17; ΔNTD = 0.55 ± 0.17; n = 3 independent preparations; ANOVA, *** p < 0.001).*

Finally, direct interactions between synthetic synaptic organiser, CPTX, and GluA1-4 NTDs were confirmed (Figure 4.16C; Suzuki et al., 2020). Here, the PTX domain of CPTX engages in direct interactions with GluA1-4 NTDs. Similarly, CPTX has a binding preference of: GluA4 > GluA3 > GluA1 > GluA2 (Figure 4.16C), consistent with those previously reported by Suzuki et al., (2020). This further emphasises the importance of the Nptx1 PTX domain in the formation of direct Nptx1-AMPAR NTD interactions.

These findings corroborate Nptx1 as an AMPAR NTD interactor, which has a subunit NTD binding preference of GluA4 > GluA3 > GluA1 > GluA2. Nptx1 was identified by PL proteomics, enriched for the GluA2 NTD (Figure 4.10B), and direct interactions were confirmed here using the cell-based binding assay (Figure 4.16). This validates the use of PL proteomics to identify synaptic cleft protein NTD interactors. The physiology of Nptx1-AMPAR NTD interactions at excitatory synapses is investigated in Chapter 5.

Confirmation of known iGluR NTD interactors in the cell-based binding assay validates the use of this assay to identify extracellular secreted protein interactions with the AMPAR NTD. Next, 33 candidate protein interactors (Figure 4.13D1) discovered using PL proteomics enriched for the AMPAR NTD, were cloned, secreted and incubated with iGluR NTDs to probe for direct protein interactions.

4.2.6 Screening candidate NTD interactors

Candidate AMPAR NTD interactors identified by PL proteomics (Figure 4.10B), were subsequently screened for direct protein interactions alongside known interactors using the cell-based binding assay established in Figure 4.13. Successful expression and secretion of synaptic proteins was confirmed by WB, before screening in the binding assay.

NTD-myc-pDisplay

33 candidate proteins were selected based on top ranked candidates from PL proteomics alongside 8 potential direct interactors from the literature (Figure 4.13D1). Candidates were screened for direct interactions with NTD-myc-pDisplay constructs; however, direct interactions were observed only for known iGluR NTD interactors (Figure 4.17). Despite numerous proteins having interesting ascribed function in the literature, many of which associated to AMPAR-mediated synaptic transmission, none of these candidate proteins directly interacted with iGluR NTDs. Examples of key candidate interactors identified by PL proteomics include disintegrin and metalloproteinase domain-containing protein 22 (Adam22) and 11 (Adam11) and leucine-rich glioma-inactivated protein 1 (Lgi1) and 3 (Lgi3). These proteins are particularly interesting in the context of the AMPAR as they form a *trans*-synaptic complex which organises postsynaptic receptors on a nanometer scale for efficient excitatory synaptic transmission (Fukata et al., 2021). Other key candidates included neurexin (Nrxn) isoforms 3a (Nrxn3a), 3b (Nrxn3b) and mKIAA0743, a neurexin-like protein, of which NTD-enrichment was considerably high (Figure 4.10B). These cell-adhesion molecules (CAMs) regulate postsynaptic AMPAR trafficking through interactions that span the synaptic cleft (Aoto et al., 2013; Aoto et al., 2015), again making them ideal candidates for direct AMPAR NTD interactions, potentially controlling receptor positioning.

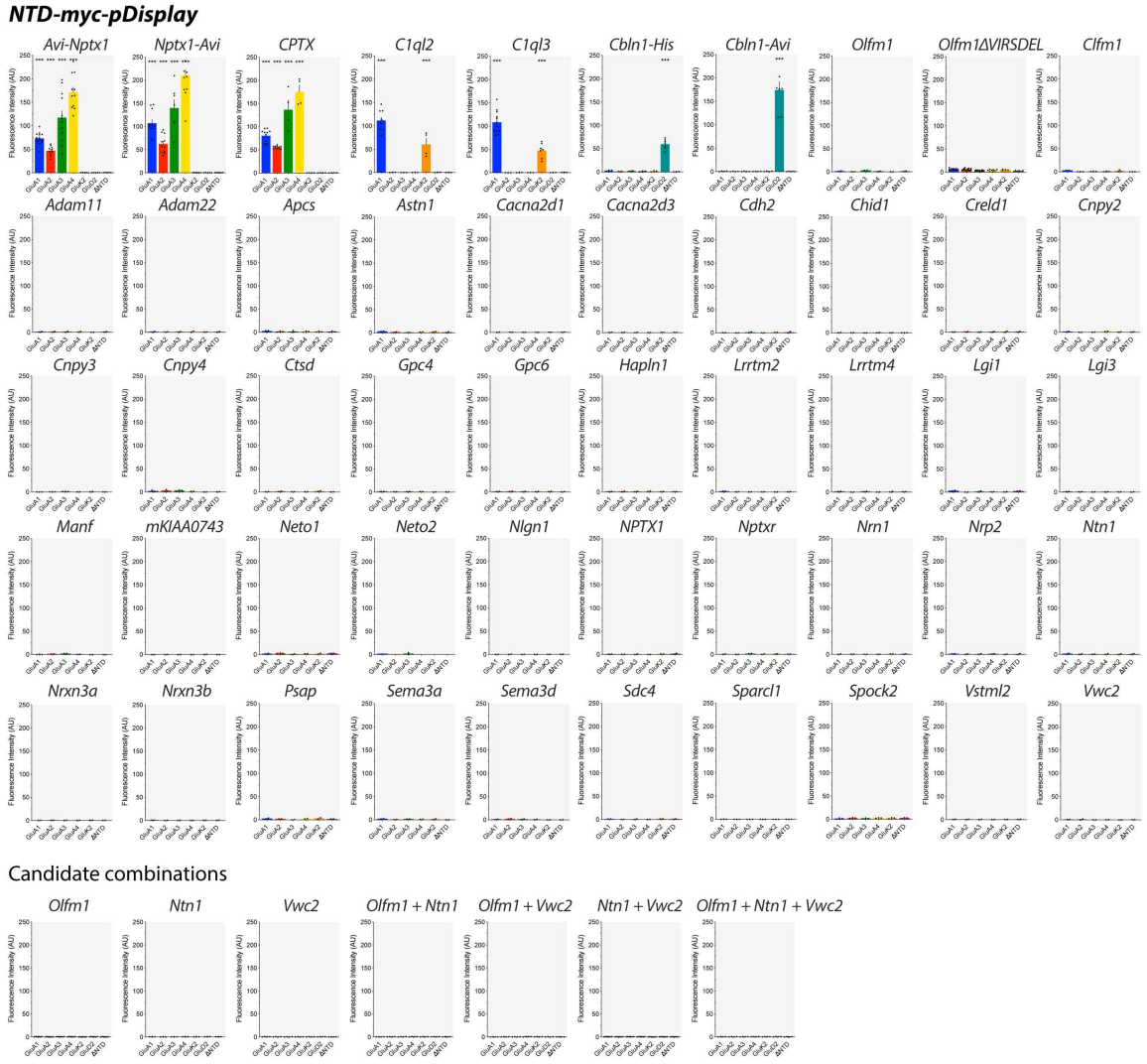

Figure 4.17 *Candidate NTD interactors screened against NTD-myc-pDisplay constructs.*

Figure 4.17 ***Candidate NTD interactors screened against NTD-myc-pDisplay constructs.*** *NTD-myc-pDisplay constructs displaying iGluR subunit NTDs were incubated with 50 different secreted proteins for 4 hrs. The PTX domain of N-ter Nptx1, C-ter Nptx1 and CPTX directly interacts with GluA1-4 NTDs with the following binding preference: GluA4 > GluA3 > GluA1 > GluA2 (data from Figure 4.16). C1q domains of C1q2 and C1ql3 directly interact with GluA1 and GluK2 NTDs (data from Figure 4.15). Cbln1-6xHis and Cbln1-AviTag interact specifically with GluD2 NTDs (data from Figure 4.14). Olfm1 constructs do not directly interact with iGluR NTDs (data from Figure 4.19). No direct interactions were detected between 40 newly identified candidate proteins and iGluR NTDs. Candidates synaptic proteins were identified by PL proteomics and selected depending on ranking from MS data and importance in the literature. All transmembrane-bound candidates were applied as 'ectodomains' and secreted candidates as full-length proteins. Olfm1 + Ntn1 + Vwc2 applied in combination also did not result in direct iGluR NTD interactions.*

Similarly, CAMs organisers leucine-rich repeat transmembrane proteins (Lrrtms) have been shown to regulate AMPAR-mediated synaptic transmission and plasticity at CA1 synapses (Soler-Llavina et al., 2011; Soler-Llavina et al., 2013), potentially through direct interactions with the AMPAR (de Wit et al., 2009; Schwenk et al., 2012; Schwenk et al., 2014). Additionally, *trans*-synaptic organisers voltage-gated calcium channel subunits Cacna2d1/3 are particularly interesting as they couple to presynaptic glutamate release sites and act as organisers of glutamatergic synapses (Schöpf et al., 2019). Despite the fascinating literature surrounding the roles of these CAMs and *trans*-synaptic organisers in AMPAR-mediated synaptic transmission, these proteins among many other candidates were found not to directly interact with the AMPAR NTD.

Additionally, a number of secreted proteins were identified by PL proteomics with interesting roles in excitatory synaptic function. Namely, astrocyte-released hevin (Spock2) and SPARC (Sparcl1), which both positively and negatively regulate synapse formation respectively (Kucukdereli et al., 2011). These proteins are particularly interesting as they are able to control postsynaptic AMPAR content (Jones et al., 2011), in a similar fashion to known AMPAR NTD interactor Nptx1. Secreted proteins netrin-1 (Ntn1; Glasgow et al., 2018) and neuritin (Nrn1; Subramanian et al., 2019) also regulate postsynaptic AMPAR content and the strength of synaptic transmission. This highlights just a few of the candidate secreted proteins with captivating literature, thought to play key roles in regulating AMPAR-mediated synaptic transmission. Despite this, no direct interactions were found with the AMPAR NTD in the cell-based binding assay (Figure 4.17).

There are numerous explanations for a lack of direct interactions between candidate synaptic proteins and the AMPAR NTD. On the face of it, one may hypothesise that only Nptx1 is capable of directly binding to the AMPAR NTD (Figure 4.16). At this stage however, candidate proteins cannot be dismissed. One possibility, is that protein interactions with the AMPAR NTD must bind as a complex of multiple proteins. This is a particularly interesting hypothesis as potential AMPAR NTD interactor, Olfm1 (Pandya et al., 2018), is identified in AMPAR proteomics in parallel with two other secreted proteins neuritin (Ntn1) and brorin (Vwc2) (Schwenk et al., 2012). To test if AMPAR NTD interactions require multiple proteins for complex formation, Olfm1, Ntn1 and Vwc2 were applied in combination to AMPAR NTDs, however, no binding was observed (Figure 4.17).

Another limitation of using the NTD-myc-pDisplay construct, is that only an NTD monomer/ dimer is displayed on the cell surface. This faces the same limitations as SPR, using NTD monomers/dimers (depending on NTD concentration; Rossmann et al., 2011) to determine binding affinity. It is possible that protein interactions require a tetrameric NTD interface in order to bind. To overcome this issue, the cell-based binding assay was repeated using homomeric and heteromeric AMPARs to form full-length tetrameric receptors (Figure 4.18).

Full-length AMPARs

The overall strength of protein-protein interactions is determined by their avidity, the accumulated strength of multiple binding affinities. It is possible that synaptic protein interactions with the AMPAR NTD may bind across NTD subunits, or even across domains (NTD-LBD), thus requiring a full-length receptor to form successful protein interactions. Therefore, candidates were applied to HEK293 cells displaying full-length and ΔNTD AMPAR subunits. The fluorescence intensity observed with AMPAR homomers is significantly lower than that observed with NTD-myc-pDisplay constructs for AMPAR NTD interactor Nptx1. This is likely due to a lower surface expression of full-length AMPARs relative to NTD-myc-pDisplay. Significant binding is detected only for the N-ter Nptx1, C-ter Nptx1 and CPTX interaction with GluA4 homomer. This is likely due to differential surface expression of AMPAR subunits affecting the apparent binding affinity, whereas NTD-myc-pDisplay constructs show comparable levels of surface expression. Furthermore, the apparent affinity of Nptx1 is greatest for GluA4 relative to other AMPAR subunits (Figure 4.16).

Taken together, NTD-myc-pDisplay constructs provide the most robust read-out for determining direct interactions between synaptic proteins and iGluR NTDs. This binding assay confirms known iGluR NTD interactors and deduces the binding preference for AMPAR NTD interactor, Nptx1 (GluA4 > GluA3 > GluA1 > GluA2).

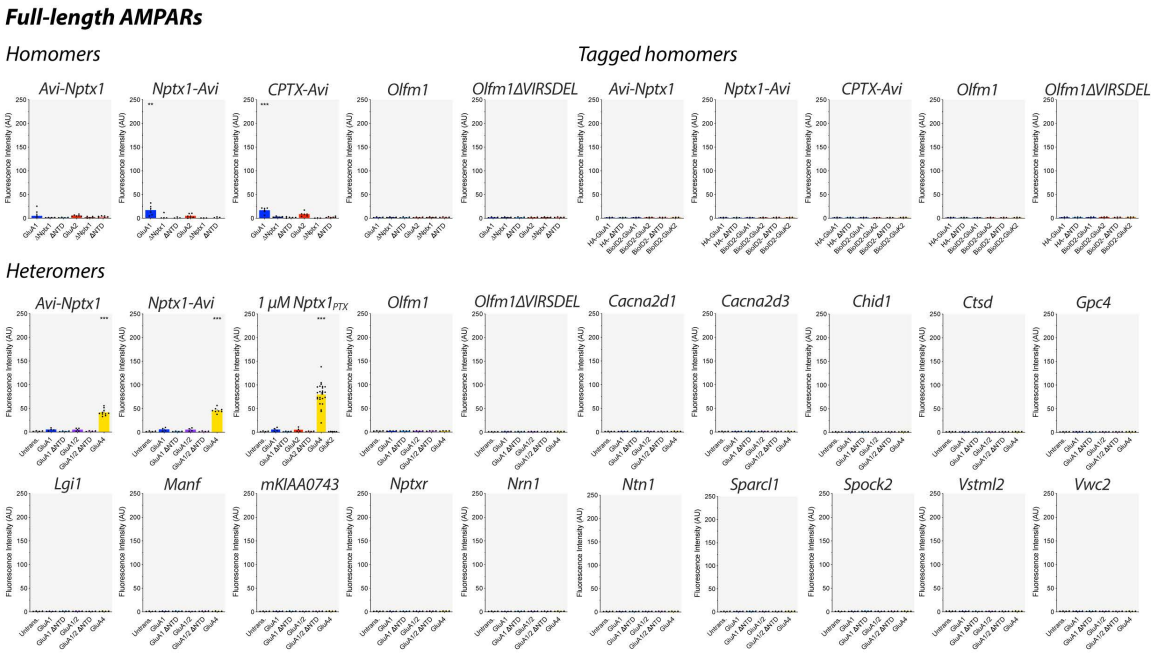

Figure 4.18 ***Candidate NTD interactors screened against full-length AMPARs.*** *Full-length tagged and un-tagged homomeric and heteromeric AMPARs expressed in HEK293 cells were incubated in candidate secreted protein interactors for 4 hrs. C-ter Nptx1 (GluA1 WT = 17.0 ± 4.29; GluA1 ΔNptx1 = 0.00 ± 2.85; GluA1 ΔNTD = 0.01 ± 1.40) and CPTX (GluA1 WT = 16.8 ± 2.45; GluA1 ΔNptx1 = 3.15 ± 0.59; GluA1 ΔNTD = 0.74 ± 0.72) directly interact with full-length GluA1, but not GluA1 ΔNTD homomers. The fluorescence intensity of this interaction was greater reduced relative to NTD-myc-pDisplay constructs. N-ter Nptx1 (Untrans. = 2.14 ± 0.37; GluA1 WT = 5.47 ± 1.32; GluA1 ΔNTD = 1.79 ± 0.36; GluA1/2 WT = 5.18 ± 1.32; GluA1/2 ΔNTD = 2.12 ± 0.41; GluA4 WT = 41.9 ± 2.28; ANOVA, *** p < 0.001), C-ter Nptx1 (Untrans. = 2.08 ± 0.38; GluA1 WT = 6.03 ± 1.78; GluA1 ΔNTD = 1.90 ± 0.25; GluA1/2 WT = 5.62 ± 1.67; GluA1/2 ΔNTD = 2.02 ± 0.37; GluA4 WT = 46.3 ± 1.90; ANOVA, *** p < 0.001) and 1 μM $Nptx1_{PTX}$ (Untrans. = 2.06 ± 0.38; GluA1 WT = 6.03 ± 1.86; GluA1 ΔNTD = 1.83 ± 0.24; GluA2Q WT = 5.53 ± 2.11; GluA2Q ΔNTD = 2.04 ± 0.30; GluA4 WT = 79.9 ± 4.67; GluK2 WT = 1.61 ± 0.07; ANOVA, *** p < 0.001) directly interact with GluA4 homomers. No direct interactions were detected between other candidate synaptic protein interactors and full-length homomers or heteromers. A number of these proteins were also applied in combination with each other, for example Olfm1+Nrn1+Vwc2, however no direct interactions were observed.*

Olfm1 does not interact directly with the AMPAR NTD

As there is strong evidence to suggest that olfactomedin-1 (Olfm1) forms part of the AMPAR macro-molecular complex (Engelhardt et al., 2010; Shanks et al., 2012; Schwenk et al., 2012; Schwenk et al., 2014; Brechet et al., 2017) at excitatory synapses (Loh et al., 2016; Cijsouw et al., 2018) and was identified by PL proteomics an NTD-enriched protein (Figure 4.10B), this protein was examined in more detail. More recently, a direct interaction between Olfm1 and the GluA2 NTD has been postulated, thought to affect the lateral mobility of synaptic AMPARs (Pandya et al., 2018).

Olfm1 is expressed and secreted into the cell media in large quantities relative to other secreted proteins as detected by WB (Figure 4.13B3). However, no direct interactions are observed between full length Olfm1 and iGluR NTDs (Figure 4.19A). To further enhance the amount of Olfm1 secretion, the C-terminal ER retention motif '*VIRSDEL*' was removed (Olfm1ΔVIRSDEL) (Pronker et al., 2015; Pronker et al., 2019). This resulted in even higher levels of protein secretion, but did not result in iGluR NTD binding (Figure 4.19B).

Finally, a synthetic version of Olfm1 was constructed (Figure 4.19C). In a similar fashion to CPTX (Suzuki et al., 2020), the coiled coil domain of Cbln1 and a GC4 triple coil helix was used to induce oligomerisation of the olfactomedin-like domain of Olfm1, named cerebellar olfactomedin (Clfm1). This ensures that oligomeric protein is formed and applied to NTD-displaying cells. However, no direct interactions were observed in the cell-based binding assay (Figure 4.19C).

Further studies are required to confirm the direct interaction between Olfm1 and the GluA2 NTD reported by Pandya et al., (2018). A possible explanation for the discrepancy between these findings, is the requirement of a full-length heteromeric AMPAR to permit protein interactions, unlike the monomeric NTDs used in this assay. This possibility was investigated by applying Olfm1 to full-length homomeric and heteromeric AMPARs, however no direct interactions were detected (Figure 4.19D). It remains unclear whether Olfm1 forms direct interactions with the AMPAR NTD, to investigate the possibility of an indirect mechanism, immunostaining of Olfm1 was performed.

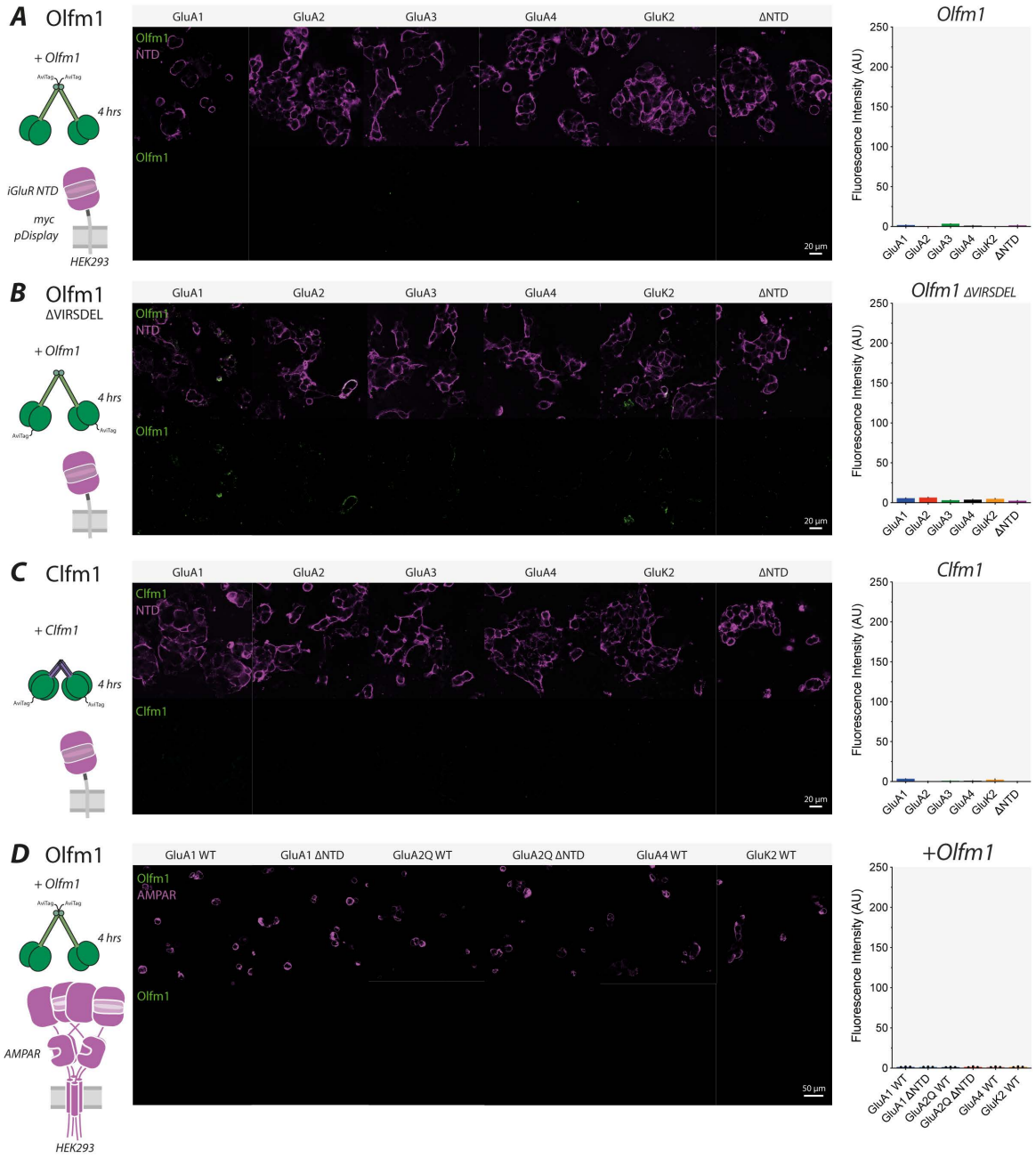

Figure 4.19 *Olfm1 does not interact directly with iGluR NTDs.*

Figure 4.19 ***Olfm1 does not interact directly with iGluR NTDs.*** *(**A**) Olfm1 does not interact with iGluR NTDs. Full length Olfm1 is incubated with NTD-displaying cells for 4 hrs before PFA fixation and immunostaining. Representative images indicate robust expression of iGluR NTDs (myc, magenta), but no binding of Olfm1 (streptavidin, green). (**B**) Olfm1Δ VIRSDEL does not interact with iGluR NTDs. Olfm1Δ VIRSDEL is incubated with iGluR NTDs for 4 hrs before PFA fixation and immunostaining. Representative images indicate iGluR NTD expression (myc, magenta), and background fluorescence from non-specific Olfm1Δ VIRSDEL binding (streptavidin, green). (**C**) Cerebellar olfactomedin (Clfm1) does not interact with iGluR NTDs. Clfm1 is incubated with iGluR NTDs for 4 hrs before PFA fixation and immunostaining. Representative images indicate iGluR NTD expression (myc, magenta) and no Clfm1 binding (streptavidin, green). (**D**) Olfm1 does not interact with full-length AMPARs. Olfm1 incubation with full-length (WT) and NTD-deleted (ΔNTD) expressing cells does not result in co-localisation despite robust AMPAR subunit expression.*

Olfm1 localises to extra-synaptic sites

The precise nature of Olfm1-AMPAR NTD interactions and its physiological function remain unresolved. Due to the lack of a reliable and specific primary antibody directed at Olfm1 (Figure 4.20A), determining its localisation is challenging. To overcome this issue, experiments were performed using exogenous application of 1 µg/ml Olfm1 conjugated to AF^{488} (Olfm1-AF^{488}) to dissociated hippocampal neurons for 12 hrs. To determine if Olfm1 co-localises with AMPARs at excitatory hippocampal synapses, incubated cultures were washed, fixed and immunostained for postsynaptic GluA2 and presynaptic marker RIM, to determine co-localisation with Olfm1 (Figure 4.20A1).

Immunofluorescence experiments demonstrated co-localisation of Olfm1-AF^{488} with endogenous GluA2. Interestingly, Olfm1-AF^{488} predominantly co-localised with GluA2 at extra-synaptic, but not synaptic sites, as indicated by line scans of hippocampal dendrites and spines (Figure 4.20 B2/ B3). GluA2 was observed on hippocampal dendrites and enriched at dendritic spines. RIM was absent from dendritic sites, but highly enriched at synaptic sites. Conversely, Olfm1 was highly enriched at extra-synaptic sites on the dendrite and was absent from hippocampal spines. These data suggest that exogenously applied Olfm1 does not localise at synaptic sites, but rather co-localises with GluA2 at extra-synaptic sites. In contrast, Pandya et al., (2018) demonstrate both extra-synaptic and synaptic localisation of Olfm1, using a commercial primary antibody (Neuromab; Cat# 75-042). This antibody however, shows little specificity for Olfm1 when co-staining for exogenously expressed HA-Olfm1 using anti-HA and anti-Olfm1 (Figure 4.20A). Exogenous application of Olfm1 therefore, offers a suitable alternative approach to study the localisation of Olfm1, where Olfm1-AF^{488} localises to extra-synaptic sites.

It is possible that Olfm1 may control entry or exit from the synapse by lateral diffusion, similarly to SynDIG4 (also known as PRRT1; Matt et al., 2018). These findings should be investigated in further detail to elucidate the localisation and protein secretion sites of endogenous Olfm1. With the lack of suitable antibodies against Olfm1, this could be achieved using a CRISPR/Cas9-based knock-in strategy to introduce small epitope tags.

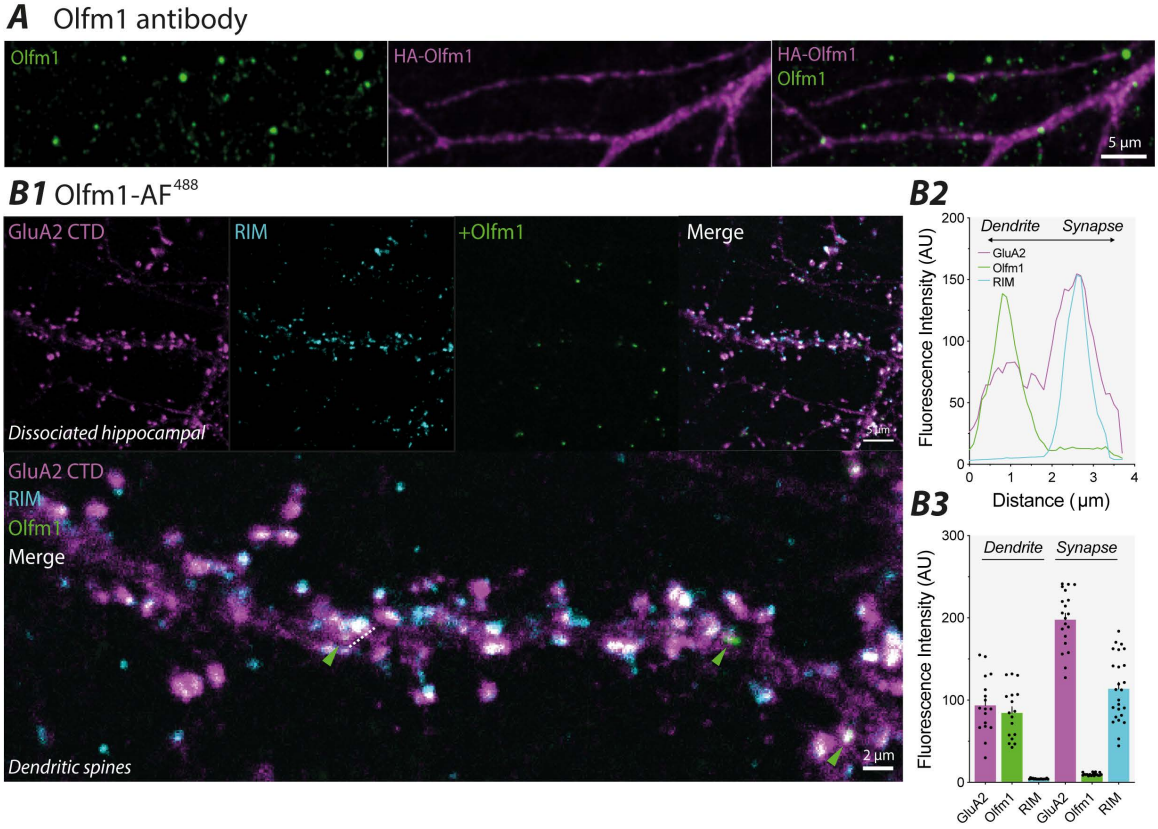

Figure 4.20 *Olfm1 localises at extra-synaptic sites in hippocampal neurons.*

Figure 4.20 ***Olfm1 localises at extra-synaptic sites in hippocampal neurons.*** *(**A**) Olfm1 (green) antibody (Neuromab; Cat# 75-042) showed no specificity for exogenously expressed HA-Olfm1 (magenta) (images kindly provided by Dr Alexandra Pinggera). No co-localisation between Olfm1 and HA-Olfm1 was observed. (**B**) Exogenously applied Olfm1 localises at extra-synaptic sites in hippocampal neurons. (**B1**) 1 µg/ml Olfm1 Alex Fluor-488 conjugate (Olfm1-AF^{488}; kindly provided by Dr Matti Pronker) was applied to dissociated hippocampal neurons for 12 hrs before PFA fixation and immunostaining. Permeabilised GluA2 CTD staining indicates receptors located throughout the dendrite and enrichment at synaptic sites. Synapses are identified by co-localisation of postsynaptic GluA2 and presynaptic marker RIM. Olfm1-AF^{488} was co-localised with GluA2 at dendritic extra-synaptic sites (green arrows). Line scans were performed from the dendrite to synaptic sites (4 µm distance on average; dotted line) (**B2**) Example line scan of dendrite to synapse indicates GluA2 throughout dendritic sites with enrichment at the synapse. RIM fluorescence was absent in the dendrite and enriched at the synapse. Conversely, Olfm1 was absent from the synapse, but present at extra-synaptic sites on hippocampal dendrites. (**B3**) Fluorescence intensity (AU) of the dendrite indicates the presence of GluA2 and Olfm1. Synapses contain postsynaptic GluA2 and presynaptic RIM, but no Olfm1.*

Screening against endogenous AMPARs

Candidate protein binding to the AMPAR NTD cannot be dismissed using the cell-based binding assay alone. Developing a robust assay for detecting NTD protein interactions, whilst recapitulating the synaptic environment is a challenging task. To further probe for candidate NTD interactions with endogenous AMPARs, secreted candidates were applied to dissociated hippocampal cultures and immunostained for endogenous GluA2-containing receptors (magenta) and presynaptic marker bassoon (cyan). This permitted screening for direct or indirect protein interactions with endogenous AMPARs positioned at excitatory synapses (Figure 4.21). Dissociated hippocampal cultures permit access of secreted proteins to synapses and the presence of endogenous synaptic proteins, hypothetically enabling indirect AMPAR protein interactions to form.

Top ranked candidates from PL proteomics and the scientific literature were secreted and applied to dissociated hippocampal cultures for 4 hrs, to match timings used to detect iGluR NTD interactions in heterologous cells (Figure 4.17), or for 12 hrs to allow for sufficient binding to occur. However, no significant fluorescence signal was observed from any of the top ranked candidates or known NTD interactors (eg. Nptx1; Figure 4.21), suggesting that protein interactions with endogenous AMPARs were either not formed or not detectable using this approach. This is likely due to the concentration of protein applied in the cell medium, as candidate screening against full-length AMPARs expressed in heterologous cells also resulted in no significant binding using small-scale protein production (Figure 4.18). A significant level of binding in this assay may require a higher concentration of secreted protein, or overexpression of full-length AMPARs. This hypothesis is supported by findings from heterologous cells, where binding was only observed with purified $Nptx1_{PTX}$ concentrated and applied at 1 μM. Application of 1 μM $Nptx1_{PTX}$ was found to co-localise with GluA4 on astrocytes (Figure 4.21), as previously reported (Sia et al., 2007). Candidate proteins in these binding assays are produced by small-scale transfection. To achieve higher concentrations of protein, large-scale purifications must be performed, which is time consuming and costly. Therefore, it is not possible to achieve high-throughput screening of candidates using this alternative approach.

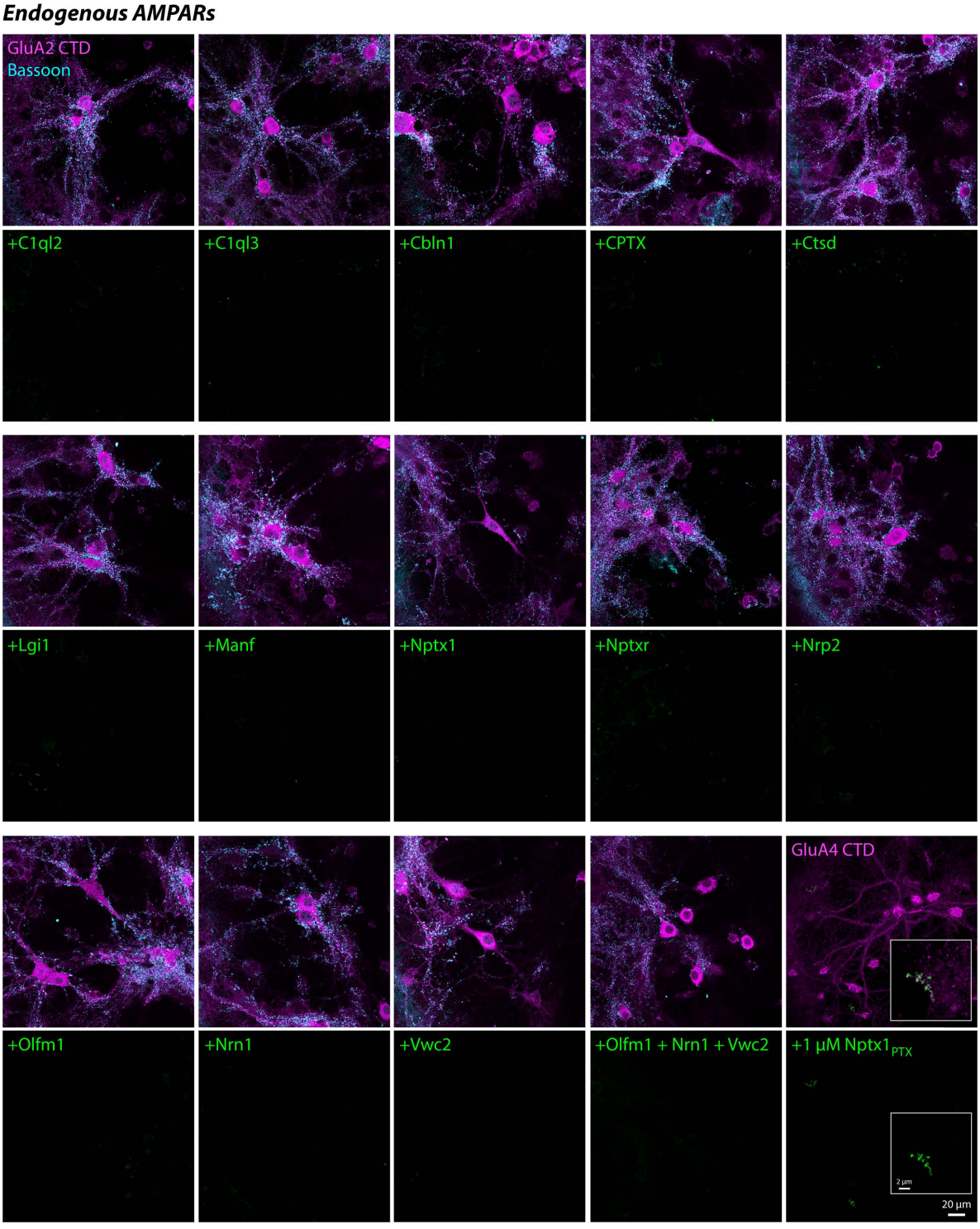

Figure 4.21 *Candidate NTD interactors screened against endogenous AMPARs.*

Figure 4.21 ***Candidate NTD interactors screened against endogenous AMPARs.*** *Candidate NTD interactors applied to dissociated hippocampal neurons for a total of 4 hrs to match application times using in heterologous cells (Figure 4.17). Experiments were also repeating using a 12 hrs incubation time to allow for sufficient binding to occur. Immunostaining for endogenous postsynaptic GluA2 (magenta), presynaptic bassoon (cyan) and candidate proteins (green) (Scale bar = 20 µm). Co-localisation of GluA2 and bassoon indicates excitatory synaptic sites. Widefield images of dissociated hippocampal neurons indicate no co-localisation with secreted candidate protein application. Known AMPAR NTD interactors Nptx1 and CPTX show no co-localisation with excitatory synapses in dissociated hippocampal cultures. Candidate proteins were applied both individually (eg. Olfm1) and in combination (eg. Olfm1 + Nrn1 + Vwc2; Schwenk et al., 2012), to see if multiple proteins are required for complex formation. Higher magnification images were also taken from synaptic localisations (magenta and cyan co-localisation); however, no significant candidate binding was observed. Application of 1 µM Nptx1 PTX domain ($Nptx1_{PTX}$) colocalises with GluA4 in astrocytes, as previously reported (Sia et al., 2007). Zoomed panel indicating $Nptx1_{PTX}$ co-localisation likely with GluA4-containing astrocytic processes.*

Np65 does not directly interact with the AMPAR NTD

Neuroplastin-65 (Np65) is a single transmembrane domain CAM involved in synaptogenesis (Vemula et al., 2020), and the expression of long-term potentiation (LTP) at CA1 synapses (Smalla et al., 2000). Np65 is highly expressed in the hippocampus, where it regulates NMDAR, GluA1-containing AMPAR (Empson et al., 2006) and $GABA_AR$ content (Herrera-Molina et al., 2014). Very recently, Jiang et al., (2021) proposed a role for Np65 in LTP maintenance through direct GluA1 NTD interactions. To investigate this novel AMPAR NTD interactor, immunofluorescence and co-IP experiments were performed on Np65 using the same experimental tools as described previously (Jiang et al., 2021). Furthermore, Np65 was screened in the cell-based binding assay established in this chapter.

Using a specific Np65 antibody (R&D systems; Cat# AF5360; Jiang et al., 2021), localisation of Np65 was investigated in dissociated hippocampal neurons (Figure 4.22A). Here, Np65 was expressed abundantly in the hippocampus, and localised throughout the neuron, particularly in hippocampal dendrites and spines (Figure 4.22A). In GFP+ transfected neurons, surface HA-GluA1 was probed for by live-labelling with a fluorescently conjugated single chain Fv-Clasp (Watson et al., 2020; kindly provided by Dr Alexandra Pinggera). Surface expression of GluA1 was both dendritic and enriched at the synapse, quantified by dendritic line scans (Figure 4.22B). Similarly, Np65 is expressed both in hippocampal dendrites, with enrichment at synaptic sites, co-localising with GluA1. These findings support those of Jiang et al., (2021), but provide further insight into the degree of spine enrichment, which was found to be 2-fold for both GluA1 and Np65.

Next, the direct interaction between Np65 and the GluA1 NTD was investigated using co-IP experiments in HEK293 cells, with the same constructs described previously (Np65 C-terminal Flag; Jiang et al., 2021). The authors report Np65 immunoprecipitation with the GluA1 NTD in brain lysates, using a lysis buffer containing 1% Triton X-100 detergent. Therefore, co-IP experiments in this chapter were first performed using an identical lysis buffer with 1% Triton X-100. However, in these experiments no direct interactions were detected between Np65 and AMPAR subunits (Figure 4.22C1; n = 2 preparations). One would expect to see a direct interaction specifically between Np65 and GluA1 full-length receptors (Jiang et al., 2021), however, no co-IP was observed.

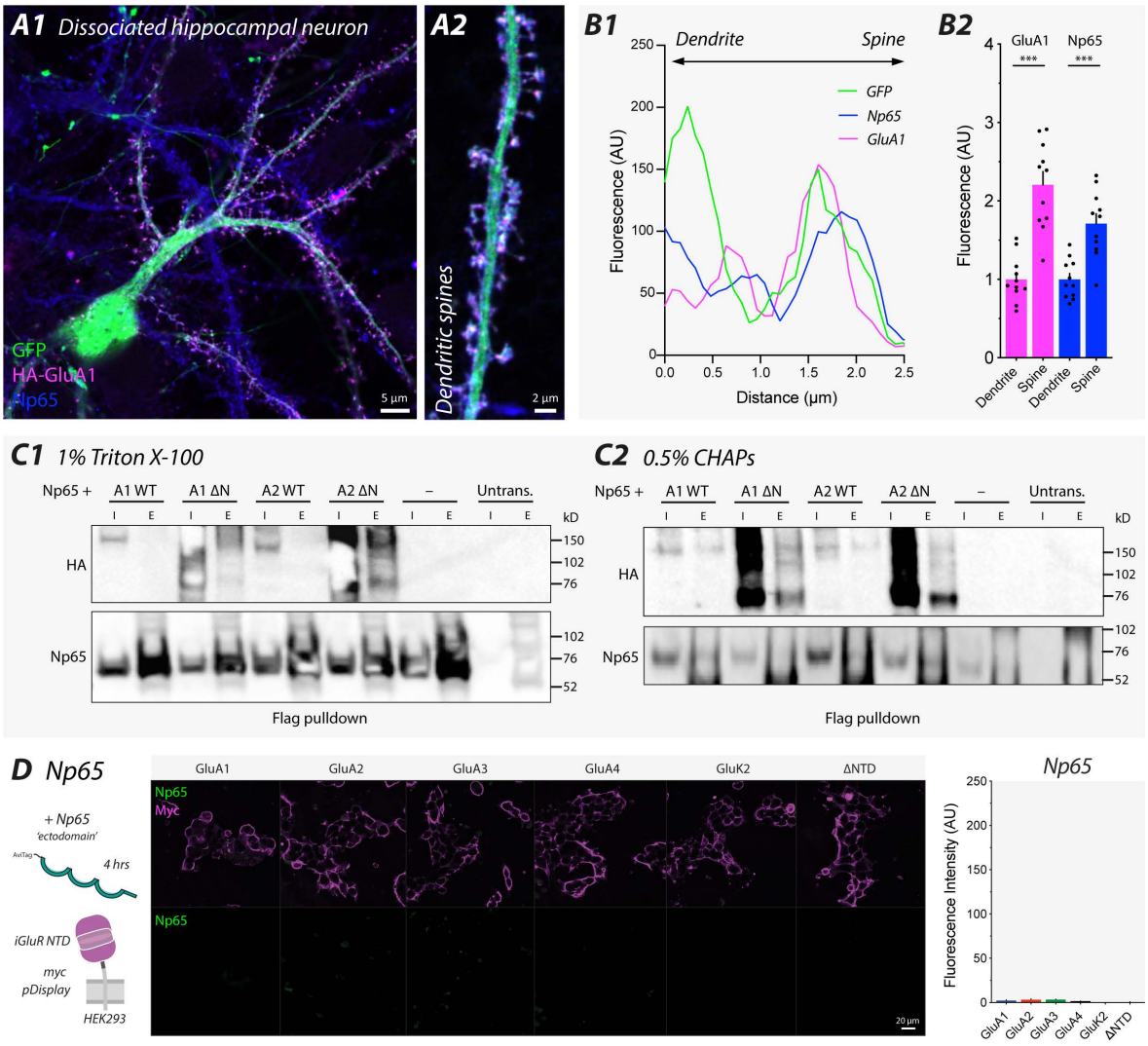

Figure 4.22 ***Np65 localises to excitatory synapses but does not interact directly with the AMPAR NTD.*** *(**A1**) Live staining of surface HA-GluA1 (magenta; kindly provided by Dr Alexandra Pinggera), permeabilised Np65 (blue) and cytosolic GFP (green). (**A2**) GluA1 localised to dendritic spines along with Np65. (**B1**) Line scan of GFP, Np65 and GluA1 revealed enrichment of GluA1 and Np65 in dendritic spines. (**B2**) Normalised fluorescence intensity revealed a significantly higher intensity from the spine relative to dendrite for GluA1 (Dendrite = 1.00 ± 0.09; Spine = 2.21 ± 0.17; n = 11 cells; paired t-test, $p < 0.001$) and Np65 (Dendrite = 1.00 ± 0.08; Spine = 1.71 ± 0.13; n = 11 cells; paired t-test, $p < 0.001$). (**C**) Flag bead co-IP of GluA1/2 ±NTD and Np65 in lysis buffer containing (**C1**) 1% Triton X-100 and (**C2**) 0.5% CHAPs revealed no direct interaction between Np65 and AMPARs (n = 2 preparations per detergent). Robust expression of Np65 (~65 kD) and AMPAR subunits (WT ~100 kD; ΔNTD ~50 kD) was detected in the input of HEK293 cell lysate using both detergents. (**D**) Np65 ectodomain does not directly interact with iGluR NTDs in the cell-based binding assay.*

Secondly, co-IPs were conducted using a milder detergent, CHAPs, which has a higher critical micelle concentration. As protein interactions with the AMPAR are sensitive to harsher detergents such as Triton X-100, CHAPs may preserve low-affinity protein interactions. However, in 0.5% CHAPs no direct interaction was detected with the GluA1 NTD. In fact, GluA1 ΔNTD and GluA2Q ΔNTD constructs were pulled down with Np65-Flag to a greater extent than full-length AMPARs, suggesting if at all, an interaction with different sites on the AMPAR.

Finally, in an attempt to resolve these discrepancies, Np65 was also screened in the cell-based binding assay (Figure 4.22D). The extracellular 'ectodomain' of Np65 was expressed, secreted and applied to NTD-displaying cells for 4 hours, as described previously (Figure 4.13). However, no fluorescence signal was detected for any iGluR NTDs, suggesting Np65 is not a direct iGluR NTD interactor.

The discrepancies between these findings and those of Jiang et al., (2021) are confusing. Immunofluorescence experiments confirm co-localisation of Np65 with GluA1 and significant enrichment in synaptic spines. However, co-IP experiments are unable to confirm direct interactions between Np65 and the GluA1 NTD. Furthermore, direct Np65-GluA1 NTD interactions were also not detected in the cell-based binding assay, which is capable of detecting other known direct NTD interactions (Figure 4.14/15/16). Taken together, these findings suggest that Np65 is abundantly expressed in hippocampal dendrites and spines, but does not directly interact with the GluA1 NTD.

4.3 Discussion

This chapter identifies a number of candidate AMPAR NTD interactors using a novel PL proteomics technique and subsequently screens these proteins for direct NTD interactions using a cell-based binding assay. Extensive screening of candidate proteins permitted identification of Nptx1, a direct GluA1-4 NTD interactor.

Proximity-labelling proteomics

Unbiased PL proteomics experiments were performed in organotypic slice culture to identify candidate protein interactors with the AMPAR NTD. Organotypic slice culture provides an intact physiological network that can be easily manipulated using AAV transduction to achieve expression of BirA*-AMPAR subunits. A functional role for the AMPAR NTD has been described at CA1 synapses using electrophysiology in organotypic hippocampal slices (Watson et al., 2017; Díaz-Alonso et al., 2017; Watson et al., 2020). An emerging hypothesis in the field is that synaptic protein interactions with the AMPAR NTD position the receptor for effective excitatory synaptic transmission (Watson et al., 2020). Therefore, the same experimental system was utilised to probe for candidate interacting proteins.

The ability of three BirA* tags (BioID2, MiniTurbo and TurboID; Figure 4.3B) and APEX2 to label and identify AMPAR-interacting proteins were compared directly. First, optimal labelling conditions for BirA* were determined in heterologous cells, by comparing the amount of biotinylated material produced with different concentrations and durations of biotin + ATP application (Figure 4.4). A concentration of 200 μM biotin and 2 mM ATP was found to produce the highest level of biotinylation intensity on WB, without compromising cell health (Figure 4.4A2). To deduce the duration of biotin application required for sufficient biotinylation, different labelling times were tested with all three BirA* tags. Where TurboID requires 2 hrs (Figure 4.4B), MiniTurbo requires 18 hrs, TurboID requires 48 hrs labelling time (Figure 4.4C) and APEX2 requires 10 mins (Figure 4.11).

BirA*-AMPARs are packaged into AAVs and introduced into organotypic hippocampal slices by global transduction of the slice (Figure 4.7A3). One concern with fusing BirA* tags to the N-terminus of AMPARs is that this may occlude synaptic incorporation of receptors. Using the RI as a measure of synaptic trafficking, the extent of synaptic trafficking with BirA*-GluA1/2 is shown to be comparable to WT receptors (Figure 4.5), validating the use of these

constructs for identifying synaptic protein interactors. Furthermore, BirA*-AMPARs localise to hippocampal dendritic spines where they label their proximal environment upon initiation with biotin + ATP (Figure 4.7).

Of the three BirA* tags, TurboID provides the deepest coverage of known synaptic proteins and greatest fold enrichment of AMPAR NTD interactors relative to BioID2 and MiniTurbo (Figure 4.10). This is most likely due to its superior temporal labelling efficiency (Branon et al., 2018). In this study TurboID is the most effective probe for resolving AMPAR ER and synaptic protein interactions in organotypic slice culture. NTD interactors are determined by comparison of AMPAR subunits expressed at the same subcellular compartment, demonstrating the remarkable molecular resolution achievable with this technique. Candidate AMPAR NTD interactors were ranked by enrichment for full-length versus ΔNTD receptors (NTD-enrichment; Figure 4.10B) and top candidates from this list were subsequently screened for direct AMPAR NTD interactions.

AMPAR NTD interactions are likely to be of low-affinity and transiently formed, therefore, PL proteomics requires high temporal labelling efficiency to capture dynamic protein interactions. Of the BirA* tags tested, TurboID requires the shortest labelling time (2 hrs) to permit protein identification (Figure 4.4B). A concern is that the temporal labelling efficiency of this enzyme is not high enough to permit successful capture of AMPAR NTD interactors. Therefore, experiments were repeated using an engineered ascorbate peroxidase tag APEX2 (Figure 4.12; Lam et al., 2015; Hung et al., 2016). Using the same protocol established with BirA*-AMPARs (Figure 4.8), but with the addition of biotin-phenol and H_2O_2 to initiate the biotinylation reaction. APEX2 only requires 10 mins to label sufficient protein material following application of biotin-phenol and H_2O_2 (Figure 4.11; Loh et al., 2016; Cijsouw et al., 2018; Li et al., 2020). Therefore, using 10 min labelling, the PL proteomes of APEX2-GluA2Q WT and ΔNTD were deduced (Figure 4.12; Appendix A Figure A.2). This permitted confirmation of proteins captured by BirA*, and identification of additional proteins (Figure 4.12). Newly identified candidate NTD interactors are potentially captured owing to proximal biotinylation of neighbouring tyrosine (APEX), opposed to lysine (BirA*) residues. Furthermore, APEX2 has a higher labelling efficiency relative to TurboID (Figure 4.11), possibly identifying transient interactors undetected by the relatively slower enzymatic efficiency of TurboID. These were however, not found to directly interact with the AMPAR NTD (Figure 4.17).

Additionally, PL proteomics was performed on AMPAR subunits GluA1/2/3 using BioID2 (Appendix A Figure A.4). Given the differential trafficking and contribution of these subunits to excitatory synaptic transmission in the hippocampus (Chapter 3; Lu et al., 2009), it was hypothesised that diverse NTD-interacting proteins may control the function of AMPARs in a subunit-specific manner. However, BioID2-AMPARs are less efficient at identifying proteins from the synapse relative to TurboID (Figure 4.10C2), making the results of these experiments unclear. These experiments should be repeated with TurboID-AMPAR subunits to permit effective capture of candidate synaptic protein interactors.

Candidate interactors

PL proteomics identifies known components of the AMPAR proteome, identified by AP-MS, (Schwenk et al., 2012; Schwenk et al., 2014; Shanks et al., 2012), and further captures novel proteins undetected by classical AP-MS. Novel candidate interactors are identified owing to the covalent modification of transient low-affinity interactors without the need for isolation based on affinity (Gingras et al., 2019). Due to the cell-permeable nature of biotin, AMPAR interactors are identified from both ER and synaptic compartments. To validate the PL proteomics method, identified proteins were first searched for known constituents of the AMPAR proteome.

AMPARs are assembled in the ER, where a number of ER-resident interacting proteins promote the biogenesis of tetrameric receptors (Schwenk and Fakler, 2020). BirA*-AMPARs successfully identify known components of the AMPAR ER proteome, including Frrs1l (Schwenk et al., 2019) and Cpt1c (Gratacòs-Batlle et al., 2018), proteins required for the forward trafficking of AMPARs to the synapse. Additionally, known ER AMPAR interactors Calx and BiP (Rubio and Wenthold, 1999) and Stim1/2 (Gruszczynska-Biegala et al., 2016) are enriched for BirA*-AMPARs (Figure 4.10B). This demonstrates that PL proteomics with BirA*-AMPARs is able to identify known constituents of the AMPAR ER proteome (Brechet et al., 2017). Furthermore, numerous ER proteins are identified by BirA*-AMPARs that currently have no ascribed function. It would be interesting to determine the effect of these proteins on AMPAR biogenesis and function. This question is particularly interesting in the context of the AMPAR NTD, as Frrs1l for example, has a high degree of NTD-enrichment in PL proteomics experiments (Figure 4.10B). Frrs1l plays a key role in AMPAR biogenesis and forward trafficking to synaptic sites, critical for synaptic

transmission and plasticity (Schwenk et al., 2019). Hypothetically, Frrs1l-AMPAR NTD interactions in the ER may regulate AMPAR forward trafficking to the synapse. This is an interesting hypothesis as the AMPAR NTD has been shown to regulate surface expression of the receptor in heterologous and neuronal cells (Möykkynen et al., 2014; Watson et al., 2020).

Auxiliary proteins modulate AMPAR trafficking and channel gating kinetics (Milstein and Nicoll, 2009; Shi et al., 2010; Jackson and Nicoll, 2011). The most predominant auxiliary proteins present at CA1 synapses are TARP-γ8 and CNIH2 (Schwenk et al., 2012). Of note, BirA*-AMPARs detect TARP-γ8, but not CNIH2 from organotypic hippocampal slices, this is likely due to the difference in topology of these two proteins. Where TARP-γ8 has an extracellular loop region, CNIH2 is fully imbedded within the membrane (Zhang et al., 2021). Consequently, N-terminally tagged BirA*-AMPARs are more likely to label surface lysine residues on TARP-γ8 than CNIH2, thus only detecting TARP-γ8 by PL proteomics. Interestingly, Shisa6 is identified as an NTD-enriched protein with PL proteomics. Shisa6, acts as an AMPAR auxiliary protein, accumulating receptors at postsynaptic sites during synaptic activity (Klaassen et al., 2016). It would be interesting to see if Shisa6 forms direct interactions with the AMPAR NTD and whether this influences channel gating or receptor positioning at the synapse.

Synaptic proteins are identified from PL proteomics by entering gene lists into the SynGO database (Koopmans et al., 2019; www.syngoportal.org). ~40% of proteins identified by TurboID are found to be associated with the synaptic cellular compartment (Figure 4.10C2). Of these proteins, a number of interesting candidates were selected based on ranking of NTD-enrichment and selection from the scientific literature. Synaptic proteins were expressed as full-length secreted proteins or 'ectodomains' (first amino acid after signal sequence and last amino acid before TMD) of transmembrane-bound candidates, before screening in the cell-based binding assay (Figure 4.13). Candidate synaptic AMPAR-interacting proteins were classified as 'secreted' or 'transmembrane-bound' based on the UNIPROT database (https://www.uniprot.org/) and available scientific literature.

Cell-based binding assay

Firstly, known iGluR NTD interactors were confirmed in a cell-based binding assay to validate this screen for extracellular protein interactions. SPR experiments with known iGluR NTD interactors indicate relatively weak binding affinities in the μM range. The PTX domain of Nptx1

has an affinity of 10 μM for GluA4 NTDs (Suzuki et al., 2020), C1ql2/3 show an affinity of 5 μM for GluK2 NTDs (Matsuda et al., 2016) and Cbln1 has an affinity of 0.2 μM for GluD2 NTDs (Matsuda et al., 2010; Elegheert et al., 2016). All of these direct protein interactions were detected and confirmed in the cell-based binding assay, demonstrating this screen is capable of detecting relatively low-affinity extracellular protein interactions with iGluR NTDs.

The cell-based binding assay was performed with both NTD-myc-pDisplay (Figure 4.17) and full-length AMPAR constructs (Figure 4.18). When directly comparing the apparent affinity of Nptx1 interactions between these two constructs, NTD-myc-pDisplay was found to be significantly more robust at detecting extracellular NTD interactions. This is most likely due to a higher level of surface expression, with a greater number of NTDs available to engage in protein interactions. As a result, NTD-myc-pDisplay constructs were employed for screening 33 candidate protein interactors identified by PL proteomics. PL proteomics identifies proteins proximal to the AMPAR NTD (Figure 4.10/12), but not necessarily those forming direct interactions. Therefore, a high number of negative hits from NTD-enriched candidates (Figure 4.17/18) is to be expected (Roux et al., 2018).

Future studies may also consider screening for protein interactions in co-culture systems (Biederer and Scheiffele, 2007), by co-expressing NTD-myc-pDisplay and secreted proteins in ‘postsynaptic’ HEK293 cells followed by immunostaining for a presynaptic marker (RIM or bassoon). This would permit robust detection of NTD interactions as demonstrated previously (Figure 4.17), but with the addition of endogenous presynaptic terminals. Therefore, allowing reliable screening for direct protein interactions that may also require presynaptic proteins for complex formation with the AMPAR NTD. This assay can also be used to detect changes in synapse formation, as observed with CPTX (Suzuki et al., 2020).

A number of CAMs were identified as part of the NTD-enriched PL proteome (Figure 4.13D1). Many of these proteins are involved in shaping glutamatergic synaptic transmission. Including, but not limited to: Adam11/22, Astn1, Cacna2d1/3, Cdh2, Lrrtm2/4, mKIAA0743, Nrxn3a, Nrxn3b, Sdc4 (Fukata et al., 2010; Horn et al., 2018; Dolphin et al., 2018; Saglietti et al., 2007; de Wit et al., 2009; Aoto et al., 2013; Siddiqui et al., 2013). However, none of these protein formed direct interactions with AMPAR NTDs in the cell-based binding assay, using NTD-myc-pDisplay (Figure 4.17), full-length AMPARs (Figure 4.18) and endogenous AMPARs (Figure 4.21).

Perhaps the most promising candidate of the CAMs identified is Cdh2 (N-cadherin), as this protein has been reported to directly interact with the GluA2 NTD regulating synapse density (Saglietti et al., 2007). However, in this study N-cadherin AMPAR NTD interactions were not detected. CAMs were screened by expressing only the 'ectodomain' of transmembrane-bound proteins. It is possible that protein interactions between CAMs and the AMPAR NTD only occur if the protein is transmembrane-bound. Therefore, another approach would be to screen CAMs using co-IP experiments in heterologous cells, as performed with Np65 (Figure 4.22C), though no direct interactions were observed.

Numerous secreted proteins were also identified as NTD-enriched synaptic proteins in PL proteomics (Figure 4.10B), with many proteins having established roles in glutamatergic synaptic transmission. Including, but not limited to: Nptx1, Nptxr, Olfm1, Ctsd, Gpc4, Lgi1, Nrp2, Ntn1, Nrn1, Sema3a, Spock2, Vwc2 (Sia et al., 2007; Lee et al., 2017; Pandya et al., 2018; Li et al., 2019; Allen et al., 2012; Fukata et al., 2010; Wang et al., 2017; Glasgow et al., 2018; Subramanian et al., 2019; Yamashita et al., 2014; Kucukdereli et al., 2011; Schwenk et al., 2012). However, these secreted proteins formed no direct protein interactions with the AMPAR NTD. Likely the most promising secreted AMPAR NTD interactors identified by PL proteomics are Olfm1 (Pandya et al., 2018) and Nptx1 (O'Brien et al., 1999; Xu et al., 2003; Sia et al., 2007; Lee et al., 2017), discussed in more detail below.

Olfm1

Olfm1 is a secreted glycoprotein that forms part of the AMPAR macromolecular complex (Engelhardt et al., 2010; Shanks et al., 2012; Schwenk et al., 2012; Schwenk et al., 2014; Brechet et al., 2017) and has an overall 2-fold enrichment for the GluA2 NTD (Figure 4.10B), however no direct interactions with the AMPAR NTD were detected (Figure 4.19). The discrepancy between the findings in this study and those of Pandya et al., (2018) are puzzling. To gain a better insight into the relative binding affinity of this proposed interaction, SPR should be conducted to permit accurate detection of binding affinity. Interestingly, exogenously applied Olfm1 appears to localise to extra-synaptic sites (Figure 4.20B), where this protein may play a role in regulating receptor motility. Although the synaptic localisation of Olfm1 needs further investigating, with previous reports using ineffective primary antibodies (Pandya et al., 2018) unspecific for exogenously expressed Olfm1 (Figure 4.20A).

Nptx1

Nptx1 is identified by PL proteomics with an overall 2.5-fold enrichment for the GluA2 NTD (Figure 4.10B). This secreted protein is detectable reproducibly by all PL tags (BioID2, MiniTurbo, TurboID and APEX2), however is undetectable using classical AP-MS (Schwenk et al., 2012; Schwenk et al., 2014). Direct binding with the AMPAR NTD is revealed using the cell-based binding assay, where the Nptx1 PTX domain interacts with the following subunit binding preference: GluA4 > GluA3 > GluA1 > GluA2 (Figure 4.16). Functionally, Nptxs are thought to promote postsynaptic clustering of AMPARs (O'Brien et al., 1999; Xu et al., 2003; Sia et al., 2007; Lee et al., 2017), with evidence for physiological function at both excitatory (Cho et al., 2008; Figueiro-Silva et al., 2015) and inhibitory (Chang et al., 2010; Gu et al., 2013; Pelkey et al., 2015) synapses. The scientific literature surrounding the physiology of Nptx1 however, is more limited and confusing. Nptx1 is identified in this chapter using PL proteomics at excitatory synapses in principle neurons of the hippocampus. Therefore, to further investigate the role of Nptx1-AMPAR NTD interactions in shaping GluA1/2-mediated excitatory synaptic transmission, electrophysiology experiments were performed to deduce its role in Chapter 5.

Chapter 5

Nptx1 shapes excitatory synaptic transmission through NTD interactions

5.1 Introduction

Neuronal pentraxins (Nptxs) are composed of secreted (Nptx1 and Nptx2) and type-II transmembrane-bound (Nptxr) proteins characterised by their pentraxin (PTX) domain. Nptxs form homo- and hetero-meric complexes (Kirkpatrick et al., 2000) and are thought to exist as hexamers (Xu et al., 2003). Nptx1 (Schlimgen et al., 1995) and Nptxr (Dodds et al., 1997) mRNA is expressed in discrete populations of neurons in the hippocampal CA3 region and dentate gyrus (DG), cerebral cortex and cerebellum. Nptx2 is also observed in these brain regions, with the exception of the cerebellum (Tsui et al., 1996). Strong protein expression of Nptx1/2/r is observed in deep layers of the cortex, hippocampal DG hilus, CA3 stratum lucidum and CA1 stratum radiatum, and the cerebellum (Gong et al., 2003; Cho et al., 2008; Apóstolo et al., 2020).

Nptxs promote the accumulation of AMPARs at postsynaptic sites (O'Brien et al., 1999; O'Brien et al., 2002; Xu et al., 2003), through direct interactions between their PTX domain and postsynaptic AMPAR NTDs both *in vitro* and *in vivo* (O'Brien et al., 1999; Xu et al., 2003; Sia et al., 2007; Lee et al., 2017). The physiology of Nptx neuronal circuit modulation has been extensively characterised using constitutive gene knockout mice. Nptx2, also known as neuronal activity-regulated pentraxin (NARP), is highly abundant at excitatory synapses onto parvalbumin-positive interneurons (PV-INs) in the hippocampus. At these aspiny synapses Nptx2 recruits GluA4-containing AMPARs to increase synaptic strength onto PV-INs, subsequently increasing inhibitory drive (Chang et al., 2010; Gu et al., 2013; Pelkey et al., 2015). Nptx2 also directly interacts with the perineuronal net (PNN), an extracellular matrix structure responsible for synaptic stabilisation. An interesting hypothesis is that Nptx-PNN interactions are additionally involved in the process of AMPAR clustering (Van't Spijker et al., 2019).

Nptxs are however not restricted to aspiny neurons, but also localise to dendritic spines in the hippocampus (O'Brien et al., 1999; Xu et al., 2003; Cho et al., 2008). At hippocampal and cerebellar synapses metabotropic glutamate receptor 1/5 (mGluR1/5)-dependent long-term depression (LTD) is mediated through cleavage of Nptxr by tumor necrosis factor α-converting enzyme (TACE) and binding to postsynaptic AMPARs capturing them for endocytosis (Cho et al., 2008). Knockdown of Nptx1 at excitatory synapses increases both AMPAR-mediated transmission and neuronal excitability, suggesting a negative modulatory role of Nptx1 at excitatory synapses (Figueiro-Silva et al., 2015). More recently, a synthetic synaptic organiser containing the Nptx1 PTX domain ($Nptx1_{PTX}$) was shown to restore glutamatergic synaptic function (Suzuki et al., 2020).

Nptxs are thought to be mainly axonally released from presynaptic sites (O'Brien et al., 1999; O'Brien et al., 2002; Reti et al., 2008; Farhy-Tselnicker et al., 2017). In retinal ganglion cells (RGCs), glypican-4 is thought to induce axonal release of Nptx1 through Gpc4 interactions with presynaptic RPTP δ. AMPARs are then accumulated at postsynaptic sites by Nptx1-induced clustering (Farhy-Tselnicker et al., 2017). This mechanism likely underlies the conversion of silent (AMPAR-lacking) to functional (AMPAR-containing) synapses (Bjartmar et al., 2006; Koch and Ullian, 2010), which is developmentally regulated by Nptxs (Bjartmar et al., 2006). This regulation is probably due to high Nptx1 expression during early neuronal development (Boles et al., 2014).

Despite evidence for Nptxs in controlling the function of excitatory synapses onto inhibitory interneurons through GluA4 NTD interactions, the physiological function of Nptx1 in shaping excitatory synaptic transmission at principal neurons in the hippocampus remains unclear. Having identified Nptx1 as a key component of the AMPAR NTD-proteome at excitatory synapses and confirmed a direct interaction between Nptx1 and GluA1-4 NTDs (Chapter 4), this chapter aims to deduce the functional role of Nptx1 at excitatory synapses in the hippocampus through interactions with GluA1/2-containing AMPAR NTDs.

5.2 Results

5.2.1 Nptx1 binding site mutants

The Nptx1 PTX domain ($Nptx1_{PTX}$) interacts directly with the AMPAR NTD (O'Brien et al., 1999; Xu et al., 2003; Sia et al., 2007; Lee et al., 2017; Suzuki et al., 2020), with the following subunit binding preference: GluA4 > GluA3 > GluA1 > GluA2 (data from cell-based binding assay established and described in Chapter 4). Until recently, the structural biology of this protein interaction was unknown. Using an X-ray crystal structure of Nptx1 in complex with the AMPAR NTD (Unpublished; collaboration with Veronica Chang and Radu Aricescu), numerous NTD mutants were designed in an attempt to obstruct Nptx1 binding. Mutating 2 amino acids in the AMPAR NTD to non-polar hydrophobic alanine residues (Confidential amino acid sequence) completely abolished Nptx1-AMPAR NTD interactions (Figure 5.1). This mutation, termed ΔNptx1, was introduced to all four AMPAR subunit NTDs by sequence alignment of GluA1-4 NTDs. Robust surface expression was observed with both WT and ΔNptx1 GluA1-4 NTDs, however Nptx1 binding was only observed with WT NTDs (Figure 5.1). Direct protein interactions with WT NTDs were found to be independent of N- or C-terminal AviTag positioning on Nptx1 (Figure 5.1A2/B2). ΔNptx1 mutants therefore, offer a powerful way to study the consequence of a loss of Nptx1 binding by minimal modification of the AMPAR NTD amino acid sequence.

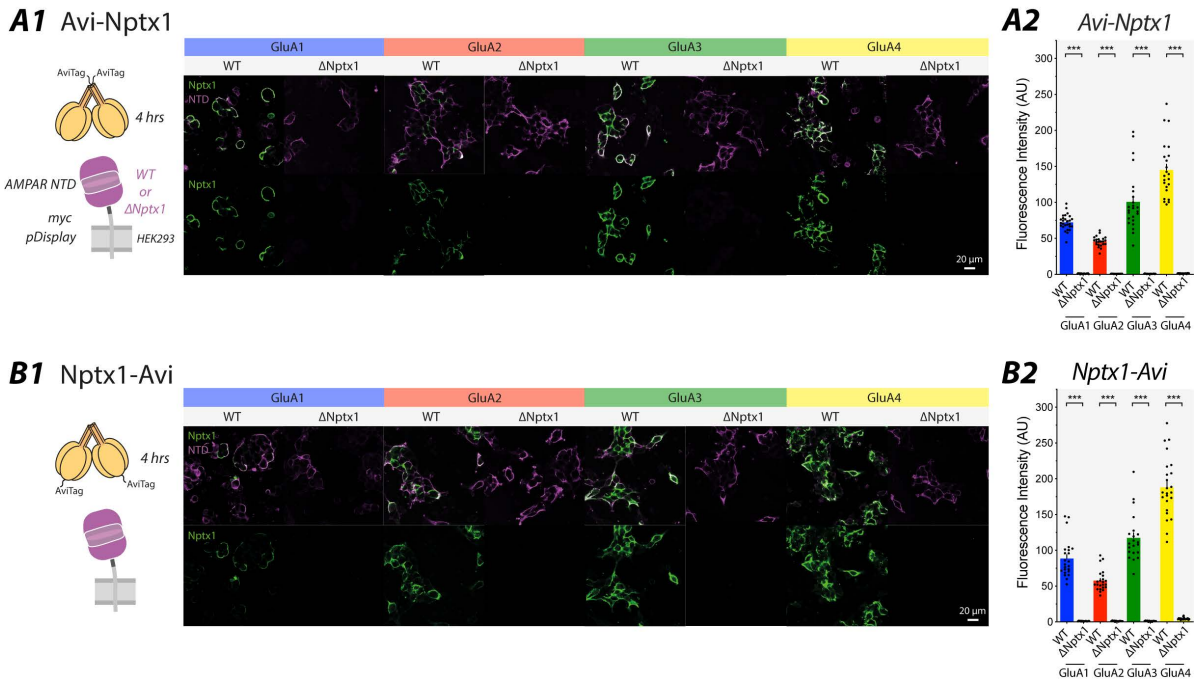

Figure 5.1 ***Nptx1-AMPAR NTD binding mutants abolish direct interactions.*** *Cell-based binding assay used to measure Nptx1 binding to WT and ΔNptx1 AMPAR NTDs in HEK293 cells (established in Chapter 4).* ***(A1)*** *N-terminal AviTag-Nptx1 (Avi-Nptx1; green) co-localised with pDisplay-myc-NTDs (magenta) indicating direct interactions with GluA1-4 WT but not ΔNptx1 NTDs, despite robust surface expression of both WT and ΔNptx1 GluA1-4 NTDs.* ***(A2)*** *Fluorescence intensity (AU) was used to measure the binding preference of direct interactions between Nptx1 and AMPAR NTDs. Avi-Nptx1 co-localised with GluA1-4 WT, but not ΔNptx1 NTDs (GluA1 WT = 72.3 ± 2.10; GluA1 ΔNptx1 = 0.93 ± 0.10; GluA2 WT = 45.8 ± 1.53; GluA2 ΔNptx1 = 0.73 ± 0.03; GluA3 WT = 100.7 ± 8.29; GluA3 ΔNptx1 = 0.73 ± 0.05; GluA4 WT = 144.9 ± 8.08; GluA4 ΔNptx1 = 1.21 ± 0.08; n = 6 preparations; ANOVA, *** p < 0.001).* ***(B1)*** *C-terminal Nptx1-AviTag (Nptx1-Avi; green) co-localised with pDisplay-myc-NTDs (magenta) of WT but not ΔNptx1 GluA1-4 NTDs.* ***(B2)*** *Nptx1-Avi co-localised with GluA1-4 WT, but not ΔNptx1 NTDs (GluA1 WT = 88.6 ± 5.48; GluA1 ΔNptx1 = 1.09 ± 0.08; GluA2 WT = 57.6 ± 0.08; GluA2 ΔNptx1 = 1.10 ± 0.15; GluA3 WT = 117.3 ± 7.18; GluA3 ΔNptx1 = 1.09 ± 0.18; GluA4 WT = 188.1 ± 8.50; GluA4 ΔNptx1 = 4.46 ± 0.32; n = 6 preparations; ANOVA, *** p < 0.01).*

5.2.2 GluA2Q ΔNptx1 gating kinetics

GFP-P2A-AMPAR vector

First, to achieve robust and reliable expression of AMPARs and fluorescent reporter GFP as a transfection marker in neurons, a bicistronic expression system was developed. Due to its smaller base pair (bp) size, the P2A 'self-cleaving' peptide (Figure 5.2A1; Liu et al., 2017) was chosen over IRES, to permit incorporation of both GFP + AMPAR encoding DNA into adeno-associated viruses (AAVs), at the packaging size limit of 4.7 kbp. Additionally, due to its equimolar expression of upstream and downstream products, P2A reduces the variability of AMPAR expression experienced with IRES vectors. Immunostaining of HEK293 cells transfected with GFP-P2A-AMPARs confirmed surface AMPAR and cytosolic GFP expression of WT and ΔNptx1 constructs (Figure 5.2B). The intensity of GFP fluorescence observed with the P2A vector was vastly enhanced over that detected with conventional IRES vectors. Moreover, AMPAR surface expression correlated with the intensity of GFP fluorescence to a greater extent than IRES (qualitative observation from immunostaining experiments).

GluA2Q ΔNptx1 gating kinetics

To assess if ΔNptx1 receptors have the same gating kinetics as WT, glutamate-evoked currents (10 mM, 200 ms, -60 mV) were recorded from outside-out patches excised from HEK293 cells expressing homomeric GluA2Q WT and ΔNptx1 (Figure 5.2C1). In the CNS, GluA2 subunits are RNA edited at the Q/R site, which lines the channel pore, conveying a linear current-voltage (IV) relationship and Ca^{2+} impermeability (Bowie and Mayer, 1995; Kamboj et al., 1995; Koh et al., 1995). In contrast, recombinant unedited GluA2Q receptors display an inwardly rectifying IV curve, through pore-block by intracellular polyamines, such as spermine at positive potentials (Figure 5.2C3; Pellegrini-Giampietro, 2003). GluA2Q receptors were used throughout this study to permit the detection of synaptic trafficking as a change in the synaptic rectification index (RI) (Hayashi et al., 2000; Shi et al., 2001).

GluA2Q WT and ΔNptx1 displayed classical fast AMPAR currents in response to 10 mM glutamate (Figure 5.2D). The current rise time (10-90 %), peak amplitude and weighted time constant of current decay (τ des.) of GluA2Q ΔNptx1 remain unchanged relative to WT receptors (Figure 5.2D3). This suggests that channel gating properties of ΔNptx1 receptors are unaltered relative to WT, permitting the use of this mutant receptor for studying the effect of a loss of Nptx1 binding on synaptic function.

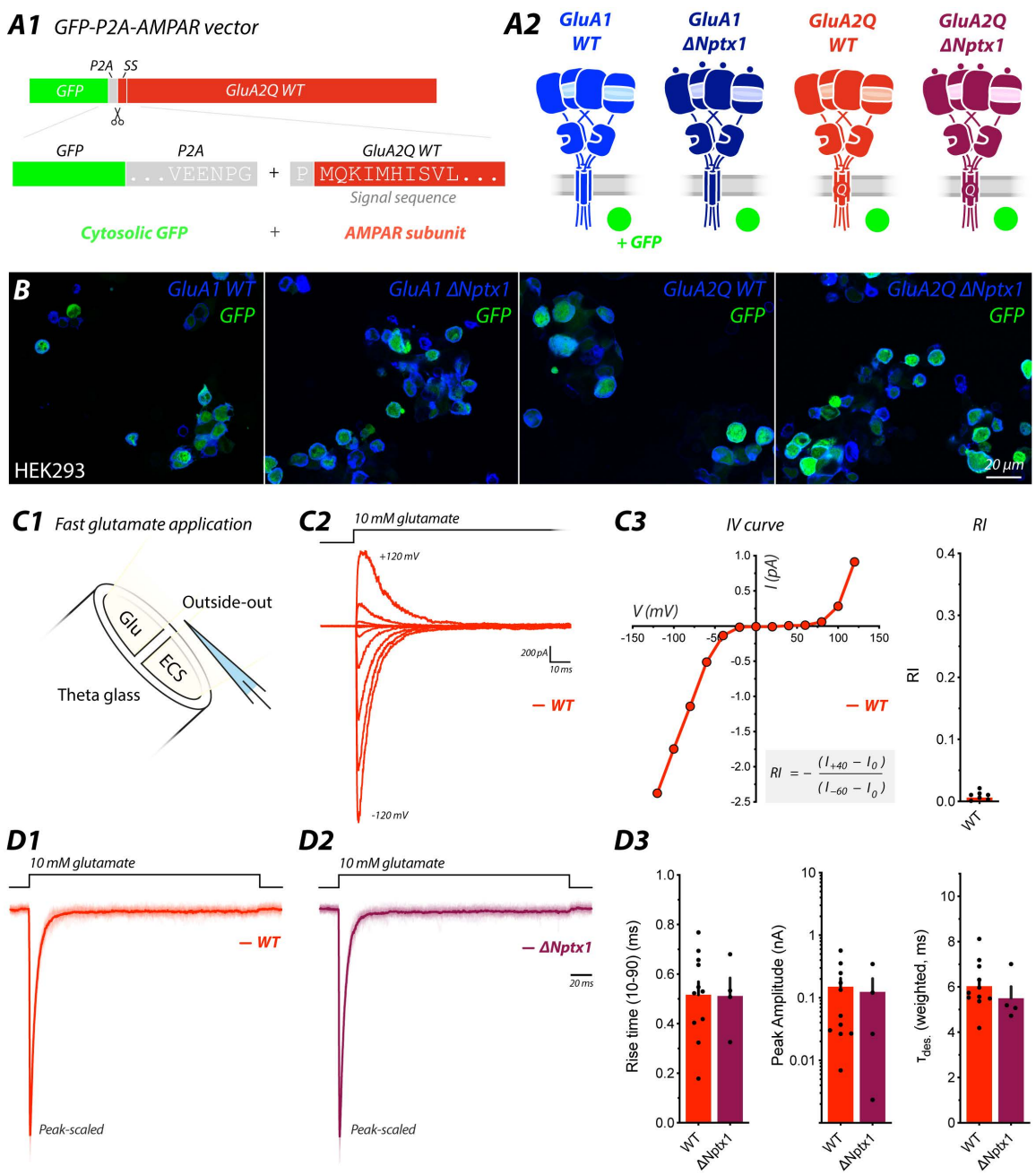

Figure 5.2 *GluA2Q ΔNptx1 gating kinetics are unchanged relative to WT.*

Figure 5.2 ***GluA2Q ΔNptx1 gating kinetics are unchanged relative to WT.*** *(**A1**) GFP-P2A-AMPAR bicistronic expression system. The self-cleaving P2A peptide results in expression of cytosolic GFP and AMPAR subunits with a proline (P) residue attached the signal sequence (SS). The signal sequence is subsequently cleaved in the ER, producing un-tagged AMPAR subunits. (**A2**) GluA1 WT, GluA1 ΔNptx1, GluA2Q WT and GluA2Q ΔNptx1 receptors. (•) 2 amino acid mutation in the AMPAR NTD, referred to as ΔNptx1. (**B**) Immunostaining of surface WT and mutant AMPARs (blue) and cytosolic GFP (green) expressed in HEK293 cells using the GFP-P2A-AMPAR vector (scale bar = 20 μm). (**C1**) Fast glutamate application system used to record AMPAR currents from GFP positive HEK293 cells. Piezoelectric-driven theta-glass capillary tube was used to switch between extracellular solution (ECS) and ECS containing 10 mM glutamate (Glu). (**C2**) Representative trace recorded from outside-out patches containing GluA2Q WT in response to 10 mM glutamate application held at membrane potentials of -120 to +120 mV (kindly provided by Dr Ondrej Cais). (**C3**) Current-voltage (IV) relationship of GluA2Q WT displaying double rectification due to intracellular spermine. Rectification index (RI) of GluA2Q WT (WT = 0.006 ± 0.003, n = 9). (**D**) AMPAR currents recorded from outside-out patches containing (**D1**) WT and (**D2**) ΔNptx1. (**D3**) Rise time (10-90 %) (WT = 0.52 ± 0.05 ms, n = 11; ΔNptx1 = 0.51 ± 0.07 ms, n = 4; unpaired t-test, p = 0.96), peak amplitude (WT = 150.6 ± 53.5 pA, n = 11; ΔNptx1 = 124.2 ± 78.4 pA, n = 4; unpaired t-test, p = 0.80) and weighted time constant (WT = 6.04 ± 0.32 ms, n = 11; ΔNptx1 = 5.50 ± 0.51 ms, n = 4; unpaired t-test, p = 0.40) remain unchanged relative to WT.*

5.2.3 GluA2Q ΔNptx1 synaptic transmission

AAV microinjection of CA1 pyramidal neurons

To increase the number of successfully transduced CA1 pyramidal neurons over that achieved with traditional single-cell electroporation (SCE), AAV transduction of GFP-P2A-AMPAR vectors was established. This required production and purification of high-titer (1.0×10^{13} GC/mL) recombinant AAVs containing GFP-P2A-AMPARs for GluA1/2 WT and ΔNptx1 constructs. AAV-GFP-P2A-AMPARs were microinjected into the CA1 region of organotypic hippocampal slices, resulting in region-specific expression across the pyramidal cell layer (Figure 5.3A1; Ehrengruber et al., 1999; Wiegert et al., 2017a). Firstly, AAV-GFP was expressed alone without the AMPAR, and pairs of uninfected (GFP-) and infected (GFP+) cells were recorded simultaneously using dual whole-cell patch-clamp. The synaptic RI and AMPAR EPSC amplitude of GFP+ cells were unchanged relative to uninfected cells (Figure 5.3A2). This demonstrates that GFP expression via AAV microinjection has no effect on AMPAR-mediated synaptic transmission, demonstrating this a suitable transduction technique.

Next, the AMPAR inward rectification property described earlier using recombinant expression (Figure 5.2C), was harnessed to study the trafficking of AMPARs to CA1 synapses (Hayashi et al., 2000; Shi et al., 2001). AMPAR EPSCs recorded at -60, 0 and +40 mV revealed a strong rectification of the synaptic response from cells expressing GluA2Q WT, transfected by SCE (Figure 5.3B3). Following microinjection of AAV-GFP-P2A-AMPAR constructs, the level of GFP fluorescence and synaptic RI of GluA2Q WT were monitored at different time points from day post infection (DPI) 3-13 (Figure 5.3B4). Dim GFP fluorescence was observed at DPI 3, with a significantly reduced synaptic RI = 0.4 relative to uninfected cells. However, from DPI 5 onwards, synaptic RI was further reduced to 0.2, consistent with that obtained after SCE in this study (Figure 5.3B3) and other reports (Watson et al., 2017). Based on this timeline experiment all subsequent recordings were performed at DPI 5-7.

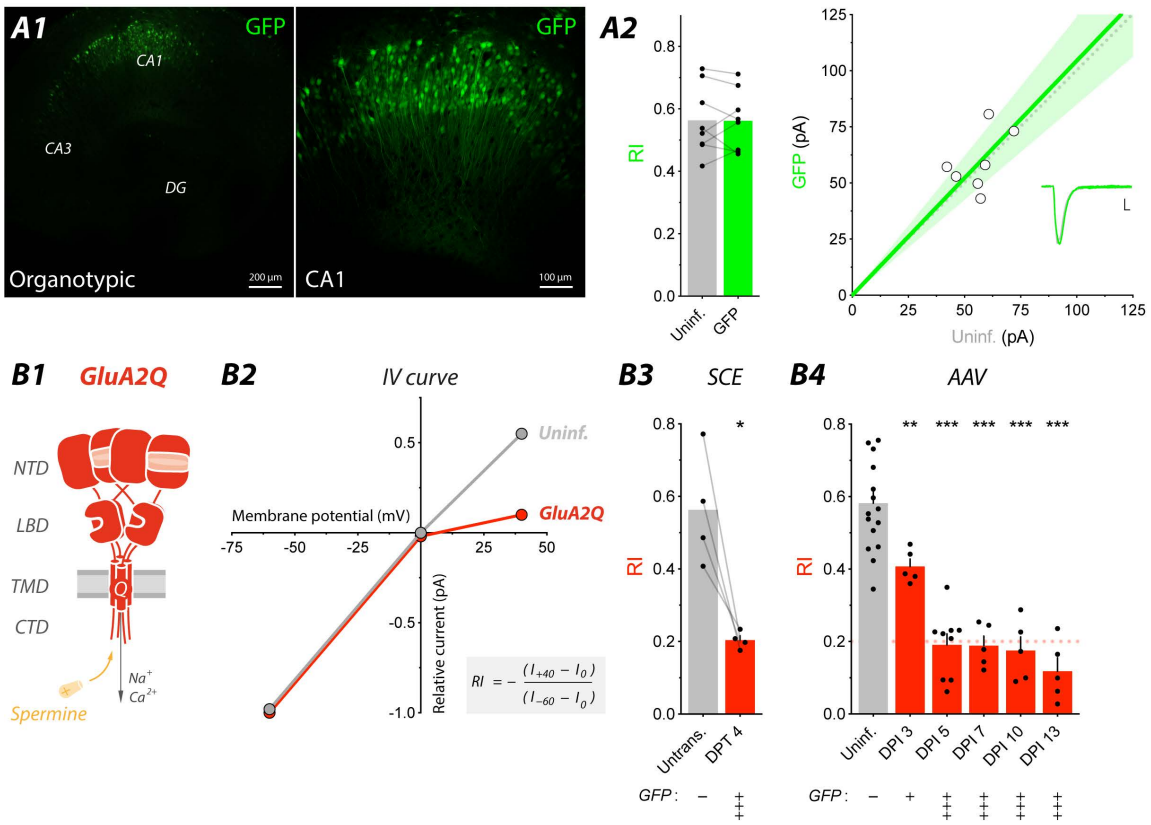

Figure 5.3 ***GFP-P2A-AMPAR expression in CA1 pyramidal neurons.*** *(**A1**) AAV microinjection of the CA1 pyramidal layer of organotypic hippocampal slices resulted in region-specific GFP expression. (**A2**) Rectification index (RI) of GFP remained unchanged relative to Uninf. (Uninf. = 0.56 ± 0.04; GFP = 0.56 ± 0.03, n = 8; paired t-test, p = 0.95). AMPAR EPSC amplitude of GFP remained unchanged relative to Uninf. (Uninf. = 56.2 ± 3.70 pA; GFP = 59.3 ± 5.0 pA; paired t-test, p = 0.52). (**B1**) GluA2Q receptors are blocked by intracellular polyamines, such as spermine, at positive potentials. (**B2**) Endogenous AMPARs in Uninf. cells have a linear current-voltage (IV) relationship, whereas exogenous GluA2Q expressing cells are inwardly rectifying, due to block at +40 mV. (**B3**) Synaptic RI recorded from GluA2Q transfected by single-cell electroporation (SCE) at day post-transfection (DPT) 4 (Untrans. = 0.56 ± 0.08, WT = 0.20 ± 0.01, n = 4; paired t-test, p < 0.05). (**B4**) Synaptic RI recorded from GluA2Q at different days post-infection (DPI) following AAV microinjection (Uninf. = 0.58 ± 0.03, n = 16; DPI 3 = 0.41 ± 0.02, n = 5; DPI 5 = 0.19 ± 0.03, n = 9; DPI 7 = 0.19 ± 0.03, n = 5; DPI 10 = 0.17 ± 0.04, n = 5; DPI 13 = 0.12 ± 0.04, n = 5; ANOVA, * p < 0.05, ** p < 0.01, *** p < 0.001).*

The GFP-P2A-AMPAR expression system offers numerous advantages over other transduction techniques such as SCE. First and foremost, increased number of expressing cells per slice (AAV = ~100 cells, SCE = ~10 cells); reduced time taken to transduce (AAV = ~5 mins per slice; SCE = ~30 mins per slice); increased success rate (AAV = 100%; SCE = ~25%); and finally, equimolar expression of GFP + AMPAR (AAV – P2A vector expresses similar quantities of GFP + AMPAR; SCE – co-transfection with GFP plasmid results in variable ratios of GFP + AMPAR expression). This permits selection of cells with similar AMPAR expression levels, undetectable with SCE.

GluA2Q ΔNptx1 synaptic trafficking

Nptx1 has been shown to localise to synapses on excitatory (O'Brien et al., 1999; Xu et al., 2003; Cho et al., 2008) and inhibitory neurons (Chang et al., 2010; Pelkey et al., 2015). Although the number of synaptic localisations on PV-INs is well-described (~95%; Chang et al., 2010), the proportion of excitatory synapses containing Nptx1 is unknown. To address this question, immunostaining of dissociated hippocampal cultures was performed using primary antibodies directed at Nptx1 (green), GluA2 (magenta) and presynaptic marker bassoon (cyan) (Figure 5.4B). Nptx1 co-localised with postsynaptic GluA2 and presynaptic bassoon at ~17% of excitatory synapses (Figure 5.4B2). However, the functional consequence of Nptx1 localisation at this fraction of excitatory synapses is unclear.

Exogenously expressed GluA2Q WT displayed a significantly reduced synaptic RI relative to paired uninfected cells in organotypic hippocampal slices (Figure 5.4C1), comparable to that achieved with SCE transfection (Figure 5.3B3; Watson et al., 2017). GluA2Q WT significantly increased the AMPAR EPSC amplitude by ~50% (Figure 5.4C1). These findings indicate that GluA2Q WT receptors traffic to CA1 synapses where they contribute to effective synaptic transmission. Similarly, GluA2Q ΔNptx1 significantly reduced the synaptic RI relative to paired uninfected cells (Figure 5.4C2). Furthermore, the EPSC amplitude of GluA2Q ΔNptx1 was significantly increased by ~50% (Figure 5.4C2), mimicking GluA2Q WT. This suggests that GluA2Q ΔNptx1 traffics to CA1 synapses where it contributes to efficient synaptic transmission. Therefore, Nptx1 binding to the GluA2 NTD appears to have no effect on the trafficking of receptors to CA1 synapses.

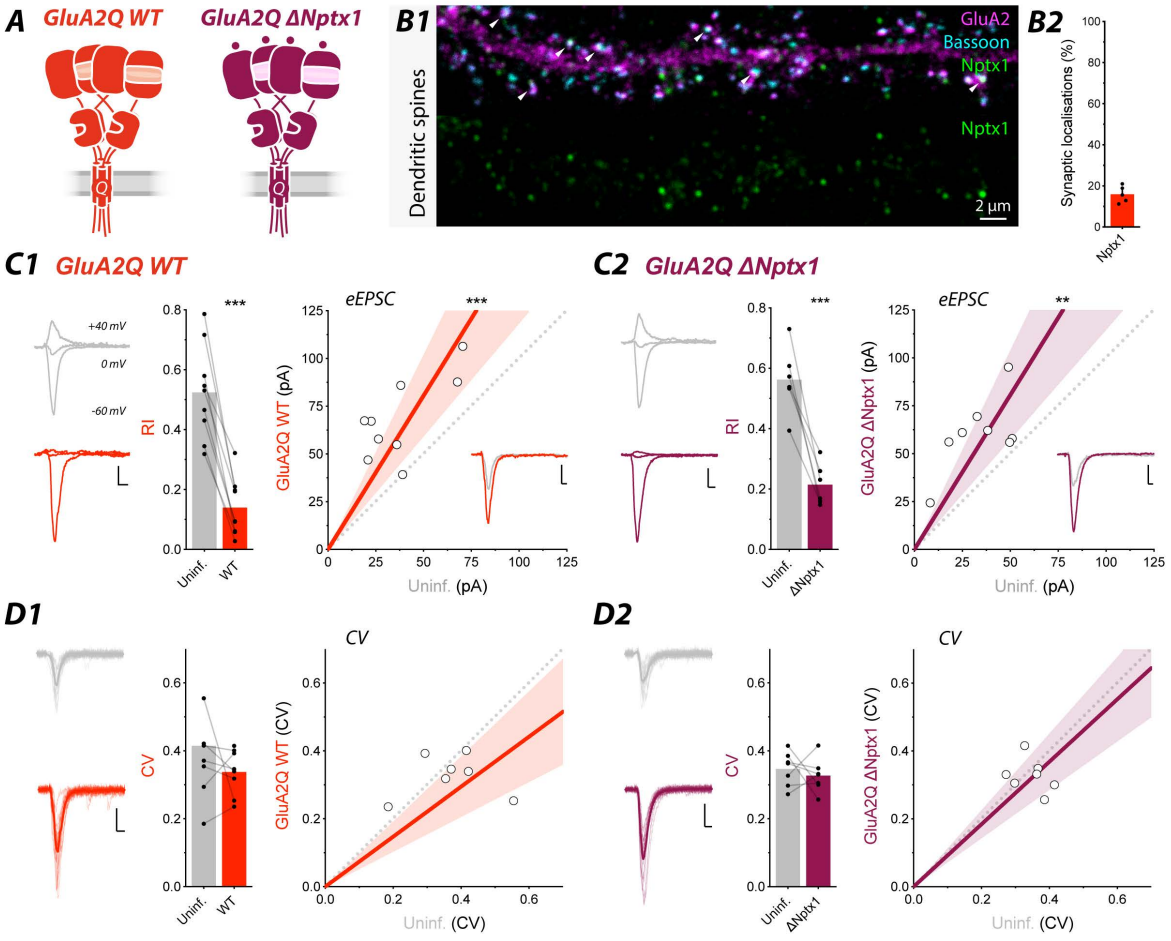

Figure 5.4 *GluA2Q ΔNptx1 traffics to CA1 synapses.*

Figure 5.4 ***GluA2Q ΔNptx1 traffics to CA1 synapses.*** *(**A**) GluA2Q WT and ΔNptx1 receptors. (•) 2 amino acid mutation in the AMPAR NTD, referred to as ΔNptx1. (**B1**) Immunostaining of hippocampal dendritic spines containing endogenous: GluA2 (magenta), bassoon (cyan) and Nptx1 (green). Triple co-localisations are marked with white arrows and quantified as synaptic localisations. (**B2**) Nptx1 localised to 17% of excitatory synapses containing GluA2 (n = 5 cells) (Nptx1 primary antibody kindly provided by Dr Kunimichi Suzuki). (**C1**) Representative synaptic RI traces of Uninf. (grey) and GluA2Q WT (red) held at -60, 0 and + 40 mV (scale bar = 20 pA; 10 ms). Synaptic RI of WT was significantly decreased relative to Uninf. (Uninf. = 0.52 0.05; WT = 0.14 0.03; n = 9; paired t-test, p < 0.001). Evoked EPSC (eEPSC) amplitude of WT was significantly increased relative to Uninf. (Uninf. = 37.8 ± 6.4 pA; WT = 68.2 ± 7.2 pA; n = 9; paired t-test, p < 0.001). (**C2**) Representative synaptic RI traces of Uninf. (grey) and GluA2Q ΔNptx1 (burgundy) (scale bar = 20 pA; 10 ms). Synaptic RI of ΔNptx1 was significantly decreased relative to Uninf. (Uninf. = 0.56 ± 0.04; ΔNptx1 = 0.21 ± 0.03; n = 8; paired t-test, p < 0.001). eEPSC amplitude of ΔNptx1 was significantly increased relative to Uninf. (Uninf. = 34.0 ± 5.6 pA; ΔNptx1 = 60.3 ± 6.9 pA; n = 8; paired t-test, p < 0.01). (**D1**) 20 representative traces recorded at -60 mV overlay with average trace (bold) of Uninf. and WT. Coefficient of variation (CV) of WT was unchanged relative to Uninf. (Uninf. = 0.41 ± 0.06; WT = 0.34 ± 0.02; n = 8; paired t-test, p = 0.19). 20 representative traces overlay with average trace of Uninf. and ΔNptx1. CV of ΔNptx1 was unchanged relative to Uninf. (Uninf. = 0.35 ± 0.02; WT = 0.33 ± 0.02; n = 7; paired t-test, p = 0.55).*

To further investigate the reliability of synaptic transmission with these receptors, the coefficient of variation (CV) was determined from EPSCs recorded at -60 mV. CV is a measure of the variability of the synaptic response, influenced by the probabilistic nature of presynaptic glutamate release and postsynaptic receptor localisation, where more effective transmission is accompanied by a reduction in the CV (Huijstee et al., 2020). The CV of both GluA2Q WT and GluA2Q ΔNptx1 were unchanged relative to paired uninfected cells (Figure 5.4D1). This suggests that Nptx1 binding to the GluA2 NTD has no effect on the reliability of CA1 synaptic transmission.

GluA2Q ΔNptx1 mEPSCs

Miniature EPSCs (mEPSCs) are postsynaptic responses to spontaneous glutamate release, activating synaptic receptors within the postsynaptic density (PSD; Hardingham and Bading, 2010). Evoked EPSCs (eEPSCs; Figure 5.4) however, can activate peri- and extra-synaptic receptors even using a low stimulation frequency (Chapter 3; Papouin and Oliet, 2014). mEPSCs therefore, were used to study solely synaptic AMPARs. Additionally, mEPSCs can be used to determine the frequency of excitatory synaptic transmission, providing further insights into presynaptic and postsynaptic function. Tetrodotoxin (TTX) was applied to organotypic hippocampal slices to prevent action potential-driven events and resultant mEPSCs were recorded from CA1 pyramidal neurons expressing WT and ΔNptx1 receptors.

Application of 1 μM TTX to organotypic hippocampal slices revealed AMPAR mEPSCs of >7 pA, detectable using a template search (Clampfit, Molecular Devices) above a noise-level of 6 pA, defined by peak to peak (Figure 5.5A). CA1 pyramidal cells expressing WT and ΔNptx1 displayed a higher proportion of AMPAR mEPSCs with an amplitude of 20-30 pA, detected for both WT and ΔNptx1 relative to uninfected cells. The AMPAR mEPSC amplitude of WT and ΔNptx1 was significantly increased relative to uninfected cells, as determined by the cumulative frequency distribution plot (Figure 5.5B1). However, mEPSC amplitude taken from the average of individual cells revealed no significant change (Figure 5.5B3). Previous reports also indicate no significant change in mEPSC amplitude with GluA2Q WT overexpression at CA1 synapses (Watson et al., 2017).

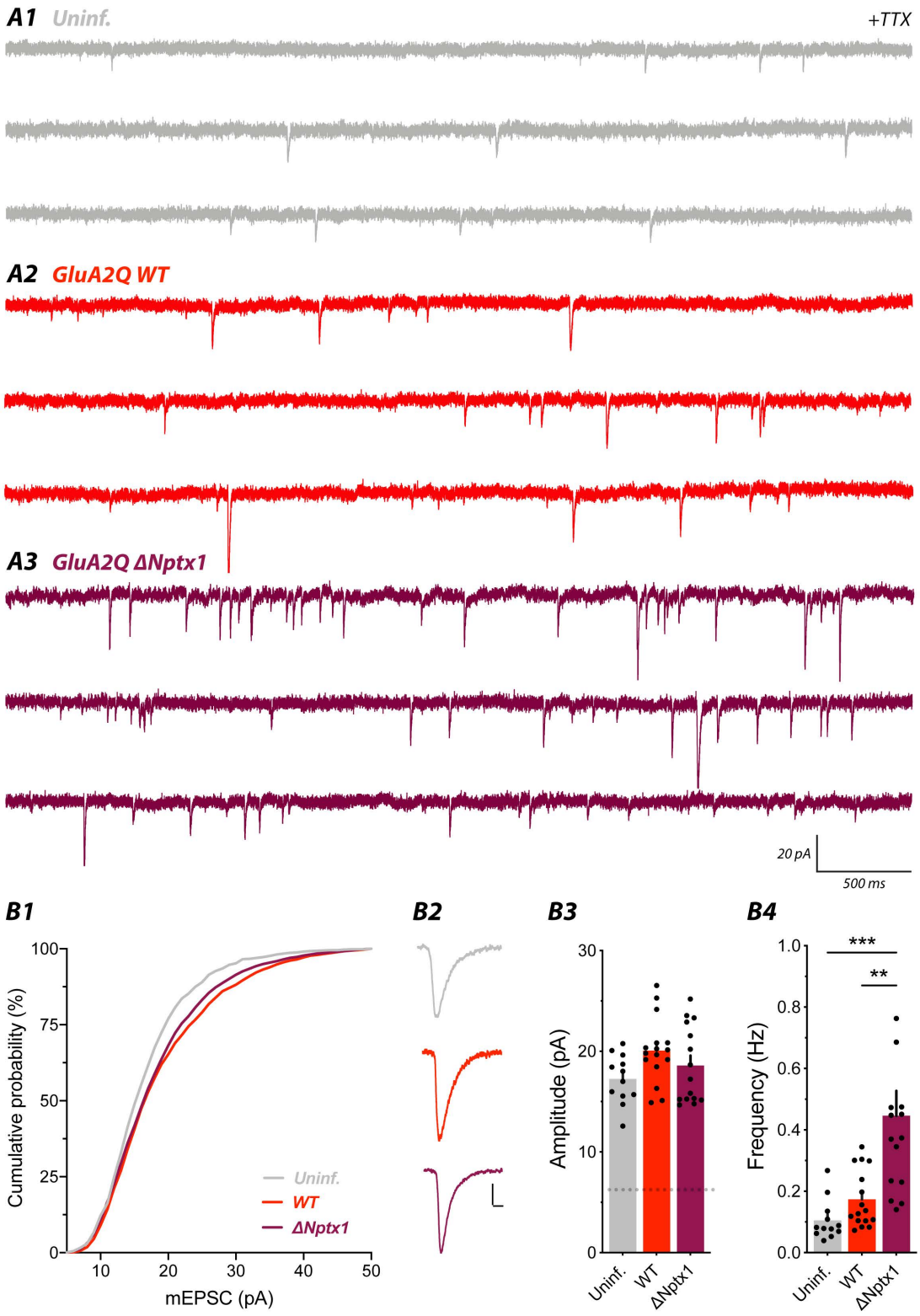

Figure 5.5 *GluA2Q ΔNptx1 increases the frequency of mEPSCs.*

Figure 5.5 ***GluA2Q ΔNptx1 increases the frequency of mEPSCs.*** *(**A**) 3 Representative mEPSC traces recorded from (**A1**) Uninf., (**A2**) WT and (**A3**) ΔNptx1 in the presence 1 μM TTX. Recordings were performed at DPI 5-7, with Uninf. cells recorded from the same slices as WT and ΔNptx1. mEPSCs were detected with an amplitude of >7 pA above a noise level of 6 pA. Example traces for each condition are taken from 3 independent preparations. (**B1**) Cumulative frequency distribution plot of mEPSC amplitude indicates a higher proportion of larger amplitude mEPSCs for WT and ΔNptx1 relative to Uninf., data from all recored events. GluA2Q WT had a significantly increased mEPSC amplitude distribution relative to Uninf. (Uninf. = 17.5 ± 0.24 pA; n = 1072 events; n = 12 cells; GluA2Q WT = 20.4 ± 0.20 pA; n = 3118 events; n = 16 cells; Kolmogorov-Smirnov test, P < 0.001). GluA2Q ΔNptx1 had a significantly increased mEPSC amplitude distribution relative to Uninf. (Uninf. = 17.5 ± 0.24 pA; n = 1072 events; n = 12 cells; GluA2Q ΔNptx1 = 19.3 ± 0.14 pA; n = 5056 events; n = 15 cells; Kolmogorov-Smirnov test, P < 0.001). (**B2**) Representative average mEPSC traces of Uninf. (grey), WT (red) and ΔNptx1 (burgundy) from individual cells (scale bar = 5 pA; 5 ms). (**B3**) mEPSC amplitude was unchanged between Uninf., WT and ΔNptx1 (Uninf. = 17.3 ± 0.70 pA, n = 12 cells; WT = 20.1 ± 0.81 pA, n = 16 cells; ΔNptx1 = 18.6 ± 0.99 pA, n = 15 cells; n = 3 independent preparations; ANOVA, p = 0.09). (**B4**) mEPSC frequency was significantly increased 2-fold for WT and 4-fold for ΔNptx1 relative to Uninf. (Uninf. = 0.081 ± 0.017 Hz, n = 13 cells; WT = 0.15 ± 0.025 Hz, n = 12 cells; ΔNptx1 = 0.49 ± 0.106 Hz, n = 11 cells; n = 3 independent preparations; ANOVA with multiple comparisons, ** p < 0.01, *** p < 0.001).*

Surprisingly, ΔNptx1 significantly increased the mEPSC frequency 4-fold relative to uninfected cells, and 2-fold relative to WT (Figure 5.5B4). This robust increase in mEPSC frequency was reproducibly observed across a total of 9 slices from 3 independent preparations for each condition. In line with these data, Nptx1 knockdown at excitatory synapses was also found to increase the frequency of mEPSCs (Figueiro-Silva et al., 2015). An increase in mEPSC frequency could be due to changes in: 1. Glutamate release probability, 2. Spine density, or 3. Postsynaptic AMPAR content. To further investigate the mechanisms underlying an increase in mEPSC frequency with ΔNptx1, additional experiments were conducted.

Probability of glutamate release

To investigate if the increase in mEPSC frequency observed with ΔNptx1 (Figure 5.5) can be attributed to changes in the presynaptic release machinery, the paired pulse ratio (PPR) was determined for WT, ΔNptx1 and uninfected cells using inter-stimulus intervals (ISIs) of 25, 50, 100 and 200 ms between $EPSC_1$ and $EPSC_2$. The PPR is calculated using the following equation:

$$PPR = EPSC_2 / EPSC_1$$

The probability of glutamate release is inversely proportional to the PPR, with alterations attributed to changes in the presynaptic calcium concentration (Zucker and Regehr, 2002). CA1 synapses of uninfected control slices exhibit classical paired pulse facilitation (PPF) (Figure 5.6A1; Zucker et al., 1989; Dobrunz and Stevens, 1997). As the ISI is increased, the probability of glutamate release is also increased, reflected by a decrease in the PPR (Figure 5.6B2).

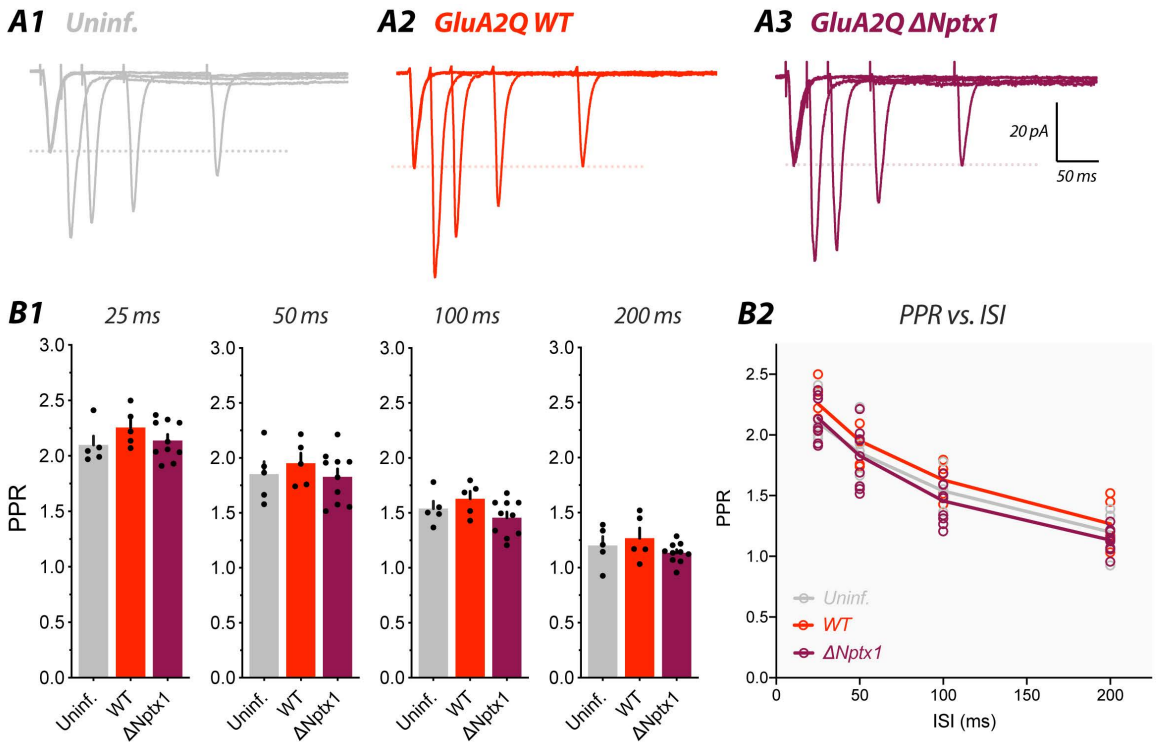

Figure 5.6 ***GluA2Q ΔNptx1 has no effect on the probability of glutamate release.*** *(**A**) Representative traces for EPSCs recorded from (**A1**) Uninf., (**A2**) GluA2Q WT and (**A3**) GluA2Q ΔNptx1 cells using an interstimulus interval (ISI) of 25, 50, 100 and 200 ms. (**B1**) Paired pulse ratio (PPR) of Uninf., WT and ΔNptx1 remained unchanged using an ISI of 25 ms (Uninf. = 2.10 ± 0.08, n = 5; WT = 2.26 ± 0.08, n = 5; ΔNptx1 = 2.14 ± 0.05, n = 10; ANOVA, p > 0.05); 50 ms (Uninf. = 1.85 ± 0.11, n = 5; WT = 1.95 ± 0.09, n = 5; ΔNptx1 = 1.83 ± 0.07, n = 10; ANOVA, p > 0.05); 100 ms (Uninf. = 1.54 ± 0.07, n = 5; WT = 1.63 ± 0.07, n = 5; ΔNptx1 = 1.46 ± 0.05, n = 10; ANOVA, p > 0.05); 200 ms (Uninf. = 1.20 ± 0.08, n = 5; WT = 1.27 ± 0.09, n = 5; ΔNptx1 = 1.13 ± 0.03, n = 10; ANOVA, p > 0.05). (**B2**) PPR versus ISI scatter plot indicates no change between Uninf., WT and ΔNptx1.*

Neuronal pentraxins have been shown to modify glutamate release at the Schaffer collateral-CA1 synapse (Cummings et al., 2017). The authors show that acute application of exogenous Nptx1/2/r to organotypic hippocampal slices increases the PPR, whereas chronic application decreases the PPR. In the context of this work, it is possible that the increase in mEPSC frequency with ΔNptx1 (Figure 5.5) may be due to changes in the probability of glutamate release. Therefore, it was hypothesised that a loss of Nptx1 binding with GluA2Q ΔNptx1, may in-turn affect the presynaptic release machinery, significantly altering the PPR.

However, there is no significant difference between the PPR of GluA2Q WT and ΔNptx1 compared to uninfected cells over a range of ISIs (Figure 5.6B). The discrepancy between these data and Cummings et al., (2017), may be explained by direct Nptx1 interactions with other elements of the presynaptic machinery, thus the ΔNptx1 mutation on the AMPAR NTD may not participate in this function. Nptx1 has been shown to directly interact with Kv7.2, localised at presynaptic sites (Figueiro-Silva et al., 2015), this interaction may influence glutamate release probability. Another explanation for these conflicting results is the potential difference in endogenous and exogenous concentrations of Nptx1, where Cummings et al., (2017) may achieve saturation of excitatory synapses with exogenous application, opposed to ~17% endogenous synaptic localisation in this study (Figure 5.4B). To investigate other potential mechanisms underlying the increase in ΔNptx1 mEPSC frequency, the AMPAR/NMDAR ratio of CA1 pyramidal neurons was investigated.

AMPAR/NMDAR ratio

A change in the number of functional excitatory synapses can have a profound effect on the frequency of mEPSC events. To investigate if the increased mEPSC frequency observed with ΔNptx1 (Figure 5.5) could be attributed to changes in the number of functional excitatory synapses, the AMPAR/NMDAR (A/N) ratio was determined. This assay was used to address two possible mechanisms: changes in synapse density and the number of 'silent synapses'. Where changes in the number of synaptic connections is accompanied by a significant change in the NMDAR EPSC (Soler-Llavina et al., 2011; Letellier et al., 2018), and a change in the number of silent synapses is reflected by a change in the A/N ratio (Kerchner and Nicoll, 2008). Interestingly, knockdown of Nptx1 has been shown to increase the number of excitatory synapses in dissociated cortical cultures, reflected by an increase in mEPSC frequency (Figueiro-Silva et al., 2015). A similar effect is observed with occlusion of Nptx1 binding to the GluA2 NTD

(Figure 5.5). This suggests that Nptx1-GluA2 NTD interactions may be involved in limiting excitatory synapse density. Alternatively, Nptx1 interactions may be involved in regulating the number of silent synapses, as in Nptx1 knockout neurons of the dorsolateral geniculate nucleus the proportion of silent synapses is either increased or decreased depending on synapse maturation (Koch and Ullian, 2010; Bjartmar et al., 2006). To investigate if there is a change in synapse density or number of silent synapses with ΔNptx1, the A/N ratio was determined. AMPAR EPSCs were resolved from the peak current of responses held at -60 mV, and NMDAR EPSCs were determined from the amplitude 50 ms after the stimulus of responses held at +40 mV, to exclude AMPAR contribution to the EPSC. This permits recording of both AMPAR and NMDAR EPSCs from the same cell, which are then expressed as a ratio (A/N). The EPSC amplitude of neurons transduced with WT GluA2Q was significantly increased compared to paired uninfected cells (Figure 5.7A1), as demonstrated previously (Figure 5.4). The size of the NMDAR EPSC, however, was unchanged relative to paired uninfected cells. This is reflected by a significant increase in the A/N ratio (Figure 5.7A2). With no changes in NMDAR EPSC amplitude, this suggests that overexpression of WT receptors has no effect on the number of functional synapses.

Expression of ΔNptx1 also significantly increased the size of the AMPAR EPSC (Figure 5.7B1), as illustrated in Figure 5.4. Interestingly, ΔNptx1 NMDAR EPSCs remain unchanged relative to paired uninfected cells. Consequently, the A/N ratio was significantly increased to a similar extent to WT (Figure 5.7B2), suggesting no change in the number of silent synapses. Since changes in spine density upon manipulation of other proteins e.g. cell-adhesion molecules, are reflected by significant changes in the NMDAR EPSC (Soler-Llavina et al., 2011; Letellier et al., 2018), it seems unlikely that occlusion of Nptx1 binding to GluA2 receptors affects synapse density. However, it is still possible that ΔNptx1 affects spine morphology, therefore future studies should address this question using imaging approaches.

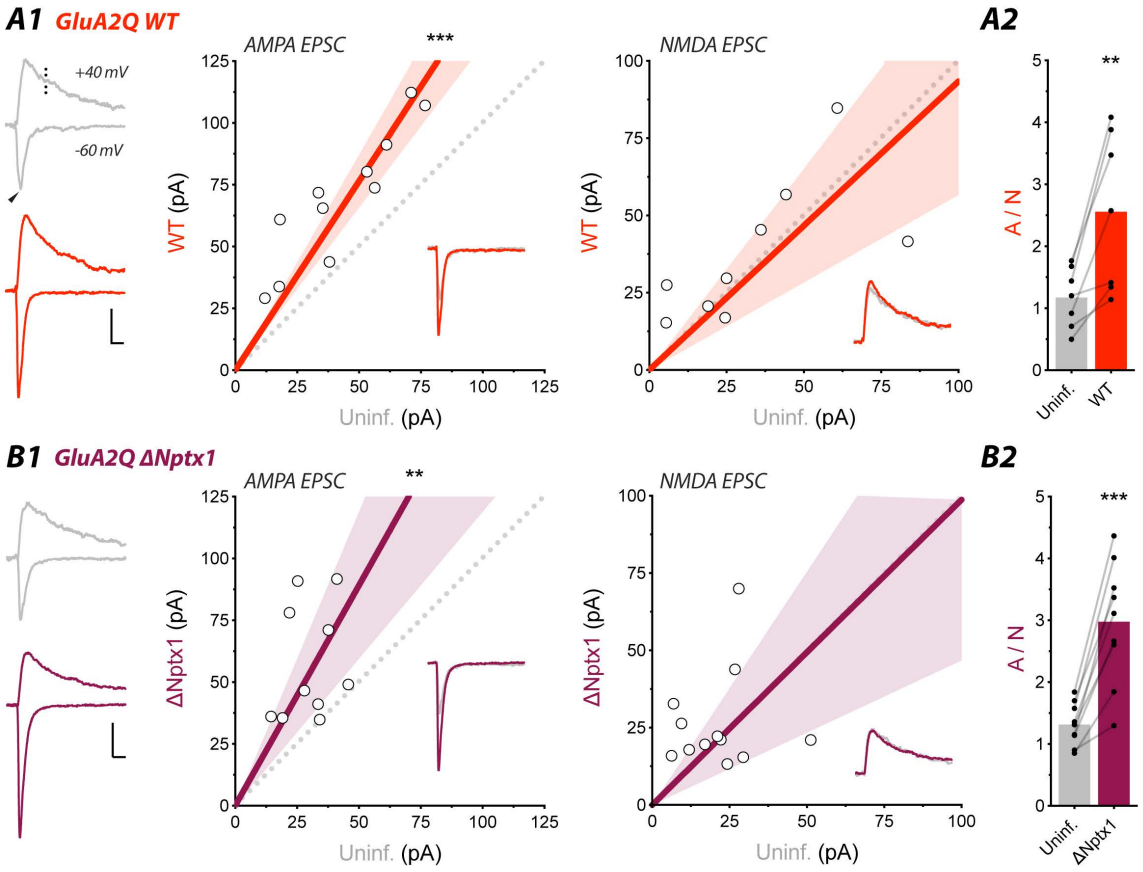

Figure 5.7 *GluA2Q ΔNptx1 has no effect on AMPAR/NMDAR ratio.*

Figure 5.7 ***GluA2Q ΔNptx1 has no effect on AMPAR/NMDAR ratio.*** *(**A1**) GluA2Q WT increased AMPAR, but not NMDAR EPSC amplitude. Representative traces of AMPAR EPSC (arrow; peak amplitude) recorded at -60 mV and NMDAR EPSC (dotted line; 50 ms after stimulus) recorded at +40 mV of Uninf. (grey) and GluA2Q WT (red) (scale bar = 20 pA; 20 ms). WT AMPAR EPSC amplitude was significantly increased relative to Uninf. (Uninf. = 43.0 ± 6.7 pA; WT = 70.0 ± 8.3 pA; n = 11; paired t-test, p < 0.001). WT NMDAR EPSC amplitude was unchanged relative to Uninf. (Uninf. = 33.8 ± 8.6 pA; WT = 37.6 ± 7.5 pA; n = 9; paired t-test, p = 0.58). (**A2**) WT AMPAR/NMDAR (A/N) ratio was significantly increased relative to Uninf. (Uninf. = 1.17 ± 0.18; WT = 2.56 0.48; n = 7; paired t-test, p < 0.01). (**B1**) GluA2Q ΔNptx1 increased AMPAR, but not NMDAR EPSC amplitude. Representative traces of AMPAR and NMDAR EPSCs of Uninf. (grey) and GluA2Q ΔNptx1 (burgundy) (scale bar = 20 pA; 20 ms). ΔNptx1 AMPAR EPSC amplitude was significantly increased relative to Uninf. (Uninf. = 30.1 ± 3.2 pA; ΔNptx1 = 57.5 ± 7.3 pA; n = 10; paired t-test, p < 0.01). ΔNptx1 NMDAR EPSC amplitude was unchanged relative to Uninf. (Uninf. = 21.2 ± 3.6 pA; ΔNptx1 = 26.6 ± 4.6 pA; n = 12; paired t-test, p = 0.35). (**B2**) ΔNptx1 A/N ratio was significantly increased relative to Uninf. (Uninf. = 1.31 ± 0.11; ΔNptx1 = 2.98 ± 0.33; n = 9; paired t-test, p < 0.001).*

Synaptic expression

Constitutive synaptic trafficking of AMPARs is thought to involve the insertion and removal of receptors by exocytotic and endocytic processes on a rapid time scale (Opazo and Choquet, 2011), influencing receptor number and ultimately the synaptic strength. Nptxs are able to dramatically control the synaptic AMPAR content at both excitatory (Cho et al., 2008; Figueiro-Silva et al., 2015) and inhibitory (Chang et al., 2010; Pelkey et al., 2015) synapses. To further investigate if the increase in ΔNptx1 mEPSC frequency (Figure 5.5) is due to a change in the number of postsynaptic AMPARs, the evoked AMPAR EPSC amplitude of WT and ΔNptx1 expressing cells was combined from several experiments (Figure 5.4 and 5.7) and normalised to paired uninfected cells (Figure 5.8A). As the peak amplitude of AMPAR EPSCs were unchanged between WT and ΔNptx1 in recombinant cells (Figure 5.2), the size of the synaptic response (AMPAR EPSC amplitude) can be used as a measure of synaptic receptor content.

Surprisingly, AMPAR surface expression is increased in Nptx knockout cortical neurons, an effect attributed to AMPAR clustering and endocytosis by Nptxs. Knockout of Nptx inhibits AMPAR endocytosis, increasing synaptic expression (Cho et al., 2008), a mechanism potentially underlying enhanced frequency of excitatory synaptic transmission (Figure 5.5; Figueiro-Silva et al., 2015). Nptx1-induced clustering and internalisation of AMPARs may explain the increased number of mEPSC events detected with GluA2Q ΔNptx1 (Figure 5.5), as AMPAR internalisation is associated with a decrease in mEPSC frequency (Beattie et al., 2000). To determine synaptic expression levels, normalised AMPAR EPSCs of GluA2Q WT and ΔNptx1 were compared directly (Figure 5.8). WT overexpression resulted in a 1.7-fold increase (Figure 5.8A2) and ΔNptx1 overexpression resulted in a 1.8-fold increase (Figure 5.8A3) in the AMPAR EPSC. Using this as a measure of synaptic receptor content at CA1 synapses, this suggests that Nptx1 binding has no effect on GluA2Q synaptic expression.

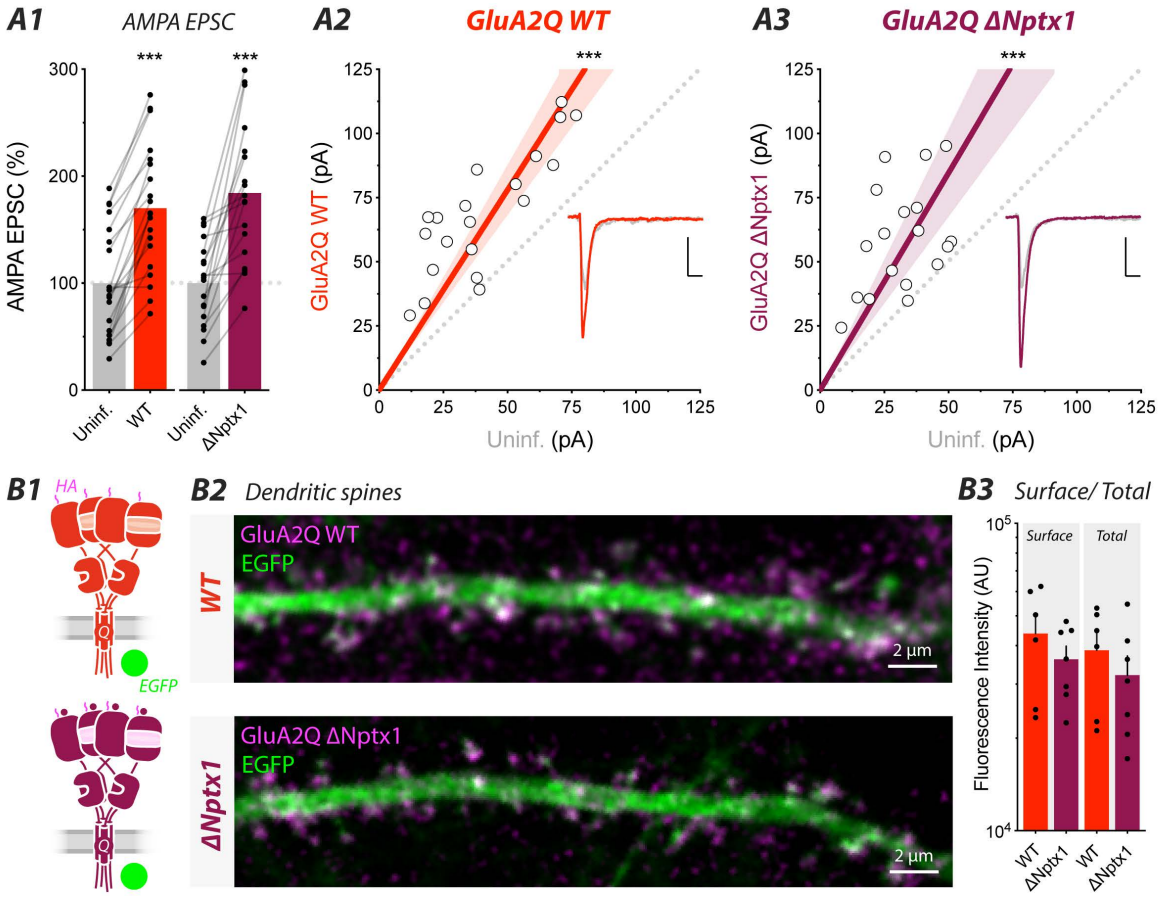

Figure 5.8 ***GluA2Q WT and ΔNptx1 localise at excitatory synapses and increase the AMPAR EPSC.*** *(**A**) Pooled data of AMPAR EPSC amplitude from GluA2Q WT and ΔNptx1 expressing cells relative to paired Uninf. control cells. (**A1**) AMPAR EPSC amplitude of WT (Uninf. = 100.0 ± 11.3 %; WT = 170.0 ± 13.4 %; n = 20 cells, n = 6 preparations; paired t-test, p < 0.001) and ΔNptx1 (Uninf. = 100.0 ± 9.44 %; ΔNptx1 = 184.4 ± 15.5 %; n = 18 cells, n = 6 preparations; paired t-test, p < 0.001) was significantly increased relative to Uninf. (**A2**) Scatter plot of WT AMPAR EPSC amplitude indicates a robust increase in amplitude relative to Uninf. (scale bar = 20 pA; 20 ms). (**A3**) Scatter plot of ΔNptx1 AMPAR EPSC amplitude shows a significant increase in amplitude relative to Uninf. (scale bar = 20 pA; 20 ms). (**B1**) HA-GluA2Q WT and ΔNptx1 transfected for immunostaining. (**B2**) WT and ΔNptx1 receptors were enriched at hippocampal dendritic spines (cytosolic GFP). ΔNptx1 surface and total expression was unchanged relative to WT (Surface: WT = 4.38 ± 0.69 x10^4 AU; ΔNptx1 = 3.61 ± 0.37 x10^4 AU; Total: WT = 3.86 ± 0.56 x10^4 AU; ΔNptx1 = 3.21 ± 0.50 x10^4 AU; n = 6; ANOVA, p > 0.05).*

To further clarify synaptic expression levels, HA-tagged WT and ΔNptx1 were overexpressed in dissociated hippocampal neurons followed by live staining of surface receptors (Figure 5.8B). both WT and ΔNptx1 enriched at dendritic spines, where they contribute to effective synaptic transmission, as determined using the synaptic RI (Figure 5.4). The surface and total receptor content were then quantified using the fluorescence intensity from live and permeabilised staining against HA-GluA2Q respectively, indicating no change in ΔNptx1 relative to WT (Figure 5.8B3). This further supports functional data (Figure 5.8A), suggesting no change significant changes in synaptic receptor expression levels between WT and ΔNptx1.

Taken together, these data imply no change in synaptic receptor expression levels with occlusion of Nptx1 binding to the GluA2 NTD. A caveat of these immunostaining experiments for studying AMPAR internalisation, is that dissociated hippocampal cultures are fixed before quantifying surface/ total receptor content. A more suitable approach for studying changes in synaptic AMPARs, is to use fluorescence recovery after photobleaching (FRAP; Watson et al., 2017), or single-particle tracking experiments on WT and ΔNptx1 receptors. This would permit live assessment of receptor motility, where changes in AMPAR internalisation can be uncovered.

5.2.4 GluA1 ΔNptx1 synaptic transmission

GluA1 NTDs have a higher binding affinity for Nptx1 than GluA2 NTDs (Figure 5.1B). Given the subunit-specific contribution of GluA1/2 NTDs to synaptic trafficking and control of transmission and plasticity (Watson et al., 2017; Díaz-Alonso et al., 2017; Watson et al., 2020; Jiang et al., 2021), it is possible that GluA1 ΔNptx1 may exert different functional effects at CA1 synapses. To test this hypothesis, GluA1 WT and ΔNptx1 receptors were expressed in CA1 pyramidal neurons and their effect on synaptic function was determined.

First the endogenous distribution of Nptx1 was investigated at GluA1-containing excitatory synapses in dissociated hippocampal neurons (Figure 5.9B). Nptx1 (green) showed co-localisation with presynaptic bassoon (cyan) and postsynaptic GluA1 (magenta) at some but not all excitatory synapses. Similarly to GluA2, Nptx1 localised at ~19% of excitatory synaptic sites containing GluA1 (Figure 5.9B2). This finding is unsurprising, as the majority of excitatory synapses contain GluA1/2 heteromers in the hippocampus (Lu et al., 2009; Schwenk et al., 2012; Schwenk et al., 2014), therefore a similar percentage co-localisation would be

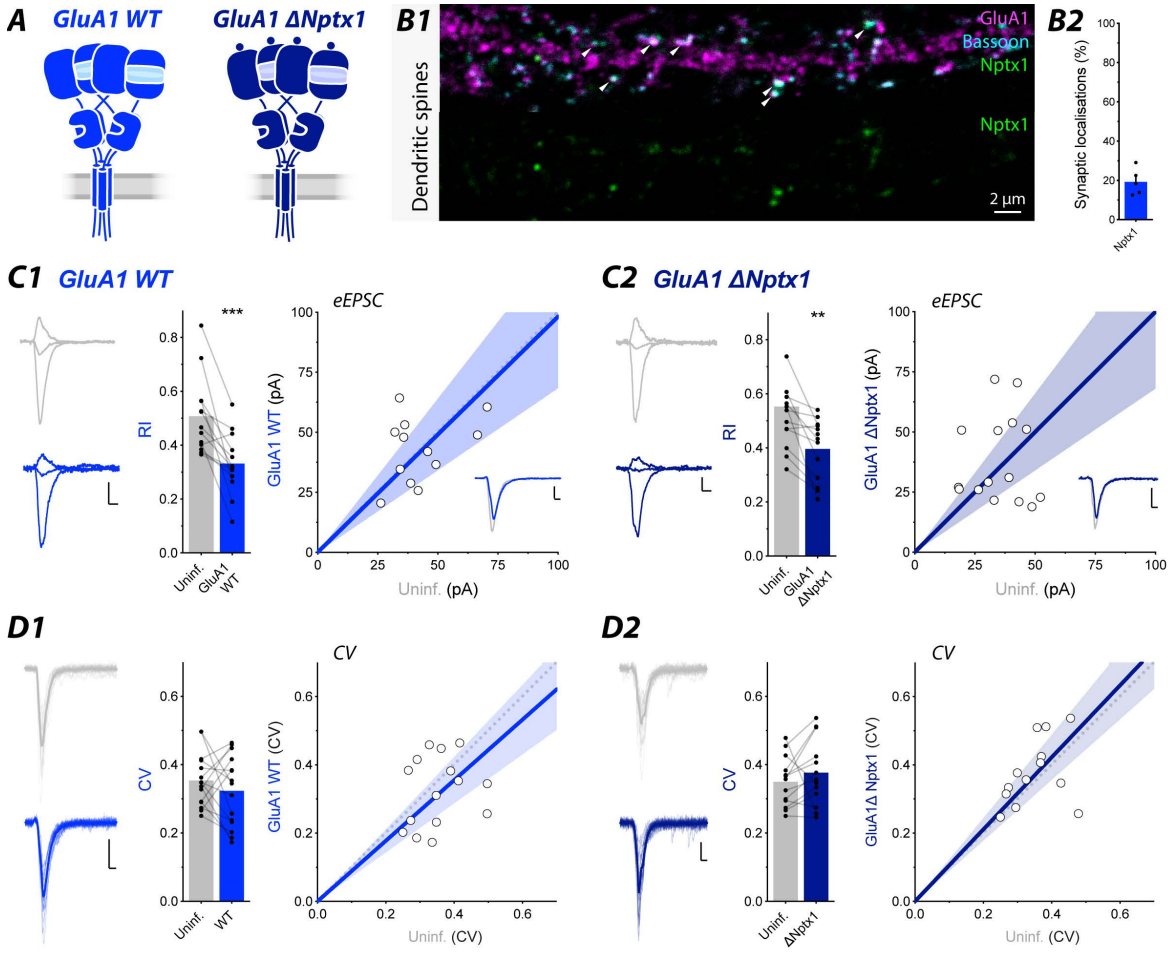

Figure 5.9 *GluA1 ΔNptx1 traffics to CA1 synapses.*

Figure 5.9 ***GluA1 ΔNptx1 traffics to CA1 synapses.*** *(**A**) GluA1 WT and ΔNptx1 receptors. (•) 2 amino acid mutation in the AMPAR NTD, referred to as ΔNptx1. (**B**) Immunostaining of hippocampal dendritic spines containing endogenous: GluA1 (magenta), bassoon (cyan) and Nptx1 (green). Triple co-localisations are marked with white arrows and quantified as synaptic localisations. (**B2**) Nptx1 localised to 19% of excitatory synapses containing GluA1 (n = 5 cells). (**C1**) Representative synaptic RI traces of Uninf. (grey) and GluA1 WT (blue) held at -60, 0 and + 40 mV (scale bar = 20 pA; 10 ms). Synaptic RI of WT was significantly decreased relative to Uninf. (Uninf. = 0.51 ± 0.04; WT = 0.33 ± 0.03; n = 13; paired t-test, p < 0.001). eEPSC amplitude of WT was unchanged relative to Uninf. (Uninf. = 65.0 ± 12.6 pA; WT = 74.6 ± 14.2 pA; n = 18; paired t-test, p = 0.42). (**C2**) Representative synaptic RI traces of Uninf. (grey) and GluA1 ΔNptx1 (navy) (scale bar = 20 pA; 10 ms). Synaptic RI of ΔNptx1 was significantly decreased relative to Uninf. (Uninf. = 0.55 ± 0.05; ΔNptx1 = 0.40 ± 0.03; n = 13; paired t-test, p < 0.01). eEPSC amplitude of ΔNptx1 was unchanged relative to Uninf. (Uninf. = 35.1 ± 2.8 pA; ΔNptx1 = 38.2 ± 4.7 pA; n = 15; paired t-test, p = 0.58). (**D1**) 20 representative traces recorded at -60 mV overlay with average trace (bold) of Uninf. and WT. Coefficient of variation (CV) of WT was unchanged relative to Uninf. (Uninf. = 0.35 ± 0.02; WT = 0.32 ± 0.03; n = 15; paired t-test, p = 0.32). 20 representative traces overlay with average trace of Uninf. and ΔNptx1. CV of ΔNptx1 was unchanged relative to Uninf. (Uninf. = 0.35 ± 0.02; WT = 0.38 ± 0.03; n = 13; paired t-test, p = 0.33).*

expected. Nptx1 localises to < 20% of GluA1/2-containing synapses, much lower than that of Nptx2 at PV-IN synapses (~95%; Chang et al., 2010).

To determine synaptic trafficking of GluA1, the synaptic RI was determined (Figure 5.9). GluA1 homomers contain a Q residue at the Q/R editing site, rendering them Ca^{2+} permeable and inwardly rectifying (Bowie and Mayer, 1995). Upon overexpression of GluA1, receptors predominantly form homomers, evident by significant rectification of the synaptic response (Watson et al., 2017; Díaz-Alonso et al., 2017). GluA1 and GluA2Q homomers have comparable single-channel conductances in heterologous expression systems ~20 pS (Coombs et al., 2012), therefore permitting comparison of the relative amplitude of GluA1 and GluA2Q synaptic responses.

The extent of synaptic rectification observed with GluA1 WT was lower than that of GluA2Q WT, confirming previous findings performed using SCE (Chapter 4; Watson et al., 2017). GluA1 WT had a significantly reduced synaptic RI relative to paired uninfected cells but showed no change in AMPAR EPSC amplitude (Figure 5.9C1). This suggests that GluA1 WT is trafficked to CA1 synapses where it contributes to synaptic transmission, although to a lesser degree than GluA2Q WT (Figure 5.4). Likewise, GluA1 ΔNptx1 also significantly reduced the synaptic RI relative to paired uninfected cells, with no change in AMPAR EPSC amplitude (Figure 5.9C2). This indicates that occlusion of Nptx1 binding to the GluA1 NTD has no effect on synaptic trafficking to CA1 synapses.

Coefficient of variation (CV) analysis on AMPAR EPSCs recorded from GluA1 WT and ΔNptx1 provides a measure of the reliability synaptic transmission at CA1 synapses. GluA1 WT CV was unchanged relative to paired uninfected cells (Figure 5.9D1). Similarly, GluA1 ΔNptx1 CV remained unchanged compared to paired uninfected cells (Figure 5.9D2). This implies that Nptx1 binding to the GluA1 NTD has no effect on in the reliability of GluA1-containing AMPAR-mediated synaptic transmission.

GluA1 ΔNptx1 mEPSCs

To investigate the effect of Nptx1-GluA1 NTD interactions on the frequency of excitatory synaptic transmission, mEPSCs were recorded from WT and ΔNptx1 receptors at CA1 synapses (Figure 5.9). In the presence of 1 μM TTX, mEPSCs with an amplitude of >7 pA were detected from Uninf., WT and ΔNptx1 expressing cells (Figure 5.10A), with uninfected cells reproducing the mEPSC amplitude and frequency determined in Figure 5.5. Strikingly, the mEPSC amplitude of ΔNptx1 was significantly decreased relative to both WT and uninfected cells (Figure 5.10B1). The cumulative distribution plot showed a significant trend towards a higher proportion of lower amplitude events (10-20 pA) for ΔNptx1 relative to WT (Figure 5.10B1). This suggests that ΔNptx1 receptors, although synaptically expressed (Figure 5.9), are unable to maintain the strength of synaptic transmission achieved by WT receptors. Interestingly, mEPSC frequency was significantly increased for both WT and ΔNptx1 relative to uninfected cells (Figure 5.10B4), suggesting WT and ΔNptx1 receptors have a similar level of overexpressed synaptic receptors. However, GluA1 ΔNptx1 receptors are unable to respond as effectively to presynaptic glutamate release, likely due to the loss of Nptx1-induced clustering. One interpretation of these data is that Nptx1 interactions with the GluA1 NTD may cluster postsynaptic receptors within the PSD for effective synaptic transmission (Savtchenko and Rusakov, 2014).

These findings are interesting when directly compared to mEPSCs recorded from GluA2Q receptors (Figure 5.5). While GluA2Q ΔNptx1 showed a trend wise increase in mEPSC amplitude (Figure 5.5B1), GluA1 ΔNptx1 had a significantly reduced mEPSC amplitude (Figure 5.10). This suggests that Nptx1 may exert subunit-specific effects on AMPAR-mediated synaptic transmission. This could be explained by the apparent higher binding affinity of Nptx1 for GluA1 relative to GluA2 NTDs (Figure 5.1), exerting subunit-specific effects on receptor function. Another interesting comparison between these subunits, is the increase in mEPSC frequency observed with GluA2Q ΔNptx1 (4-fold) relative to GluA1 ΔNptx1 (2-fold). GluA2Q ΔNptx1 dramatically increased mEPSC frequency, whereas GluA1 ΔNptx1 did not. This again raises the possibility of a subunit-specific regulation of AMPAR function by Nptx1, or indeed other interactors that engage with this binding site.

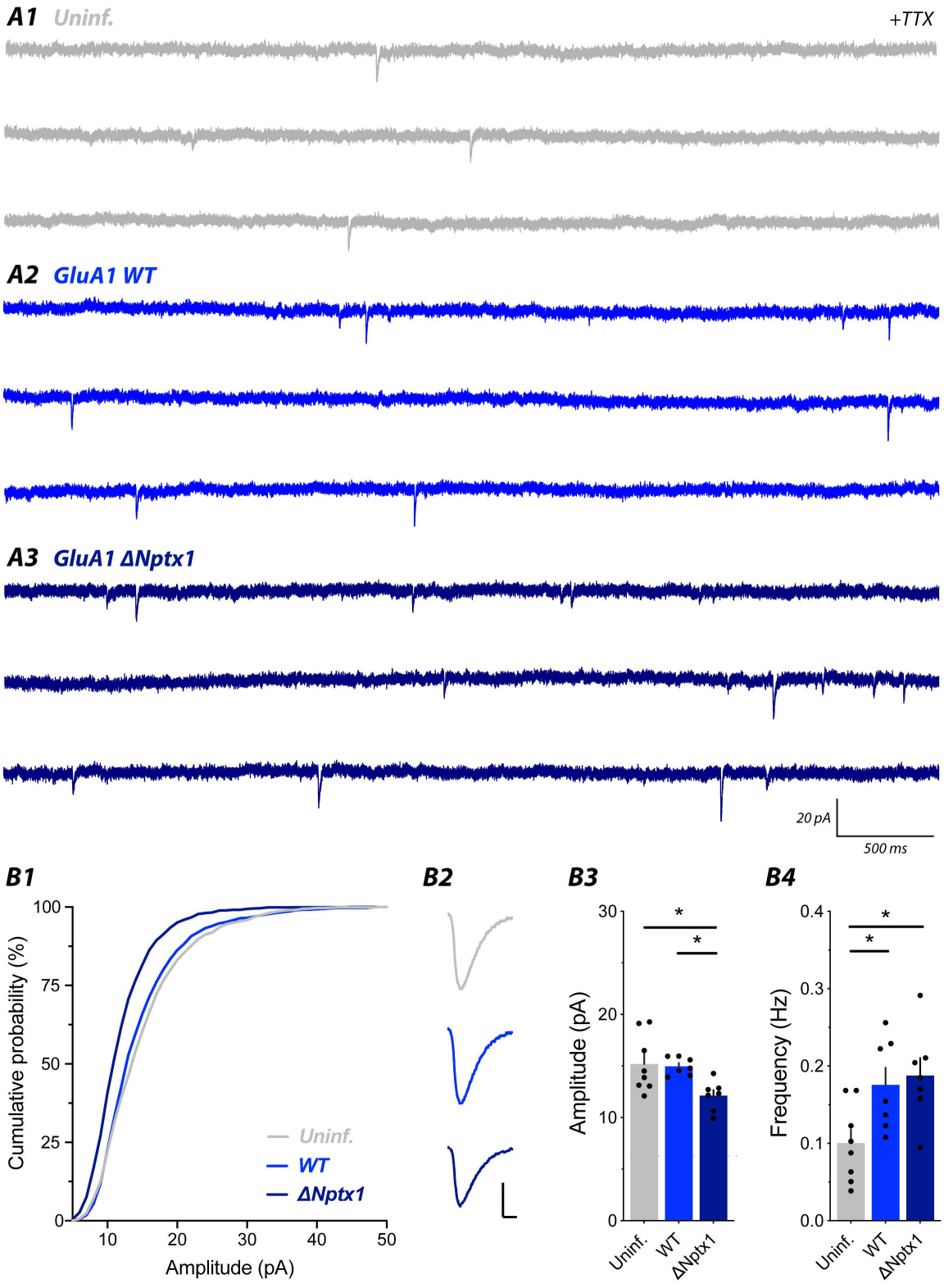

Figure 5.10 *GluA1 ΔNptx1 decreases mEPSC amplitude.*

Figure 5.10 ***GluA1 ΔNptx1 decreases mEPSC amplitude.*** *(**A**) 3 Representative mEPSC traces recorded from (**A1**) Uninf., (**A2**) WT and (**A3**) ΔNptx1 in the presence 1 μM TTX. Example traces for each condition are taken from 2 independent preparations. (**B1**) Cumulative frequency distribution plot of mEPSC amplitude indicates a significant decrease in ΔNptx1 mEPSC amplitude distribution relative to WT (WT = 14.9 ± 0.20 pA, n = 982 events; ΔNptx1 = 12.3 ± 0.11 pA, n = 1487 events; Kolmogorov-Smirnov test, P < 0.001). (**B2**) Average mEPSC traces of Uninf. (grey), WT (blue) and ΔNptx1 (navy) (scale bar = 5 pA; 5 ms). (**B3**) mEPSC amplitude of ΔNptx1 was significantly decreased relative to both Uninf., and WT (Uninf. = 15.2 ± 0.99 pA, n = 8 cells; WT = 15.0 ± 0.36 pA, n = 7 cells; ΔNptx1 = 12.1 ± 0.55 pA, n = 7 cells; n = 2 independent preparations; ANOVA with multiple comparisons, *p < 0.05). (**B4**) mEPSC frequency was unchanged for WT and significantly increased 2-fold for ΔNptx1 relative to Uninf. (Uninf. = 0.10 ± 0.018 Hz, n = 8 cells; WT = 0.18 ± 0.022 Hz, n = 7 cells; ΔNptx1 = 0.19 ± 0.023 Hz, n = 7 cells; n = 2 independent preparations; ANOVA with multiple comparisons, * p < 0.05).*

5.2.5 Exogenous $Nptx1_{PTX}$ application

Throughout this Chapter synaptic recordings have been performed on overexpressed WT and ΔNptx1 AMPARs to examine the functional effect of blocking endogenous Nptx1 binding. To approach this question from a different angle, exogenous Nptx1 PTX domains ($Nptx1_{PTX}$) were purified and applied to organotypic hippocampal slices to interfere with endogenous Nptx1-AMPAR interactions (Figure 5.11). As mentioned above, endogenous Nptx1 forms hexameric assemblies, containing 6 PTX domains, which are thought to cluster AMPARs (Xu et al., 2003), whereas $Nptx1_{PTX}$ lacks the domains involved in oligomerisation. 100 nM $Nptx1_{PTX}$ binds to GluA1-4 NTDs (Chapter 4), similarly to full-length Nptx1 (Figure 5.1A). $Nptx1_{PTX}$ is hypothesised to compete with endogenous Nptx1 for binding sites on the AMPAR NTD. However, with only one PTX domain of the oligomeric hexamer that makes up Nptx1 (Xu et al., 2003), AMPAR clustering by hexameric Nptxs should be prevented (Figure 5.1) and reflected by a change in the AMPAR EPSC.

AMPAR EPSCs were recorded from CA1 pyramidal neurons at a basal stimulation frequency of 0.2 Hz for a duration of 40 mins (Figure 5.11A1). Application of buffer solution had no considerable effect on the amplitude of AMPAR EPSCs over time (Figure 5.11A1/2). Similarly, 100 nM $Nptx1_{PTX}$ application had no significant effect on AMPAR EPSC amplitude (Figure 5.11A1/2). This suggests that $Nptx1_{PTX}$ binding to endogenous AMPAR NTDs has no effect on the strength of AMPAR-mediated synaptic transmission at CA1 synapses. The lack of an observable change in the size of the AMPAR EPSC with $Nptx1_{PTX}$ however, has a number of potential explanations discussed below.

CPTX, a synthetic synaptic organiser containing the $Nptx1_{PTX}$ domain, enhances AMPAR-mediated synaptic transmission at CA1 synapses after 4 hours or 3 days incubation (Suzuki et al., 2020). It is possible therefore, that wash-in of $Nptx1_{PTX}$ over 35 mins is not sufficient time for the protein to penetrate through the slice and enter CA1 synapses. An alternative strategy would be to pre-incubate slices for around 12 hours, as demonstrated with purified GluA1-3 NTDs (Chapter 3). Another possibility is that the functional effect of endogenous Nptx1 may occur at other hippocampal synapses. PL proteomics was performed on entire hippocampal slices in (Chapter 4), including CA1, CA3 and DG hippocampal regions. In these experiments therefore, Nptx1 identification could be from any of these hippocampal synapse types. The strongest endogenous signal for Nptx1 was observed in the hilus of the dentate gyrus (Figure 5.11B3), suggesting that Nptx1 may exert its functional effect at DG-CA3 synapses.

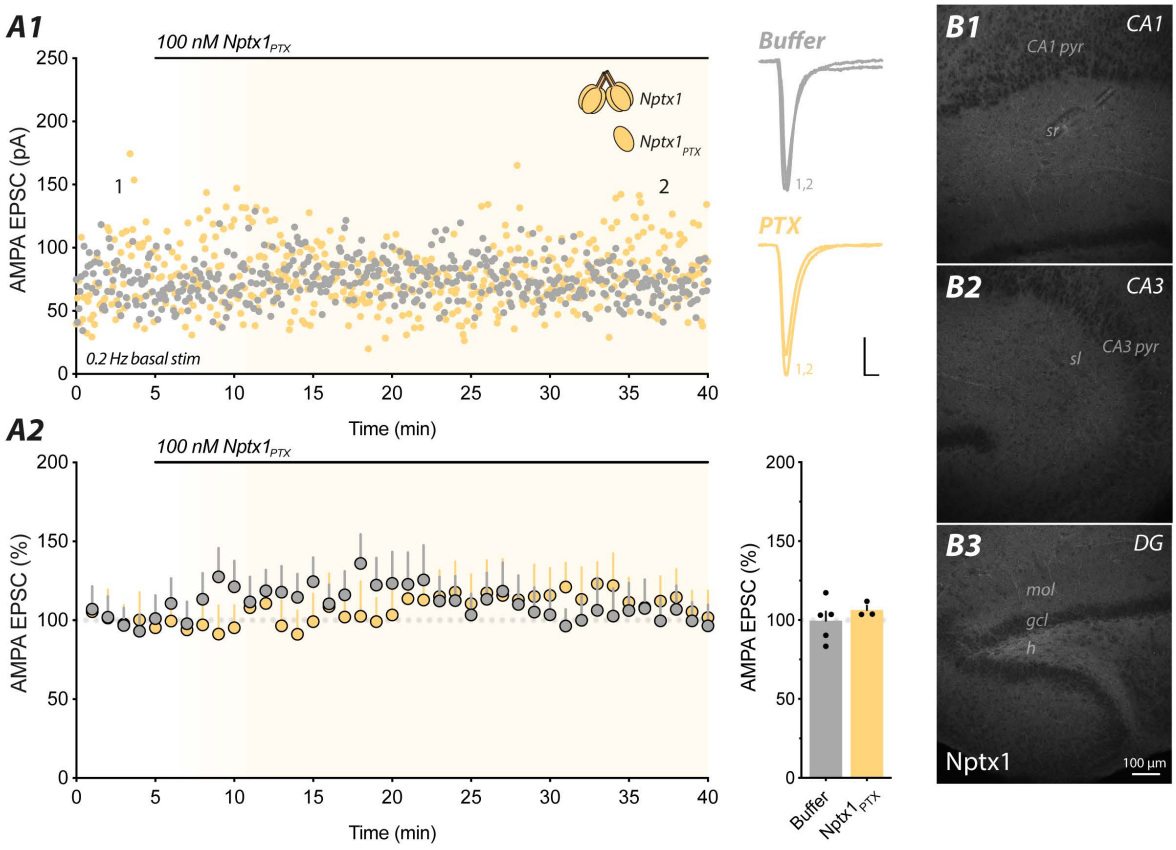

Figure 5.11 ***Nptx1$_{PTX}$ has no effect on AMPAR-mediated transmission at CA1 synapses.*** *(**A1**) Nptx1 cartoon (top) indicates full-length oligomeric hexamer formed in vivo (Xu et al., 2003). Nptx1$_{PTX}$ cartoon (bottom) indicates the Nptx1 PTX domain, lacking the domains involved in protein oligomerisation. AMPAR EPSCs recorded at a basal stimulation frequency of 0.2 Hz indicate no change in amplitude following application of 100 nM Nptx1$_{PTX}$ (kindly provided by Dr Veronica Chang) or buffer control after a 35 mins incubation. (Scale bar: 20 pA; 20 ms). (**A2**) No significant change in AMPAR EPSC amplitude over time. AMPAR EPSC of Nptx1$_{PTX}$ was unchanged relative to buffer control after 35 mins (Buffer = 99.5 ± 5.9 %, n = 4; Nptx1$_{PTX}$ = 106.4 ± 2.7 %, n = 3; unpaired t-test, p = 0.43). (**B**) Immunostaining of endogenous Nptx1 in the (**B1**) CA1, (**B2**) CA3 and (**B3**) dentate gyrus (DG) regions of organotypic hippocampal slices (pepsin-reated), with the strongest signal observed in the hilus (h) of the DG. Lower Nptx1 expression was observed in the stratum radiatum (sr) of the CA1 region, where schaffer collaterals synapse onto CA1 pyramidal neurons recorded in these experiments.*

Future experiments therefore, should aim to deduce the functional effect of Nptx1 at DG-CA3 synapses, where expression appears to be highest. Finally, application of only $Nptx1_{PTX}$ domain will result in a much lower affinity for AMPAR NTDs than that of oligomeric hexamers, due to multivalent avidity (Elegheert et al., 2016). Therefore, it can be expected that Nptx1 PTX domain binding in organotypic slices will have a much lower affinity than that of endogenous Nptx1 interactions. Thus, a much higher concentration than 100 nM will be required to out-compete endogenous Nptx1-induced AMPAR clustering. A concentration of 100 nM $Nptx1_{PTX}$ was used in these experiments as this is the highest concentration achievable with protein purification ($Nptx1_{PTX}$ kindly provided by Dr Veronica Chang).

5.2.6 GluA2Q ΔNptx1 neuronal excitability

In addition to Nptx1-AMPAR NTD interactions, a direct interaction between Nptx1 and Kv7.2 has also been reported (Figueiro-Silva et al., 2015). The authors have shown that Nptx1 and Kv7.2 co-immunoprecipitate in brain lysates and co-localise at presynaptic terminals. This interaction was found to modulate Kv7.2 surface expression and subsequently potassium M-current amplitude. Kv7 potassium channel subunits regulate neuronal excitability, by setting the action potential threshold (Brown and Passmore, 2009). Neuronal excitability is increased in Nptx1 knockdown neurons, suggestive of a negative regulatory role in shaping neuronal excitability. To determine if Nptx1 interactions with Kv7.2 are linked to Nptx1-AMPAR NTD interactions, the neuronal excitability of CA1 pyramidal neurons expressing GluA2Q WT and ΔNptx1 was assessed.

Neuronal excitability was measured by determining the number of action potential spikes in response to a +350 pA current injection (Figure 5.12). Spike number was significantly increased in both WT and ΔNptx1 relative to uninfected cells (Figure 5.12B). Surprisingly, the neuronal excitability of ΔNptx1 was further increased relative to WT (Figure 5.12B). This suggests that occlusion of Nptx1 binding to the GluA2 NTD results in increased action potential firing through an unknown molecular mechanism. Further investigation into the effect of ΔNptx1 on neuronal excitability is required, these experiments could be repeated in the presence of AMPAR antagonists, to remove the contribution of an increased frequency of excitatory synaptic transmission with ΔNptx1 relative to WT receptors (Figure 5.5).

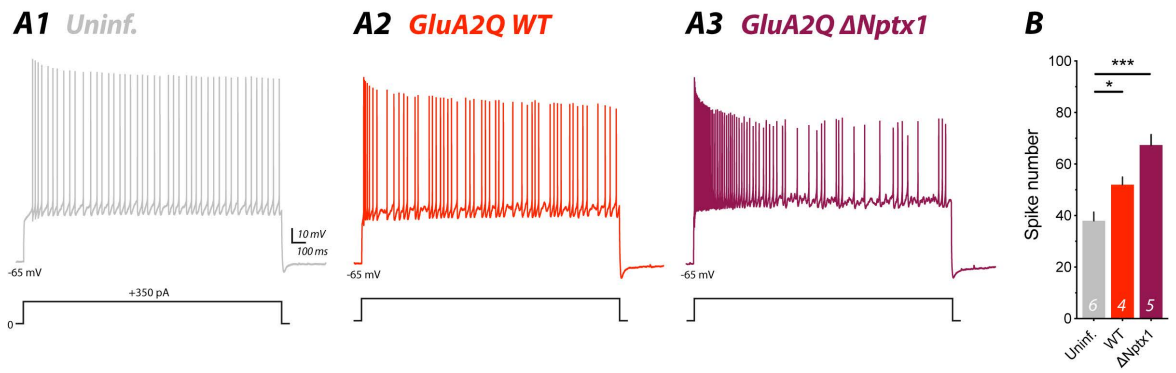

Figure 5.12 ***GluA2Q ΔNptx1 increases neuronal excitability.*** *(**A**) Action potential firing of CA1 pyramidal neurons in response to a +350 pA current injection for (**A1**) Uninf., (**A2**) GluA2Q WT, and (**A3**) GluA2Q ΔNptx1 (scale bar: 10 mV; 100 ms). Resting membrane potentials of Uninf., GluA2Q WT and GluA2Q ΔNptx1 were unchanged, with an average of -65 mV. GluA2Q WT and ΔNptx1 recordings were performed from DPI 5-7 CA1 pyramidal neurons, with Uninf. cells recorded from the same slices. (**B**) GluA2Q WT and ΔNptx1 spike number were significantly increased relative to Uninf. (Uninf. = 38 ± 3.34; n = 6; GluA2Q WT = 52 ± 2.97; n = 4; GluA2Q ΔNptx1 = 67 ± 4.03; n = 5; ANOVA with multiple comparisons, * p < 0.05, *** p < 0.001).*

5.3 Discussion

This chapter aims to resolve the influence of Nptx1-AMPAR NTD interactions on excitatory synaptic transmission. Occlusion of Nptx1 binding to the GluA1/2 NTD has a subunit-specific effect on the efficiency of AMPAR-mediated synaptic transmission. While Nptx1 interactions with the GluA2 NTD appear to negatively regulate, GluA1 NTD interactions appear to positively regulate spontaneous excitatory synaptic transmission.

Nptx1 directly interacts with AMPAR subunits GluA1-4, engaging with the AMPAR NTD at an undisclosed binding site (Figure 5.1). NTD mutants occlude Nptx1 binding (ΔNptx1) and have the same channel gating kinetics as WT receptors (Figure 5.2). AMPARs are expressed selectively in the CA1 region of the hippocampus using AAV microinjection of the GFP-P2A-AMPAR expression vector (Figure 5.3). Endogenous Nptx1 binding to the AMPAR NTD has no effect on the trafficking of exogenous GluA1 (Figure 5.9) or GluA2Q (Figure 5.4) receptors to CA1 synapses, as ΔNptx1 mutants contribute to excitatory synaptic transmission to the same extent as WT receptors. However, when positioned at excitatory synapses, GluA2Q ΔNptx1 significantly increases mEPSC frequency (Figure 5.5), whereas GluA1 significantly reduces mEPSC amplitude (Figure 5.10). These functional effects could be attributed to a number of different mechanisms, namely changes in 1. Glutamate release probability; 2. Spine density; 3. Postsynaptic AMPAR content. Occlusion of Nptx1 binding to the GluA2 NTD appears to have no effect on the probability of glutamate release (Figure 5.6), or spine density (Figure 5.7), leaving the possibility of a change in postsynaptic AMPAR content. The following mechanisms are postulated as possible explanations for an increased GluA2 ΔNptx1 mEPSC frequency: lateral diffusion or endocytosis of receptors (Figure 5.13). Blocking Nptx1 interactions with the GluA1 NTD appears to reduce the number of functional postsynaptic AMPARs, likely through preventing receptor clustering and reducing the efficacy of synaptic transmission. The following mechanism is postulated for a reduced GluA1 ΔNptx1 mEPSC amplitude: postsynaptic receptor clustering (Figure 5.14). Nptx1 regulates excitatory synaptic transmission in a subunit-specific manner through direct interactions with the AMPAR NTD. Hypothetical mechanisms for Nptx1 regulation are discussed below.

Probability of glutamate release

Changes in mEPSC are often accompanied by changes in the presynaptic release machinery, therefore the PPR was used a measure of glutamate release probability. CA1 pyramidal neurons were selectively transduced as to only affect the postsynaptic neuron, so changes in presynaptic activity cannot be attributed to expression in CA3 pyramidal neurons. No significant change in the PPR (Figure 5.6), or CV (Figure 5.4) was detected between GluA2Q WT and ΔNptx1. This suggests that there is no change in the probability of glutamate release with a loss of Nptx1-AMPAR NTD interactions. These experiments were conducted using eEPSCs, relying on action-potential driven vesicular release of glutamate. However, experiments demonstrating a significant change in mEPSC frequency were performed using spontaneous EPSCs. It is possible therefore, that increases in mEPSC frequency (Figure 5.5; Figure 5.10) may be due to changes in the presynaptic release machinery affecting only spontaneous release. As spontaneous and evoked transmission are differentially regulated at excitatory synapses (Ramirez and Kavalali, 2011), Nptx1 binding may selectively affect spontaneous transmission through undetermined mechansims. This can be further investigated by recording asynchronous EPSCs (aEPSCs) in the presence of Sr^{2+}. Where replacing Ca^{2+} with Sr^{2+} in the ACSF results in 'asynchronous release' of glutamate onto postsynaptic AMPARs, a distinct form of glutamate release (Oliet et al., 1996).

Functional synapses

A/N ratio can be used as a proxy for studying changes in the number of functional synapses, where significant changes in the NMDAR EPSC reflect a change in spine density (Letellier et al., 2018), and changes in the A/N ratio reflect a change in the number of silent synapses (Kerchner and Nicoll, 2008). Although no significant changes between GluA2Q WT and ΔNptx1 are observed using this read-out, it remains possible that a subtle change in spine density or morphology may occur, which can be detected using confocal microscopy of dendritic spines filled with cytosolic fluorescent reporter. To further address changes in silent synapses, GluA2Q WT and ΔNptx1 receptors should be studied using knockout and replacement to achieve endogenous AMPAR expression levels. Additionally, the number of silent synapses could be studied by recording aEPSCs in the presence of Sr^{2+} and detecting changes in aEPSC frequency (Chapter 3; Sheng et al., 2015). At this stage, the possibility of Nptx1 increasing the proportion of silent synapses via a negative regulation mechanism cannot be ruled out.

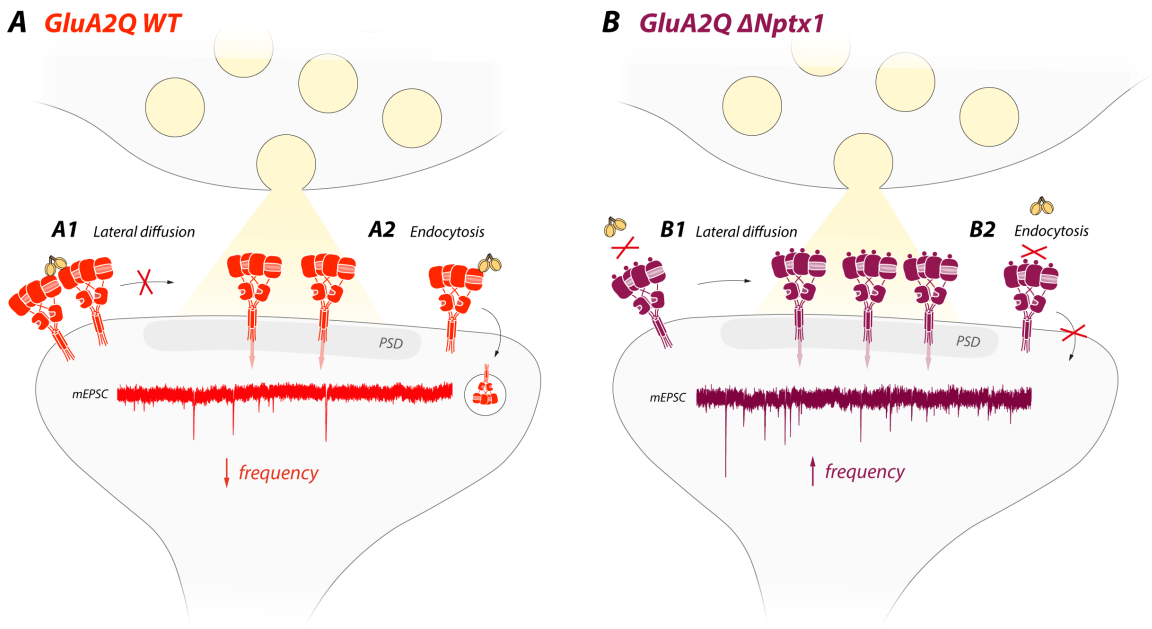

Figure 5.13 ***Nptx1 negatively regulates GluA2-mediated synaptic transmission.*** *(**A**) Hypothetical mechanisms for Nptx1-GluA2 NTD interactions with WT receptors at excitatory synapses. GluA2Q WT receptors bind Nptx1 resulting in a lower frequency of mEPSCs. Proposed mechanisms for negative regulation of synaptic transmission include: (**A1**) reduced lateral diffusion of AMPARs from extra-/peri-synaptic sites into the synapse; or (**A2**) increased AMPAR endocytosis. (**B**) Hypothetical mechanisms for a loss of Nptx1 binding to GluA2Q ΔNptx1 receptors at excitatory synapses. (•) GluA2Q ΔNptx1 mutation occludes Nptx1 binding resulting in a higher frequency of mEPSCs. Proposed mechanisms of increased excitatory synaptic transmission with GluA2Q ΔNptx1 include: (**B1**) increased lateral diffusion into the synapse from peri-/extra-synaptic sites; or (**B2**) decreased AMPAR endocytosis. Ultimately, a high proportion of GluA2Q ΔNptx1 receptors are expected within the postsynaptic density (PSD), resulting in a higher frequency of mEPSC events.*

AMPAR clustering

Nptx1 promotes postsynaptic receptor clustering through direct interactions with the AMPAR NTD (O'Brien et al., 1999; O'Brien et al., 2002; Xu et al., 2003; Sia et al., 2007; Lee et al., 2017). The functional consequence of Nptx1-induced AMPAR clustering however, remains unresolved at CA1 synapses. In this study, AMPAR-mediated synaptic transmission appears to be regulated by Nptx1 in a subunit-specific manner, where GluA2Q negative regulates (Figure 5.5) and GluA1 positively regulates (Figure 5.10) the strength of spontaneous synaptic transmission. This is puzzling, as Nptx1 binding occurs at both GluA1/2 NTDs, however the functional outcome appears to differ. This may be the consequence of differential Nptx1 binding affinity or even other protein interactors docking at the same binding site. Potential AMPAR clustering mechansims of these subunits are discussed below.

AMPARs are incorporated into the synapse via surface diffusion from extra-synaptic sites (Opazo and Choquet, 2011; Penn et al., 2017). Protein interactions with the AMPAR influence receptor mobility, resulting in the insertion, retention or exclusion of receptors from the synapse. Interestingly, synaptic protein SynDIG4 has been shown to establish an 'reserve pool' of extra-synaptic AMPARs (Kirk et al., 2015), fundamental for the expression of long-term potentiation (Granger et al., 2013; Matt et al., 2018). In the context of this study, it is possible that Nptx1 interactions with GluA2Q are responsible for limiting insertion of AMPARs into the synapse, limiting the frequency of mEPSC events (Figure 5.13A1). Blockade of Nptx1 binding with GluA2Q ΔNptx1 therefore, may result in a loss of this regulatory mechanism, culminating in an increased frequency of spontaneous synaptic transmission (Figure 5.13B1).

In contrast to this, Nptx1-GluA1 NTD interactions appear to be crucial for the maintenance of synaptic strength. The reduction in GluA1 ΔNptx1 mEPSC amplitude (Figure 5.10) may be due to a loss of AMPAR clustering within the PSD (Figure 5.14). Similarly, synaptic protein Olfm1 appears to trap AMPARs at the synapses by decreasing receptor lateral diffusion through direct interactions with the AMPAR NTD (Pandya et al., 2018). A loss of Nptx1 binding to GluA1 ΔNptx1 therefore, may also result in 'un-clustering' of receptors and exclusion from the PSD (Figure 5.14B1). To address this hypothesis, FRAP or single-particle tracking experiments could be performed on GluA1/2 WT and ΔNptx1 receptors to assess the mobility of synaptic receptors. Similar experiments have been used to demonstrate a role for the AMPAR (Watson et al., 2017) and NMDAR (Washburn et al., 2020) NTD in trapping receptors at the synapse.

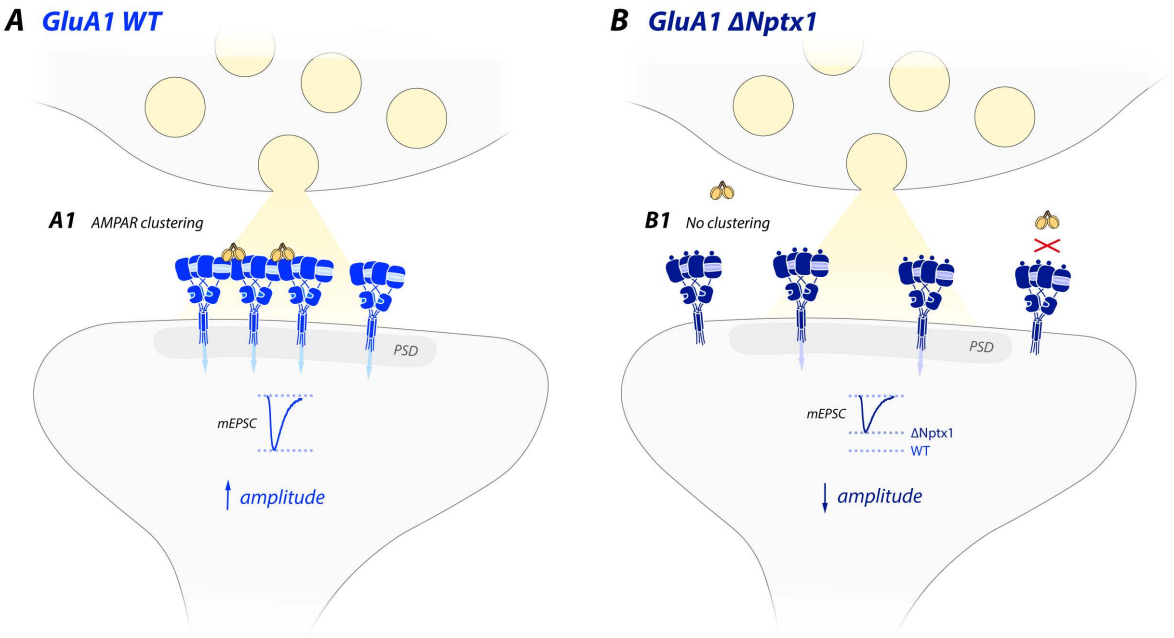

Figure 5.14 ***Nptx1-induced clustering potentiates GluA1-mediated synaptic transmission.*** *(**A**) GluA1 WT receptors are clustered by Nptx1 through direct NTD interactions. (**A1**) Hypothetical mechanism underlying GluA1 WT mEPSC amplitude. A moderate clustering of AMPARs on a nanoscale permits potentiation of the synaptic response (Savtchenko and Rusakov, 2014). Nptx1-induced accumulation of GluA1-containing AMPARs within the postsynaptic density (PSD) enables receptors to respond more effectively to presynaptic glutamate release. As a consequence, mEPSC amplitude is increased. (**B**) GluA1 ΔNptx1 receptors are unable to cluster due to a loss of Nptx1-AMPAR NTD interactions. (•) GluA1 ΔNptx1 mutation occludes Nptx1 binding resulting in a decreased mEPSC amplitude. (**B1**) Hypothetical mechanism responsible for a reduced mEPSC amplitude with GluA1 ΔNptx1. Occlusion of Nptx1 binding results in a disperse arrangement of postsynaptic AMPARs, with some receptors unable to respond to glutamate positioned outside the PSD. This may result in a lower mEPSC amplitude as fewer receptors are positioned within the PSD for effective signal transduction.*

Taken together, it is postulated that GluA2 NTD clustering may manifest as a 'trapping' of receptors at peri-synaptic sites, whereas GluA1 NTD clustering may result in immobilisation of receptors within the PSD, promoting effective signal transduction (Savtchenko and Rusakov, 2014). In line with this evidence, the AMPAR NTD has been shown to exert a subunit-specific effect on excitatory synaptic transmission and plasticity (Watson et al., 2017; Díaz-Alonso et al., 2017; Watson et al., 2020; Jiang et al., 2021). The findings in this study however, should be interpreted with caution, as the ΔNptx1 mutation may also serve as a binding site for other AMPAR NTD interactors. Therefore, subunit-specific effects deduced using ΔNptx1 constructs could be the result of other synaptic proteins engaging in interactions with the AMPAR NTD at the same binding site.

Endocytosis

Another potential postsynaptic mechanism for Nptx1 in excitatory synaptic transmission is GluA2 NTD clustering and endocytosis. For Nptxr, TACE-induced cleavage of the Nptxr PTX domain promotes postsynaptic clustering of AMPARs and subsequent endocytosis during mGluR1/5-dependent long-term depression at hippocampal and cerebellar synapses (Cho et al., 2008). The authors propose that AMPARs are captured by PTX domain interactions with the AMPAR NTD and targeted to sites of endocytosis. The role of Nptx1 in AMPAR endocytosis has not been investigated, but it would be interesting to see if $Nptx1_{PTX}$ binding were able to induce AMPAR internalisation. In this model, occlusion of Nptx1 binding to ΔNptx1 receptors at the synapse may prevent regulated endocytosis of AMPARs, subsequently increasing the frequency of mEPSC events (Figure 5.13B2). Whereas WT receptors, which bind Nptx1, are able to undergo endocytosis and thus the strength of excitatory synaptic transmission can be negatively regulated successfully (Figure 5.13A2). No significant difference in WT and ΔNptx1 synaptic expression is observed using immunostaining of fixed hippocampal neurons and microscopy (Figure 5.8B). To better answer this question of AMPAR endocytosis, a knockout and replacement strategy should be employed with single particle tracking of live AMPARs.

Negative regulation

Several publications point towards a role for Nptx1 in the negative regulation of excitatory synaptic transmission (Figueiro-Silva et al., 2015; Koch and Ullian, 2010; Bjartmar et al., 2006). Considerable lines of evidence in this Chapter support the findings of Figueiro-Silva et al., (2015). GluA2Q ΔNptx1 often mimics the effects observed with Nptx1 knockdown, including: increased mEPSC frequency (Figure 5.5) and increased neuronal excitability (Figure 5.12). It is likely that Nptx1 in turn binds to other synaptic proteins, as is the case for C1ql2/3 (Matsuda

et al., 2016; Straub et al., 2016) and Cbln1/2/4 (Matsuda et al., 2010; Elegheert et al., 2016), which bind iGluR NTDs and presynaptic neurexin simultaneously (Favuzzi et al., 2019). Nptx1 has been shown to interact with presynaptic potassium channel subunit Kv7.2, regulating neuronal excitability (Figueiro-Silva et al., 2015). It would be interesting to confirm this interaction and deduce whether this forms a *trans*-synaptic complex with the AMPAR NTD.

The findings in this study could be explained by the presence of simultaneous interactions between secreted Nptx1, postsynaptic GluA2 NTDs and presynaptic Kv7.2, in a *trans*-synaptic complex. Where occluding Nptx1 binding may result in a loss of Kv7.2 surface expression and increased neuronal excitability. Nptx1-AMPAR NTD interactions may regulate neuronal firing rate (Figure 5.12), through potential simultaneous interactions with presynaptic Kv7.2 (Figueiro-Silva et al., 2015) and the AMPAR NTD in concert. Following confirmation of the direct Nptx1-Kv7.2 interaction, it would be interesting to see if all three components interact simultaneously in a cell-based binding assay or neuronal co-culture system. Interestingly, *trans*-synaptic complex ADAM22-LGI1-ADAM23 requires all components to participate in the complex, otherwise AMPAR function and neuronal excitability is perturbed (Fukata et al., 2021).

Developmental regulation

Studying the functional effect of Nptx1 is made more challenging due to its developmental expression and activity-dependent release (Chang et al., 2010; Schaukowitch et al., 2017; Dörrbaum et al., 2020). Nptx1 expression in organotypic hippocampal slices (Figure 5.11B) appears to be lower than that of adult acute slices, where the more well-defined layers of the adult hippocampus show strong expression of Nptx1 (Cho et al., 2008; Apóstolo et al., 2020). Physiologically, this expression profile results in developmental regulation of silent synapse conversion at RGC synapses (Bjartmar et al., 2006; Koch and Ullian, 2010). These differences may account for discrepancies in functional effects uncovered at different synapse-types and developmental age. Nptx1 binding affinity is highest for GluA4 across the AMPAR NTD subunits; future studies may aim to determine the effect of a loss of Nptx1-GluA4 NTD binding, where this higher affinity may translate into a more profound functional effect. This interaction is particularly interesting in the context of neuronal development, as GluA4-containing AMPARs contribute to synaptic transmission during early-postnatal stages of hippocampal development (Zhu et al., 2000). Although the physiology of the Nptxs has been

well-described for excitatory synapses onto PV-INs (Chang et al., 2010; Gu et al., 2013; Pelkey et al., 2015), this cell-type makes up only ~10% of hippocampal neurons. It is unlikely therefore, that this is the only role of Nptxs. Indeed, Nptx1 and Nptxr are detected with high levels of AMPAR NTD-enrichment in PL proteomics from excitatory synapses onto principal neurons in the hippocampus (Chapter 4).

This chapter uses organotypic hippocampal slices to permit modification of the CA1 pyramidal neurons AMPAR content using AAV transduction. Future studies however, should aim to study later developmental stages when Nptx1 expression is increased (Cho et al., 2008; Apóstolo et al., 2020), using P0/1 stereotactic injection of AAV particles in in vivo (Ho et al., 2020) followed by acute brain slice preparation from adult mice. Furthermore, the effect of occluding Nptx1 binding with the ΔNptx1 mutation should be studied on endogenous AMPARs, using CRISPR/Cas9 modification of post-mitotic neurons (Nishiyama et al., 2017), opposed to overexpression used throughout this study.

This chapter provides novel insights into the subunit-specific role of Nptx1-AMPAR NTD interactions on CA1 synaptic transmission. Interestingly, Nptx1 binding appears to selectively affect spontaneous, but not evoked transmission. Future studies should aim to deduce the mechanism of Nptx1 modulation on spontaneous AMPAR-mediated synaptic transmission.

Chapter 6

Conclusions

This investigation has identified synaptic cleft proteins that interact with the AMPAR NTD and characterised their functional importance. The NTD projects mid-way into the synaptic cleft, exposing it to a protein-rich environment. This large extracellular domain acts as a docking platform for synaptic proteins, hypothetically modulating receptor sub-synaptic positioning and function. This study identified Nptx1 as a direct AMPAR NTD interactor involved in modulating excitatory synaptic transmission at hippocampal CA1 synapses.

AMPARs concentrate within clusters in the postsynaptic density, potentially *trans*-synaptically aligning with presynaptic glutamate release sites. Sub-synaptic arrangement of receptors on a nanometer scale is thought to enhance synaptic efficacy. The AMPAR NTD plays a role in the maintenance of synaptic transmission and plasticity at hippocampal synapses. To determine the physiological role of the NTD in sub-synaptic positioning, glutamate spillover was induced onto potentially 'mis-aligned' peri-synaptic receptors. These experiments provided the first functional assessment of sub-synaptic AMPAR positioning. Increasing the spatio-temporal spillover of glutamate from the synaptic cleft did not however, result in the activation of additional 'mis-aligned' NTD-deleted AMPARs, suggesting no detectable change in the nanometer arrangement of WT and ΔNTD receptors.

A wealth of AMPAR-interacting proteins have been identified using classical affinity-purification mass spectrometry. However, this technique does not permit capture of weak and transient AMPAR-interacting proteins. Therefore, proximity-labelling proteomics was established in organotypic slice culture, allowing capture of synaptic proteins within the vicinity of AMPAR-fusion constructs. The efficiency of 4 different labelling tags were assessed, derived from biotin ligase (BioID2, MiniTurbo and TurboID) and ascorbate peroxidase (APEX2) enzymes. Proximity-labelling proteomics enabled identification of novel candidate interactors

from the synaptic cleft, in addition to known constituents of the AMPAR proteome. Candidate proteins were subsequently screened in a cell-based binding assay, capable of detecting known iGluR NTD interactors Cbln1, C1ql2 and C1ql3. Over 40 synaptic proteins were screened in the binding assay, resolving Nptx1 as a direct GluA1-4 NTD interactor.

Nptx1 binds directly to the AMPAR at an undisclosed site within the NTD. A 2 amino acid mutation within the NTD, termed ΔNptx1, completely abolished Nptx1 interactions, permitting study of the functional consequence of Nptx1 binding. ΔNptx1 receptors had the same channel gating kinetics as WT receptors, however, when incorporated into synaptic sites, occlusion of Nptx1 binding was found to affect AMPAR-mediated synaptic transmission in a subunit-specific manner. Nptx1 interactions with the GluA1 and GluA2 NTD appear to both negatively and positively regulate the strength of synaptic transmission respectively. This study determined the role of Nptx1 in shaping excitatory synaptic transmission through direct interactions with a specific site on the AMPAR NTD.

It has been postulated that N-cadherin, Olfm1 and Np65 all engage in protein interactions with the AMPAR NTD. However, direct interactions were not observed using various binding assays, raising questions over the reproducibility of reported NTD interactors. Using the comprehensive proteomic lists determined in this study, future investigations should focus on determining protein interactions with different sites on the AMPAR or explore the synaptic function of undescribed cleft proteins.

AMPAR-interacting proteins modulate numerous aspects of receptor function, from early biogenesis to synaptic function. The AMPAR NTD is thought to engage in subunit-specific interactions with proteins in the synaptic cleft, regulating functional output from the postsynaptic cell. Understanding how synaptic proteins bind to the AMPAR NTD and the physiological consequence of these interactions is crucial for understanding the mechanisms of synaptic transmission and plasticity. Ultimately, an appreciation of these molecular processes will improve our knowledge of how information is transferred and stored in the brain.

Bibliography

Allen, N.J., Bennett, M.L., Foo, L.C., Wang, G.X., Chakraborty, C., Smith, S.J., Barres, B.A., 2012. Astrocyte glypicans 4 and 6 promote formation of excitatory synapses via GluA1 AMPA receptors. *Nature*, 486:410–414.

Anderson, C.T., Radford, R.J., Zastrow, M.L., Zhang, D.Y., Apfel, U.P., Lippard, S.J., Tzounopoulos, T., 2015. Modulation of extrasynaptic NMDA receptors by synaptic and tonic zinc. *Proceedings of the National Academy of Sciences of the United States of America*, 112:E2705–E2714.

Aoto, J., Földy, C., Ilcus, S.M.C., Tabuchi, K., Südhof, T.C., 2015. Distinct circuit-dependent functions of presynaptic neurexin-3 at GABAergic and glutamatergic synapses. *Nature Neuroscience*, 18:997–1007.

Aoto, J., Martinelli, D.C., Malenka, R.C., Tabuchi, K., Südhof, T.C., 2013. Presynaptic neurexin-3 alternative splicing trans-synaptically controls postsynaptic AMPA receptor trafficking. *Cell*, 154:75.

Apóstolo, N., Smukowski, S.N., Vanderlinden, J., Condomitti, G., Rybakin, V., ten Bos, J., Trobiani, L., Portegies, S., Vennekens, K.M., Gounko, N. V., Comoletti, D., Wierda, K.D., Savas, J.N., de Wit, J., 2020. Synapse type-specific proteomic dissection identifies IgSF8 as a hippocampal CA3 microcircuit organizer. *Nature Communications*, 11:5171.

Araki, Y., Lin, D.T., Huganir, R.L., 2010. Plasma membrane insertion of the AMPA receptor GluA2 subunit is regulated by NSF binding and Q/R editing of the ion pore. *Proceedings of the National Academy of Sciences of the United States of America*, 107:11080–11085.

Aricescu, A.R., Lu, W., Jones, E.Y., 2006. A time- and cost-efficient system for high-level protein production in mammalian cells. *Acta Crystallographica Section D: Biological Crystallography*, 62:1243–1250.

Armbruster, M., Hanson, E., Dulla, C.G., 2016. Glutamate clearance is locally modulated by presynaptic neuronal activity in the cerebral cortex. *Journal of Neuroscience*, 36:10404–10415.

Arnth-Jensen, N., Jabaudon, D., Scanziani, M., 2002. Cooperation between independent hippocampal synapses is controlled by glutamate uptake. *Nature Neuroscience*, 5:325–331.

Asztely, F., Erdemli, G., Kullmann, D.M., 1997. Extrasynaptic glutamate spillover in the hippocampus: Dependence on temperature and the role of active glutamate uptake. *Neuron*, 18:281–293.

Ayalon, G., Segev, E., Elgavish, S., Stern-Bach, Y., 2005. Two regions in the N-terminal domain of ionotropic glutamate receptor 3 form the subunit oligomerization interfaces that control subtype-specific receptor assembly. *Journal of Biological Chemistry*, 280:15053–15060.

Balik, A., Penn, A.C., Nemoda, Z., Greger, I.H., 2013. Activity-regulated RNA editing in select neuronal subfields in hippocampus. *Nucleic Acids Research*, 41:1124–1134.

Balmer, T.S., Borges-Merjane, C., Trussell, L.O., 2021. Incomplete removal of extracellular glutamate controls synaptic transmission and integration at a cerebellar synapse. *eLife*, 10:e63819.

Bannerman, D.M., Good, M.A., Butcher, S.P., Morris, R.G.M., 1995. Distinct components of spatial learning revealed by prior training and NMDA receptor blockade. *Nature*, 378:182–186.

Barria, A., Malinow, R., 2005. NMDA receptor subunit composition controls synaptic plasticity by regulating binding to CaMKII. *Neuron*, 48:289–301.

Beattie, E.C., Carroll, R.C., Yu, X., Morishita, W., Yasuda, H., Von Zastrow, M., Malenka, R.C., 2000. Regulation of AMPA receptor endocytosis by a signaling mechanism shared with LTD. *Nature Neuroscience*, 3:1291–1300.

Beaudoin, G.M.J., Lee, S.H., Singh, D., Yuan, Y., Ng, Y.G., Reichardt, L.F., Arikkath, J., 2012. Culturing pyramidal neurons from the early postnatal mouse hippocampus and cortex. *Nature Protocols*, 7:1741–1754.

Bedoukian, M.A., Weeks, A.M., Partin, K.M., 2006. Different domains of the AMPA receptor direct stargazin-mediated trafficking and stargazin-mediated modulation of kinetics. *Journal of Biological Chemistry*, 281:23908–23921.

Bekkers, J.M., Stevens, C.F., 1989. NMDA and non-NMDA receptors are co-localized at individual excitatory synapses in cultured rat hippocampus. *Nature*, 341:230–233.

Bhouri, M., Morishita, W., Temkin, P., Goswami, D., Kawabe, H., Brose, N., Südhof, T.C., Craig, A.M., Siddiqui, T.J., Malenka, R., 2018. Deletion of LRRTM1 and LRRTM2 in adult mice impairs basal AMPA receptor transmission and LTP in hippocampal CA1 pyramidal neurons. *Proceedings of the National Academy of Sciences of the United States of America*, 115:E5382–E5389.

Biederer, T., Kaeser, P.S., Blanpied, T.A., 2017. Transcellular Nanoalignment of Synaptic Function. *Neuron*, 96:680–696.

Biederer, T., Scheiffele, P., 2007. Mixed-culture assays for analyzing neuronal synapse formation. *Nature Protocols*, 2:670–676.

Biou, V., Bhattacharyya, S., Malenka, R.C., 2008. Endocytosis and recycling of AMPA receptors lacking GluR2/3. *Proceedings of the National Academy of Sciences of the United States of America*, 105:1038–1043.

Bjartmar, L., Huberman, A.D., Ullian, E.M., Rentería, R.C., Liu, X., Xu, W., Prezioso, J., Susman, M.W., Stellwagen, D., Stokes, C.C., Cho, R., Worley, P., Malenka, R.C., Ball, S., Peachey, N.S., Copenhagen, D., Chapman, B., Nakamoto, M., Barres, B.A., Perin, M.S., 2006. Neuronal pentraxins mediate synaptic refinement in the developing visual system. *The Journal Neuroscience*, 26:6269–6281.

Bliss, T.V.P. & Collingridge, G.L., 1993. A synaptic model of memory: LTP in the hippocampus. *Nature*, 361:31–39.

Bliss, T.V.P., T, L., 1973. Long-lasting potentiation of synaptic transmission in the dentate area of the unanaesthetized rabbit following stimulation of the perforant path. *The Journal of Physiology*, 232:331–356.

Boillot, M., Lee, C.Y., Allene, C., Leguern, E., Baulac, S., Rouach, N., 2016. LGI1 acts presynaptically to regulate excitatory synaptic transmission during early postnatal development. *Scientific Reports*, 6:21769.

Boles, N.C., Hirsch, S.E., Le, S., Corneo, B., Najm, F., Minotti, A.P., Wang, Q., Lotz, S., Tesar, P.J., Fasano, C.A., 2014. NPTX1 Regulates Neural Lineage Specification from Human Pluripotent Stem Cells. *Cell Reports*, 6:724–736.

Boudkkazi, S., Brechet, A., Schwenk, J., Fakler, B., 2014. Cornichon2 Dictates the Time Course of Excitatory Transmission at Individual Hippocampal Synapses. *Neuron*, 82:848–858.

Bowie, D., Mayer, M.L., 1995. Inward rectification of both AMPA and kainate subtype glutamate receptors generated by polyamine-mediated ion channel block. *Neuron*, 15:453–462.

Branon, T.C., Bosch, J.A., Sanchez, A.D., Udeshi, N.D., Svinkina, T., Carr, S.A., Feldman, J.L., Perrimon, N., Ting, A.Y., 2018. Efficient proximity labeling in living cells and organisms with TurboID. *Nature Biotechnology*, 36:880–898.

Brechet, A., Buchert, R., Schwenk, J., Boudkkazi, S., Zolles, G., Siquier-Pernet, K., Schaber, I., Bildl, W., Saadi, A., Bole-Feysot, C., Nitschke, P., Reis, A., Sticht, H., Al-Sanna'a, N., Rolfs, A., Kulik, A., Schulte, U., Colleaux, L., Abou Jamra, R., Fakler, B., 2017. AMPA-receptor specific biogenesis complexes control synaptic transmission and intellectual ability. *Nature Communications*, 8:15910.

Brown, D.A., Passmore, G.M., 2009. Neural KCNQ (Kv7) channels. *British Journal of Pharmacology*, 156:1185–1195.

Burada, A.P., Vinnakota, R., Kumar, J., 2020. Cryo-EM structures of the ionotropic glutamate receptor GluD1 reveal a non-swapped architecture. *Nature Structural and Molecular Biology*, 27:84–91.

Bushell, K.M., Söllner, C., Schuster-Boeckler, B., Bateman, A., Wright, G.J., 2008. Large-scale screening for novel low-affinity extracellular protein interactions. *Genome Research*, 18:622–630.

Cai, H., Reed, R.R., 1999. Cloning and characterization of neuropilin-1-interacting protein: A PSD-95/Dlg/ZO-1 domain-containing protein that interacts with the cytoplasmic domain of neuropilin-1. *Journal of Neuroscience*, 19:6519–6527.

Cais, O., Herguedas, B., Krol, K., Cull-Candy, S.G., Farrant, M., Greger, I.H., 2014. Mapping the interaction sites between AMPA receptors and TARPs reveals a role for the receptor N-terminal domain in channel gating. *Cell Reports*, 9:728–740.

Carter, A.G., Regehr, W.G., 2000. Prolonged synaptic currents and glutamate spillover at the parallel fiber to stellate cell synapse. *Journal of Neuroscience*, 20:4423–4434.

Castillo, P.E., Malenka, R.C., Nicoll, R.A., 1997. Kainate receptors mediate a slow postsynaptic current in hippocampal CA3 neurons. *Nature*, 388:182–186.

Chabrol, E., Navarro, V., Provenzano, G., Cohen, I., Dinocourt, C., Rivaud-Péchoux, S., Fricker, D., Baulac, M., Miles, R., Leguern, E., Baulac, S., 2010. Electroclinical characterization of epileptic seizures in leucine-rich, glioma-inactivated 1-deficient mice. *Brain*, 133:2749–2762.

Chamma, I., Letellier, M., Butler, C., Tessier, B., Lim, K.H., Gauthereau, I., Choquet, D., Sibarita, J.B., Park, S., Sainlos, M., Thoumine, O., 2016. Mapping the dynamics and nanoscale organization of synaptic adhesion proteins using monomeric streptavidin. *Nature Communications*, 7:10773.

Chan, K.Y., Jang, M.J., Yoo, B.B., Greenbaum, A., Ravi, N., Wu, W.L., Sánchez-Guardado, L., Lois, C., Mazmanian, S.K., Deverman, B.E., Gradinaru, V., 2017. Engineered AAVs for efficient noninvasive gene delivery to the central and peripheral nervous systems. *Nature Neuroscience*, 20:1172–1179.

Chang, M.C., Park, J.M., Pelkey, K.A., Grabenstatter, H.L., Xu, D., Linden, D.J., Sutula, T.P., McBain, C.J., Worley, P.F., 2010. Narp regulates homeostatic scaling of excitatory synapses on parvalbumin-expressing interneurons. Nature Neuroscience, 13:1090–1097.

Chapman-Smith, A., Cronan, J.E., 1999. In vivo enzymatic protein biotinylation. Biomolecular Engineering, 16:119–125.

Chen, L., Chetkovich, D.M., Petralia, R.S., Sweeney, N.T., Kawasaki, Y., Wenthold, R.J., Bredt, D.S., Nicoll, R.A., 2000. Stargazin regulates synaptic targeting of AMPA receptors by two distinct mechanisms. *Nature*, 408:936–943.

Chen, S., Diamond, J.S., 2002. Synaptically released glutamate activates extrasynaptic NMDA receptors on cells in the ganglion cell layer of rat retina. *Journal of Neuroscience*, 22:2165–2173.

Cho, R.W., Park, J.M., Wolff, S.B.E., Xu, D., Hopf, C., Kim, J.A., Reddy, R.C., Petralia, R.S., Perin, M.S., Linden, D.J., Worley, P.F., 2008. mGluR1/5-Dependent Long-Term Depression Requires the Regulated Ectodomain Cleavage of Neuronal Pentraxin NPR by TACE. *Neuron*, 57:858–871.

Choi-Rhee, E., Schulman, H., Cronan, J.E., 2008. Promiscuous protein biotinylation by Escherichia coli biotin protein ligase. *Protein Science*, 13:3043–3050.

Choi, J.H., Yu, N.K., Baek, G.C., Bakes, J., Seo, D., Nam, H.J., Baek, S.H., Lim, C.S., Lee, Y.S., Kaang, B.K., 2014. Optimization of AAV expression cassettes to improve packaging capacity and transgene expression in neurons. *Molecular Brain*, 7:17.

Christie, J.M., Jahr, C.E., 2006. Multivesicular release at Schaffer collateral-CA1 hippocampal synapses. *Journal of Neuroscience*, 26:210–216.

Cijsouw, T., Ramsey, A.M., Lam, T.K.T., Carbone, B.E., Blanpied, T.A., Biederer, T., 2018. Mapping the proteome of the synaptic cleft through proximity labeling reveals new cleft proteins. *Proteomes*, 6:48.

Citri, A., Bhattacharyya, S., Ma, C., Morishita, W., Fang, S., Rizo, J., Malenka, R.C., 2010. Calcium binding to PICK1 is essential for the intracellular retention of AMPA receptors underlying long-term depression. *Journal of Neuroscience*, 30:16437–16452.

Clark, B.A., Cull-Candy, S.G., 2002. Activity-Dependent Recruitment of Extrasynaptic NMDA Receptor Activation at an AMPA Receptor-only Synapse. *Journal of Neuroscience*, 22:4428–4436.

Coleman, S.K., Möykkynen, T., Cai, C., Von Ossowski, L., Kuismanen, E., Korpi, E.R., Keinänen, K., 2006. Isoform-specific early trafficking of AMPA receptor flip and flop variants. *Journal of Neuroscience*, 26:11220–11229.

Collingridge, G.L., Kehl, S.J., McLennan, H., 1983. Excitatory amino acids in synaptic transmission in the Schaffer collateral-commissural pathway of the rat hippocampus. *The Journal of Physiology*, 334:33–46.

Collingridge, G.L., Lester, R.A.J., 1989. Excitatory amino acid receptors in the vertebrate central nervous system. *Pharmacological Reviews*, 41:143–210.

Contractor, A., Mulle, C., Swanson, G.T., 2011. Kainate receptors coming of age: Milestones of two decades of research. *Trends in Neurosciences*, 34:154–163.

Coombs, I.D., Soto, D., Zonouzi, M., Renzi, M., Shelley, C., Farrant, M., Cull-Candy, S.G., 2012. Cornichons modify channel properties of recombinant and glial AMPA receptors. *Journal of Neuroscience*, 32:9796–9804.

Copits, B.A., Robbins, J.S., Frausto, S., Swanson, G.T., 2011. Synaptic targeting and functional modulation of GluK1 kainate receptors by the auxiliary neuropilin and tolloid-like (NETO) Proteins. *Journal of Neuroscience*, 31:7334–7340.

Cronan, J.E., 2005. Targeted and proximity-dependent promiscuous protein biotinylation by a mutant Escherichia coli biotin protein ligase. *Journal of Nutritional Biochemistry*, 16:416–418.

Cummings, D.M., Benway, T.A., Ho, H., Tedoldi, A., Fernandes Freitas, M.M., Shahab, L., Murray, C.E., Richard-Loendt, A., Brandner, S., Lashley, T., Salih, D.A., Edwards, F.A., 2017. Neuronal and Peripheral Pentraxins Modify Glutamate Release and may Interact in Blood-Brain Barrier Failure. *Cerebral Cortex*, 27:3437–3448.

Dalva, M.B., Takasu, M.A., Lin, M.Z., Shamah, S.M., Hu, L., Gale, N.W., Greenberg, M.E., 2000. EphB receptors interact with NMDA receptors and regulate excitatory synapse formation. *Cell*, 103:945–956.

de Wit, J., O'Sullivan, M.L., Savas, J.N., Condomitti, G., Caccese, M.C., Vennekens, K.M., Yates, J.R., Ghosh, A., 2013. Unbiased discovery of Glypican as a receptor for LRRTM4 in regulating excitatory synapse development. *Neuron*, 79:696–711.

de Wit, J., Sylwestrak, E., O'Sullivan, M.L., Otto, S., Tiglio, K., Savas, J.N., Yates, J.R., Comoletti, D., Taylor, P., Ghosh, A., 2009. LRRTM2 Interacts with Neurexin1 and Regulates Excitatory Synapse Formation. *Neuron*, 64:799–806.

Deverman, B.E., Pravdo, P.L., Simpson, B.P., Kumar, S.R., Chan, K.Y., Banerjee, A., Wu, W.L., Yang, B., Huber, N., Pasca, S.P., Gradinaru, V., 2016. Cre-dependent selection yields AAV variants for widespread gene transfer to the adult brain. *Nature Biotechnology*, 34:204–209.

Diamond, J.S., 2001. Neuronal glutamate transporters limit activation of NMDA receptors by neurotransmitter spillover on CA1 pyramidal cells. *Journal of Neuroscience*, 21:8328–8338.

Díaz-Alonso, J., Morishita, W., Incontro, S., Simms, J., Holtzman, J., Gill, M., Mucke, L., Malenka, R.C., Nicoll, R.A., 2020. Long-term potentiation is independent of the C-tail of the GluA1 AMPA receptor subunit. *eLife*, 9:e58042.

Díaz-Alonso, J., Sun, Y.J., Granger, A.J., Levy, J.M., Blankenship, S.M., Nicoll, R.A., 2017. Subunit-specific role for the amino-terminal domain of AMPA receptors in synaptic targeting. *Proceedings of the National Academy of Sciences of the United States of America*, 114:7136–7141.

Diering, G.H., Heo, S., Hussain, N.K., Liu, B., Huganir, R.L., 2016. Extensive phosphorylation of AMPA receptors in neurons. *Proceedings of the National Academy of Sciences of the United States of America*, 113:E4920–E4927.

Diering, G.H., Huganir, R.L., 2018. The AMPA Receptor Code of Synaptic Plasticity. *Neuron*, 100:314–329.

DiGregorio, D.A., Nusser, Z., Silver, R.A., 2002. Spillover of glutamate onto synaptic AMPA receptors enhances fast transmission at a cerebellar synapse. *Neuron*, 35:521–533.

Dobrunz, L.E., Stevens, C.F., 1997. Heterogeneity of release probability, facilitation, and depletion at central synapses. *Neuron*, 18:995–1008.

Dodds, D.C., Omeis, I.A., Cushman, S.J., Helms, J.A., Perin, M.S., 1997. Neuronal pentraxin receptor, a novel putative integral membrane pentraxin that interacts with neuronal pentraxin 1 and 2 and taipoxin-associated calcium-binding protein 49. *Journal of Biological Chemistry*, 272:21488–21494.

Dohrke, J.N., Watson, J.F., Birchall, K., Greger, I.H., 2020. Characterizing the binding and function of TARP g8-selective AMPA receptor modulators. *Journal of Biological Chemistry*, 295:14565–14577.

Dolphin, A.C., 2018. Voltage-gated calcium channel α2δ subunits: an assessment of proposed novel roles. *F1000Research*, 7:1830.

Dong, H., O'Brien, R.J., Fung, E.T., Lanahant, A.A., Worley, P.F., Huganir, R.L., 1997. GRIP: a synaptic PDZ domain- containing protein that interacts with AMPA receptors. *Nature*, 386:279–284.

Dörrbaum, A.R., Alvarez-Castelao, B., Nassim-Assir, B., Langer, J.D., Schuman, E.M., 2020. Proteome dynamics during homeostatic scaling in cultured neurons. *eLife*, 9:e52939.

Dutta, A., Shrivastava, I.H., Sukumaran, M., Greger, I.H., Bahar, I., 2012. Comparative dynamics of NMDA- and AMPA-glutamate receptor n-terminal domains. *Structure*, 20:1838–1849.

Dzubay, J.A., Jahr, C.E., 1999. The concentration of synaptically released glutamate outside of the climbing fiber-Purkinje cell synaptic cleft. *Journal of Neuroscience*, 19:5265–5274.

Ehrengruber, M.U., Lundstrom, K., Schweitzer, C., Heuss, C., Schlesinger, S., Gähwiler, B.H., 1999. Recombinant Semliki Forest virus and Sindbis virus efficiently infect neurons in hippocampal slice cultures. *Proceedings of the National Academy of Sciences of the United States of America*, 96:7041–7046.

Elegheert, J., Kakegawa, W., Clay, J.E., Shanks, N.F., Behiels, E., Matsuda, K., Kohda, K., Miura, E., Rossmann, M., Mitakidis, N., Motohashi, J., Chang, V.T., Siebold, C., Greger, I.H., Nakagawa, T., Yuzaki, M., Aricescu, A.R., 2016. Structural basis for integration of GluD receptors within synaptic organizer complexes. *Science*, 353:295–300.

Empson, R.M., Buckby, L.E., Kraus, M., Bates, K.J., Crompton, M.R., Gundelfinger, E.D., Beesley, P.W., 2006. The cell adhesion molecule neuroplastin-65 inhibits hippocampal long-term potentiation via a mitogen-activated protein kinase p38-dependent reduction in surface expression of GluR1-containing glutamate receptors. *Journal of Neurochemistry*, 99:850–860.

Erlenhardt, N., Yu, H., Abiraman, K., Yamasaki, T., Wadiche, J.I., Tomita, S., Bredt, D.S., 2016. Porcupine Controls Hippocampal AMPAR Levels, Composition, and Synaptic Transmission. *Cell Reports*, 14:782–794.

Fadó, R., Soto, D., Miñano-Molina, A.J., Pozo, M., Carrasco, P., Yefimenko, N., Rodríguez-Álvarez, J., Casals, N., 2015. Novel regulation of the synthesis of α-Amino-3-hydroxy-5-methyl-4-isoxazolepropionic Acid (ampa) receptor subunit glua1 by carnitine palmitoyltransferase 1C (CPT1C) in the Hippocampus. *Journal of Biological Chemistry*, 290:25548–25560.

Farhy-Tselnicker, I., van Casteren, A.C.M., Lee, A., Chang, V.T., Aricescu, A.R., Allen, N.J., 2017. Astrocyte-Secreted Glypican 4 Regulates Release of Neuronal Pentraxin 1 from Axons to Induce Functional Synapse Formation. *Neuron*, 96:428-445.e13.

Farrow, P., Khodosevich, K., Sapir, Y., Schulmann, A., Aslam, M., Stern-Bach, Y., Monyer, H., von Engelhardt, J., 2015. Auxiliary subunits of the CKAMP family differentially modulate AMPA receptor properties. *eLife*, 4:e09693.

Favuzzi, E., Deogracias, R., Marques-Smith, A., Maeso, P., Jezequel, J., Exposito-Alonso, D., Balia, M., Kroon, T., Hinojosa, A.J., Maraver, E.F., Rico, B., 2019. Distinct molecular programs regulate synapse specificity in cortical inhibitory circuits. *Science*, 363:413–417.

Figueiro-Silva, J., Gruart, A., Clayton, K.B., Podlesniy, P., Abad, M.A., Gasull, X., Delgado-García, J.M., Trullas, R., 2015. Neuronal pentraxin 1 negatively regulates excitatory synapse density and synaptic plasticity. *Journal of Neuroscience*, 35:5504–5521.

Fossati, M., Assendorp, N., Gemin, O., Colasse, S., Dingli, F., Arras, G., Loew, D., Charrier, C., 2019. Trans-Synaptic Signaling through the Glutamate Receptor Delta-1 Mediates Inhibitory Synapse Formation in Cortical Pyramidal Neurons. *Neuron*, 104:1081-1094.e7.

Franks, K.M., Stevens, C.F., Sejnowski, T.J., 2003. Independent Sources of Quantal Variability at Single Glutamatergic Synapses. *Journal of Neuroscience*, 23:3186–3195.

Fukata, Y., Adesnik, H., Iwanaga, T., Bredt, D.S., Nicoll, R.A., Fukata, M., 2006. Epilepsy-Related Ligand/Receptor Complex LGI1 and ADAM22 Regulate Synaptic Transmission. *Science*, 313:1792–1796.

Fukata, Y., Chen, X., Chiken, S., Hirano, Y., Yamagata, A., Inahashi, H., Sanbo, M., Sano, H., Goto, T., Hirabayashi, M., Kornau, H.-C., Prüss, H., Nambu, A., Fukai, S., Nicoll, R.A., Fukata, M., 2021. LGI1–ADAM22–MAGUK configures transsynaptic nanoalignment for synaptic transmission and epilepsy prevention. *Proceedings of the National Academy of Sciences*, 118:e2022580118.

Fukata, Y., Lovero, K.L., Iwanaga, T., Watanabe, A., Yokoi, N., Tabuchi, K., Shigemoto, R., Nicoll, R.A., Fukata, M., 2010. Disruption of LGI1-linked synaptic complex causes abnormal synaptic transmission and epilepsy. *Proceedings of the National Academy of Sciences of the United States of America*, 107:3799–3804.

Fukata, Y., Tzingounis, A. V., Trinidad, J.C., Fukata, M., Burlingame, A.L., Nicoll, R.A., Bredt, D.S., 2005. Molecular constituents of neuronal AMPA receptors. *Journal of Cell Biology*, 169:399–404.

Gähwiler, B.H., Capogna, M., Debanne, D., McKinney, R.A., Thompson, S.M., 1997. Organotypic slice cultures: A technique has come of age. *Trends in Neurosciences*, 20:471–477.

García-Nafría, J., Herguedas, B., Watson, J.F., Greger, I.H., 2016a. The dynamic AMPA receptor extracellular region: a platform for synaptic protein interactions. *Journal of Physiology*, 594:5449–5458.

García-Nafría, J., Watson, J.F., Greger, I.H., 2016b. IVA cloning: A single-tube universal cloning system exploiting bacterial In Vivo Assembly. *Scientific Reports*, 6:27459.

Gerstner, W., Kistler, W.M., Naud, R., Paninski, L., Gerstner, W., Kistler, W.M., Naud, R., Paninski, L., 2014. Synaptic plasticity and learning. *Neuronal Dynamics*, 21:50–62.

Gibson, D.G., Glass, J.I., Lartigue, C., Noskov, V.N., Chuang, R.Y., Algire, M.A., Benders, G.A., Montague, M.G., Ma, L., Moodie, M.M., Merryman, C., Vashee, S., Krishnakumar, R., Assad-Garcia, N., Andrews-Pfannkoch, C., Denisova, E.A., Young, L., Qi, Z.N., Segall-Shapiro, T.H., Calvey, C.H., Parmar, P.P., Hutchison, C.A., Smith, H.O., Venter, J.C., 2010. Creation of a bacterial cell controlled by a chemically synthesized genome. *Science*, 329:52–56.

Gibson, D.G., Young, L., Chuang, R.Y., Venter, J.C., Hutchison, C.A., Smith, H.O., 2009. Enzymatic assembly of DNA molecules up to several hundred kilobases. *Nature Methods*, 6:343–345.

Gill, M.B., Kato, A.S., Roberts, M.F., Yu, H., Wang, H., Tomita, S., Bredt, D.S., 2011. Cornichon-2 modulates AMPA receptor-transmembrane AMPA receptor regulatory protein assembly to dictate gating and pharmacology. *Journal of Neuroscience*, 31:6928–6938.

Gingras, A.C., Abe, K.T., Raught, B., 2019. Getting to know the neighborhood: using proximity-dependent biotinylation to characterize protein complexes and map organelles. *Current Opinion in Chemical Biology*, 48:44–54.

Glasgow, S.D., Labrecque, S., Beamish, I. V., Aufmkolk, S., Gibon, J., Han, D., Harris, S.N., Dufresne, P., Wiseman, P.W., McKinney, R.A., Séguéla, P., De Koninck, P., Ruthazer, E.S., Kennedy, T.E., 2018. Activity-Dependent Netrin-1 Secretion Drives Synaptic Insertion of GluA1-Containing AMPA Receptors in the Hippocampus. *Cell Reports*, 25:168-182.e6.

Gogolla, N., Galimberti, I., DePaola, V., Caroni, P., 2006. Staining protocol for organotypic hippocampal slice cultures. *Nature Protocols*, 1:2452–2456.

Gong, S., Zheng, C., Doughty, M.L., Losos, K., Didkovsky, N., Schambra, U.B., Nowak, N.J., Joyner, A., Leblanc, G., Hatten, M.E., Heintz, N., 2003. A gene expression atlas of the central nervous system based on bacterial artificial chromosomes. *Nature*, 425:917–925.

Granger, A.J., Shi, Y., Lu, W., Cerpas, M., Nicoll, R.A., 2013. LTP requires a reserve pool of glutamate receptors independent of subunit type. *Nature*, 493:495–500.

Gratacòs-Batlle, E., Olivella, M., Sánchez-Fernández, N., Yefimenko, N., Miguez-Cabello, F., Fadó, R., Casals, N., Gasull, X., Ambrosio, S., Soto, D., 2018. Mechanisms of CPT1C-Dependent AMPAR Trafficking Enhancement. *Frontiers in Molecular Neuroscience*, 11:275.

Gratacòs-Batlle, E., Yefimenko, N., Cascos-García, H., Soto, D., 2015. AMPAr interacting protein CPT1C enhances surface expression of GluA1-containing receptors. *Frontiers in Cellular Neuroscience*, 8:469.

Gray, S.J., Choi, V.W., Asokan, A., Haberman, R.A., McCown, T.J., Samulski, R.J., 2011. Production of recombinant adeno-associated viral vectors and use in in vitro and in vivo administration, *Current Protocols in Neuroscience*, 57:4.17.1-4.17.30.

Greger, I.H., Esteban, J.A., 2007. AMPA receptor biogenesis and trafficking. *Current Opinion in Neurobiology*, 17:289-297.

Greger, I.H., Khatri, L., Kong, X., Ziff, E.B., 2003. AMPA receptor tetramerization is mediated by Q/R editing. *Neuron*, 40:763–774.

Greger, I.H., Khatri, L., Ziff, E.B., 2002. RNA editing at Arg607 controls AMPA receptor exit from the endoplasmic reticulum. *Neuron*, 34:759–772.

Gruszczynska-Biegala, J., Sladowska, M., Kuznicki, J., 2016. AMPA receptors are involved in store-operated calcium entry and interact with STIM proteins in rat primary cortical neurons. *Frontiers in Cellular Neuroscience*, 10:251.

Gu, X., Mao, X., Lussier, M.P., Hutchison, M.A., Zhou, L., Hamra, F.K., Roche, K.W., Lu, W., 2016. GSG1L suppresses AMPA receptor-mediated synaptic transmission and uniquely modulates AMPA receptor kinetics in hippocampal neurons. *Nature Communications*, 7:10873.

Gu, Y., Huang, S., Chang, M.C., Worley, P., Kirkwood, A., Quinlan, E.M., 2013. Obligatory role for the immediate early gene NARP in critical period plasticity. *Neuron*, 79:335–346.

Han, W., Li, J., Pelkey, K.A., Pandey, S., Chen, X., Wang, Y.-X., Wu, K., Ge, L., Li, T., Castellano, D., Liu, C., Wu, L.-G., Petralia, R.S., Lynch, J.W., McBain, C.J., Lu, W., 2019. Shisa7 is a GABAA receptor auxiliary subunit controlling benzodiazepine actions. *Science*, 366:246–250.

Han, W., Wang, H., Li, J., Zhang, S., Lu, W., 2017. Ferric chelate reductase 1 like protein (FRRS1L) associates with dynein vesicles and regulates glutamatergic synaptic transmission. *Frontiers in Molecular Neuroscience*, 10:402.

Hangen, E., Cordelières, F.P., Petersen, J.D., Choquet, D., Coussen, F., 2018. Neuronal Activity and Intracellular Calcium Levels Regulate Intracellular Transport of Newly Synthesized AMPAR. *Cell Reports*, 24:1001-1012.e3.

Hardingham, G.E., Bading, H., 2010. Synaptic versus extrasynaptic NMDA receptor signalling: Implications for neurodegenerative disorders. *Nature Reviews Neuroscience*, 11:682–696.

Hayashi, T., Rumbaugh, G., Huganir, R.L., 2005. Differential regulation of AMPA receptor subunit trafficking by palmitoylation of two distinct sites. *Neuron*, 47:709–723.

Hayashi, Y., Shi, S.H., Esteban, J.A., Piccini, A., Poncer, J.C., Malinow, R., 2000. Driving AMPA receptors into synapses by LTP and CaMKII: Requirement for GluR1 and PDZ domain interaction. *Science*, 287:2262–2267.

He, K., Song, L., Cummings, L.W., Goldman, J., Huganir, R.L., Lee, H.K., 2009. Stabilization of Ca^{2+}-permeable AMPA receptors at perisynaptic sites by GluR1-S845 phosphorylation. *Proceedings of the National Academy of Sciences of the United States of America*, 106:20033–20038.

He, X.Y., Li, Y.J., Kalyanaraman, C., Qiu, L.L., Chen, C., Xiao, Q., Liu, W.X., Zhang, W., Yang, J.J., Chen, G., Jacobson, M.P., Shi, Y.S., 2016. GluA1 signal peptide determines the spatial assembly of heteromeric AMPA receptors. *Proceedings of the National Academy of Sciences of the United States of America*, 113:E5645–E5654.

Hebert, D.N., Molinari, M., 2007. In and out of the ER: Protein folding, quality control, degradation, and related human diseases. *Physiological Reviews*, 87:1377–1408.

Herguedas, B., Watson, J.F., Ho, H., Cais, O., García-Nafría, J., Greger, I.H., 2019. Architecture of the heteromeric GluA1/2 AMPA receptor in complex with the auxiliary subunit TARP g8. *Science*, 364:6438.

Herman, M.A., Jahr, C.E., 2007. Extracellular glutamate concentration in hippocampal slice. *Journal of Neuroscience*, 27:9736–9741.

Herrera-Molin, R., Sarto-Jackson, I., Montenegro-Venegas, C., Heine, M., Smalla, K.H., Seidenbecher, C.I., Beesley, P.W., Gundelfinger, E.D., Montag, D., 2014. Structure of excitatory synapses and GABAA receptor localization at inhibitory synapses are regulated by neuroplastin-65. *Journal of Biological Chemistry*, 289:8973–8988.

Herring, B.E., Shi, Y., Suh, Y.H., Zheng, C.Y., Blankenship, S.M., Roche, K.W., Nicoll, R.A., 2013. Cornichon Proteins Determine the Subunit Composition of Synaptic AMPA Receptors. *Neuron*, 77:1083–1096.

Hirai, H., Pang, Z., Bao, D., Miyazaki, T., Li, L., Miura, E., Parris, J., Rong, Y., Watanabe, M., Yuzaki, M., Morgan, J.I., 2005. Cbln1 is essential for synaptic integrity and plasticity in the cerebellum. *Nature Neuroscience*, 8:1534–1541.

Hires, S.A., Zhu, Y., Tsien, R.Y., 2008. Optical measurement of synaptic glutamate spillover and reuptake by linker optimized glutamate-sensitive fluorescent reporters. *Proceedings of the National Academy of Sciences of the United States of America*, 105:4411–4416.

Ho, H., Fowle, A., Coetzee, M., Greger, I.H., Watson, J.F., 2020. An inhalation anaesthesia approach for neonatal mice allowing streamlined stereotactic injection in the brain. *Journal of Neuroscience* Methods, 342:108824.

Hollmann, M., Hartley, M., Heinemann, S., 1991. Ca^{2+} permeability of KA-AMPA - gated glutamate receptor channels depends on subunit composition. *Science*, 252:851–853.

Hollmann, M., Heinemann, S., 1994. Cloned Glutamate Receptors. *Annual Review of Neuroscience*, 17:31–108.

Horn, Z., Behesti, H., Hatten, M.E., 2018. N-cadherin provides a cis and trans ligand for astrotactin that functions in glial-guided neuronal migration. *Proceedings of the National Academy of Sciences of the United States of America*, 115:10556–10563.

Howard, M.A., Elias, G.M., Elias, L.A.B., Swat, W., Nicoll, R.A., 2010. The role of SAP97 in synaptic glutamate receptor dynamics. *Proceedings of the National Academy of Sciences of the United States of America*, 107:3805–3810.

Howarth, M., Liu, W., Puthenveetil, S., Zheng, Y., Marshall, L.F., Schmidt, M.M., Wittrup, K.D., Bawendi, M.G., Ting, A.Y., 2008. Monovalent, reduced-size quantum dots for imaging receptors on living cells. *Nature Methods*, 5:397–399.

Hruska, M., Henderson, N., Le Marchand, S.J., Jafri, H., Dalva, M.B., 2018. Synaptic nanomodules underlie the organization and plasticity of spine synapses. *Nature Neuroscience*, 21:671–682.

Huang, Y.H., Sinha, S.R., Tanaka, K., Rothstein, J.D., Bergles, D.E., 2004. Astrocyte glutamate transporters regulate metabotropic glutamate receptor-mediated excitation of hippocampal interneurons. *Journal of Neuroscience*, 24:4551–4559.

Hung, V., Udeshi, N.D., Lam, S.S., Loh, K.H., Cox, K.J., Pedram, K., Carr, S.A., Ting, A.Y., 2016. Spatially resolved proteomic mapping in living cells with the engineered peroxidase APEX2. *Nature Protocols*, 11:456–475.

Jackman, S.L., Regehr, W.G., 2017. The Mechanisms and Functions of Synaptic Facilitation. *Neuron*, 94:447–464.

Jackson, A.C., Nicoll, R.A., 2011. The Expanding Social Network of Ionotropic Glutamate Receptors: TARPs and Other Transmembrane Auxiliary Subunits. *Neuron*, 70:178–199.

Jiang, C.H., Wei, M., Zhang, C., Shi, Y.S., 2021. The amino-terminal domain of GluA1 mediates LTP maintenance via interaction with neuroplastin-65. *Proceedings of the National Academy of Sciences of the United States of America*, 118:e2019194118.

Jiang, S., Kotani, N., Ohnishi, T., Miyagawa-Yamguchi, A., Tsuda, M., Yamashita, R., Ishiura, Y., Honke, K., 2012. A proteomics approach to the cell-surface interactome using the enzyme-mediated activation of radical sources reaction. *Proteomics*, 12:54–62.

Jones, E. V., Bernardinelli, Y., Tse, Y.C., Chierzi, S., Wong, T.P., Murai, K.K., 2011. Astrocytes control glutamate receptor levels at developing synapses through SPARC-β-integrin interactions. *Journal of Neuroscience*, 31:4154–4165.

Kalashnikova, E., Lorca, R.A., Kaur, I., Barisone, G.A., Li, B., Ishimaru, T., Trimmer, J.S., Mohapatra, D.P., Díaz, E., 2010. SynDIG1: An Activity-Regulated, AMPA- Receptor-Interacting Transmembrane Protein that Regulates Excitatory Synapse Development. *Neuron*, 65:80–93.

Kamalova, A., Futai, K., Delpire, E., Nakagawa, T., 2020. AMPA Receptor Auxiliary Subunit GSG1L Suppresses Short-Term Facilitation in Corticothalamic Synapses and Determines Seizure Susceptibility. *Cell Reports*, 32:107921.

Kamboj, S.K., Swanson, G.T., Cull-Candy, S.G., 1995. Intracellular spermine confers rectification on rat calcium-permeable AMPA and kainate receptors. *The Journal of Physiology*, 486:297–303.

Karakas, E., Furukawa, H., 2014. Crystal structure of a heterotetrameric NMDA receptor ion channel. *Science*, 344:992–997.

Kato, A.S., Burris, K.D., Gardinier, K.M., Gernert, D.L., Porter, W.J., Reel, J., Ding, C., Tu, Y., Schober, D.A., Lee, M.R., Heinz, B.A., Fitch, T.E., Gleason, S.D., Catlow, J.T., Yu, H., Fitzjohn, S.M., Pasqui, F., Wang, H., Qian, Y., Sher, E., Zwart, R., Wafford, K.A., Rasmussen, K., Ornstein, P.L., Isaac, J.T.R., Nisenbaum, E.S., Bredt, D.S., Witkin, J.M., 2016. Forebrain-selective AMPA-receptor antagonism guided by TARP γ-8 as an antiepileptic mechanism. *Nature Medicine*, 22:1496–1501.

Kato A.S., Siuda E.R., Nisenbaum, E.S., Bredt, D.S., 2008. AMPA Receptor Subunit-Specific Regulation by a Distinct Family of Type II TARPs. *Neuron*, 59:986–996.

Kerchner, G.A., Nicoll, R.A., 2008. Silent synapses and the emergence of a postsynaptic mechanism for LTP. *Nature Reviews Neuroscience*, 9:813–825.

Khodosevich, K., Jacobi, E., Farrow, P., Schulmann, A., Rusu, A., Zhang, L., Sprengel, R., Monyer, H., von Engelhardt, J., 2014. Coexpressed Auxiliary Subunits Exhibit Distinct Modulatory Profiles on AMPA Receptor Function. *Neuron*, 83:601–615.

Kim, D.I., Birendra, K.C., Zhu, W., Motamedchaboki, K., Doye, V., Roux, K.J., 2014. Probing nuclear pore complex architecture with proximity-dependent biotinylation. *Proceedings of the National Academy of Sciences of the United States of America*, 111:2453–2461.

Kim, D.I., Jensen, S.C., Noble, K.A., Kc, B., Roux, K.H., Motamedchaboki, K., Roux, K.J., 2016. An improved smaller biotin ligase for BioID proximity labeling. *Molecular Biology of the Cell*, 27:1188–1196.

Kirk, L.M., Ti, S.W., Bishop, H.I., Orozco-Llamas, M., Pham, M., Trimmer, J.S., Díaz, E., 2016. Distribution of the SynDIG4/proline-rich transmembrane protein 1 in rat brain. *Journal of Comparative Neurology*, 524:2266–2280.

Kirkpatrick, L.L., Matzuk, M.M., Dodds, D.C., Perin, M.S., 2000. Biochemical interactions of the neuronal pentraxins. Neuronal pentraxin (NP) receptor binds to taipoxin and taipoxin-associated calcium-binding protein 49 via NP1 and NP2. *Journal of Biological Chemistry*, 275:17786–17792.

Klaassen, R. V., Stroeder, J., Coussen, F., Hafner, A.S., Petersen, J.D., Renancio, C., Schmitz, L.J.M., Normand, E., Lodder, J.C., Rotaru, D.C., Rao-Ruiz, P., Spijker, S., Mansvelder, H.D., Choquet, D., Smit, A.B., 2016. Shisa6 traps AMPA receptors at postsynaptic sites and prevents their desensitization during synaptic activity. *Nature Communications*, 7:10682.

Ko, J., Fuccillo, M. V., Malenka, R.C., Südhof, T.C., 2009. LRRTM2 Functions as a Neurexin Ligand in Promoting Excitatory Synapse Formation. *Neuron*, 64:791–798.

Ko, J.S., Pramanik, G., Um, J.W., Shim, J.S., Lee, D., Kim, K.H., Chung, G.-Y., Condomitti, G., Kim, H.M., Kim, H., Wit, J. de, Park, K.-S., Tabuchi, K., Ko, J., 2015. Ptpσ functions as a presynaptic receptor for the glypican-4/LRRTM4 complex and is essential for excitatory synaptic transmission. *Proceedings of the National Academy of Sciences of the United States of America*, 112:1874–1879.

Koch, S.M., Ullian, E.M., 2010. Neuronal pentraxins mediate silent synapse conversion in the developing visual system. *Journal of Neuroscience*, 30:5404–5414.

Koh, D.S., Burnashev, N., Jonas, P., 1995. Block of native Ca($^{2+}$)-permeable AMPA receptors in rat brain by intracellular polyamines generates double rectification. *The Journal of Physiology*, 486:305–312.

Kohda, K., Kakegawa, W., Matsuda, S., Yamamoto, T., Hirano, H., Yuzaki, M., 2013. The δ2 glutamate receptor gates long-term depression by coordinating interactions between two AMPA receptor phosphorylation sites. *Proceedings of the National Academy of Sciences of the United States of America*, 110:E948–E957.

Koopmans, F., van Nierop, P., Andres-Alonso, M., Byrnes, A., Cijsouw, T., Coba, M.P., Cornelisse, L.N., Farrell, R.J., Goldschmidt, H.L., Howrigan, D.P., Hussain, N.K., Imig, C., de Jong, A.P.H., Jung, H., Kohansalnodehi, M., Kramarz, B., Lipstein, N., Lovering, R.C., MacGillavry, H., Mariano, V., Mi, H., Ninov, M., Osumi-Sutherland, D., Pielot, R., Smalla, K.H., Tang, H., Tashman, K., Toonen, R.F.G., Verpelli, C., Reig-Viader, R., Watanabe, K., van Weering, J., Achsel, T., Ashrafi, G., Asi, N., Brown, T.C., De Camilli, P., Feuermann, M., Foulger, R.E., Gaudet, P., Joglekar, A., Kanellopoulos, A., Malenka, R., Nicoll, R.A., Pulido, C., de Juan-Sanz, J., Sheng, M., Südhof, T.C., Tilgner, H.U., Bagni, C., Bayés, À., Biederer, T., Brose, N., Chua, J.J.E., Dieterich, D.C., Gundelfinger, E.D., Hoogenraad, C., Huganir, R.L., Jahn, R., Kaeser, P.S., Kim, E., Kreutz, M.R., McPherson, P.S., Neale, B.M., O'Connor, V., Posthuma, D., Ryan, T.A., Sala, C., Feng, G., Hyman, S.E., Thomas, P.D., Smit, A.B., Verhage, M., 2019. SynGO: An Evidence-Based, Expert-Curated Knowledge Base for the Synapse. *Neuron*, 103:217-234.e4.

Krieger, J., Bahar, I., Greger, I.H., 2015. Structure, Dynamics, and Allosteric Potential of Ionotropic Glutamate Receptor N-Terminal Domains. *Biophysical Journal*, 109:1136–1148.

Kristensen, A.S., Jenkins, M.A., Banke, T.G., Schousboe, A., Makino, Y., Johnson, R.C., Huganir, R., Traynelis, S.F., 2011. Mechanism of Ca^{2+}/calmodulin-dependent kinase II regulation of AMPA receptor gating. *Nature Neuroscience*, 14:727–735.

Kucukdereli, H., Allen, N.J., Lee, A.T., Feng, A., Ozlu, M.I., Conatser, L.M., Chakraborty, C., Workman, G., Weaver, M., Sage, E.H., Barres, B.A., Eroglu, C., 2011. Control of excitatory CNS synaptogenesis by astrocyte-secreted proteins hevin and SPARC. *Proceedings of the National Academy of Sciences of the United States of America*, 108:E440–E449.

Kuner, T., Beck, C., Sakmann, B., Seeburg, P.H., 2001. Channel-lining residues of the AMPA receptor M2 segment: Structural environment of the Q/R site and identification of the selectivity filter. *Journal of Neuroscience*, 21:4162–4172.

Lam, S.S., Martell, J.D., Kamer, K.J., Deerinck, T.J., Ellisman, M.H., Mootha, V.K., Ting, A.Y., 2014. Directed evolution of APEX2 for electron microscopy and proximity labeling. *Nature Methods*, 12:51–54.

Laurén, J., Airaksinen, M.S., Saarma, M., Timmusk, T., 2003. A novel gene family encoding leucine-rich repeat transmembrane proteins differentially expressed in the nervous system. *Genomics*, 81:411–421.

Lauri, S.E., Bortolotto, Z.A., Bleakman, D., Ornstein, P.L., Lodge, D., Isaac, J.T.R., Collingridge, G.L., 2001. A critical role of a facilitatory presynaptic kainate receptor in mossy fiber LTP. *Neuron*, 32:697–709.

Lee, H.K., Takamiya, K., Han, J.S., Man, H., Kim, C.H., Rumbaugh, G., Yu, S., Ding, L., He, C., Petralia, R.S., Wenthold, R.J., Gallagher, M., Huganir, R.L., 2003. Phosphorylation of the AMPA receptor GluR1 subunit is required for synaptic plasticity and retention of spatial memory. *Cell*, 112:631–643.

Lee, S.H., Liu, L., Wang, Y.T., Sheng, M., 2002. Clathrin adaptor AP2 and NSF interact with overlapping sites of GluR2 and play distinct roles in AMPA receptor trafficking and hippocampal LTD. *Neuron*, 36:661–674.

Lemoine, D., Mondoloni, S., Tange, J., Lambolez, B., Faure, P., Taly, A., Tricoire, L., Mourot, A., 2020. Probing the ionotropic activity of glutamate GluD2 receptor in HEK cells with genetically-engineered photopharmacology. eLife, 9:e59026

Lei, N., Mellem, J.E., Brockie, P.J., Madsen, D.M., Maricq, A. V., 2017. NRAP-1 Is a Presynaptically Released NMDA Receptor Auxiliary Protein that Modifies Synaptic Strength. *Neuron*, 96:1303-1316.e6.

Lei, N., Mellem, J.E., Brockie, P.J., Madsen, D.M., Maricq, A. V., 2017. NRAP-1 Is a Presynaptically Released NMDA Receptor Auxiliary Protein that Modifies Synaptic Strength. *Neuron*, 96:1303-1316.e6.

Letellier, M., Szíber, Z., Chamma, I., Saphy, C., Papasideri, I., Tessier, B., Sainlos, M., Czöndör, K., Thoumine, O., 2018. A unique intracellular tyrosine in neuroligin-1 regulates AMPA receptor recruitment during synapse differentiation and potentiation. *Nature Communications*, 9:3979.

Li, J., Han, S., Li, H., Udeshi, N.D., Svinkina, T., Mani, D.R., Xu, C., Guajardo, R., Xie, Q., Li, T., Luginbuhl, D.J., Wu, B., McLaughlin, C.N., Xie, A., Kaewsapsak, P., Quake, S.R., Carr, S.A., Ting, A.Y., Luo, L., 2020. Cell-Surface Proteomic Profiling in the Fly Brain Uncovers Wiring Regulators. *Cell*, 180:373-386.e15.

Li, X., Qin, L., Li, Y., Yu, H., Zhang, Z., Tao, C., Liu, Y., Xue, Y., Zhang, X., Xu, Z., Wang, Y., Lou, H., Tan, Z., Saftig, P., Chen, Z., Xu, T., Bi, G., Duan, S., Gao, Z., 2019. Presynaptic Endosomal Cathepsin D Regulates the Biogenesis of GABAergic Synaptic Vesicles. *Cell Reports*, 28:1015-1028.e5.

Li, Y.J., Duan, G.F., Sun, J.H., Wu, D., Ye, C., Zang, Y.Y., Chen, G.Q., Shi, Y.Y., Wang, J., Zhang, W., Shi, Y.S., 2019. Neto proteins regulate gating of the kainate-type glutamate receptor GluK2 through two binding sites. *Journal of Biological Chemistry*, 294:17889–17902.

Linhoff, M.W., Laurén, J., Cassidy, R.M., Dobie, F.A., Takahashi, H., Nygaard, H.B., Airaksinen, M.S., Strittmatter, S.M., Craig, A.M., 2009. An Unbiased Expression Screen for Synaptogenic Proteins Identifies the LRRTM Protein Family as Synaptic Organizers. *Neuron*, 61:734–749.

Lisman, J., 2017. Glutamatergic synapses are structurally and biochemically complex because of multiple plasticity processes: Long-term potentiation, long-term depression, short-term potentiation and scaling. *Philosophical Transactions of the Royal Society B: Biological Sciences*, 372:20160260.

Lisman, J., Raghavachari, S., 2006. A Unified Model of the Presynaptic and Post- synaptic Changes During LTP at CA1 Synapses. *Science's STKE*, 356:re11.

Lisman, J.E., Raghavachari, S., Tsien, R.W., 2007. The sequence of events that underlie quantal transmission at central glutamatergic synapses. *Nature Reviews Neuroscience*, 8:597–609.

Liu, A., Ji, H., Ren, Q., Meng, Y., Zhang, H., Collingride, G., Xie, W., Jia, Z., 2020. The Requirement of the C-Terminal Domain of GluA1 in Different Forms of Long-Term Potentiation in the Hippocampus Is Age-Dependent. *Frontiers in Synaptic Neuroscience*, 12:588785.

Liu, G., Choi, S., Tsien, R.W., 1999. Variability of neurotransmitter concentration and nonsaturation of postsynaptic AMPA receptors at synapses in hippocampal cultures and slices. *Neuron*, 22:395–409.

Liu, Z., Chen, O., Wall, J.B.J., Zheng, M., Zhou, Y., Wang, L., Ruth Vaseghi, H., Qian, L., Liu, J., 2017. Systematic comparison of 2A peptides for cloning multi-genes in a polycistronic vector. *Scientific Reports*, 7:2193.

Lomeli, H., Mosbacher, J., Melcher, T., Höger, T., Geiger, J.R.P., Kuner, T., Monyer, H., Higuchi, M., Bach, A., Seeburg, P.H., 1994. Control of kinetic properties of AMPA receptor channels by nuclear RNA editing. *Science*, 266:1709–1713.

Lovero, K.L., Blankenship, S.M., Shi, Y., Nicoll, R.A., 2013. SynDIG1 Promotes Excitatory Synaptogenesis Independent of AMPA Receptor Trafficking and Biophysical Regulation. *PLoS ONE*, 8:e66171.

Lovero, K.L., Fukata, Y., Granger, A.J., Fukata, M., Nicoll, R.A., 2015. The LGI1-ADAM22 protein complex directs synapse maturation through regulation of PSD-95 function. *Proceedings of the National Academy of Sciences of the United States of America*, 112:E4129–E4137.

Lu, W., Shi, Y., Jackson, A.C., Bjorgan, K., During, M.J., Sprengel, R., Seeburg, P.H., Nicoll, R.A., 2009. Subunit Composition of Synaptic AMPA Receptors Revealed by a Single-Cell Genetic Approach. *Neuron*, 62:254–268.

Lu, W., Ziff, E.B., 2005. PICK1 interacts with ABP/GRIP to regulate AMPA receptor trafficking. *Neuron*, 47:407–421.

MacGillavry, H.D., Song, Y., Raghavachari, S., Blanpied, T.A., 2013. Nanoscale scaffolding domains within the postsynaptic density concentrate synaptic ampa receptors. *Neuron*, 78:615–622.

Maher, M.P., Wu, N., Ravula, S., Ameriks, M.K., Savall, B.M., Liu, C., Lord, B., Wyatt, R.M., Matta, J.A., Dugovic, C., Yun, S., Ver Donck, L., Steckler, T., Wickenden, A.D., Carruthers, N.I., Lovenberg, T.W., 2016. Discovery and characterization of AMPA receptor modulators selective for TARP-γ8. *Journal of Pharmacology and Experimental Therapeutics*, 357:394–414.

Malinow, R., Tsien, R.W., 1990. Presynaptic enhancement shown by whole-cell recordings of long-term potentiation in hippocampal slices. *Nature*, 346:177–180.

Mao, X., Gu, X., Lu, W., 2017. GSG1L regulates the strength of AMPA receptor-mediated synaptic transmission but not AMPA receptor kinetics in hippocampal dentate granule neurons. *Journal of Neurophysiology*, 117:28–35.

Martell, J.D., Deerinck, T.J., Sancak, Y., Poulos, T.L., Mootha, V.K., Sosinsky, G.E., Ellisman, M.H., Ting, A.Y., 2012. Engineered ascorbate peroxidase as a genetically encoded reporter for electron microscopy. *Nature Biotechnology*, 30:1143–1148.

Martinelli, D.C., Chew, K.S., Rohlmann, A., Lum, M.Y., Ressl, S., Hattar, S., Brunger, A.T., Missler, M., Südhof, T.C., 2016. Expression of C1ql3 in Discrete Neuronal Populations Controls Efferent Synapse Numbers and Diverse Behaviors. *Neuron*, 91:1034–1051.

Matsuda, K., Budisantoso, T., Mitakidis, N., Sugaya, Y., Miura, E., Kakegawa, W., Yamasaki, M., Konno, K., Uchigashima, M., Abe, M., Watanabe, I., Kano, M., Watanabe, M., Sakimura, K., Aricescu, A.R., Yuzaki, M., 2016. Transsynaptic Modulation of Kainate Receptor Functions by C1q-like Proteins. *Neuron*, 90:752–767.

Matsuda, K., Miura, E., Miyazaki, T., Kakegawa, W., Emi, K., Narumi, S., Fukazawa, Y., Ito-lshida, A., Kondo, T., Shigemoto, R., Watanabe, M., Yuzaki, M., 2010. Cbln1 is a ligand for an orphan glutamate receptor δ2, a bidirectional synapse organizer. *Science*, 328:363–368.

Matsuda, S., Launey, T., Mikawa, S., Hirai, H., 2000. Disruption of AMPA receptor GluR2 clusters following long-term depression induction in cerebellar Purkinje neurons. *EMBO Journal*, 19:2765–2774.

Matt, L., Kirk, L.M., Chenaux, G., Speca, D.J., Puhger, K.R., Pride, M.C., Qneibi, M., Haham, T., Plambeck, K.E., Stern-Bach, Y., Silverman, J.L., Crawley, J.N., Hell, J.W., Díaz, E., 2018. SynDIG4/Prrt1 Is Required for Excitatory Synapse Development and Plasticity Underlying Cognitive Function. *Cell Reports*, 22:2246–2253.

May, D.G., Scott, K.L., Campos, A.R., Roux, K.J., 2020. Comparative Application of BioID and TurboID for Protein-Proximity Biotinylation. *Cells*, 9:1070.

Mayer, M.L., Westbrookt, G.L., Guthriet, P.B., 1984. Responses in Spinal Cord Neurones. *Nature*, 309:261–263.

McAllister, A.K., Stevens, C.F., 2000. Nonsaturation of AMPA and NMDA receptors at hippocampal synapses. *Proceedings of the National Academy of Sciences of the United States of America*, 97:6173–6178.

McGee, T.P., Bats, C., Farrant, M., Cull-Candy, S.G., 2015. Auxiliary subunit GSG1L acts to suppress calcium- permeable AMPA receptor function. *Journal of Neuroscience*, 35:16171–16179.

Meyerson, J.R., Chittori, S., Merk, A., Rao, P., Han, T.H., Serpe, M., Mayer, M.L., Subramaniam, S., 2016. Structural basis of kainate subtype glutamate receptor desensitization. *Nature*, 537:567–571.

Milstein, A.D., Nicoll, R.A., 2009. TARP modulation of synaptic AMPA receptor trafficking and gating depends on multiple intracellular domains. *Proceedings of the National Academy of Sciences of the United States of America*, 106:11348–11351.

Mitchell, S.J., Silver, R.A., 2000. Glutamate spillover suppresses inhibition by activating presynaptic mGluRs. *Nature*, 404:498–502.

Möykkynen, T., Coleman, S.K., Semenov, A., Keinänen, K., 2014. The N-terminal domain modulates α-Amino-3-hydroxy-5-methyl-4- isoxazolepropionic acid (AMPA) receptor desensitization. *Journal of Biological Chemistry*, 289:13197–13205.

Nair, D., Hosy, E., Petersen, J.D., Constals, A., Giannone, G., Choquet, D., Sibarita, J.B., 2013. Super-resolution imaging reveals that AMPA receptors inside synapses are dynamically organized in nanodomains regulated by PSD95. *Journal of Neuroscience*, 33:13204–13224.

Nakagawa, T., 2019. Structures of the AMPA receptor in complex with its auxiliary subunit cornichon. *Science*, 366:1259–1263.

Nakaya, N., Sultana, A., Tomarev, S.I., 2017. Impaired AMPA receptor trafficking by a double knockout of zebrafish olfactomedin1a/b. *Journal of Neurochemistry*, 143:635–644.

Naur, P., Hansen, K.B., Kristensen, A.S., Dravid, S.M., Pickering, D.S., Olsen, L., Vestergaard, B., Egebjerg, J., Gajhede, M., Traynelis, S.F., Kastrup, J.S., 2007. Ionotropic glutamate-like receptor δ2 binds D-serine and glycine. *Proceedings of the National Academy of Sciences of the United States of America*, 104:14116–14121.

Nietz, A.K., Vaden, J.H., Coddington, L.T., Overstreet-Wadiche, L., Wadiche, J.I., 2017. Non-synaptic signaling from cerebellar climbing fibers modulates Golgi cell activity. *eLife*, 6:e29215.

Nishimune, A., Isaac, J.T.R., Molnar, E., Noel, J., Nash, S.R., Tagaya, M., Collingridge, G.L., Nakanishi, S., Henley, J.M., 1998. NSF binding to GluR2 regulates synaptic transmission. *Neuron*, 21:87–97.

Nishiyama, J., Mikuni, T., Yasuda, R., 2017. Virus-Mediated Genome Editing via Homology-Directed Repair in Mitotic and Postmitotic Cells in Mammalian Brain. *Neuron*, 96:755-768.e5.

Nolt, M.J., Lin, Y., Hruska, M., Murphy, J., Sheffler-Colins, S.I., Kayser, M.S., Passer, J., Bennett, M.V.L., Zukin, R.S., Dalva, M.B., 2011. EphB controls NMDA receptor function and synaptic targeting in a subunit-specific manner. *Journal of Neuroscience*, 31:5353–5364.

Nowak, L., Bregestovski, P., Ascher, P., Herbet, A., Prochiantz, A., 1984. Magnesium gates glutamate-activated channels in mouse central neurones. *Nature*, 307:462–465.

O'Brien, R., Xu, D., Mi, R., Tang, X., Hopf, C., Worley, P., 2002. Synaptically Targeted Narp Plays an Essential Role in the Aggregation of AMPA Receptors at Excitatory Synapses in Cultured Spinal Neurons. *Journal of Neuroscience*, 22:4487–4498.

O'Brien, R.J., Desheng, X., Petralia, R.S., Steward, O., Huganir, R.L., Worley, P., 1999. Synaptic clustering of AMPA receptors by the extracellular immediate- early gene product Narp. *Neuron*, 23:309–323.

Oliet, S.H.R., Malenka, R.C., Nicoll, R.A., 1996. Bidirectional control of quantal size by synaptic activity in the hippocampus. *Science*, 271:1294–1297.

Opazo, P., Choquet, D., 2011. A three-step model for the synaptic recruitment of AMPA receptors. *Molecular and Cellular Neuroscience*, 46:1–8.

Orth, A., Tapken, D., Hollmann, M., 2013. The delta subfamily of glutamate receptors: Characterization of receptor chimeras and mutants. *European Journal of Neuroscience*, 37:1620–1630.

Osten, P., Khatri, L., Perez, J.L., Köhr, G., Giese, G., Daly, C., Schulz, T.W., Wensky, A., Lee, L.M., Ziff, E.B., 2000. Mutagenesis reveals a role for ABP/GRIP binding to GluR2 in synaptic surface accumulation of the AMPA receptor. *Neuron*, 27:313–325.

Osten, P., Srivastava, S., Inman, G.J., Vilim, F.S., Khatri, L., Lee, L.M., States, B.A., Einheber, S., Milner, T.A., Hanson, P.I., Ziff, E.B., 1998. The AMPA receptor GluR2 C terminus can mediate a reversible, ATP- dependent interaction with NSF and α- and β-SNAPs. *Neuron*, 21:99–110.

Osterweil, E., Wells, D.G., Mooseker, M.S., 2005. A role for myosin VI in postsynaptic structure and glutamate receptor endocytosis. *Journal of Cell Biology*, 168:329–338.

Overstreet, L.S., Kinney, G.A., Liu, Y.B., Billups, D., Slater, N.T., 1999. Glutamate transporters contribute to the time course of synaptic transmission in cerebellar granule cells. *Journal of Neuroscience*, 19:9663–9673.

Pandya, N.J., Seeger, C., Babai, N., Gonzalez-Lozano, M.A., Mack, V., Lodder, J.C., Gouwenberg, Y., Mansvelder, H.D., Danielson, U.H., Li, K.W., Heine, M., Spijker, S., Frischknecht, R., Smit, A.B., 2018. Noelin1 Affects Lateral Mobility of Synaptic AMPA Receptors. *Cell Reports*, 24:1218–1230.

Paoletti, P., Bellone, C., Zhou, Q., 2013. NMDA receptor subunit diversity: Impact on receptor properties, synaptic plasticity and disease. *Nature Reviews Neuroscience*, 14:383–400.

Papouin, T., Oliet, S.H.R., 2014. Organization, Control and function of extrasynaptic NMDA receptors. *Philosophical Transactions of the Royal Society B: Biological Sciences*, 369: 20130601.

Passafaro, M., Nakagawa, T., Sala, C., Sheng, M., 2003. Induction of dendritic spines by an extracellular domain of AMPA receptor subunit GluR2. *Nature*, 424:677–681.

Pasternack, A., Coleman, S.K., Jouppila, A., Mottershead, D.G., Lindfors, M., Pasternack, M., Keinänen, K., 2002. α-amino-3-hydroxy-5-methyl-4-isoxazolepropionic acid (AMPA) receptor channels lacking the N-terminal domain. *Journal of Biological Chemistry*, 277:49662–49667.

Pelkey, K.A., Barksdale, E., Craig, M.T., Yuan, X., Sukumaran, M., Vargish, G.A., Mitchell, R.M., Wyeth, M.S., Petralia, R.S., Chittajallu, R., Karlsson, R.M., Cameron, H.A., Murata, Y., Colonnese, M.T., Worley, P.F., McBain, C.J., 2015. Pentraxins coordinate excitatory synapse maturation and circuit integration of parvalbumin interneurons. *Neuron*, 85:1257–1272.

Pellegrini-Giampietro, D.E., 2003. An activity-dependent spermine-mediated mechanism that modulates glutamate transmission. *Trends in Neurosciences*, 26:9–11.

Penn, A.C., Balik, A., Wozny, C., Cais, O., Greger, I.H., 2012. Activity-Mediated AMPA Receptor Remodeling, Driven by Alternative Splicing in the Ligand-Binding Domain. *Neuron*, 76:503–510.

Penn, A.C., Zhang, C.L., Georges, F., Royer, L., Breillat, C., Hosy, E., Petersen, J.D., Humeau, Y., Choquet, D., 2017. Hippocampal LTP and contextual learning require surface diffusion of AMPA receptors. *Nature*, 549:384–388.

Perez de Arce, K., Schrod, N., Metzbower, S.W.R., Allgeyer, E., Kong, G.K.W., Tang, A.H., Krupp, A.J., Stein, V., Liu, X., Bewersdorf, J., Blanpied, T.A., Lučić, V., Biederer, T., 2015. Topographic Mapping of the Synaptic Cleft into Adhesive Nanodomains. *Neuron*, 88:1165–1172.

Perez, J.L., Khatri, L., Chang, C., Srivastava, S., Osten, P., Ziff, E.B., 2001. PICK1 targets activated protein kinase Cα to AMPA receptor clusters in spines of hippocampal neurons and reduces surface levels of the AMPA-type glutamate receptor subunit 2. *Journal of Neuroscience*, 21:5417–5428.

Petit-Pedrol, M., Sell, J., Planagumà, J., Mannara, F., Radosevic, M., Haselmann, H., Ceanga, M., Sabater, L., Spatola, M., Soto, D., Gasull, X., Dalmau, J., Geis, C., 2018. LGI1 antibodies alter K v 1.1 and AMPA receptors changing synaptic excitability, plasticity and memory. *Brain*, 141:3144–3159.

Pinky, N.F., Wilkie, C.M., Barnes, J.R., Parsons, M.P., 2018. Region-and activity-dependent regulation of extracellular glutamate. *Journal of Neuroscience*, 38:5351–5366.

Pronker, M.F., Bos, T.G.A.A., Sharp, T.H., Thies-Weesie, D.M.E., Janssen, B.J.C., 2015. Olfactomedin-1 has a V-shaped disulfide-linked tetrameric structure. *Journal of Biological Chemistry*, 290:15092–15101.

Pronker, M.F., Van Den Hoek, H., Janssen, B.J.C., 2019. Design and structural characterisation of olfactomedin-1 variants as tools for functional studies. *BMC Molecular and Cell Biology*, 20:50.

Raghavachari, S., Lisman, J.E., 2004. Properties of quantal transmission at CA1 synapses. *Journal of Neurophysiology*, 92:2456–2467.

Ramanathan, M., Majzoub, K., Rao, D.S., Neela, P.H., Zarnegar, B.J., Mondal, S., Roth, J.G., Gai, H., Kovalski, J.R., Siprashvili, Z., Palmer, T.D., Carette, J.E., Khavari, P.A., 2018. RN A-protein interaction detection in living cells. *Nature Methods*, 15:207–212.

Ramirez, D.M.O., Kavalali, E.T., 2011. Differential regulation of spontaneous and evoked neurotransmitter release at central synapses. *Current Opinion in Neurobiology*, 21:275–282.

Ranaivoson, F.M., Turk, L.S., Ozgul, S., Kakehi, S., von Daake, S., Lopez, N., Trobiani, L., De Jaco, A., Denissova, N., Demeler, B., Özkan, E., Montelione, G.T., Comoletti, D., 2019. A Proteomic Screen of Neuronal Cell-Surface Molecules Reveals IgLONs as Structurally Conserved Interaction Modules at the Synapse. *Structure*, 27:893-906.e9.

Rathenberg, J., Nevian, T., Witzemann, V., 2003. High-efficiency transfection of individual neurons using modified electrophysiology techniques. *Journal of Neuroscience Methods*, 126:91–98.

Reiner, A., Levitz, J., 2018. Glutamatergic Signaling in the Central Nervous System: Ionotropic and Metabotropic Receptors in Concert. *Neuron*, 98:1080–1098.

Reti, I.M., Miskimon, M., Dickson, M., Petralia, R.S., Takamiya, K., Bland, R., Saini, J., During, M.J., Huganir, R.L., Baraban, J.M., 2008. Activity-dependent secretion of neuronal activity regulated pentraxin from vasopressin neurons into the systemic circulation. *Neuroscience*, 151:352–360.

Roppongi, R.T., Dhume, S.H., Padmanabhan, N., Silwal, P., Zahra, N., Karimi, B., Bomkamp, C., Patil, C.S., Champagne-Jorgensen, K., Twilley, R.E., Zhang, P., Jackson, M.F., Siddiqui, T.J., 2020. LRRTMs Organize Synapses through Differential Engagement of Neurexin and PTPσ. *Neuron*, 106:108-125.e12.

Rossmann, M., Sukumaran, M., Penn, A.C., Veprintsev, D.B., Babu, M.M., Greger, I.H., 2011. Subunit-selective N-terminal domain associations organize the formation of AMPA receptor heteromers. *EMBO Journal*, 30:959–971.

Rouach, N., Byrd, K., Petralia, R.S., Elias, G.M., Adesnik, H., Tomita, S., Karimzadegan, S., Kealey, C., Bredt, D.S., Nicoll, R.A., 2005. TARP γ-8 controls hippocampal AMPA receptor number, distribution and synaptic plasticity. *Nature Neuroscience*, 8:1525–1533.

Roux, K.J., Kim, D.I., Burke, B., May, D.G., 2018. BioID: A Screen for Protein-Protein Interactions. *Current Protocols in Protein Science*, 91:19.23.1-19.23.15.

Roux, K.J., Kim, D.I., Raida, M., Burke, B., 2012. A promiscuous biotin ligase fusion protein identifies proximal and interacting proteins in mammalian cells. *Journal of Cell Biology*, 196:801–810.

Royo, N.C., Vandenberghe, L.H., Ma, J.Y., Hauspurg, A., Yu, L.Y., Maronski, M., Johnston, J., Dichter, M.A., Wilson, J.M., Watson, D.J., 2008. Specific AAV serotypes stably transduce primary hippocampal and cortical cultures with high efficiency and low toxicity. *Brain Research*, 1190:15–22.

Rubio, M.E., Wenthold, R.J., 1999. Calnexin and the immunoglobulin binding protein (BiP) coimmunoprecipitate with AMPA receptors. *Journal of Neurochemistry*, 73:942–948.

Rusakov, D.A., Kullmann, D.M., 1998. Extrasynaptic glutamate diffusion in the hippocampus: Ultrastructural constraints, uptake, and receptor activation. *Journal of Neuroscience*, 18:3158–3170.

Saglietti, L., Dequidt, C., Kamieniarz, K., Rousset, M.C., Valnegri, P., Thoumine, O., Beretta, F., Fagni, L., Choquet, D., Sala, C., Sheng, M., Passafaro, M., 2007. Extracellular Interactions between GluR2 and N-Cadherin in Spine Regulation. *Neuron*, 54:461–477.

Sanderson, T.M., Bradley, C.A., Georgiou, J., Hong, Y.H., Ng, A.N., Lee, Y., Kim, H.D., Kim, D., Amici, M., Son, G.H., Zhuo, M., Kim, K., Kaang, B.K., Kim, S.J., Collingridge, G.L., 2018. The Probability of Neurotransmitter Release Governs AMPA Receptor Trafficking via Activity-Dependent Regulation of mGluR1 Surface Expression. *Cell Reports*, 25:3631-3646.e3.

Savall, B.M., Wu, D., Swanson, D.M., Seierstad, M., Wu, N., Vives Martinez, J., García Olmos, B., Lord, B., Coe, K., Koudriakova, T., Lovenberg, T.W., Carruthers, N.I., Maher, M.P., Ameriks, M.K., 2019. Discovery of Imidazo[1,2-a]pyrazines and Pyrazolo[1,5-c]pyrimidines as TARP γ-8 Selective AMPAR Negative Modulators. *ACS Medicinal Chemistry Letters*, 10:267–272.

Savtchenko, L.P., Rusakov, D.A., 2014. Moderate AMPA receptor clustering on the nanoscale can efficiently potentiate synaptic current. *Philosophical Transactions of the Royal Society B: Biological Sciences*, 369:20130167.

Scanziani, M., Salin, P.A., Vogt, K.E., Malenka, R.C., Nicoll, R.A., 1997. Use-dependent increases in glutamate concentration activate presynaptic metabotropic glutamate receptors Massimo. *Nature*, 385:630–634.

Schaukowitch, K., Reese, A.L., Kim, S.K., Kilaru, G., Joo, J.Y., Kavalali, E.T., Kim, T.K., 2017. An Intrinsic Transcriptional Program Underlying Synaptic Scaling during Activity Suppression. *Cell Reports*, 18:1512–1526.

Schlimgen, A.K., Helms, J.A., Vogel, H., Perin, M.S., 1995. Neuronal pentraxin, a secreted protein with homology to acute phase proteins of the immune system. *Neuron*, 14:519–526.

Schmid, S.M., Hollmann, M., 2008. To gate or not to gate: Are the delta subunits in the glutamate receptor family functional ion channels? *Molecular Neurobiology*, 37:126–141.

Schmid, S.M., Kott, S., Sager, C., Huelsken, T., Hollmann, M., 2009. The glutamate receptor subunit delta2 is capable of gating its intrinsic ion channel as revealed by ligand binding domain transplantation. *Proceedings of the National Academy of Sciences of the United States of America*, 106:10320–10325.

Schmitz, L.J.M., Klaassen, R. V., Ruiperez-Alonso, M., Zamri, A.E., Stroeder, J., Rao-Ruiz, P., Lodder, J.C., van der Loo, R.J., Mansvelder, H.D., Smit, A.B., Spijker, S., 2017. The AMPA receptor-associated protein Shisa7 regulates hippocampal synaptic function and contextual memory. *eLife*, 6:e24192.

Schöpf, C.L., Geisler, S., Stanika, R.I., Campiglio, M., Kaufmann, W.A., Nimmervoll, B., Schlick, B., Shigemoto, R., Obermair, G.J., 2019. Presynaptic α2δ subunits are key organizers of glutamatergic synapses. *bioRxiv*, doi: https://doi.org/10.1101/826016.

Schulte, U., Thumfart, J.O., Klöcker, N., Sailer, C.A., Bildl, W., Biniossek, M., Dehn, D., Deller, T., Eble, S., Abbass, K., Wangler, T., Knaus, H.G., Fakler, B., 2006. The epilepsy-linked Lgi1 protein assembles into presynaptic Kv1 channels and inhibits inactivation by Kvβ1. *Neuron*, 49:697–706.

Schwenk, J., Baehrens, D., Haupt, A., Bildl, W., Boudkkazi, S., Roeper, J., Fakler, B., Schulte, U., 2014. Regional diversity and developmental dynamics of the AMPA-receptor proteome in the mammalian brain. *Neuron*, 84:41–54.

Schwenk, J., Boudkkazi, S., Kocylowski, M.K., Brechet, A., Zolles, G., Bus, T., Costa, K., Kollewe, A., Jordan, J., Bank, J., Bildl, W., Sprengel, R., Kulik, A., Roeper, J., Schulte, U., Fakler, B., 2019. An ER Assembly Line of AMPA-Receptors Controls Excitatory Neurotransmission and Its Plasticity. *Neuron*, 104:680-692.e9.

Schwenk, J., Fakler, B., 2020. Building of AMPA-type glutamate receptors in the endoplasmic reticulum and its implication for excitatory neurotransmission. *Journal of Physiology*, JP279025.

Schwenk, J., Harmel, N., Brechet, A., Zolles, G., Berkefeld, H., Müller, C.S., Bildl, W., Baehrens, D., Hüber, B., Kulik, A., Klöcker, N., Schulte, U., Fakler, B., 2012. High-Resolution Proteomics Unravel Architecture and Molecular Diversity of Native AMPA Receptor Complexes. *Neuron*, 74:621–633.

Schwenk, J., Harmel, N., Zolles, G., Bildl, W., Kulik, A., Heimrich, B., Chisaka, O., Jonas, P., Schulte, U., Fakler, B., Klöcker, N., 2009. Functional Proteomics Identify Cornichon Proteins as Auxiliary Subunits of AMPA Receptors. *Science*, 323:1313–1319.

Schwiebert, E.M., Zsembery, A., 2003. Extracellular ATP as a signaling molecule for epithelial cells. *Biochimica et Biophysica Acta - Biomembranes*, 1615:7–32.

Seagar, M., Russier, M., Caillard, O., Maulet, Y., Fronzaroli-Molinieres, L., De San Feliciano, M., Boumedine-Guignon, N., Rodriguez, L., Zbili, M., Usseglio, F., Formisano-Tréziny, C., Youssouf, F., Sangiardi, M., Boillot, M., Baulac, S., Benitez, M.J., Garrido, J.J., Debanne, D., El Far, O., 2017. LGI1 tunes intrinsic excitability by regulating the density of axonal Kv1 channels. *Proceedings of the National Academy of Sciences of the United States of America*, 114:7719–7724.

Setou, M., Seog, D.H., Tanaka, Y., Kanai, Y., Takei, Y., Kawagishi, M., Hirokawa, N., 2002. Glutamate-receptor-interacting protein GRIP1 directly steers kinesin to dendrites. *Nature*, 417:83–87.

Shanks, N.F., Savas, J.N., Maruo, T., Cais, O., Hirao, A., Oe, S., Ghosh, A., Noda, Y., Greger, I.H., Yates, J.R., Nakagawa, T., 2012. Differences in AMPA and Kainate Receptor Interactomes Facilitate Identification of AMPA Receptor Auxiliary Subunit GSG1L. *Cell Reports*, 1:590–598.

Shen, L., Liang, F., Walensky, L.D., Huganir, R.L., 2000. Regulation of AMPA receptor GluR1 subunit surface expression by a 4.1N-linked actin cytoskeletal association. *Journal of Neuroscience*, 20:7932–7940.

Sheng, N., Bemben, M.A., Díaz-Alonso, J., Tao, W., Shi, Y.S., Nicoll, R.A., 2018. LTP requires postsynaptic PDZ-domain interactions with glutamate receptor/auxiliary protein complexes. *Proceedings of the National Academy of Sciences of the United States of America*, 115:3948–3953.

Sheng, N., Shi, Y.S., Lomash, R.M., Roche, K.W., Nicoll, R.A., 2015. Neto auxiliary proteins control both the trafficking and biophysical properties of the kainate receptor GluK1. *eLife*, 4:e11682.

Sheng, N., Shi, Y.S., Nicoll, R.A., 2017a. Amino-terminal domains of kainate receptors determine the differential dependence on Neto auxiliary subunits for trafficking. *Proceedings of the National Academy of Sciences of the United States of America*, 114:1159–1164.

Sheng, N., Yang, J., Silm, K., Edwards, R.H., Nicoll, R.A., 2017b. A slow excitatory postsynaptic current mediated by a novel metabotropic glutamate receptor in CA1 pyramidal neurons. *Neuropharmacology*, 115:4–9.

Shepherd, J.D., Huganir, R.L., 2007. The cell biology of synaptic plasticity: AMPA receptor trafficking. *Annual Review of Cell and Developmental Biology*, 23:613-43.

Sheridan, D.L., Robert, A., Cho, C.H., Howe, J.R., Hughes, T.E., 2006. Regions of α-amino-5-methyl-3-hydroxy-4-isoxazole propionic acid receptor subunits that are permissive for the insertion of green fluorescent protein. *Neuroscience*, 141:837–849.

Shi, S.-H., Hayashi, Y., Esteban, J.A., Malinow, R., 2001. Subunit-Specific Rules Governing AMPA Receptor Trafficking to Synapses in Hippocampal Pyramidal Neurons. *Cell*, 105:331–343.

Shi, Y., Suh, Y.H., Milstein, A.D., Isozaki, K., Schmid, S.M., Roche, K.W., Nicoll, R.A., 2010. Functional comparison of the effects of TARPs and cornichons on AMPA receptor trafficking and gating. *Proceedings of the National Academy of Sciences of the United States of America*, 107:16315–16319.

Shimamoto, K., LeBrun, B., Yasuda-Kamatani, Y., Sakaitani, M., Shigeri, Y., Yumoto, N., Nakajima, T., 1998. DL-threo-β-benzyloxyaspartate, a potent blocker of excitatory amino acid transporters. *Molecular Pharmacology*, 53:195–201.

Shimamoto, K., Sakai, R., Takaoka, K., Yumoto, N., Nakajima, T., Amara, S.G., Shigeri, Y., 2004. Characterization of Novel L-threo-β-Benzyloxyaspartate Derivatives, Potent Blockers of the Glutamate Transporters. *Molecular Pharmacology*, 65:1008–1015.

Shimamoto, K., Shigeri, Y., Yasuda-Kamatani, Y., Lebrun, B., Yumoto, N., Nakajima, T., 2000. Syntheses of optically pure β-hydroxyaspartate derivatives as glutamate transporter blockers. *Bioorganic and Medicinal Chemistry Letters*, 10:2407–2410.

Sia, G.M., Béïque, J.C., Rumbaugh, G., Cho, R., Worley, P.F., Huganir, R.L., 2007. Interaction of the N-Terminal Domain of the AMPA Receptor GluR4 Subunit with the Neuronal Pentraxin NP1 Mediates GluR4 Synaptic Recruitment. *Neuron*, 55:87–102.

Siddiqui, T.J., Tari, P.K., Connor, S.A., Zhang, P., Dobie, F.A., She, K., Kawabe, H., Wang, Y.T., Brose, N., Craig, A.M., 2013. An LRRTM4-HSPG complex mediates excitatory synapse development on dentate gyrus granule cells. *Neuron*, 79:680–695.

Smalla, K.H., Matthies, H., Langnäse, K., Shabir, S., Böckers, T.M., Wyneken, U., Staak, S., Krug, M., Beesley, P.W., Gundelfinger, E.D., 2000. The synaptic glycoprotein neuroplastin is involved in long-term potentiation at hippocampal CA1 synapses. *Proceedings of the National Academy of Sciences of the United States of America*, 97:4327–4332.

Sobolevsky, A.I., Rosconi, M.P., Gouaux, E., 2009. X-ray structure, symmetry and mechanism of an AMPA-subtype glutamate receptor. *Nature*, 462:745–756.

Soler-Llavina, G.J., Arstikaitis, P., Morishita, W., Ahmad, M., Südhof, T.C., Malenka, R.C., 2013. Leucine-rich repeat transmembrane proteins are essential for maintenance of long-term potentiation. *Neuron*, 79:439–446.

Soler-Llavina, G.J., Fuccillo, M. V., Ko, J., Südhof, T.C., Malenka, R.C., 2011. The neurexin ligands, neuroligins and leucine-rich repeat transmembrane proteins, perform convergent and divergent synaptic functions in vivo. *Proceedings of the National Academy of Sciences of the United States of America*, 108:16502–16509.

Sommer, B., Keinänen, K., Verdoorn, T.A., Wisden, W., Burnashev, N., Herb, A., Köhler, M., Takagi, T., Sakmann, B., Seeburg, P.H., 1990. Flip and flop: A cell-specific functional switch in glutamate-operated channels of the CNS. *Science*, 249:1580–1585.

Sommer, B., Köhler, M., Sprengel, R., Seeburg, P.H., 1991. RNA editing in brain controls a determinant of ion flow in glutamate-gated channels. *Cell*, 67:11–19.

Spence, E.F., Dube, S., Uezu, A., Locke, M., Soderblom, E.J., Soderling, S.H., 2019. In vivo proximity proteomics of nascent synapses reveals a novel regulator of cytoskeleton-mediated synaptic maturation. *Nature Communications*, 10:386.

Spruston, N., 2008. Pyramidal neurons: Dendritic structure and synaptic integration. *Nature Reviews Neuroscience*, 9:206–221.

Stoppini, L., Buchs, P.A., Muller, D., 1991. A simple method for organotypic cultures of nervous tissue. *Journal of Neuroscience Methods*, 37:173–182.

Straub, C., Noam, Y., Nomura, T., Yamasaki, M., Yan, D., Fernandes, H.B., Zhang, P., Howe, J.R., Watanabe, M., Contractor, A., Tomita, S., 2016. Distinct Subunit Domains Govern Synaptic Stability and Specificity of the Kainate Receptor. *Cell Reports*, 16:531–544.

Subramanian, J., Michel, K., Benoit, M., Nedivi, E., 2019. CPG15/Neuritin Mimics Experience in Selecting Excitatory Synapses for Stabilization by Facilitating PSD95 Recruitment. *Cell Reports*, 28:1584-1595.e5.

Südhof, T.C., 2017. Synaptic Neurexin Complexes: A Molecular Code for the Logic of Neural Circuits. *Cell*, 171:745–769.

Sultana, A., Nakaya, N., Dong, L., Abu-Asab, M., Qian, H., Tomarev, S.I., 2014. Deletion of olfactomedin 2 induces changes in the AMPA receptor complex and impairs visual, olfactory, and motor functions in mice. *Experimental Neurology*, 261:802–811.

Sun, Y., Smirnov, M., Kamasawa, N., Yasuda, R., 2019. Rapid ultrastructural changes of PSD and extrasynaptic axon-spine interface membrane during LTP induced in single dendritic spine. *bioRxiv*, doi: https://doi.org/10.1101/840629.

Suzuki, K., Elegheert, J., Song, I., Sasakura, H., Senkov, O., Matsuda, K., Kakegawa, W., Clayton, A.J., Chang, V.T., Ferrer-Ferrer, M., Miura, E., Kaushik, R., Ikeno, M., Morioka, Y., Takeuchi, Y., Shimada, T., Otsuka, S., Stoyanov, S., Watanabe, M., Takeuchi, K., Dityatev, A., Radu Aricescu, A., Yuzaki, M., 2020. A synthetic synaptic organizer protein restores glutamatergic neuronal circuits. *Science*, 369:6507.

Swanson, G.T., Kamboj, S.K., Cull-Candy, S.G., 1997. Single-channel properties of recombinant AMPA receptors depend on RNA editing, splice variation, and subunit composition. *Journal of Neuroscience*, 17:58–69.

Takano, T., Wallace, J.T., Baldwin, K.T., Purkey, A.M., Uezu, A., Courtland, J.L., Soderblom, E.J., Shimogori, T., Maness, P.F., Eroglu, C., Soderling, S.H., 2020. Chemico-genetic discovery of astrocytic control of inhibition in vivo. *Nature*, 588:296–302.

Tan, H.L., Chiu, S.L., Zhu, Q., Huganir, R.L., 2020. GRIP1 regulates synaptic plasticity and learning and memory. *Proceedings of the National Academy of Sciences of the United States of America*, 117:25085–25091.

Tang, A.H., Chen, H., Li, T.P., Metzbower, S.R., MacGillavry, H.D., Blanpied, T.A., 2016. A trans-synaptic nanocolumn aligns neurotransmitter release to receptors. *Nature*, 536:210–214.

Tang, S., Wang, T., Zhang, X., Guo, Y., Xu, P., Zeng, J., Luo, Z., Li, D., Zheng, Y., Luo, Y., Yu, C., Xu, Z., 2020. Olfactomedin-3 Enhances Seizure Activity by Interacting With AMPA Receptors in Epilepsy Models. *Frontiers in Cell and Developmental Biology*, 8:722.

Tao, W., Díaz-Alonso, J., Sheng, N., Nicoll, R.A., 2018. Postsynaptic d1 glutamate receptor assembles and maintains hippocampal synapses via Cbln2 and neurexin. *Proceedings of the National Academy of Sciences of the United States of America*, 115:E5373–E5381.

Ting, A.Y., Stawski, P.S., Draycott, A.S., Udeshi, N.D., Lehrman, E.K., Wilton, D.K., Svinkina, T., Deerinck, T.J., Ellisman, M.H., Stevens, B., Carr, S.A., Ting, A.Y., 2016. Proteomic Analysis of Unbounded Cellular Compartments: Synaptic Clefts. *Cell*, 166:1295-1307.e21.

Tomita, S., Adesnik, H., Sekiguchi, M., Zhang, W., Wada, K., Howe, J.R., Nicoll, R.A., Bredt, D.S., 2005. Stargazin modulates AMPA receptor gating and trafficking by distinct domains. *Nature*, 435:1052–1058.

Tomita, S., Chen, L., Kawasaki, Y., Petralia, R.S., Wenthold, R.J., Nicoll, R.A., Bredt, D.S., 2003. Functional studies and distribution define a family of transmembrane AMPA receptor regulatory proteins. *Journal of Cell Biology*, 161:805–816.

Traynelis, S.F., Wollmuth, L.P., McBain, C.J., Menniti, F.S., Vance, K.M., Ogden, K.K., Hansen, K.B., Yuan, H., Myers, S.J., Dingledine, R., 2010. Glutamate receptor ion channels: Structure, regulation, and function. *Pharmacological Reviews*, 62:405–496.

Trinkle-Mulcahy, L., 2019. Recent advances in proximity-based labeling methods for interactome mapping. *F1000Research*, 8:135.

Tsui, C.C., Copeland, N.G., Gilbert, D.J., Jenkins, N.A., Barnes, C., Worley, P.F., 1996. Narp, a novel member of the pentraxin family, promotes neurite outgrowth and is dynamically regulated by neuronal activity. *Journal of Neuroscience*, 16:2463–2478.

Twomey, E.C., Yelshanskaya, M. V., Grassucci, R.A., Frank, J., Sobolevsky, A.I., 2017. Structural Bases of Desensitization in AMPA Receptor-Auxiliary Subunit Complexes. *Neuron*, 94:569-580.e5.

Twomey, E.C., Yelshanskaya, M. V., Vassilevski, A.A., Sobolevsky, A.I., 2018. Mechanisms of Channel Block in Calcium-Permeable AMPA Receptors. *Neuron*, 99:956-968.e4.

Tzingounis, A. V., Wadiche, J.I., 2007. Glutamate transporters: Confining runaway excitation by shaping synaptic transmission. *Nature Reviews Neuroscience*, 8:935–947.

Uezu, A., Kanak, D.J., Bradshaw, T.W.A., Soderblom, E.J., Catavero, C.M., Burette, A.C., Weinberg, R.J., Soderling, S.H., 2016. Identification of an elaborate complex mediating postsynaptic inhibition. *Science*, 353:1123–1129.

Um, J.W., Choi, T.Y., Kang, H., Cho, Y.S., Choii, G., Uvarov, P., Park, D., Jeong, D., Jeon, S., Lee, D., Kim, H., Lee, S.H., Bae, Y.C., Choi, S.Y., Airaksinen, M.S., Ko, J., 2016. LRRTM3 Regulates Excitatory Synapse Development through Alternative Splicing and Neurexin Binding. *Cell Reports*, 14:808–822.

van Huijstee, A.N., Kessels, H.W., 2020. Variance analysis as a tool to predict the mechanism underlying synaptic plasticity. *Journal of Neuroscience Methods*, 331:108526.

Van't Spijker, H., Rowlands, D., Rossier, J., Haenzi, B., Fawcett, J., Kwok, J., 2019. Neuronal Pentraxin 2 Binds PNNs and Enhances PNN Formation. Neural Plasticity, 2019, 1-13.

Vemula, S.K., Malci, A., Junge, L., Lehmann, A.-C., Rama, R., Hradsky, J., Matute, R.A., Weber, A., Prigge, M., Naumann, M., Kreutz, M.R., Seidenbecher, C.I., Gundelfinger, E.D., Herrera-Molina, R., Vemula, S.K., Malci, A., Junge, L., Lehmann, A.-C., Rama, R., Hradsky, J., Matute, R.A., Weber, A., Prigge, M., Naumann, M., Kreutz, M.R., Seidenbecher, C.I., Gundelfinger, E.D., Herrera-Molina, R., 2020. TRAF6 controls spinogenesis instructing synapse density and neuronal activity through binding neuroplastin. *bioRxiv*, doi: https://doi.org/10.1101/768341.

Vignes, M., Collingridge, G.L., 1997. The synaptic activation of kainate receptors. *Nature*, 388:179–182.

von Engelhardt, J., Mack, V., Sprengel, R., Kavenstock, N., Li, K.W., Stern-bach, Y., Smit, A.B., Seeburg, P.H., Monyer, H., 2010. CKAMP44: A Brain-Specific Protein Attenuating Short-Term Synaptic Plasticity in the Dentate Gyrus. *Science*, 327:1518–1522.

Wang, Q., Chiu, S.L., Koropouli, E., Hong, I., Mitchell, S., Easwaran, T.P., Hamilton, N.R., Gustina, A.S., Zhu, Q., Ginty, D.D., Huganir, R.L., Kolodkin, A.L., 2017. Neuropilin-2/PlexinA3 Receptors Associate with GluA1 and Mediate Sema3F-Dependent Homeostatic Scaling in Cortical Neurons. *Neuron*, 96:1084-1098.e7.

Wang, R., Mellem, J.E., Jensen, M., Brockie, P.J., Walker, C.S., Hoerndli, F.J., Hauth, L., Madsen, D.M., Maricq, A. V., 2012. The SOL-2/Neto Auxiliary Protein Modulates the Function of AMPA-Subtype Ionotropic Glutamate Receptors. *Neuron*, 75:838–850.

Wang, X., Zhang, C., Szábo, G., Sun, Q.Q., 2013. Distribution of CaMKIIα expression in the brain in vivo, studied by CaMKIIα-GFP mice. *Brain Research*, 1518:9–25.

Washburn, H.R., Xia, N.L., Zhou, W., Mao, Y.T., Dalva, M.B., 2020. Positive surface charge of GluN1 N-terminus mediates the direct interaction with EphB2 and NMDAR mobility. *Nature Communications*, 11:570.

Watkins, J.C., Evans, R.H., 1981. Excitatory amino acid transmitters. *Annual review of pharmacology and toxicology*, 21:165–204.

Watson, J., Pinggera, A., Ho, H., Greger, I., 2020. AMPA receptor anchoring at CA1 synapses is determined by an interplay of N-terminal domain and TARP γ8 interactions. *bioRxiv*, doi: https://doi.org/10.1101/2020.07.09.196154.

Watson, J.F., García-Nafría, J., 2019. In vivo DNA assembly using common laboratory bacteria: A re-emerging tool to simplify molecular cloning. *Journal of Biological Chemistry*, 294:15271–15281.

Watson, J.F., Ho, H., Greger, I.H., 2017. Synaptic transmission and plasticity require AMPA receptor anchoring via its N-terminal domain. *eLife*, 6:e23024.

Wei, M., Wang, M., Wang, J., Su, F., Wang, Y., Sun, M., Wang, S., Liu, M., Wang, H., Lu, M., Li, W., Gong, Y., Yang, L., Zhang, C., 2020. PORCN Negatively Regulates AMPAR Function Independently of Subunit Composition and the Amino-Terminal and Carboxy-Terminal Domains of AMPARs. *Frontiers in Cell and Developmental Biology*, 8:829.

Wei, M., Zhang, J., Jia, M., Yang, C., Pan, Y., Li, S., Luo, Y., Zheng, J., Ji, J., Chen, J., Hu, X., Xiong, J., Shi, Y., Zhang, C., 2016. α/β-Hydrolase domain-containing 6 (ABHD6) negatively regulates the surface delivery and synaptic function of AMPA receptors. *Proceedings of the National Academy of Sciences of the United States of America*, 113:E2695–E2704.

Wiegert, J.S., Gee, C.E., Oertner, T.G., 2017a. Viral vector-based transduction of slice cultures. *Cold Spring Harbor Protocols*, 2017:131–134.

Wiegert, J.S., Gee, C.E., Oertner, T.G., 2017b. Single-cell electroporation of neurons. *Cold Spring Harbor Protocols*, 2017:135–138.

Wisden, W., Seeburg, P.H., 1993. A complex mosaic of high-affinity kainate receptors in rat brain. *Journal of Neuroscience*, 13:3582–3598.

Wozny, C., Breustedt, J., Wolk, F., Varoqueaux, F., Boretius, S., Zivkovic, A.R., Neeb, A., Frahm, J., Schmitz, D., Brose, N., Ivanovic, A., 2009. The function of glutamatergic synapses is not perturbed by severe knockdown of 4.1N and 4.1G expression. *Journal of Cell Science*, 122:735–744.

Wu, H., Nash, J.E., Zamorano, P., Garner, C.C., 2002. Interaction of SAP97 with minus-end-directed actin motor myosin VI: Implications for AMPA receptor trafficking. *Journal of Biological Chemistry*, 277:30928–30934.

Xie, X., Liaw, J.S., Baudry, M., Berger, T.W., 1997. Novel expression mechanism for synaptic potentiation: Alignment of presynaptic release site and postsynaptic receptor. *Proceedings of the National Academy of Sciences of the United States of America*, 94:6983–6988.

Xu, D., Hopf, C., Reddy, R., Cho, R.W., Guo, L., Lanahan, A., Petralia, R.S., Wenthold, R.J., O'Brien, R.J., Worley, P., 2003. Narp and NP1 form heterocomplexes that function in developmental and activity-dependent synaptic plasticity. *Neuron*, 39:513–528.

Yamasaki, M., Fukaya, M., Yamazaki, M., Azechi, H., Natsume, R., Abe, M., Sakimura, K., Watanabe, M., 2016. TARP γ-2 and γ-8 differentially control AMPAR density across schaffer collateral/commissural synapses in the hippocampal CA1 area. *Journal of Neuroscience*, 36:4296–4312.

Yamashita, N., Usui, H., Nakamura, F., Chen, S., Sasaki, Y., Hida, T., Suto, F., Taniguchi, M., Takei, K., Goshima, Y., 2014. Plexin-A4-dependent retrograde semaphorin 3A signalling regulates the dendritic localization of GluA2-containing AMPA receptors. *Nature Communications*, 5:3424.

Yamazaki, M., Araki, K., Shibata, A., Mishina, M., 1992. Molecular cloning of a cDNA encoding a novel member of the mouse glutamate receptor channel family. *Biochemical and Biophysical Research Communications*, 183:886–892.

Yamazaki, M., Fukaya, M., Hashimoto, K., Yamasaki, M., Tsujita, M., Itakura, M., Abe, M., Natsume, R., Takahashi, M., Kano, M., Sakimura, K., Watanabe, M., 2010. TARPs γ-2 and γ-7 are essential for AMPA receptor expression in the cerebellum. *European Journal of Neuroscience*, 31:2204–2220.

Yang, Y., Wang, X. Bin, Frerking, M., Zhou, Q., 2008. Delivery of AMPA receptors to perisynaptic sites precedes the full expression of long-term potentiation. *Proceedings of the National Academy of Sciences of the United States of America*, 105:11388–11393.

Yang, Y., Wang, X. Bin, Zhou, Q., 2010. Perisynaptic GluR2-lacking AMPA receptors control the reversibility of synaptic and spines modifications. *Proceedings of the National Academy of Sciences of the United States of America*, 107:11999–12004.

Yuzaki, M., 2018. Two Classes of Secreted Synaptic Organizers in the Central Nervous System. *Annual Review of Physiology*, 80:243–262.

Zeng, M., Díaz-Alonso, J., Ye, F., Chen, X., Xu, J., Ji, Z., Nicoll, R.A., Zhang, M., 2019. Phase Separation-Mediated TARP/MAGUK Complex Condensation and AMPA Receptor Synaptic Transmission. *Neuron*, 104:529-543.e6.

Zhang, D., Watson, J.F., Matthews, P.M., Cais, O., Greger, I.H., 2021. Gating and modulation of a hetero-octameric AMPA glutamate receptor. *Nature*, doi, https://doi.org/10.1038/s41586-021-03613-0

Zhang, W., St-Gelais, F., Grabner, C.P., Trinidad, J.C., Sumioka, A., Morimoto-Tomita, M., Kim, K.S., Straub, C., Burlingame, A.L., Howe, J.R., Tomita, S., 2009. A Transmembrane Accessory Subunit that Modulates Kainate-Type Glutamate Receptors. *Neuron*, 61:385–396.

Zhao, Y., Chen, S., Swensen, A.C., Qian, W-J., Gouaux, E., Architecture and subunit arrangement of native AMPA receptors elucidated by cryo-EM. *Science*, 364:355–362.

Zheng, Y., Brockie, P.J., Mellem, J.E., Madsen, D.M., Walker, C.S., Francis, M.M., Maricq, A. V., 2006. SOL-1 is an auxiliary subunit that modulates the gating of GLR-1 glutamate receptors in Caenorhabditis elegans. *Proceedings of the National Academy of Sciences of the United States of America*, 103:1100–1105.

Zheng, Y., Mellem, J.E., Brockie, P.J., Madsen, D.M., Maricq, A.V., 2004. SOL-1 is a CUB-domain protein required for GLR-1 glutamate receptor function in C. elegans. *Nature*, 427:451–457.

Zhou, Z., Hu, J., Passafaro, M., Xie, W., Jia, Z., 2011. GluA2 (GluR2) regulates metabotropic glutamate receptor-dependent long-term depression through N-cadherin-dependent and cofilin-mediated actin reorganization. *Journal of Neuroscience*, 31:819–833.

Zhu, J.J., Esteban, J.A., Hayashi, Y., Malinow, R., 2000. Postnatal synaptic potentiation: Delivery of GluR4-containing AMPA receptors by spontaneous activity. *Nature Neuroscience*, 3:1098–1106.

Zolotukhin, S., Byrne, B.J., Mason, E., Zolotukhin, I., Potter, M., Chesnut, K., Summerford, C., Samulski, R.J., Muzyczka, N., 1999. Recombinant adeno-associated virus purification using novel methods improves infectious titer and yield. *Gene Therapy*, 6:973–985.

Zucker, R.S., 1989. Short-term synaptic plasticity. *Annual Review of Neuroscience*, 12:13–31.

Zucker, R.S., Regehr, W.G., 2002. Short-term synaptic plasticity. *Annual Review of Physiology*, 64:355–405.

Zuo, J., De Jager, P.L., Takahashi, K.A., Jiang, W., Linden, D.J., Heintz, N., 1997. Neurodegeneration in Lurcher mice caused by mutation in δ2 glutamate receptor gene. *Nature*, 388:769–773.

Appendix A

Proximity-labelling proteomics datasets

Enrichment values are Log_2 transformed and displayed as a heat map according to intensity.

Detection of NTD interactors from the literature marked as yes (Y) or no (N)

Ranking	BioID2_1	BioID2_2	BioID2_3	BioID2_Average	BioID2_P value	MiniTurbo_1	MiniTurbo_2	MiniTurbo_3	MiniTurbo_Average	MiniTurbo_P value	TurboID_1	TurboID_2	TurboID_3	Turbo_Average	Turbo_P value	Overall	Uniprot	Gene names	Protein names
1	0.0	0.0	0.0	0.0	0.5	-0.4	-0.6	-0.1	0.1	5.0	6.3	5.1	5.4	2.9	2.7	CA2D1_MOUSE	Cacna2d1	Voltage-dependent calcium channel subunit alpha-2/delta-1
2	0.0	0.0	0.0	0.0	-0.7	-2.1	-0.7	-1.2	0.8	3.2	7.4	6.7	5.8	1.3	2.6	VTM2L_MOUSE	Vstm2l	V-set and transmembrane domain-containing protein 2-like protein
3	1.4	0.1	0.4	0.6	0.3	2.0	4.1	3.1	3.1	1.3	2.7	3.4	2.8	3.0	2.8	NPTX1_MOUSE	Nptx1	Neuronal pentraxin-1
4	0.0	0.0	0.0	0.0	0.0	0.0	0.0	0.0	0.0	4.4	3.8	5.4	4.5	3.5	2.3	NOE1_MOUSE	Olfm1	Olfactomedin-1/ Noelin-1
5	0.7	-1.5	-0.1	-0.3	0.2	0.7	6.1	6.9	4.6	0.7	-1.7	4.3	4.1	2.2	0.5	2.2	FRS1L_MOUSE	Frrs1l	DOMON domain-containing protein FRRS1L
6	0.0	0.0	0.0	0.0	-1.0	0.0	0.4	-0.2	0.0	2.5	5.7	5.2	4.4	1.3	2.2	NELL2_MOUSE	Nell2	Protein kinase C-binding protein NELL2
7	-0.1	-0.9	-0.5	-0.5	0.4	1.1	1.0	-0.8	0.4	0.2	3.9	4.4	4.2	4.2	3.4	2.1	STIM2_MOUSE	Stim2	Stromal interaction molecule 2
8	0.0	0.0	0.0	0.0	0.0	0.0	0.0	0.0	0.0	0.0	0.9	4.1	7.1	4.0	0.8	2.0	DYN2_MOUSE	Dnm2	Dynamin-2
9	0.0	0.0	0.0	0.0	-1.0	1.5	1.9	0.8	0.2	3.3	3.2	4.2	3.6	2.3	2.0	TMX4_MOUSE	Tmx4	Thioredoxin-related transmembrane protein 4
10	-0.1	-0.3	-0.9	-0.5	0.2	1.7	1.5	0.9	1.4	0.6	2.9	3.1	3.9	3.3	2.1	1.9	CHID1_MOUSE	Chid1	Chitinase domain-containing protein 1
11	0.2	0.3	-0.3	0.1	0.0	0.0	0.9	-0.4	0.2	0.1	1.0	4.8	5.0	3.6	1.0	1.9	PPIB_MOUSE	Ppib	Peptidyl-prolyl cis-trans isomerase B;Peptidyl-prolyl cis-trans isomerase
12	0.0	0.0	0.0	0.0	0.0	0.4	5.0	5.6	3.7	0.8	1.7	2.0	2.0	1.9	3.5	1.9	NPTXR_MOUSE	Nptxr	Neuronal pentraxin receptor
13	0.0	0.0	0.0	0.0	0.6	0.0	2.2	0.9	0.8	5.0	2.0	2.6	3.2	1.0	1.8	ABCA2_MOUSE	Abca2	ATP-binding cassette sub-family A member 2
14	0.0	0.0	0.0	0.0	0.5	-1.5	-1.0	-0.6	0.4	3.4	3.8	4.1	3.8	2.5	1.7	Q6ZQ56_MOUSE	mKIAA0743	Neurexin-3
15	-0.1	-0.2	-1.1	-0.4	0.1	-1.3	0.0	-0.9	-0.8	0.5	3.4	3.2	5.3	4.0	1.9	1.7	RYR2_MOUSE	Ryr2	Ryanodine receptor 2
16	0.0	0.0	0.0	0.0	0.7	-0.1	-0.2	0.1	0.1	4.3	4.0	1.3	3.2	1.1	1.6	EXTL2_MOUSE	Extl2	Exostosin-like 2
17	-0.1	-1.6	-0.8	-0.8	0.5	3.0	2.2	2.1	2.5	0.8	2.3	2.4	2.1	2.3	3.2	1.5	CNTP1_MOUSE	Cntnap1	Contactin-associated protein 1
18	-0.2	1.1	0.8	0.6	0.5	0.0	0.0	0.0	0.0	3.1	0.5	4.6	2.7	0.9	1.5	SYPH_MOUSE	Syp	Synaptophysin
19	0.0	0.0	0.0	0.0	0.0	0.9	1.7	0.8	1.1	0.5	0.6	1.6	4.8	2.3	0.7	1.5	NCAN_MOUSE	Ncan	Neurocan core protein
20	0.0	0.0	0.0	0.0	0.0	-0.3	3.7	2.5	2.0	0.6	2.6	1.2	1.8	1.9	1.7	1.4	P4HA1_MOUSE	P4ha1	Prolyl 4-hydroxylase subunit alpha-1
21	0.1	0.9	0.7	0.5	0.8	0.3	6.5	0.7	2.5	0.6	-0.3	0.8	3.4	1.3	0.3	1.4	EFTU_MOUSE	Tufm	Elongation factor Tu, mitochondrial
22	0.0	0.0	0.0	0.0	0.3	0.1	-0.1	0.1	0.0	2.3	2.8	3.2	2.8	1.7	1.4	L1CAM_MOUSE	L1cam	Neural cell adhesion molecule L1
23	0.9	0.1	-0.5	0.2	0.1	1.3	4.6	7.5	4.5	0.7	0.4	0.0	0.9	0.4	0.1	1.4	CNPY3_MOUSE	Cnpy3	Protein canopy homolog 3
24	0.0	-0.1	0.5	0.2	0.3	0.0	0.0	0.0	0.0	3.4	4.1	0.4	2.6	0.8	1.4	SHSA6_MOUSE	Shisa6	Protein shisa-6 homolog
25	1.0	0.2	-0.6	0.2	0.2	2.6	0.4	1.1	1.3	0.6	1.0	0.4	4.1	1.8	0.6	1.3	LGI1_MOUSE	Lgi1	Leucine-rich glioma-inactivated protein 1
26	0.0	0.0	0.0	0.0	-0.5	3.5	4.6	2.5	0.7	0.6	1.3	1.4	1.1	1.4	1.2	TICN2_MOUSE	Spock2	SPARC/ Osteonectin
27	0.0	0.0	0.0	0.0	0.0	2.5	0.2	0.9	0.5	2.0	-1.8	5.1	1.7	0.4	1.1	ALDH2_MOUSE	Aldh2	Aldehyde dehydrogenase, mitochondrial
28	0.0	0.0	0.0	0.0	-1.4	0.3	1.6	0.2	0.1	1.2	3.7	1.5	2.1	0.9	1.1	PP2BA_MOUSE	Ppp3ca	Serine/threonine-protein phosphatase 2B catalytic subunit alpha isoform
29	0.5	-0.3	0.5	0.2	0.2	0.0	0.0	0.0	0.0	-1.2	2.9	4.4	2.1	0.6	1.1	1433F_MOUSE	Ywhah	14-3-3 protein eta
30	2.9	0.4	-1.6	0.6	0.2	1.1	1.6	2.4	1.7	2.2	1.0	1.2	0.8	1.0	2.1	1.1	ERO1A_MOUSE	Ero1l	ERO1-like protein alpha
31	0.2	1.1	-0.2	0.4	0.4	0.0	6.6	5.5	4.0	0.9	0.9	-0.8	-0.3	-0.1	0.0	1.1	THIL_MOUSE	Acat1	Acetyl-CoA acetyltransferase, mitochondrial
32	0.2	0.4	-0.5	0.1	0.1	4.5	6.3	0.8	3.9	1.1	0.5	-0.9	0.9	0.2	0.1	1.1	IDH3A_MOUSE	Idh3b	Isocitrate dehydrogenase [NAD] subunit, mitochondrial
33	-0.5	2.4	0.7	0.9	0.3	2.6	1.7	-0.8	1.2	0.7	3.2	0.0	1.1	0.3	1.0	ECHB_MOUSE	Hadhb	Trifunctional enzyme subunit beta, mitochondrial
34	0.0	0.0	0.0	0.0	0.0	0.0	0.0	0.0	0.0	1.2	3.0	2.0	2.1	1.0	1.0	CTP5C_MOUSE	Cntnap5c	Contactin-associated protein like 5-3
35	0.3	0.5	0.2	0.3	0.4	0.0	0.0	0.0	0.0	1.0	3.8	0.8	1.9	0.6	1.0	1433G_MOUSE	Ywhag	14-3-3 protein gamma;14-3-3 protein gamma, N-terminally processed
36	0.4	0.9	0.6	0.6	1.1	0.0	0.0	0.0	0.0	1.2	2.8	1.2	1.7	1.2	1.0	PTPRS_MOUSE	Ptprs	Receptor-type tyrosine-protein phosphatase S
37	-0.1	-0.1	0.5	0.1	0.1	5.9	4.8	-0.1	3.5	0.9	0.6	-0.6	0.3	0.1	0.1	1.0	TBA4A_MOUSE	Tuba4a	Tubulin alpha-4A chain
38	0.0	0.0	0.0	0.0	0.7	6.2	1.5	2.8	0.6	-0.1	0.2	1.4	0.5	0.6	1.0	IDH3A_MOUSE	Idh3a	Isocitrate dehydrogenase [NAD] subunit alpha, mitochondrial
39	-0.5	-0.1	-0.3	0.8	-0.7	-0.1	-2.8	-1.2	0.4	3.6	2.0	2.3	2.6	2.0	1.0	GRM1_MOUSE	Grm1	Metabotropic glutamate receptor 1
40	-0.2	-0.9	2.0	0.3	0.1	-1.0	3.4	1.4	1.3	0.5	2.1	0.9	0.4	1.1	0.5	0.9	GLT17_MOUSE	Wbscr17	Polypeptide N-acetylgalactosaminyltransferase
41	0.0	0.0	0.0	0.0	0.0	0.7	3.3	3.8	2.6	0.7	-0.1	1.4	0.5	0.6	0.5	0.9	CNPY4_MOUSE	Cnpy4	Protein canopy homolog 4
42	0.0	0.0	0.0	0.0	1.5	-2.0	-2.7	-1.1	0.4	1.8	1.9	3.4	2.4	1.4	0.9	SLIT1_MOUSE	Slit1	Slit homolog 1 protein
43	2.3	-0.1	0.3	0.8	0.2	0.2	2.2	2.2	1.5	1.4	0.6	0.4	1.0	0.6	1.3	0.9	LRP1B_MOUSE	Lrp1b	Low-density lipoprotein receptor-related protein 1B
44	0.2	0.0	-0.8	-0.2	0.2	1.0	3.3	1.7	2.0	0.6	0.6	1.2	1.0	0.9	1.8	0.9	GHC1_MOUSE	Slc25a22	Mitochondrial glutamate carrier 1
45	0.0	0.0	0.0	0.0	0.0	0.0	0.0	0.0	0.0	-0.2	2.8	2.8	1.8	0.7	0.9	CUL2_MOUSE	Cul2	Cullin-2
46	0.0	0.0	0.0	0.0	-1.3	-2.2	-0.4	-1.3	0.9	2.8	3.3	1.2	2.4	2.0	0.9	SORT_MOUSE	Sort1	Sortilin
47	0.3	0.2	-0.4	0.0	0.0	0.0	0.0	0.0	0.0	-0.9	2.5	3.7	1.8	0.7	0.9	SYN2_MOUSE	Syn2	Synapsin-2
48	-1.1	-2.0	-4.4	-2.5	0.7	-1.6	-0.7	-1.8	-1.3	1.3	4.4	4.4	2.2	3.7	1.6	0.9	CA2D3_MOUSE	Cacna2d3	Voltage-dependent calcium channel subunit alpha-2/delta-3
49	0.0	0.0	0.0	0.0	0.5	-2.8	-1.4	-1.3	0.7	1.0	1.2	4.9	2.3	1.2	0.9	THTM_MOUSE	Mpst	3-mercaptopyruvate sulfurtransferase
50	0.1	0.1	0.7	0.3	0.5	0.0	0.0	0.0	0.0	3.0	1.0	0.7	1.6	0.7	0.8	VGLU1_MOUSE	Slc17a7	Vesicular glutamate transporter 1

Figure A.1 *GluA2Q NTD-enriched proteins identified by BirA* PL proteomics.*

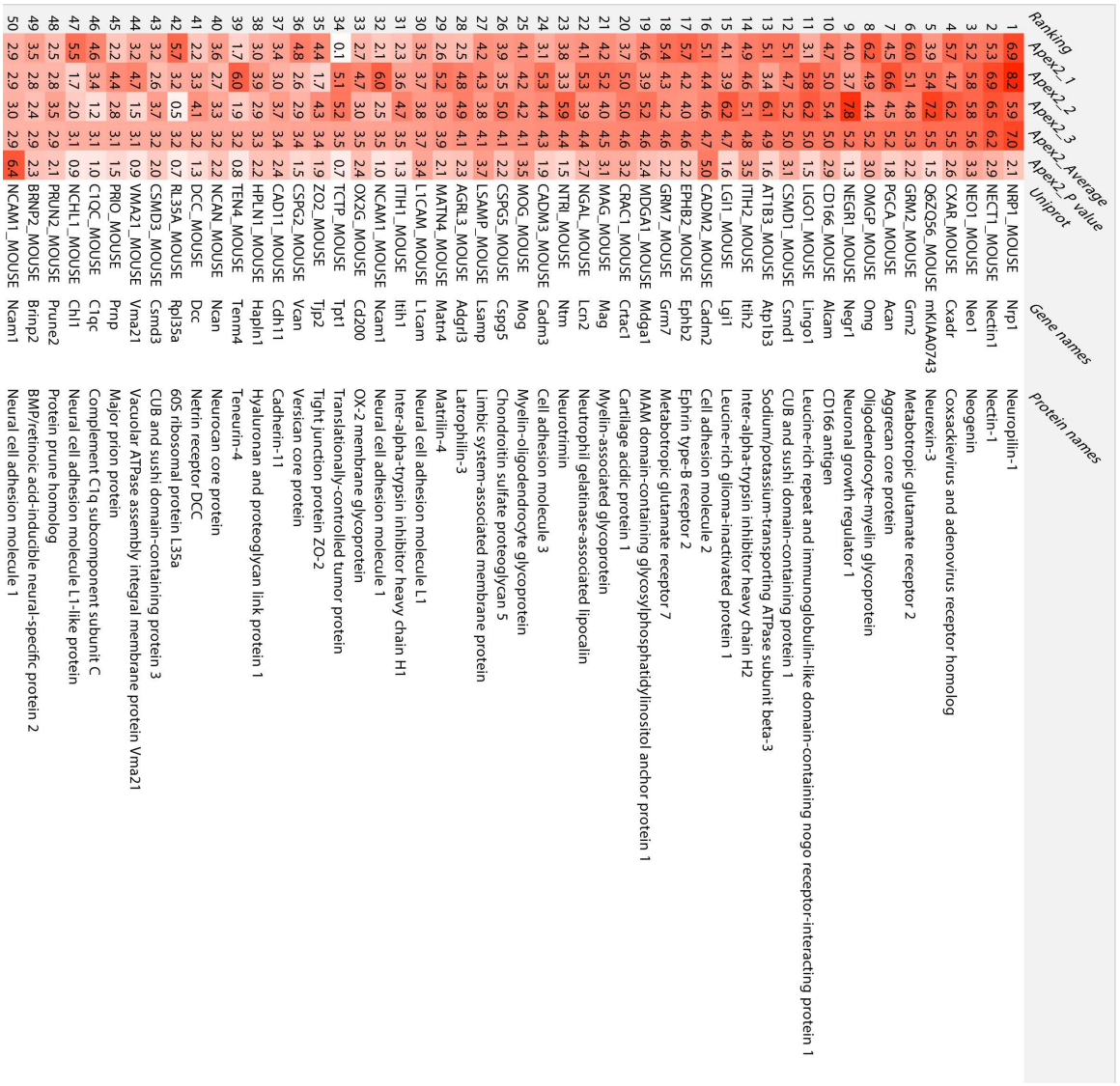

Ranking	Apex2_1	Apex2_2	Apex2_3	Apex2_Average	Apex2_P value	Uniprot	Gene names	Protein names
1	6.9	8.2	5.9	7.0	2.1	NRP1_MOUSE	Nrp1	Neuropilin-1
2	5.3	6.9	6.5	6.2	2.9	NECT1_MOUSE	Nectin1	Nectin-1
3	5.2	5.8	5.8	5.6	3.3	NEO1_MOUSE	Neo1	Neogenin
4	5.7	4.7	6.2	5.5	2.6	CXAR_MOUSE	Cxadr	Coxsackievirus and adenovirus receptor homolog
5	3.9	5.4	7.2	5.5	1.5	Q6ZQ56_MOUSE	mKIAA0743	Neurexin-3
6	6.0	5.1	4.8	5.3	2.2	GRM2_MOUSE	Grm2	Metabotropic glutamate receptor 2
7	4.5	6.6	4.5	5.2	1.8	PGCA_MOUSE	Acan	Aggrecan core protein
8	6.2	4.9	4.4	5.2	3.0	OMGP_MOUSE	Omg	Oligodendrocyte-myelin glycoprotein
9	4.0	3.7	7.8	5.2	1.3	NEGR1_MOUSE	Negr1	Neuronal growth regulator 1
10	4.7	5.0	5.4	5.0	2.9	CD166_MOUSE	Alcam	CD166 antigen
11	3.1	5.8	6.2	5.0	1.5	LIGO1_MOUSE	Lingo1	Leucine-rich repeat and immunoglobulin-like domain-containing nogo receptor-interacting protein 1
12	5.1	4.7	5.2	5.0	3.1	CSMD1_MOUSE	Csmd1	CUB and sushi domain-containing protein 1
13	5.1	3.4	6.1	4.9	1.6	AT1B3_MOUSE	Atp1b3	Sodium/potassium-transporting ATPase subunit beta-3
14	4.9	4.6	5.1	4.8	3.5	ITIH2_MOUSE	Itih2	Inter-alpha-trypsin inhibitor heavy chain H2
15	4.1	3.9	6.2	4.7	1.6	LGI1_MOUSE	Lgi1	Leucine-rich glioma-inactivated protein 1
16	5.1	4.4	4.6	4.7	5.0	CADM2_MOUSE	Cadm2	Cell adhesion molecule 2
17	5.7	4.2	4.0	4.6	2.2	EPHB2_MOUSE	Ephb2	Ephrin type-B receptor 2
18	5.4	4.3	4.2	4.6	2.2	GRM7_MOUSE	Grm7	Metabotropic glutamate receptor 7
19	4.6	3.9	5.2	4.6	2.4	MDGA1_MOUSE	Mdga1	MAM domain-containing glycosylphosphatidylinositol anchor protein 1
20	3.7	5.0	5.0	4.6	3.2	CRAC1_MOUSE	Crtac1	Cartilage acidic protein 1
21	4.2	5.2	4.0	4.5	3.1	MAG_MOUSE	Mag	Myelin-associated glycoprotein
22	4.1	5.3	3.9	4.4	2.7	NGAL_MOUSE	Lcn2	Neutrophil gelatinase-associated lipocalin
23	3.8	3.3	5.9	4.4	1.5	NTRI_MOUSE	Ntm	Neurotrimin
24	3.1	5.3	4.4	4.3	1.9	CADM3_MOUSE	Cadm3	Cell adhesion molecule 3
25	4.1	4.2	4.2	4.1	3.5	MOG_MOUSE	Mog	Myelin-oligodendrocyte glycoprotein
26	3.9	3.5	5.0	4.1	2.2	CSPG5_MOUSE	Cspg5	Chondroitin sulfate proteoglycan 5
27	4.2	4.3	3.8	4.1	3.7	LSAMP_MOUSE	Lsamp	Limbic system-associated membrane protein
28	2.5	4.8	4.9	4.1	2.3	AGRL3_MOUSE	Adgrl3	Latrophilin-3
29	2.6	5.2	3.9	3.9	2.1	MATN4_MOUSE	Matn4	Matrilin-4
30	3.5	3.7	3.8	3.7	3.4	L1CAM_MOUSE	L1cam	Neural cell adhesion molecule L1
31	2.3	3.6	4.7	3.5	1.3	ITIH1_MOUSE	Itih1	Inter-alpha-trypsin inhibitor heavy chain H1
32	2.1	6.0	2.5	3.5	1.0	NCAM1_MOUSE	Ncam1	Neural cell adhesion molecule 1
33	2.7	4.7	3.0	3.5	2.4	OX2G_MOUSE	Cd200	OX-2 membrane glycoprotein
34	0.1	5.1	5.2	3.5	0.7	TCTP_MOUSE	Tpt1	Translationally-controlled tumor protein
35	4.4	1.7	4.3	3.4	1.9	ZO2_MOUSE	Tjp2	Tight junction protein ZO-2
36	4.8	2.6	2.9	3.4	1.5	CSPG2_MOUSE	Vcan	Versican core protein
37	3.4	3.0	3.7	3.4	2.4	CAD11_MOUSE	Cdh11	Cadherin-11
38	3.0	3.9	2.9	3.3	2.2	HPLN1_MOUSE	Hapln1	Hyaluronan and proteoglycan link protein 1
39	1.7	6.0	1.9	3.2	0.8	TEN4_MOUSE	Tenm4	Teneurin-4
40	3.6	2.7	3.3	3.2	2.2	NCAN_MOUSE	Ncan	Neurocan core protein
41	2.2	3.3	4.1	3.2	1.3	DCC_MOUSE	Dcc	Netrin receptor DCC
42	5.7	3.2	0.5	3.2	0.7	RL35A_MOUSE	Rpl35a	60S ribosomal protein L35a
43	3.2	2.6	3.7	3.2	2.0	CSMD3_MOUSE	Csmd3	CUB and sushi domain-containing protein 3
44	3.2	4.7	1.5	3.1	0.9	VMA21_MOUSE	Vma21	Vacuolar ATPase assembly integral membrane protein Vma21
45	2.2	4.4	2.8	3.1	1.5	PRIO_MOUSE	Prnp	Major prion protein
46	4.6	3.4	1.2	3.1	1.0	C1QC_MOUSE	C1qc	Complement C1q subcomponent subunit C
47	5.5	1.7	2.0	3.1	0.9	NCHL1_MOUSE	Chl1	Neural cell adhesion molecule L1-like protein
48	2.5	2.8	3.5	2.9	2.1	PRUN2_MOUSE	Prune2	Protein prune homolog
49	3.5	2.8	2.4	2.9	2.3	BRNP2_MOUSE	Brinp2	BMP/retinoic acid-inducible neural-specific protein 2
50	2.9	2.9	3.0	2.9	6.4	NCAM1_MOUSE	Ncam1	Neural cell adhesion molecule 1

Figure A.2 *GluA2Q NTD-enriched proteins identified by Apex2 PL proteomics.*

Ranking	BioID2_1	BioID2_2	BioID2_3	BioID2_Average	BioID2_P value	MiniTurbo_1	MiniTurbo_2	MiniTurbo_3	MiniTurbo_Average	MiniTurbo_P value	TurboID_1	TurboID_2	TurboID_3	Turbo_Average	Turbo_P value	Apex2_1	Apex2_2	Apex2_3	Apex2_Average	Apex2_P value	Overall	Uniprot	Gene names	Protein names
1	0.0	0.0	0.0	0.0	0.5	-1.5	-1.0	-0.6	0.4	3.4	3.8	4.1	3.8	2.5	3.9	5.4	7.2	5.5	1.5	2.2	Q6ZQ56_MOUSE	mKIAA0743	Neurexin-3
2	1.0	0.2	-0.6	0.2	0.2	2.6	0.4	1.1	1.3	0.6	1.0	0.4	4.1	1.8	0.6	4.1	3.9	6.2	4.7	1.6	2.0	LGI1_MOUSE	Lgi1	Leucine-rich glioma-inactivated protein 1
3	1.4	0.1	0.4	0.6	0.3	2.0	4.1	3.1	3.1	1.3	2.7	3.4	2.8	3.0	2.8	0.6	0.4	1.0	0.7	2.1	1.8	NPTX1_MOUSE	Nptx1	Neuronal pentraxin-1
4	0.0	0.0	0.0	0.0	0.0	0.0	0.0	0.0	0.0	0.0	0.0	0.0	0.0	0.0	6.9	8.2	5.9	7.0	2.1	1.8	NRP1_MOUSE	Nrp1	Neuropilin-1
5	0.0	0.0	0.0	0.0	0.5	-0.4	-0.6	-0.1	0.1	5.0	6.3	5.1	5.4	2.9	1.7	3.0	0.0	1.6	0.6	1.7	CA2D1_MOUSE	Cacna2d1	Voltage-dependent calcium channel subunit alpha-2/delta-1
6	0.0	0.0	0.0	0.0	0.9	1.7	0.8	1.1	0.5	0.6	1.6	4.8	2.3	0.7	3.6	2.7	3.3	3.2	2.2	1.7	NCAN_MOUSE	Ncan	Neurocan core protein
7	0.0	0.0	0.0	0.0	0.3	0.1	-0.1	0.1	0.0	2.3	2.8	3.2	2.8	1.7	3.5	3.7	3.8	3.7	3.4	1.6	LICAM_MOUSE	L1cam	Neural cell adhesion molecule L1
8	0.0	0.0	0.0	0.0	0.0	0.0	0.0	0.0	0.0	0.0	0.0	0.0	0.0	0.0	5.3	6.9	6.5	6.2	2.9	1.6	NECT1_MOUSE	Nectin1	Nectin-1
9	0.7	-1.5	-0.1	-0.3	0.2	0.7	6.1	6.9	4.6	0.7	-1.7	4.3	4.1	2.2	0.5	-0.4	-0.7	0.0	-0.4	0.6	1.5	FRS1L_MOUSE	Frs1l	DOMON domain-containing protein FRRS1L
10	0.0	0.0	0.0	0.0	0.0	0.0	0.0	0.0	0.0	0.0	0.0	0.0	0.0	0.0	5.2	5.8	5.8	5.6	3.3	1.4	NEO1_MOUSE	Neo1	Neogenin
11	0.0	0.0	0.0	0.0	0.4	5.0	5.6	3.7	0.8	1.7	2.0	2.0	1.9	3.5	-0.4	0.2	-0.6	-0.2	0.5	1.3	NPTXR_MOUSE	Nptxr	Neuronal pentraxin receptor
12	-0.3	0.0	-0.1	-0.1	0.1	0.0	0.0	0.0	0.0	-0.2	1.7	1.2	0.9	0.7	5.4	4.3	4.2	4.6	2.2	1.3	GRM7_MOUSE	Grm7	Metabotropic glutamate receptor 7
13	0.0	0.0	0.0	0.0	0.0	0.0	0.0	0.0	0.0	0.0	0.0	0.0	0.0	0.0	6.0	5.1	4.8	5.3	2.2	1.3	GRM2_MOUSE	Grm2	Metabotropic glutamate receptor 2
14	0.0	0.0	0.0	0.0	0.0	0.0	0.0	0.0	0.0	0.0	0.0	0.0	0.0	0.0	4.5	6.6	4.5	5.2	1.8	1.3	PGCA_MOUSE	Acan	Aggrecan core protein
15	0.0	0.0	0.0	0.0	0.0	0.0	0.0	0.0	0.0	0.0	0.0	0.0	0.0	0.0	6.2	4.9	4.4	5.2	3.0	1.3	OMGP_MOUSE	Omg	Oligodendrocyte-myelin glycoprotein
16	0.0	0.0	0.0	0.0	0.0	0.0	0.0	0.0	0.0	0.0	0.0	0.0	0.0	0.0	4.0	3.7	7.8	5.2	1.3	1.3	NEGR1_MOUSE	Negr1	Neuronal growth regulator 1
17	0.0	0.0	0.0	0.0	0.0	0.0	0.0	0.0	0.0	4.4	3.8	5.4	4.5	3.5	0.7	0.3	0.8	0.6	1.6	1.3	NOE1_MOUSE	Olfm1	Olfactomedin-1/ Noelin-1
18	0.0	0.0	0.0	0.0	0.0	0.0	0.0	0.0	0.0	0.0	0.0	0.0	0.0	0.0	4.7	5.0	5.4	5.0	2.9	1.3	CD166_MOUSE	Alcam	CD166 antigen
19	0.0	0.0	0.0	0.0	0.0	0.0	0.0	0.0	0.0	0.0	0.0	0.0	0.0	0.0	3.1	5.8	6.2	5.0	1.5	1.3	LIGO1_MOUSE	Lingo1	Leucine-rich repeat and immunoglobulin-like domain-containing nogo receptor-interacting protein 1
20	0.0	0.0	0.0	0.0	0.0	0.0	0.0	0.0	0.0	0.0	0.0	0.0	0.0	0.0	5.1	4.7	5.2	5.0	3.1	1.3	CSMD1_MOUSE	Csmd1	CUB and sushi domain-containing protein 1
21	0.0	0.0	0.0	0.0	0.0	0.0	0.0	0.0	0.0	0.0	0.0	0.0	0.0	0.0	5.1	3.4	6.1	4.9	1.6	1.2	AT1B3_MOUSE	Atp1b3	Sodium/potassium-transporting ATPase subunit beta-3
22	0.0	0.0	0.0	0.0	0.0	0.0	0.0	0.0	0.0	0.0	0.0	0.0	0.0	0.0	4.9	4.6	5.1	4.8	3.5	1.2	ITIH2_MOUSE	Itih2	Inter-alpha-trypsin inhibitor heavy chain H2
23	0.0	0.0	0.0	0.0	0.0	0.0	0.0	0.0	0.0	0.0	0.0	0.0	0.0	0.0	5.1	4.4	4.6	4.7	5.0	1.2	CADM2_MOUSE	Cadm2	Cell adhesion molecule 2
24	0.0	0.0	0.0	0.0	0.0	0.0	0.0	0.0	0.0	0.0	0.0	0.0	0.0	0.0	3.0	3.9	2.9	3.3	2.2	1.2	HPLN1_MOUSE	Hapln1	Hyaluronan and proteoglycan link protein 1
25	0.0	0.0	0.0	0.0	0.0	0.0	0.0	0.0	0.0	0.0	0.0	0.0	0.0	0.0	5.7	4.2	4.0	4.6	2.2	1.2	EPHB2_MOUSE	Ephb2	Ephrin type-B receptor 2
26	0.9	0.1	-0.5	0.2	0.1	1.3	4.6	7.5	4.5	0.7	0.4	0.0	0.9	0.4	0.1	-0.1	-0.8	-0.3	-0.4	1.0	1.2	CNPY3_MOUSE	Cnpy3	Protein canopy homolog 3
27	0.0	0.0	0.0	0.0	0.0	0.0	0.0	0.0	0.0	0.0	0.9	4.1	7.1	4.0	0.8	0.5	0.2	1.0	0.6	1.1	1.2	DYN2_MOUSE	Dnm2	Dynamin-2
28	0.0	0.0	0.0	0.0	0.0	-0.7	-2.1	-0.7	-1.2	0.8	3.2	7.4	6.7	5.8	1.3	-0.7	0.5	0.1	0.0	0.1	1.1	VTM2L_MOUSE	Vstm2l	V-set and transmembrane domain-containing protein 2-like protein
29	0.2	0.3	-0.3	0.1	0.0	0.0	0.9	-0.4	0.2	0.1	1.0	4.8	5.0	3.6	1.0	0.3	0.9	0.6	0.6	1.7	1.1	PPIB_MOUSE	Ppib	Peptidyl-prolyl cis-trans isomerase B
30	0.0	0.0	0.0	0.0	0.0	0.0	0.0	0.0	0.0	0.0	0.0	0.0	0.0	0.0	4.1	5.3	3.9	4.4	2.7	1.1	NGAL_MOUSE	Lcn2	Neutrophil gelatinase-associated lipocalin
31	0.4	0.9	0.6	0.6	1.1	0.0	0.0	0.0	0.0	0.0	1.2	2.8	1.2	1.7	1.2	1.6	4.7	-0.1	2.0	1.1	PTPRS_MOUSE	Ptprs	Receptor-type tyrosine-protein phosphatase S
32	0.0	0.0	0.0	0.0	0.0	0.0	0.0	0.0	0.0	0.0	0.0	0.0	0.0	0.0	3.8	3.3	5.9	4.4	1.5	1.1	NTRL_MOUSE	Ntm	Neurotrimin
33	-0.1	-0.9	-0.5	-0.5	0.4	1.1	1.0	-0.8	0.4	0.2	3.9	4.4	4.2	4.2	3.4	0.0	0.2	0.4	0.2	0.8	1.1	STIM2_MOUSE	Stim2	Stromal interaction molecule 2
34	0.0	0.0	0.0	0.0	0.0	-1.0	1.5	1.9	0.8	0.2	3.3	3.2	4.2	3.6	2.3	-0.2	0.2	0.0	0.0	0.0	1.1	TMX4_MOUSE	Tmx4	Thioredoxin-related transmembrane protein 4
35	0.0	0.0	0.0	0.0	0.0	0.0	0.0	0.0	0.0	0.0	0.0	0.0	0.0	0.0	3.1	5.3	4.4	4.3	1.9	1.1	CADM3_MOUSE	Cadm3	Cell adhesion molecule 3
36	-0.1	-0.3	-0.9	-0.5	0.2	1.7	1.5	0.9	1.4	0.6	2.9	3.1	3.9	3.3	2.1	0.0	0.3	-0.3	0.0	0.0	1.1	CHID1_MOUSE	Chid1	Chitinase domain-containing protein 1
37	0.2	1.1	-0.2	0.4	0.4	0.0	6.6	5.5	4.0	0.9	0.9	-0.8	-0.3	-0.1	0.0	0.0	0.2	-0.5	-0.1	0.3	1.1	THIL_MOUSE	Acat1	Acetyl-CoA acetyltransferase, mitochondrial
38	-0.1	-1.6	-0.8	-0.8	0.5	3.0	2.2	2.1	2.5	0.8	2.3	2.4	2.1	2.3	3.2	0.3	0.4	0.1	0.3	1.0	1.0	CNTP1_MOUSE	Cntnap1	Contactin-associated protein 1
39	0.0	0.0	0.0	0.0	0.0	0.0	0.0	0.0	0.0	0.0	0.0	0.0	0.0	0.0	4.1	4.2	4.2	4.1	3.5	1.0	MOG_MOUSE	Mog	Myelin-oligodendrocyte glycoprotein
40	0.0	-0.1	0.5	0.2	0.3	0.0	0.0	0.0	0.0	0.0	3.4	4.1	0.4	2.6	0.8	0.9	1.7	1.5	1.4	2.8	1.0	SHSA6_MOUSE	Shisa6	Protein shisa-6 homolog
41	0.0	0.0	0.0	0.0	0.0	0.0	0.0	0.0	0.0	0.0	0.0	0.0	0.0	0.0	0.0	3.9	3.5	5.0	4.1	2.2	1.0	CSPG5_MOUSE	Cspg5	Chondroitin sulfate proteoglycan 5
42	0.0	0.0	0.0	0.0	0.0	0.0	0.0	0.0	0.0	0.0	0.0	0.0	0.0	0.0	4.2	4.3	3.8	4.1	3.7	1.0	LSAMP_MOUSE	Lsamp	Limbic system-associated membrane protein
43	0.1	0.9	0.7	0.5	0.8	0.3	6.5	0.7	2.5	0.6	-0.3	0.8	3.4	1.3	0.3	-0.4	0.0	-0.3	-0.2	0.9	1.0	EFTU_MOUSE	Tufm	Elongation factor Tu, mitochondrial
44	0.0	0.0	0.0	0.0	0.0	-0.5	3.5	4.6	2.5	0.7	0.6	1.3	1.4	1.1	1.4	0.4	0.9	0.1	0.5	0.6	1.0	TICN2_MOUSE	Spock2	SPARC/ Osteonectin
45	0.0	0.0	0.0	0.0	0.0	0.6	0.0	2.2	0.9	0.8	5.0	2.0	2.6	3.2	1.0	0.0	-0.1	-0.1	0.4	1.0	ABCA2_MOUSE	Abca2	ATP-binding cassette sub-family A member 2
46	0.0	0.0	0.0	0.0	0.0	0.0	0.0	0.0	0.0	0.0	0.0	0.0	0.0	0.0	0.0	2.5	4.8	4.9	4.1	2.3	1.0	AGRL3_MOUSE	Adgrl3	Latrophilin-3
47	0.0	0.0	0.0	0.0	0.0	-1.0	0.0	0.4	-0.2	0.0	2.5	5.7	5.2	4.4	1.3	-0.4	-0.3	-0.3	-0.3	1.5	1.0	NELL2_MOUSE	Nell2	Protein kinase C-binding protein NELL2
48	0.2	0.4	-0.5	0.1	0.1	4.5	6.3	0.8	3.9	1.1	0.5	-0.9	0.9	0.2	0.1	-0.1	0.0	-0.4	-0.2	0.4	1.0	IDH3A_MOUSE	Idh3b	Isocitrate dehydrogenase [NAD] subunit, mitochondrial
49	0.0	0.0	0.0	0.0	0.0	0.0	0.0	0.0	0.0	0.0	0.0	0.0	0.0	0.0	0.0	2.6	5.2	3.9	3.9	2.1	1.0	MATN4_MOUSE	Matn4	Matrilin-4
50	0.0	0.0	0.0	0.0	0.0	1.2	-0.5	0.0	0.2	0.2	1.1	1.0	2.5	1.5	1.1	2.3	2.0	2.1	2.1	2.9	1.0	THY1_MOUSE	Thy1	Thy-1 membrane glycoprotein

Figure A.3 *GluA2Q NTD-enriched proteins identified by all 4 PL proteomics tags.*

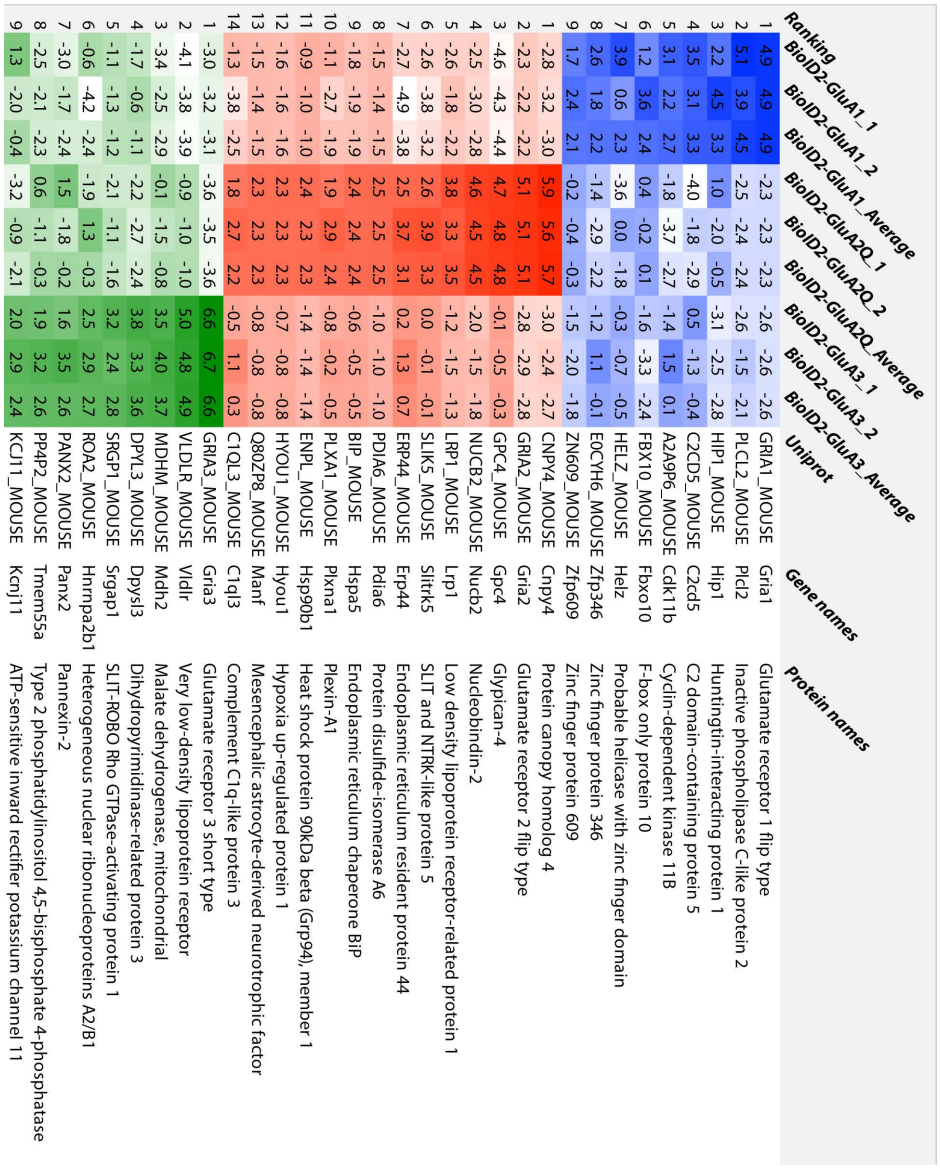

Ranking	BioID2-GluA1_1	BioID2-GluA1_2	BioID2-GluA1_Average	BioID2-GluA2Q_1	BioID2-GluA2Q_2	BioID2-GluA2Q_Average	BioID2-GluA3_1	BioID2-GluA3_2	BioID2-GluA3_Average	Uniprot	Gene names	Protein names
1	4.9	4.9	4.9	-2.3	-2.3	-2.6	-2.6	-2.6	-2.6	GRIA1_MOUSE	Gria1	Glutamate receptor 1 flip type
2	5.1	3.9	4.5	-2.5	-2.4	-2.4	-2.6	-1.5	-2.1	PLCL2_MOUSE	Plcl2	Inactive phospholipase C-like protein 2
3	2.2	4.5	3.3	1.0	-2.0	-0.5	-3.1	-2.5	-2.8	HIP1_MOUSE	Hip1	Huntingtin-interacting protein 1
4	3.5	3.1	3.3	-4.0	-1.8	-2.9	0.5	-1.3	-0.4	C2CD5_MOUSE	C2cd5	C2 domain-containing protein 5
5	3.1	2.2	2.7	-1.8	-3.7	-2.7	-1.4	1.5	0.1	A2A9P6_MOUSE	Cdk11b	Cyclin-dependent kinase 11B
6	1.2	3.6	2.4	0.4	-0.2	0.1	-1.6	-3.3	-2.4	FBX10_MOUSE	Fbxo10	F-box only protein 10
7	3.9	0.6	2.3	-3.6	0.0	-1.8	-0.3	-0.7	-0.5	HELZ_MOUSE	Helz	Probable helicase with zinc finger domain
8	2.6	1.8	2.2	-1.4	-2.9	-2.2	-1.2	1.1	-0.1	E0CYH6_MOUSE	Zfp346	Zinc finger protein 346
9	1.7	2.4	2.1	-0.2	-0.4	-0.3	-1.5	-2.0	-1.8	ZN609_MOUSE	Zfp609	Zinc finger protein 609
1	-2.8	-3.2	-3.0	5.9	5.6	5.7	-3.0	-2.4	-2.7	CNPY4_MOUSE	Cnpy4	Protein canopy homolog 4
2	-2.3	-2.2	-2.2	5.1	5.1	5.1	-2.8	-2.9	-2.8	GRIA2_MOUSE	Gria2	Glutamate receptor 2 flip type
3	-4.6	-4.3	-4.4	4.7	4.8	4.8	-0.1	-0.5	-0.3	GPC4_MOUSE	Gpc4	Glypican-4
4	-2.5	-3.0	-2.8	4.6	4.5	4.5	-2.0	-1.5	-1.8	NUCB2_MOUSE	Nucb2	Nucleobindin-2
5	-2.6	-1.8	-2.2	3.8	3.3	3.5	-1.2	-1.5	-1.3	LRP1_MOUSE	Lrp1	Low density lipoprotein receptor-related protein 1
6	-2.6	-3.8	-3.2	2.6	3.9	3.3	0.0	-0.1	-0.1	SLIK5_MOUSE	Slitrk5	SLIT and NTRK-like protein 5
7	-2.7	-4.9	-3.8	2.5	3.7	3.1	0.2	1.3	0.7	ERP44_MOUSE	Erp44	Endoplasmic reticulum resident protein 44
8	-1.5	-1.4	-1.5	2.5	2.5	2.5	-1.0	-1.0	-1.0	PDIA6_MOUSE	Pdia6	Protein disulfide-isomerase A6
9	-1.8	-1.9	-1.9	2.4	2.4	2.4	-0.6	-0.5	-0.5	BIP_MOUSE	Hspa5	Endoplasmic reticulum chaperone BiP
10	-1.1	-2.7	-1.9	1.9	2.9	2.4	-0.8	-0.2	-0.5	PLXA1_MOUSE	Plxna1	Plexin-A1
11	-0.9	-1.0	-1.0	2.4	2.3	2.3	-1.4	-1.4	-1.4	ENPL_MOUSE	Hsp90b1	Heat shock protein 90kDa beta (Grp94), member 1
12	-1.6	-1.6	-1.6	2.3	2.3	2.3	-0.7	-0.8	-0.8	HYOU1_MOUSE	Hyou1	Hypoxia up-regulated protein 1
13	-1.5	-1.4	-1.5	2.3	2.3	2.3	-0.8	-0.8	-0.8	Q80ZP8_MOUSE	Manf	Mesencephalic astrocyte-derived neurotrophic factor
14	-1.3	-3.8	-2.5	1.8	2.7	2.2	-0.5	1.1	0.3	C1QL3_MOUSE	C1ql3	Complement C1q-like protein 3
1	-3.0	-3.2	-3.1	-3.6	-3.5	-3.6	6.6	6.7	6.6	GRIA3_MOUSE	Gria3	Glutamate receptor 3 short type
2	-4.1	-3.8	-3.9	-0.9	-1.0	-1.0	5.0	4.8	4.9	VLDLR_MOUSE	Vldlr	Very low-density lipoprotein receptor
3	-3.4	-2.5	-2.9	-0.1	-1.5	-0.8	3.5	4.0	3.7	MDHM_MOUSE	Mdh2	Malate dehydrogenase, mitochondrial
4	-1.7	-0.6	-1.1	-2.2	-2.7	-2.4	3.8	3.3	3.6	DPYL3_MOUSE	Dpysl3	Dihydropyrimidinase-related protein 3
5	-1.1	-1.3	-1.2	-2.1	-1.1	-1.6	3.2	2.4	2.8	SRGP1_MOUSE	Srgap1	SLIT-ROBO Rho GTPase-activating protein 1
6	-0.6	-4.2	-2.4	-1.9	1.3	-0.3	2.5	2.9	2.7	ROA2_MOUSE	Hnrnpa2b1	Heterogeneous nuclear ribonucleoproteins A2/B1
7	-3.0	-1.7	-2.4	1.5	-1.8	-0.2	1.6	3.5	2.6	PANX2_MOUSE	Panx2	Pannexin-2
8	-2.5	-2.1	-2.3	0.6	-1.1	-0.3	1.9	3.2	2.6	PP4P2_MOUSE	Tmem55a	Type 2 phosphatidylinositol 4,5-bisphosphate 4-phosphatase
9	1.3	-2.0	-0.4	-3.2	-0.9	-2.1	2.0	2.9	2.4	KCJ11_MOUSE	Kcnj11	ATP-sensitive inward rectifier potassium channel 11

Figure A.4 *GluA1/2/3-enriched proteins identified by BioID2 PL proteomics.*

Protein	Gene	Acc. No.	Construct	NTD-pDisplay	Full-length receptor	BioID2	MiniTurbo	TurboID	APEX2	Direct AMPAR interaction	PMID	Experimental evidence
Neuronal pentraxin-1	Nptx1	Q62443	*Full-length*	Y	Y	Y	Y	Y	Sia et al., 2007. Neuron Xu et al., 2003. Neuron		PMID: 17610819 PMID: 12895424	Co-IP with GluA4 Co-IP with GluA4
Neuronal pentraxin-2	Nptx2	O70340	*Full-length*			N	N	N	Xu et al., 2003. Neuron		PMID: 12895424	Co-IP with GluA4
Neuronal pentraxin receptor	Nptxr	Q99J85	*PTX domain*	N	N	Y	Y	Y	Lee *et al.*, 2017. J Neurosci		PMID: 27986928	Co-IP and binding assay with GluA1/2 NTD
Neuropilin-2	Nrp2	O35375	*Full-length*	N		N	N	N	Wang *et al.*, 2017, Neuron		PMID: 29154130	Co-IP with GluA1/2 via CUB domain
Neuritin	Nrn1	Q8CFV4	*Full-length*	N	N	Y	Y	Y	Subramanian *et al.*, 2019, Cell Rep.		PMID: 31390571	Co-IP with GluA1
Olfactomedin-1/ Noelin-1	Olfm1	O88998	*Full-length*	N	N	N	N	Y	Pandya *et al.*, 2018. Cell Reports.		PMID: 30067977	SPR of unpurified Noelin-1 with GluA2 NTD
Complement C1q-like protein 2	C1ql2	Q8CFR0	*C1q domain*	Y		N	N	N	Matsuda *et al.*, 2016, Neuron		PMID: 27133466	SPR and binding assay with GluA1/K2/K4 NTD
Complement C1q-like protein 3	C1ql3	Q9ESN4	*C1q domain*	Y		N	N	N	Y Matsuda *et al.*, 2016, Neuron		PMID: 27133466	SPR and binding assay with GluA1/K2/K4 NTD
Brorin	Vwc2	Q8C8N3	*Full-length*	N	N	N	N	N	Schwenk et al., 2012. Neuron		PMID: 22632720	Native AMPAR complex
Leucine-rich repeat transmembrane neuronal protein 2	Lrrtm2	Q8BGA3	*Ectodomain*	N		N	N	N	de Wit *et al.*, 2009. Neuron		PMID: 20064388	Co-IP with GluA1/2
Leucine-rich repeat transmembrane neuronal protein 4	Lrrtm4	Q80XG9	*Ectodomain*	N		N	N	N	Schwenk et al., 2012. Neuron		PMID: 22632720	Native AMPAR complex
N-Cadherin	Cdh2	P15116	*Ectodomain*	N		N	Y	Y	Y Saglietti *et al.*, 2007. Neuron		PMID: 17481398	Co-IP and binding assay with GluA2 NTD
Neuroplastin-65	Nptn	P97300	*Ectodomain*	N		N	N	N	Y Jiang *et al.*, 2021. PNAS		PMID: 33627404	Co-IP with GluA1 NTD

Figure A.5 *NTD interactors identified from the current literature screened in cell-based binding assay and proximity-labelling proteomics.*